DIAGENETIC EVOLUTION OF THE MIDDLE DEVONIAN STONE AND DUNEDIN FORMATIONS OF THE LIARD BASIN, NORTHEAST BRITISH COLUMBIA

A Thesis

Submitted to the Faculty of Graduate Studies and Research

In Partial Fulfillment of the Requirements

for the Degree of

Master of Science

in

Geology

University of Regina

by

Sze Shan Yip

Regina, Saskatchewan

May, 2013

UNIVERSITY OF REGINA

FACULTY OF GRADUATE STUDIES AND RESEARCH

SUPERVISORY AND EXAMINING COMMITTEE

Sze Shan Yip, candidate for the degree of Master of Science in Geology**,** has presented a thesis titled, ***Diagenetic Evolution of the Middle Devonian Stone and Dunedin Formations of the Liard Basin, Northeast British Columbia,*** in an oral examination held on April 29, 2013. The following committee members have found the thesis acceptable in form and content, and that the candidate demonstrated satisfactory knowledge of the subject material.

External Examiner:	Dr. Ihsan Al-Aasm, University of Windsor
Co-Supervisor:	Dr. Osman Salad Hersi, Department of Geology
Co-Supervisor:	*Dr. Hairuo Qing, Department of Geology
Committee Member:	Dr. Guoxiang Chi, Department of Geology
Chair of Defense:	Dr. Gang Zhao, Petroleum Systems Engineering

*Not present at defense

Abstract

The Middle Devonian Stone and Dunedin formations are correlative to the Chinchaga and Keg River formations in Northwest Alberta, as well as the Headless and Nahanni formations in Southern Yukon. Core study has identified twenty carbonate sedimentary facies in the Stone and Dunedin formations. The lower to middle Stone Formation comprises of a subtle vertical facies transition from intertidal mudstones to lagoonal wackestones and amphiporid floatstone. The upper Stone Formation in c-10-E/94-N-7 comprises of dominantly clast-rich silty dolomudstone to silty dolomudstone, which is interpreted to have deposited in peritidal settings and represent the middle Chinchaga depositional break caused by the middle Eifelian regression. The Stone Formation as a whole is interpreted to be shallowing upward sequence. The Dunedin Formation comprises of a vertical facies transition from mudstones of restricted shallow marine origin, to reefal floatstones and boundstones, and to clast-bearing crystalline rock of slope facies. These are interpreted to be a deepening upward sequence.

Integrated geochemical and geophysical analysis have identified two sets of fractures and three stages of local structural deformations, all of which postdate the precipitation of the coarsely crystalline saddle dolomite and calcite cements in the Stone and Dunedin formations. Systematic sampling and geochemical analysis including stable oxygen and carbon isotopes, radiogenic strontium isotopic ratio, and fluid inclusion microthermometry on various diagenetic phases were conducted. The most significant

finding is that several samples of the coarsely crystalline calcite cement are highly depleted in $\delta^{13}C$ stable carbon isotope values and as low as -11.23 ‰ V-PDB. Pseudo-secondary to secondary carbonic (vapor only?) inclusions were also found in the coarsely crystalline calcite cement. These can be correlated to a major phase of organic maturation.

These new structural and geochemical findings led to a reinterpretation that the coarsely crystalline saddle dolomite and calcite in the Middle Devonian Stone and Dunedin formations of the Liard Basin in Northeast British Columbia were precipitated during the Carboniferous and Permian.

Acknowledgements

The funding for this thesis research project is provided by the British Columbia Ministry of Energy, Mines and Natural Gas grant to Dr. Salad Hersi. A Graduate Teaching Assistantship (GTA) award from The Faculty of Graduate Studies and Research was granted to Sze Shan Yip.

I thank the BC Ministry of Energy Core Warehouse and Subsurface Geological Laboratory of Saskatchewan Industry and Resources for providing access to their core examination facilities. I thank the staff of the Department of Geology at the University of Regina for their office and lab operation support. Unlimited access to the Geofluids Laboratory and facilities at the University of Regina was authorized by Dr. Guoxiang Chi.

I cannot thank my supervisors enough. I thank Dr. Osman Salad Hersi for his trust and faith in me. I thank Dr. Hairuo Qing for providing all the necessary resource and administrative support. I benefited immensely from working with my colleagues. Dr. Guoxiang Chi and Liu Yongxing introduced me into fluid inclusion analysis and enlightened me in conducting combined fluid inclusion/fracture analysis. Wang Yuchang made me aware of the importance of the coarsely crystalline calcite cement and that ultimately led to the final interpretation.

Table of Contents

List of Tables

CHAPTER 1: Introduction

CHAPTER 3: Sedimentary Facies

CHAPTER 5: Geochemistry

List of Figures

CHAPTER 1: Introduction

CHAPTER 2: Regional Geology

CHAPTER 3: Sedimentary Facies

CHAPTER 4: Diagenesis

CHAPTER 5: Geochemistry

CHAPTER 6: Discussion and Interpretation

CHAPTER 1: Introduction

1.1 Overview

Gas-bearing, dolomitized carbonate reservoir of the Middle Devonian Stone and Dunedin formations occur in the Beaver River gas fields (B.C.), Crow River gas fields (B.C.) Kotaneelee gas fields (Yukon) and Point Mountain gas fields (NWT) in Northeast British Columbia and adjacent subsurface (Morrow et al. 1986; Aulstead 1987), where Middle Devonian carbonate plays constitute upwards of 2.35 Tcf of remaining undiscovered gas in place (National Energy Board 2000). Investigating the sedimentologic, diagenetic, and geochemical attributes of the Stone and Dunedin formations provide a renewed opportunity for expanding our knowledge on dolomitization and dolomite reservoirs in Northeast British Columbia (Walsh et al. 2005).

The study area of this research project covers map areas 94N and 94O in Northeast British Columbia (Fig. 1.1), where major gas-bearing Middle Devonian strata are found in and adjacent to the study area. These include the Dunedin Formation (Morrow et al. 1986; Nadjiwon 2001), Presqu'ile barrier (Qing and Mountjoy 1994; Morrow et al. 2002), Sulphur Point Formation (Lonnee 1999), Slave Point Formation (Lonnee 2005; Lonnee and Machel 2006), and Jean-Marie Formation (Wendte et al. 2007). The study area was chosen by the Dr. Osman Salad Hersi of the University of Regina and accepted

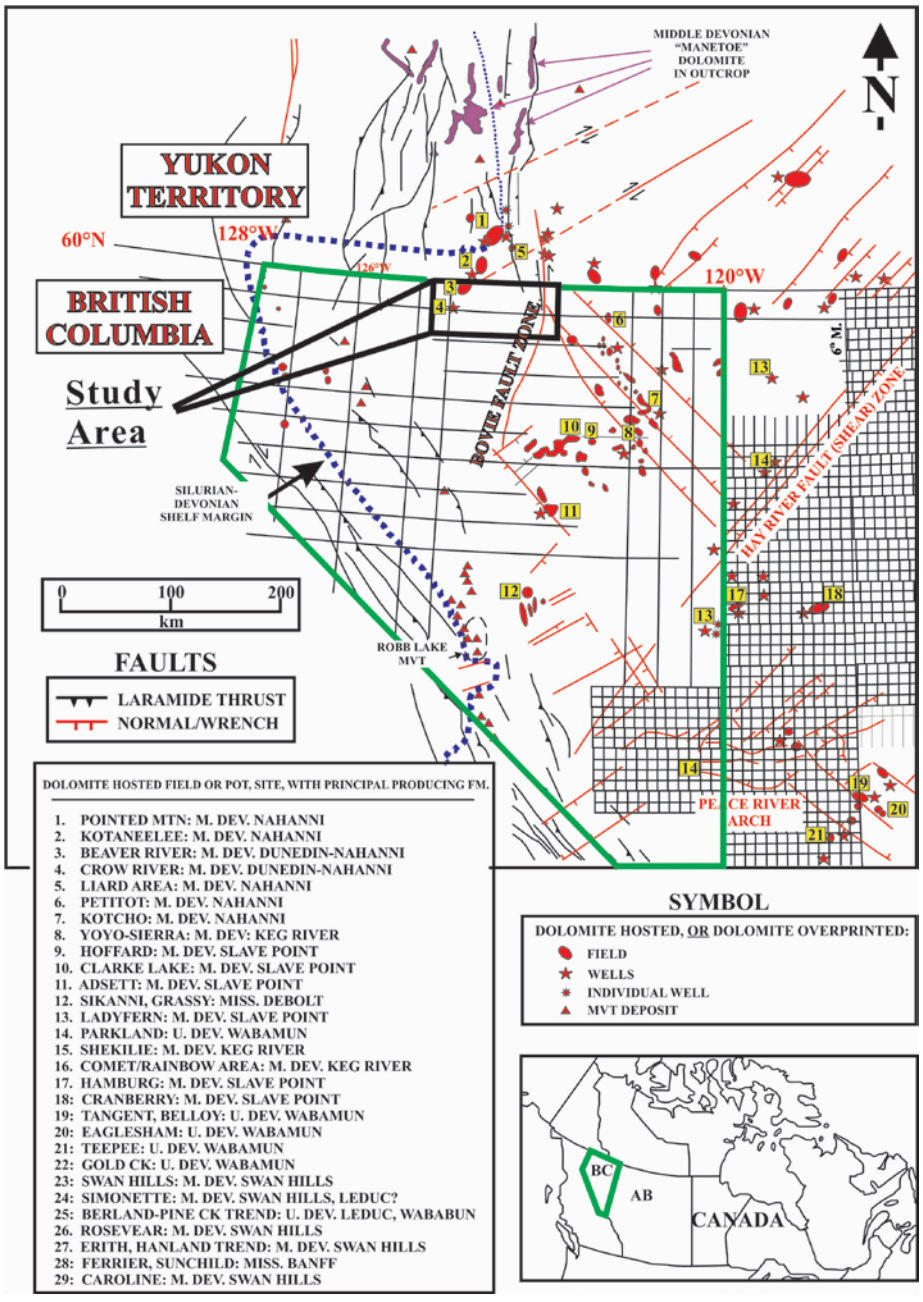

Figure 1.1: Geographic map of western Canada with the location of gas fields that are hosted in Devonian carbonate rocks. Modified from Davies and Smith (2006). (original in color)

by the project sponsor, the Ministry of Energy of the British Columbia government, for the availability of geologic cores (Fig. 1.2), natural gas potential, and proximity to major pipelines which would reduce the costs in future drillings.

1.2 Previous studies

The porosity in the Stone and Dunedin formations is dominantly intercrystalline porosity (Morrow et al. 1990; Nadjiwon 2001) resulted from fabric-destructive dolomitization and subsequent coarsely crystalline saddle dolomite precipitation. Three models were proposed to account for the fabric-destructive dolomitization and subsequent coarsely crystalline saddle dolomite precipitation in some of the Middle Devonian carbonate rock formations in Western Canada including the Stone and Dunedin formations. A combined structurally- stratigraphically controlled dolomitization model for the Nahanni Formation in southernmost Yukon and correlative Dunedin Formation in Northeast British Columbia were proposed by Morrow et al. (1990). A regional-scale hydrothermal reaction and dolomitization model for the Middle and Upper Devonian carbonate rocks in northeastern British Columbia was proposed by Reimer and Teare (1992), which is also known as the "furnace model". A structurally-controlled dolomitization model for the Dunedin Formation was proposed by Nadjiwon (2001). The ideas of these models are summarized in Table 1.1 and presented in Figures 1.3, 1.4 and 1.5. There is no representative model to account for the fracture development in Middle Devonian strata.

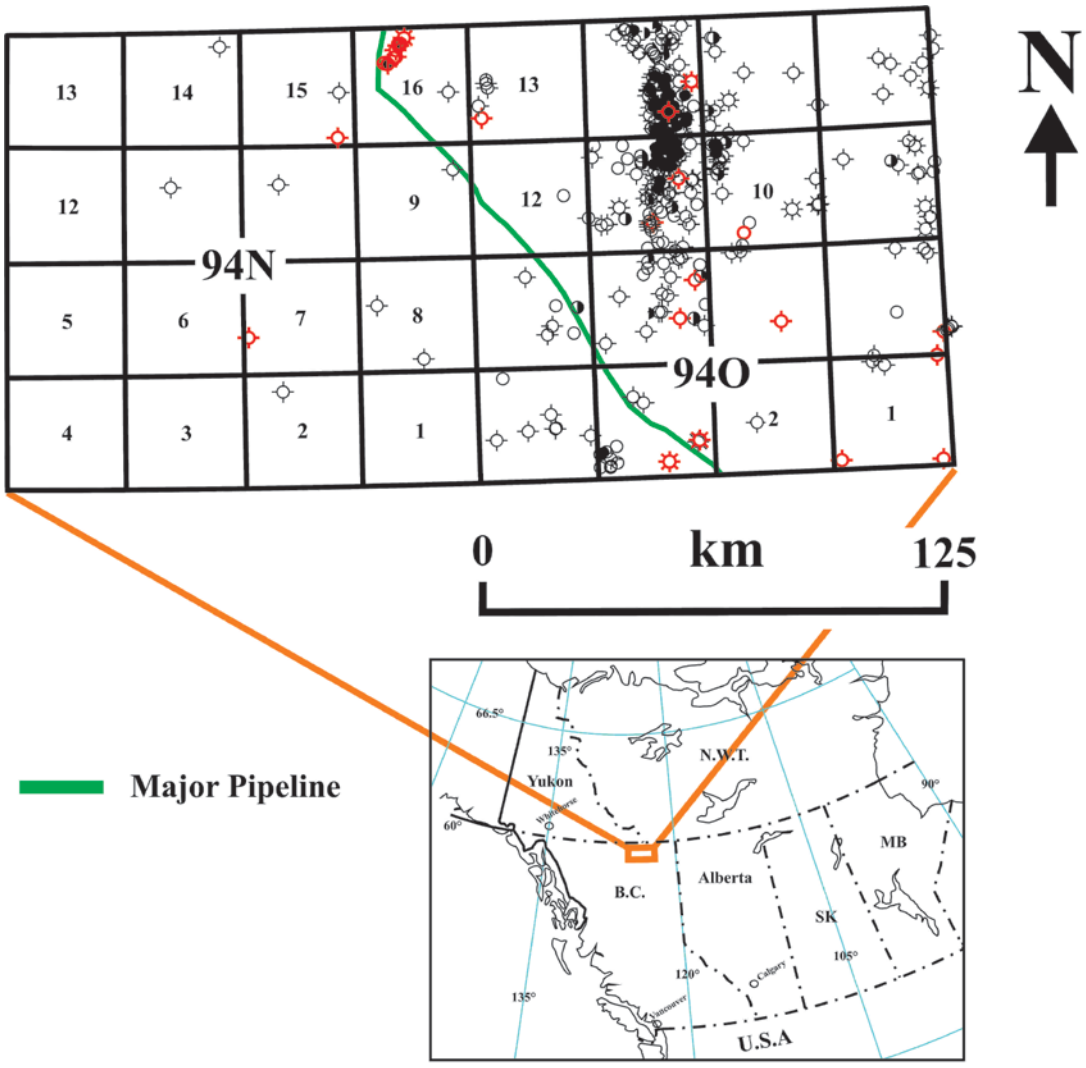

Figure 1.2: Well locations in map area 94N and 94O. Twenty three wells are highlighted in red which indicate that core samples were recovered from Stone and /or Dunedin formations (well data was acquired through the AccuMap® package provided by the Dr. Osman Salad Hersi, University of Regina; last update Fall 2004). Petroleum land grid and well locations were acquired from the Web Map Services hosted on the B.C. government website (http://webmap.em.gov.bc.ca/mapplace/minpot/Pet_map_search.cfm. Retrieved 20 Oct 2009). Matching geographic map of Lambert conical projection was acquired from the University of Texas library website (www.lib.utexas.edu/maps/americas/canada_rel97.jpg. Retrieved 20 Oct 2009). (original in color)

Table 1.1: Summary of the three dolomitization models from previous studies for the Middle Devonian carbonate rocks including the Stone and Dunedin formations in Northeast British Columbia.

Previous Studies	Precondition(s)	Supply of Mg and CO_3	Delivery Mechanism	Heat Source	Timing (or Relative Timing) of Dolomitization
Morrow et al. (1990; Fig. 1.3)	- Cavern system and influx of water dissolved limestone and created porosity. - Fault conduit systems	Elk Point brine(s)/ Brine(s) from the Devonian Elk Point Basin	Fluid circulation through fault conduit systems	Igneous pluton(?)	Middle to Late Devonian
Reimer and Teare (1992; Fig. 1.4)	Pre-existing oil pools/oil accumulation in the carbonate rocks	Supply of Mg was not stated. Supply of CO_3 is from dissolution of limestone and natural gases.	Thermochemical sulphate reduction (TSR) and aggressive hydrothermal reactions	Geothermal heat	Not stated. But postdates oil accumulation.
Nadjiwon (2001; Fig. 1.5)	Fault conduit systems	Residual brine from the Devonian Elk Point Basin	Fluid circulation through fault conduit systems	Some geothermal anomalies	Late Devonian to Mississippian

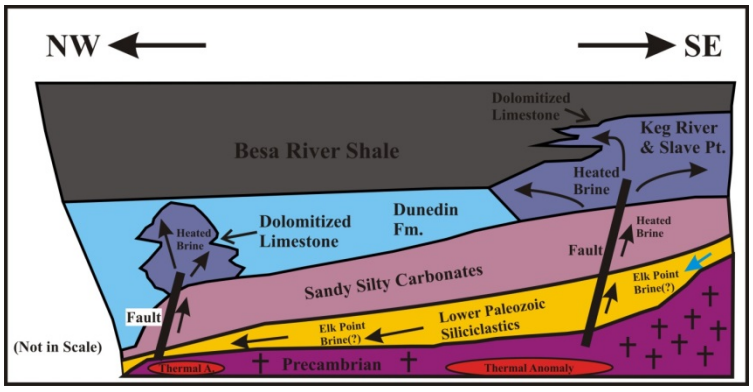

Figure 1.3: A dolomitization model for the Dunedin Formation (Diagram is modified from Nadjiwon 2001). (original in color)

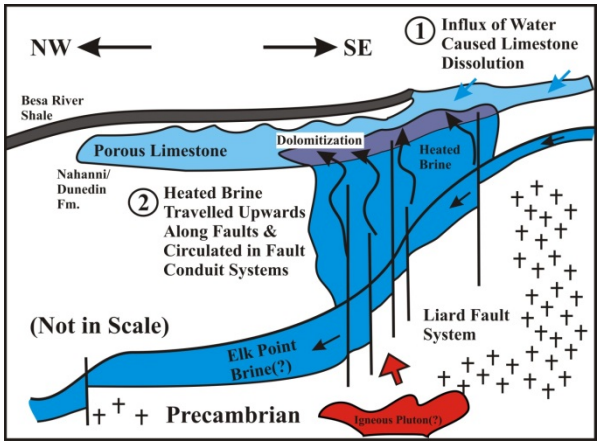

Figure 1.4: A dolomitization model for the Nahanni and correlative Dunedin formations (Diagram is modified from Morrow et al. 1990). (original in color)

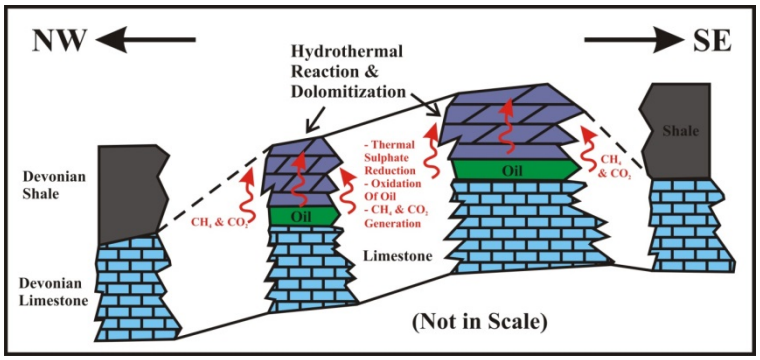

Figure 1.5: A schematic diagram of the “furnace model” showing dolomitization processes suggested by Reimer and Teare (1992) for the Middle Devonian carbonate rocks in Northeastern British Columbia. (original in color)

The model from Morrow et al. (1990; Fig. 1.3) proposed that dolomitization occurred in two phases. A cavern system developed during Early to Middle Devonian time by the actively moving Watt Mountain aquifer, influx of water dissolved the limestone and created porosity. Then fabric-destructive dolomitization took place during Middle to Late Devonian and saddle dolomite was precipitated from superheated hypersaline brine that circulated through the porous zone that was created by the cavern system. Maturation of organic-rich Devonian Besa River shale occurred during the Late Paleozoic to Early Mesozoic. Hydrocarbons were expelled and migrated laterally and downward into the permeable dolomitized strata. Intense deformation during the Tertiary Laramide Orogeny has resulted in further fracturing and additional permeability. Anticlinal folding and thrust faulting also occurred during the Tertiary Laramide Orogeny.

Reimer and Teare (1992; Fig. 1.4) suggested an alternate explanation for the fabric-destructive dolomitization in the Middle and Devonian carbonate rocks in Northeast B.C. They suggested that fabric-destructive dolomitization was caused by aggressive hydrothermal reactions that were initiated by thermochemical sulphate reduction (TSR) during the oxidation of pre-existing oil pools within the limestone strata. This reaction caused dissolution of the limestone, followed by hydrothermal dolomitization, and pyrobitumen, barite, and galena mineralization. The heat source is suggested to be geothermal heat. Methane and carbon dioxide evolved as by-products of the thermochemical sulphate reduction processes.

Nadjiwon (2001; Fig. 1.5) proposed that fabric-destructive dolomitization occurred during the Late Devonian to Mississippian. A thermal anomaly in the Precambrian basement heated the residual brine and the brine circulated through fault conduit systems. The fluid source is suggested to be modified Devonian seawater possibly the Elk Basin Brine from Western Alberta, based on fluid inclusion microthermometric analysis and calculated salinity range, and oxygen isotopic values.

Oxygen isotopic values of coarsely crystalline saddle dolomite from the Dunedin Formation are from -9.7 to -13.1 ‰ VPDB (Nadjiwon 2001). The measured fluid inclusion homogenization temperatures are from 108 to 238 ºC. The calculated oxygen isotopic composition of dolomite precipitating diagenetic fluid is from 1.5 to 2.8 ‰ SMOW by using the equation from Friedman and O'Neil (1977). The oxygen isotopic values are close to evaporated Devonian seawater (~5.0 ‰ SMOW; Morrow and Aulstead 1995), and higher than the Middle Devonian seawater of -3.8 ‰ SMOW (Shackleton and Kennett 1975) to -2.0 ‰ SMOW (Morrow and Aulstead 1995).

More remarkable stratal dolomitization models for the Middle Devonian carbonate rocks in Northwest Territories were developed by Qing and Mountjoy (1994), Morrow et al. (2002), Lonnee and Machel (2006), and Davies and Smith (2006). These models concern about 1) diagenetic fluid source, 2) structural controls, 3) stratigraphic controls, and 4) relative timing of dolomitization.

Surface and subsurface sedimentologic studies on the Stone and Dunedin formations by Nadjiwon (2001) identified 8 facies within the Dunedin Formation. The strata were concluded to be a succession of intertidal to platformal and reefal facies. Diagenetic fluid possibly migrated through porous and permeable zones and dolomitized the strata.

Fractures in the Stone and Dunedin formations were documented by Snowdon (1977). The open fractures have been suggested to have developed from tectonic deformation (Morrow et al. 1990). Dolomite cement was found in some of these fractures by Davies and Smith (2006), who interpreted the fractures with dolomite cement as shear microfractures which developed shortly before massive fluid loading and predates coarsely crystalline saddle dolomite precipitation.

The interpretation which dolomitization and saddle dolomite precipitation occurred during the Late Devonian to Carboniferous is largely based on fluid inclusion microthermometric analysis. Aulstead (1987) reported that the homogenization temperatures of primary inclusions in coarsely crystalline saddle dolomite are between 150 and 215 °C with a mean of around 185 °C, which corresponds to the calculated geothermal temperature during the Late Devonian to Carboniferous in southernmost Yukon and the adjacent 94N map area in Northeast British Columbia (Morrow et al. 1993; Morrow and Aulstead 1995; Davies and Smith 2006). Similar fluid inclusion microthermometric data was obtained by Nadjiwon (2001), who made a similar interpretation.

1.3 Problems, purposes and objectives

1.3.1 Problems

The three major dolomitization models from previous studies provided insights into the process of dolomitization in the Devonian carbonate rocks, but the relative timing of dolomitization is loosely constrained. There are also four elements that were under-explored.

1) Nadjiwon (2001) identified 8 facies within the Dunedin Formation, which her study covers both surface outcrops and subsurface cores. Outcrops of the Dunedin Formation are highly inaccessible and that field mapping requires aerial transportation. Subsurface cores of the Dunedin Formation are limited due to the cost and risk of drilling into the deep Liard basin. In order to develop a stratigraphic framework which can help to correlate the Stone and Dunedin formations with the adjacent Middle Devonian strata, a more comprehensive sedimentologic study is required.

2) The dolomite cement in fractures in the Middle Devonian Slave Point Formation in British Columbia was documented by Lonnee (2005). Lonnee (2005) and Davies and Smith (2006) interpreted the fractures that are filled with dolomite cement are shear microfractures developed shortly before massive fluid loading and predates coarsely crystalline saddle dolomite precipitation. The fracturing pattern of the Stone and Dunedin formations has been overlooked in previous studies. The Stone and Dunedin

formations have undergone 3 orogenic events. If the fractures that are filled with medium crystalline saddle dolomite cement are cut by a majority of fractures, it implies that fabric-destructive dolomitization and saddle dolomite precipitation occurred prior to, or during, the first Antler Orogeny from the Late Devonian to Mississippian. If medium crystalline saddle dolomite cement fills into a pre-existing network of fractures, this implies that fabric-destructive dolomitization and saddle dolomite precipitation might have occurred after the Late Devonian to Mississippian when the fractures had already developed. However, there is still a possibility that the hydraulic loading prior to the fabric-destructive dolomitzation has created fractures which medium crystalline saddle dolomite cement filled in (Davies and Smith 2006).

3) Fluid inclusion microthermometric analysis by Aulstead (1987) reported that the homogenization temperatures measured in the primary inclusions in coarsely crystalline saddle dolomite in the Dunedin Formation are between 150 and 215 °C with a mean of 185 °C. Nadjiwon (2001) reported similar results. The variation in temperature can be resulted from analytical precision, or the samples were collected from different depth and location, or the Dunedin Formation has already been structurally deformed after the first Antler Orogeny, which the structural blocks of the Stone and Dunedin formations were at different depth, hence different geothermal conditions and yield variation in microthermometric data. A fluid inclusion microthermometric study with systematic geochemical sampling and carefully constructed stratigraphic and structural cross-sections may generate a more refined interpretation.

4) The coarsely crystalline calcite cement postdates and directly cross-cuts coarsely crystalline saddle dolomite cement (Nadjiwon 2001). There are limited geochemial studies on the coarsely crystalline calcite cement. The relative timing of dolomitization proposed by the three major dolomitization models are supported by geochemistry and fluid inclusion microthermometric studies on the coarsely crystalline saddle dolomite. Investigating the coarsely crystalline calcite cement may lead to a discovery of new evidences which provides new insights into the relative timing of dolomitization.

1.3.2 Purposes and objectives

Collaborative studies on the Stone and Dunedin formations between the BC Ministry of Energy and University of Regina were initiated in 2004. The main purposes of this thesis are 1) to summarize and interpret the unpublished sedimentologic data collected by Dr. Osman Salad Hersi and Akhtar Khan of the University of Regina during the first phase of this collective project, as well as presenting new sedimentologic data collected by Sze Shan Yip; and 2) to interpret the relative timing of fabric-destructive dolomitization and coarsely crystalline saddle dolomite precipitation in the Middle Devonian Stone and Dunedin formations, based on and beyond previous studies. The main objectives of this graduate thesis are:

- To compile unpublished sedimentologic data of the Stone and Dunedin formations collected during the first phase of this project.

- To present new sedimentologic data, and conduct a more comprehensive study on the sedimentology of the Stone and Dunedin formations.
- To reconstruct the diagenetic history of the Stone and Dunedin formations;
- To investigate the origin of the two sets of fractures which are filled with dolomite and calcite.
- To conduct systematic geochemical sampling and geochemical analysis on different diagenetic phases, with increased emphasis on the coarsely crystalline calcite cement.
- To refine or reinterpret the relative timing of dolomitization for the Stone and Dunedin formations, and correlate the diagenetic phases and fractures with regional tectonic events and geothermal gradient.

This graduate project is a core-based study on the Stone and Dunedin formations across the 94N and 94O map areas in the Liard Basin area, Northeast British Columbia. It involves sedimentary facies analysis, petrographic investigation, fracture analysis, geochemical analysis, and fluid inclusion microthermometric analysis. This thesis is organized as the followings: A summary of the regional geology is presented in Chapter 2. Sedimentology and sedimentary facies are presented in Chapter 3. The diagenetic phases are presented in Chapter 4. Geochemistry analytical results are presented in Chapter 5. An integrated geochemical data discussion and interpretation is presented in Chapter 6.

1.4 Methodology

1.4.1 Geologic cores

Initial subsurface data quarrying was performed by Dr. Osman Salad Hersi by using AccuMap® with a well data subscription last updated in Fall 2004, which showed that core samples were recovered from the Stone and /or Dunedin formations in 23 wells in map areas 94N and 94O. The cores were studied by Dr. Osman Salad Hersi and A. Khan at the Ministry of Energy Core Warehouse in Charlie Lake, B.C. in the summer of 2005. Eleven wells and 88 cores were chosen by Dr. Osman Salad Hersi and Sze Shan Yip for further studies. Ten wells and 83 cores from ~3 to 18 m in length were chosen by Sze Shan Yip for this study (The locales of these 10 wells are presented in Table 1.2. For the depth and length measurements of these 83 cores, see Appendix A). These 10 wells were selected based on 1) the length of the cores recovered; 2) the quality of the cores recovered; and 3) the location of the wells, which an east-west trending cross-section can be constructed; such that the orientation of the cross-section is perpendicular to both the structural strike and the Middle Devonian shoreline. Comprehensive facies analysis was conducted. Core photos were taken. Maps, cross-sections, and graphic logs were drawn with CorelDRAW X4™ and CorelDRAW X5™.

Table 1.2: Well list showing the studied ten wells in this thesis. Eighty-three cores were recovered from these 10 wells. For UWIDs of the wells, and depth and length measurements of the cores, see Appendix A.

Petroleum wells studied (From east to west)
c-10-E/94-N-7
c-16-A/94-N-15
b-19-K/94-N-16
c-27-K/94N-16
c-45-K/94-N-16
c-54-K/94-N-16
d-64-K/94-N-16
d-73-K/94-N-16
a-67-D/94-O-13
b-21-G/94-O-6

1.4.2 Petrographic studies

About 150 core slabs were sampled for thin section preparation. Samples were collected from the representative units from the recovered cores, polished and documented. One hundred and nineteen samples were sent to AGAT Lab for standard thin section preparation. Core samples recovered from 8 of the 10 studied wells are dolostone (91 to ~100 %). The white card method outlined by Folk (1987) was used in petrographic studies. Description and interpretation were made based on the available cores samples.

Thin sections are half-stained with Alizarin red-S and K-ferricyanide solutions following the techniques and procedures outlined by Dickson (1966). Diagenetic phases were identified and documented from petrographic investigation. Further petrographic investigation was made by using an optical microscope equipped with a Cambridge cold-cathodoluminescence. Mineral zonings were identified from diagenetic phases and documented.

1.4.3 Geochemical sampling and analyzes

A stratigraphic cross-section with 10 wells was constructed and all samples were collected systematically over the strata (Fig. 1.6). Well logs were provided by Dr. Osman Salad Hersi of the University of Regina and Filippo Ferri of the British Columbia Ministry of Energy and Mine through AccuMap®.

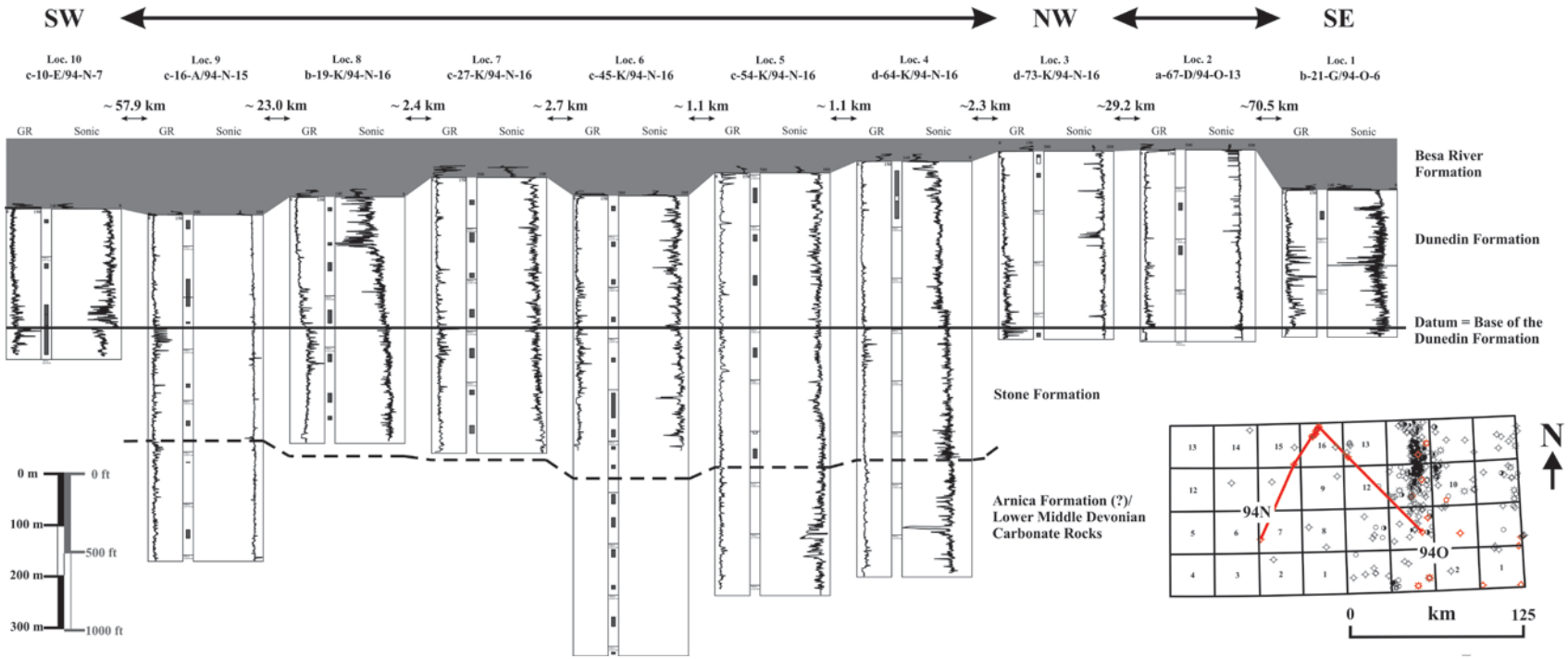

Figure 1.6: A cross-section constructed with gamma and sonic rays wire logs of the studied 10 wells. This cross-section is oriented from southeast (94O6) to northwest (94N16), and from northwest (94N16) to southwest (94N7). The base of the Dunedin Formation is used as datum. (original in color)

Seventy-nine samples were systematically chosen over the strata and sent for geochemical analyzes. Nineteen samples of which were sent to Vancouver Petrography for doubly polished, 100-um thin section preparation. Forty-five samples were selected for micro-sampling. Seventy-nine cement crystals of 7 diagenetic phases were drilled with a craftman's drill press or extracted with a pen knife. Eighty-six samples were sent to the University of Saskatchewan for oxygen and carbon stable isotopes analyzes. Forty-five samples were sent to University of Calgary for strontium radiogenic isotopes analyzes.

Carbonate samples for stable carbon and oxygen analysis were analyzed by the Saskatchewan Isotopes Lab. The procedures were outlined in the analytical report as the following: “Samples were roasted in a vacuum oven at 200 °C for 1 hour to remove water and volatile organic contaminants that may confound stable isotope values of carbonate minerals. Twenty to fifty micrograms of powdered sample was reacted at 70 °C with 3 drops of anhydrous phosphoric acid for 420 seconds. The evolved CO_2 gas was then purified and passed to a Finnigan MAT 253 isotope ratio mass spectrometer for stable carbon and oxygen isotopes analysis. Isotope ratios were corrected for acid fractionation and ^{17}O contribution. Data was directly calibrated against the international standard NBS-19 that is by definition $\delta^{13}C$ = 1.95 ‰ VPDB and $\delta^{18}O$ = -2.2 ‰ VPDB. Accuracy of $\delta^{13}C$ and $\delta^{18}O$ are ±0.05 ‰ and ±0.11 ‰, respectively. Dolomite $\delta^{18}O$ values are calculated by using the fractionation factors of 1.009926 from Rosenbaum and Sheppard (1986) at 70 °C. Calcite $\delta^{18}O$ values are calculated by using the fractionation factors of 1.008698 from Swart et al (1991) at 70 °C.”

Forty-one samples were analyzed for Sr isotopic ratios ($^{87}Sr/^{86}Sr$) at the Radiogenic Isotopes Facility of the University of Alberta supervised by Dr. Robert Creaser. The procedures were outlined by the lab as the following: “Approximately 50mg of sample was dissolved in 0.75N HCl under clean-room conditions, which strontium was chemically separated by conventional cation chromatography. Strontium isotopic abundances were measured in static mode by a multi-collector ICP Mass Spectrometry instrument. Result was normalized for variable mass fractionation to a value of 0.1194 for $^{86}Sr/^{88}Sr$ by using the exponential law. The ratios are reported relative to an $^{87}Sr/^{86}Sr$ ratio of 0.710245 for the NIST SRM987 International Sr isotope standard."

Fluid inclusion petrographic and microthermometric studies were conducted at the Geofluids Lab of the University of Regina with a Linkam Fluid Inc-modified heating-cooling system equipment on an Olympus research microscope. The trendicator thermocouple of the heating-cooling stage was calibrated and gave a melting temperature of -56.6 ℃ for synthetic CO_2 inclusions. Calibration and maintenance of the equipment was conducted by Dr. Guoxiang Chi. Eighteen samples were selected from 8 wells for fluid inclusion studies, based on 1) the location of the wells where the samples were recovered; 2) the depth where the samples were recovered from the wells; 3) the size the mineral crystals; 4) the quality of the mineral crystals. Doubly polished, 100 μm thick thin sections were prepared by Vancouver Petrography. The mineral slices were detached from the thin section glass slides in a beaker filled with acetone prior to analyze.

CHAPTER 2: Regional Geology

2.1 Paleogeography

The Middle Devonian (Elfelian to Givetian; 397.5 ± 2.7 Ma to 385.3 ± 2.6 Ma) Stone and Dunedin formations represent a westward succession of intertidal to platformal and shelfal carbonate rocks that were deposited on the MacDonald platform north of the Peace River Arch between 10° S to 10° N (Fig. 2.1 and 2.2; Morrow 1978; Morrow and Geldsetzer 1988; Cecile et al. 1997; House and Gradstein 2004; Blakey 2009). The MacDonald platform was located along a passive plate margin that was resulted from asymmetric rifting and crustal extension during the Late Proterozoic (Lister et al. 1991).

2.2 Stratigraphic nomenclature

Stratigraphy of the Devonian strata in the Northern Plains was firstly defined by Law (1955). These strata were further mapped and documented by Belyea and Norris (1962), Griffin (1967), Taylor (1967a and 1967b), Taylor and MacKenzie (1970); Taylor and Stott (1973) and Taylor and MacKenzie (1976), with the type sections of the Stone and Dunedin formations being measured by Taylor and MacKenzie (1970). More recent stratigraphic studies were conducted by Nadjiwon (2001), Petrel Robertson (2003) and Salad Hersi et al. (Fig. 2.3; 2006). Outcrops of the Stone and Dunedin formations are located in and along the One Ten Creek adjacent to the Alaska Highway, Tuchodi Lakes map area (94K), northeastern British Columbia (58°41' N, 124°48' W).

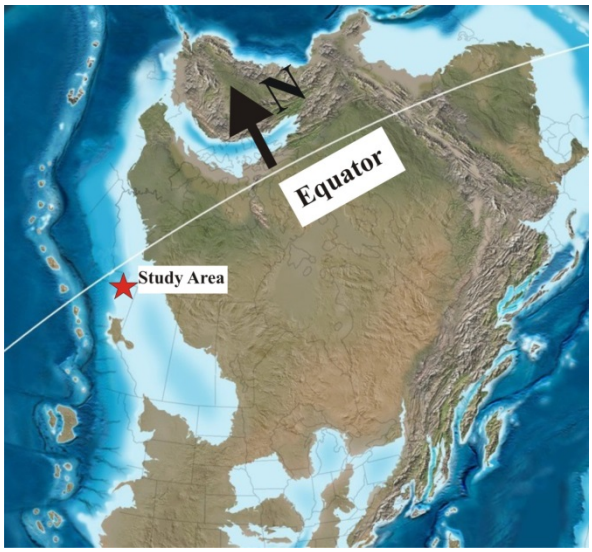

Figure 2.1: Paleographic map of the North America during the Middle Devonian time (~385 Ma). Paleogeographic map from Blakey (2009). (original in color)

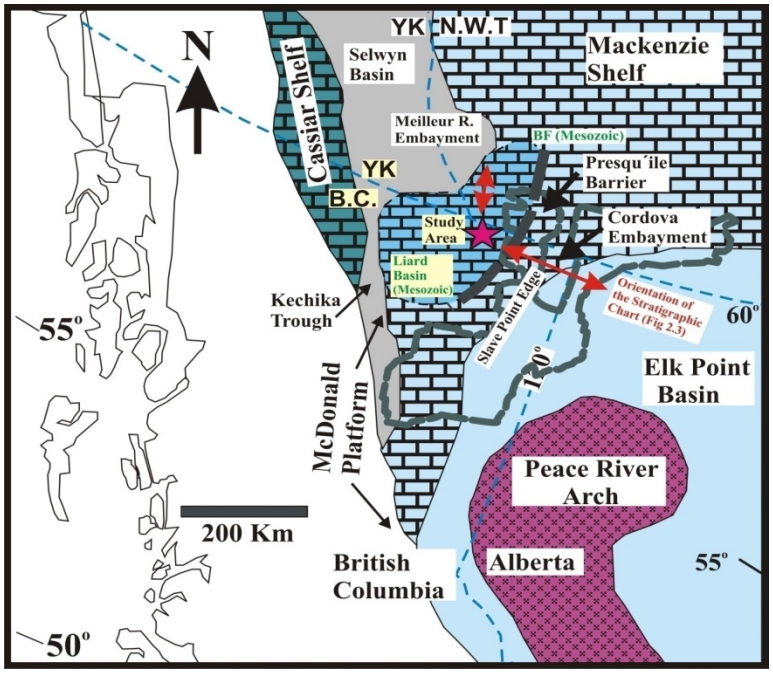

Figure 2.2: Selected Devonian and Mesozoic geologic elements in Northeast British Columbia and vicinity. BF: Mesozoic Bovie Fault, which defines the eastern limit of the Mesozoic Liard Basin structure (modified from Morrow and Geldsetzer 1988; Morrow et al. 2002; Salad Hersi et al. 2006). (original in color)

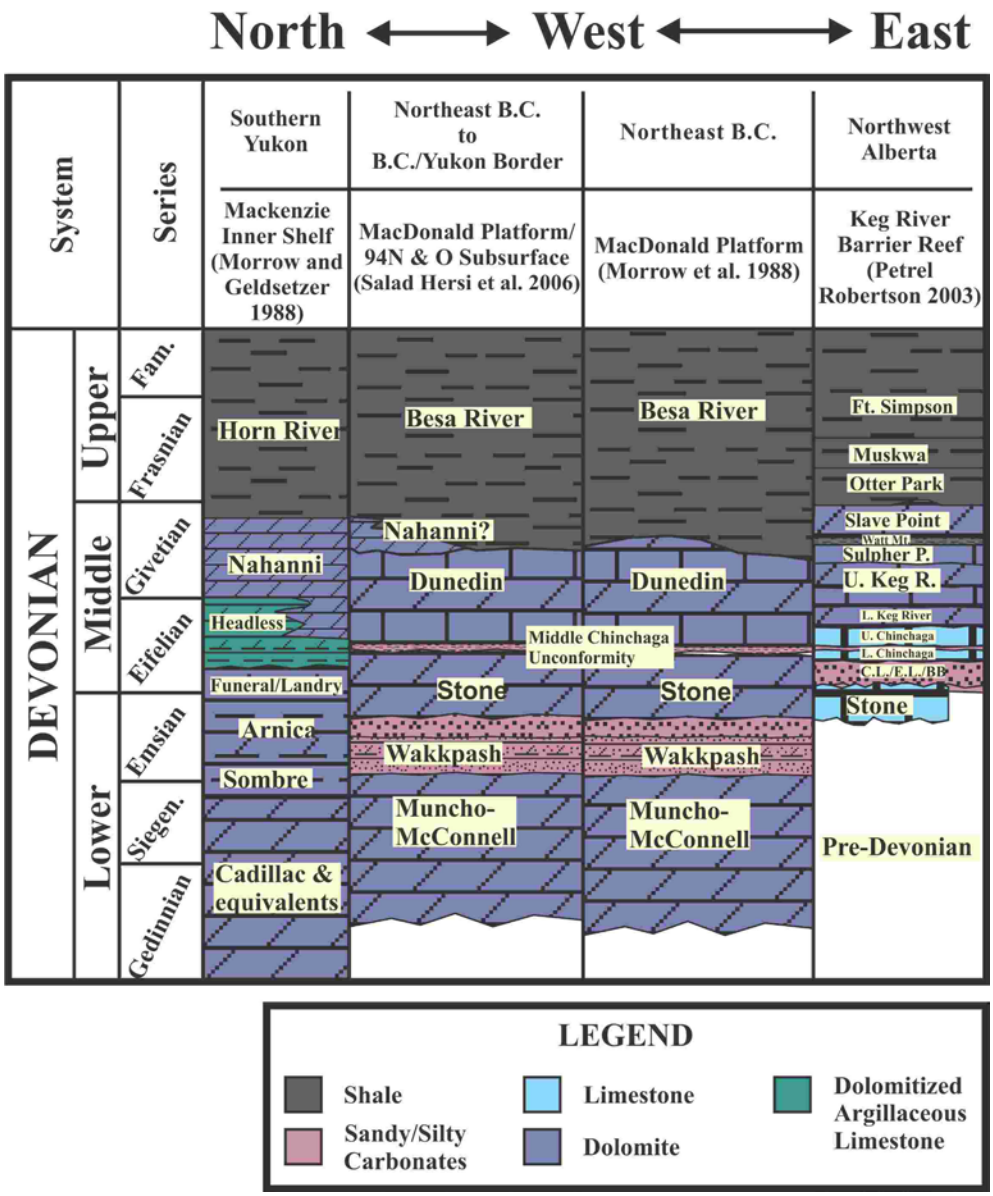

Figure 2.3: Stratigraphic correlation chart across Northwest Alberta, Northeast British Columbia and Yukon Territory (compiled from Morrow and Geldsetzer 1988; Petrel Robertson 2003 and Salad Hersi et al. 2006). (original in color)

Those outcrops were studied by Taylor (1967a and 1967b) and Taylor and MacKenzie (1970). The Nahanni Formation was firstly studied by Hage (1945) at the Nahanni Butte (Fig. 2.4; 61°03' N, 123°37' W; approximately 75 km north of the British Columbia and Yukon Territory border). Both Dunedin and Nahanni formations are conformably overlain by the Besa River Shale (Morrow et al. 1986; 1990). The Dunedin and Nahanni formations have been interpreted to be stratigraphically correlative to each other by Taylor (1967b), Taylor and MacKenzie (1970) and Morrow et al. (1986; 1990). The Stone and Dunedin strata are stratigraphically correlative to the Chinchaga and Keg River strata in northwestern Alberta (Meijer Drees 1994; Nadjiwon 2001; Petrel Robertson 2003).

The Stone Formation and middle Chinchaga unconformity

Taylor (1967a) and Taylor and Mackenzie (1970) described the Stone Formation as a sequence of very light grey dolostones and dolomite breccias in the Tuchodi Lakes map area (94K; Fig. 2.4). Floating quartz sand grains are common in the lower three quarters of the Stone formation and well-bedded sandy dolostones dominate the lithology in the Halfway map area (94B). The lithology shifts from sandy dolomites into finely crystalline dolomites with minor interbedded limestones westward. The formation thickens westward, from meters at the Alberta-British Columbia border, to

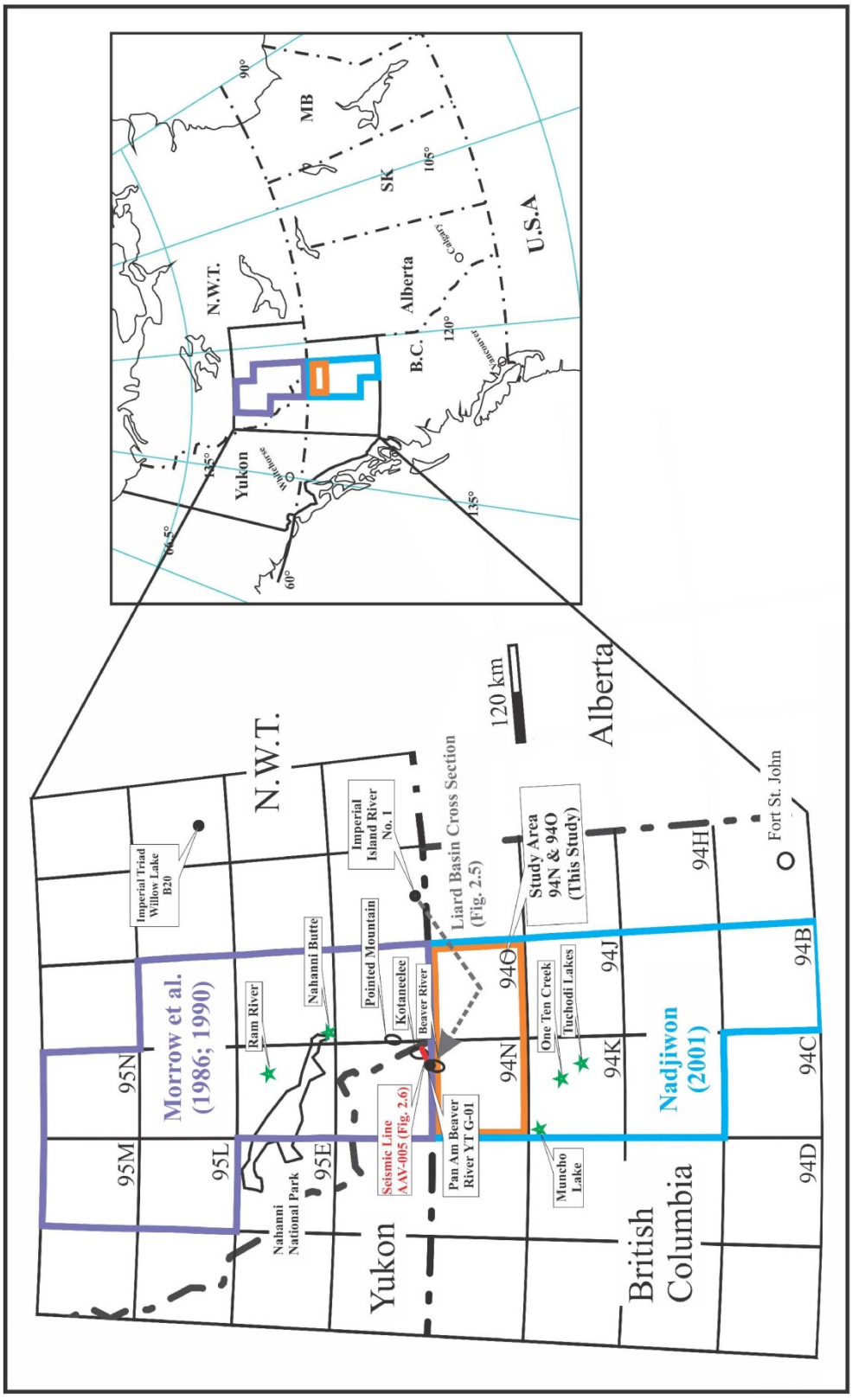
MB
SK
Alberta
B.C.
N.W.T.
Yukon
U.S.A
Whitehorse
Yellowknife
Calgary
90°
105°
120°
135°
60°
67.5°
Morrow et al. (1986; 1990)
Nadjiwon (2001)
Imperial Triad Willow Lake B20
Imperial Island River No. 1
Nahanni Butte
Ram River
Pointed Mountain
Kotaneelee
Beaver River
Seismic Line AAV-005 (Fig. 2.6)
Pan Am Beaver River YT G-01
Liard Basin Cross Section (Fig. 2.5)
Study Area 94N & 94O (This Study)
One Ten Creek
Tuchodi Lakes
Muncho Lake
Nahanni National Park
120 km
Fort St. John
95N
95M
95L
95E
94O
94N
94J
94K
94H
94B
94C
94D
N.W.T.
Yukon
Alberta
British Columbia

Figure 2.4: Geographic map showing the locations of previous mapping and subsurface core studies of the Stone Formation, Dunedin Formation and Dunedin-correlative Nahanni Formation. These include One Ten Creek in 94K map area, where the Stone and Dunedin formations type sections were measured by Taylor (1967a and 1967b) and Taylor and MacKenzie (1970) and Nadjiwon (2001), Tuchodi Lakes and Muncho Lake, 94K map area, mapped by Taylor (1967a and 1967b) and Taylor and MacKenzie (1970), Nahanni Butte, Yukon, where the Nahanni Formation type section was originally measured by Hage (1945), surface exposure of Nahanni Formation at the Ram River outcrop studied by Aulstead (1987), Pan Am Beaver River YT G-01 and Imperial Island River No. 1 in Northwest Territories, well cuttings studied by Morrow et al. (1993), Beaver River, Kotanneelee and Pointed Mountain gas fields, cores studied by Aulstead (1987), and Seismic Line AAV-005 across the Kotaneelee gas field drawn in red line (National Energy Board 2001). The subsurface study area by Morrow et al. (1986; 1990) is highlighted in purple whereas the surface and subsurface study by Nadjiwon (2001) is highlighted in blue. The current study area (subsurface of the 94N and 94O map areas) is highlighted in orange. This map is modified from Nadjiwon (2000; 2001). (original in color)

approximately 400 m thick at the One Ten Creek type section at Tuchodi Lakes map area (94K; Fig. 2.4) and approximately 600 m near Muncho Lake map area (94K; Fig. 2.4). The Stone Formation is overlain unconformably by the Dunedin Formation in the east and south of the Liard region, but both formations become conformable towards north and west of the Liard region (Taylor and MacKenzie 1970). This unconformity was named by Belyea (1970) as the middle Chinchaga unconformity, which is represented by meters of silty dolomitic limestone and siltstone. In this study, approximately 20 m of clast-bearing, silty dolomitic limestone cores were identified between the Stone and Dunedin formations in c-10-E/94-N-7. No evidence of surface exposure was observed.

The middle Chinchaga unconformity was suggested by Morrow and Geldsetzer (1988) as a representation of depositional break caused by a short-term (10 Ma?) relative sea level fall during the end of Eifelian. Minor erosion occurred before the deposition of the Dunedin Formation (Meijer Drees 1994).

The Dunedin Formation

The Dunedin Formation was documented by Taylor (1967b) and Taylor and Mackenzie (1970) as a sequence from the basal sandy dolomitic limestone, to a monotonous sequence of argillaceous and locally siliceous and dolomitic dark grey, well-bedded limestones. Two facies recognized by Morrow (1978) include a lower dolomitic

wackestone facies of shoreface environment, and an upper grainstone-wackestone facies of subtidal origin. Bafflestones are also locally present in the upper section of the Dunedin Formation. The Dunedin Formation was measured by Taylor (1967b) and Taylor and Mackenzie (1970). It is approximately 250 m thick in the Tuchodi Lakes and increases in thickness westward to approximately 400 m near Muncho Lake (Fig. 2.4).

The Nahanni Formation

The Nahanni Formation is dark grey to grey, bedded, finely crystalline dolomitic limestone, containing corals, brachiopods and trilobites (Hage 1945; Douglas and Norris 1960). The formation was measured 137 m thick at the type locality at Nahanni Butte in the Yukon Territory by Hage (1945).

The Besa River Formation

The Besa River Formation is dominantly shale, dark grey to black, slightly calcareous to siliceous, containing sponge spicules and radiolarians (Pelzer 1966). The formation was measured up to 1655 m thick in southeastern Yukon (Richards 1989). The Dunedin Formation is conformably overlain by the Besa River Formation of Late Middle Devonian (Fig. 2.3; Morrow and Geldsetzer 1988). The Besa River Formation in British Columbia and southeastern Yukon is stratigraphically correlative to the Horn River Formation in the MacKenzie Inner Shelf in the Yukon Territory.

2.3 Regional depositional pattern

The Devonian sediments in western Canada were deposited during the Kaskaskia transgression (Morrow and Geldsetzer 1988). The transgression began in the Latest Silurian, as recorded by the Muncho-McConnell Formation (Fig. 2.5). The Stone and Dunedin formations belong to a depositional package that was deposited over the Middle Devonian Elfelian stage (Morrow 1978; Morrow and Geldsetzer 1988), and the middle Chinchaga unconformity between the two formations recorded a depositional break caused by the middle Eifelian regression. Shales were deposited to the west and north of the McDonald Shelf, where the Devonian Horn River basin and ocean troughs were located (Figs. 2.2 and 2.5). Carbonate built-ups occurred in the east and south on the McDonald Shelf, where the Stone, Dunedin, Nahanni and Keg River formations were deposited (Figs. 2.2 and 2.5).

2.4 Structural development

2.4.1 Regional deformation pattern

The Stone and Dunedin formations in the 94N and 94O subsurface are within the Liard Basin region (Fig. 2.6), which is bounded by the Bovie fault in the east and structural deformation extends to the west (Fig. 2.2). The Devonian strata were displaced westward along the footwall of the Bovie fault, and form a series of horse and graben blocks (MacLean and Morrow 2004).

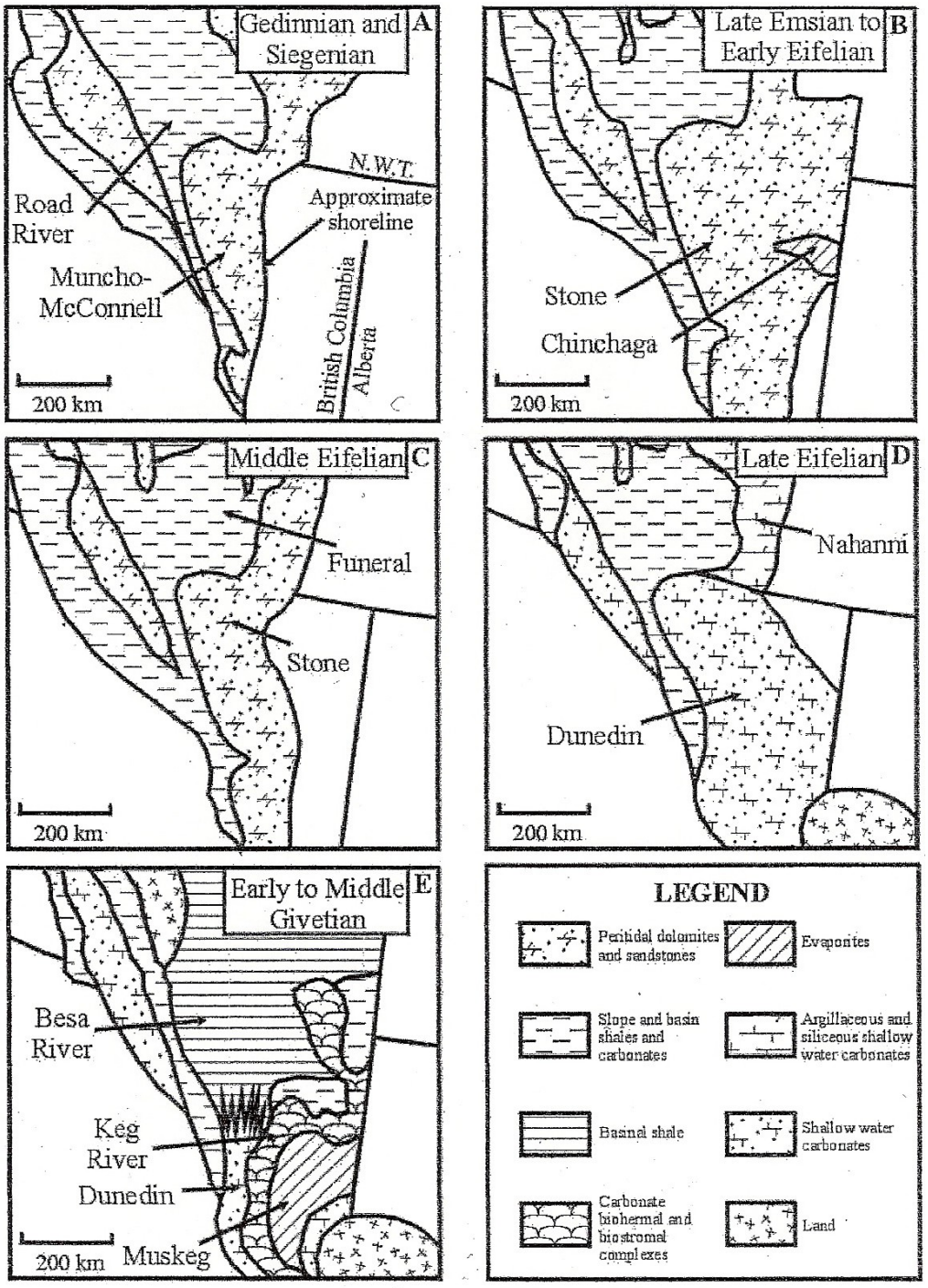

Figure 2.5: Depositional sequences and environments for the Stone and Dunedin formations (Morrow and Geldsetzer 1988).

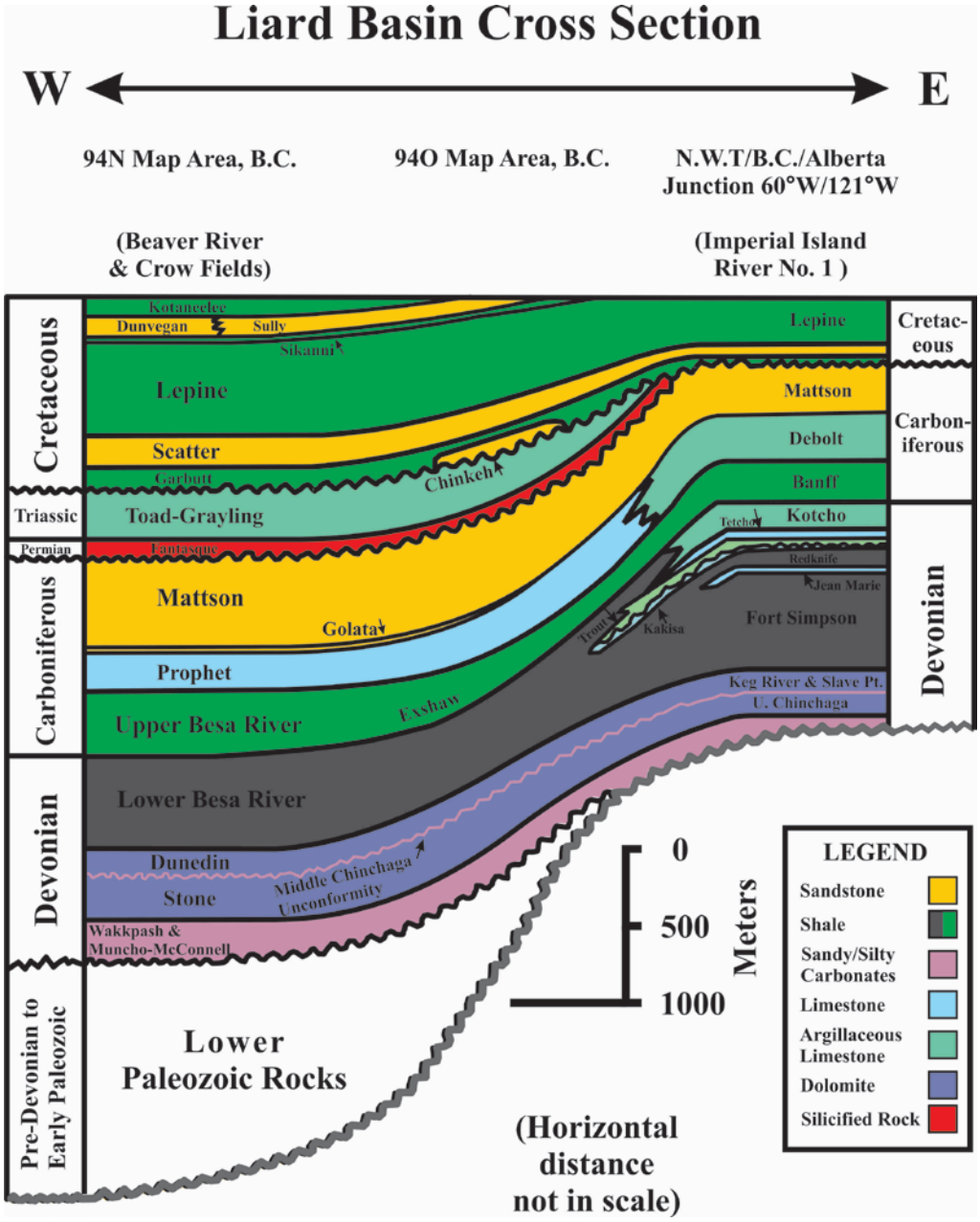

Figure 2.6: General stratigraphy of the Liard Basin from British Columbia/Alberta/ N.W.T junction in the east, to the 94N map area in the west. Modified from Morrow et al. (1993) and Morrow and Shinduke (2003). (original in color)

2.4.2 Local deformation pattern

A more detailed structural profile adjacent to the study area is shown in the interpreted seismic profile AAV-005 shot by Columbia Oil and Gas in 1978, achieved by the National Energy Board, and published in report by the Government of Yukon in 2001 (Fig. 2.7; refer to Fig 2.2 for the location of the seismic line), which demonstrates 3 stages of structural deformation (F1, F2 & F3). The first stage of structural folding (F1) is identified in the Devonian and Carboniferous strata where both strata were folded in the same fashion. The folded strata were further displaced along faults (F2). Structures of F1 and F2 were cut by a kilometer-scale thrust fault (F3), which the axis of F3 is roughly north-south oriented. F1 folding is interpreted to have occurred during the Late Carboniferous or after Carboniferous because both the Devonian and Early Carboniferous strata were folded in the same fashion. The timing of F2 and F3 are not clear. No interpretation was found in the report by National Energy Board (2001). The kilometer-scale thrust fault (F3) might be a sub-structure of the north-south trending Bovie fault.

2.5 Burial history and gas maturation

Vitrinite reflectances data of the Pan Am Beaver River YT G-01, Beaver River gas field was measured by Morrow et al. (1993) from well cuttings (Fig. 2.8; refer to Fig. 2.4 for the well location of Pan Am Beaver River YT G-01). The maximum burial depths of the

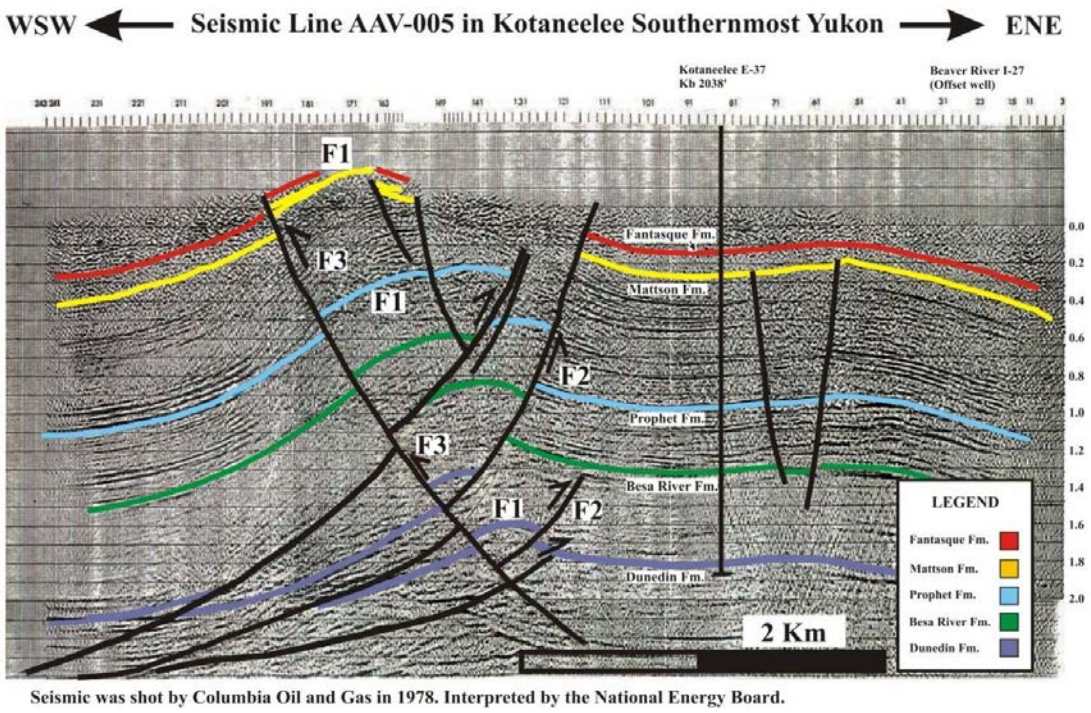

Figure 2.7: Seismic line AAV-005 showing the structural deformation history of the Devonian and Carboniferous strata underneath the Kotaneelee gas field, southernmost Yukon (immediate north of the study area of this project; see Fig. 2.4 for the location of seismic line across the Kotaneelee gas field). Both Devonian and Carboniferous strata were folded in the same fashion. This indicates that folding (F1) occurred after the deposition of the Carboniferous Mattson and Pantasque formations (MacLean and Morrow 2002). The folded blocks were further displaced (F2). A larger-scale thrusting (F3) created a kilometer-scale reverse fault which cuts the F1 folding and F2 faulting. This seismic profile was shot by Columbia Oil and Gas in 1978 (author not known), it was later compiled by the National Energy Board (2001) with other information, and published by the Government of Yukon, Oil and Gas Resources Branch in 2001. (original in color)

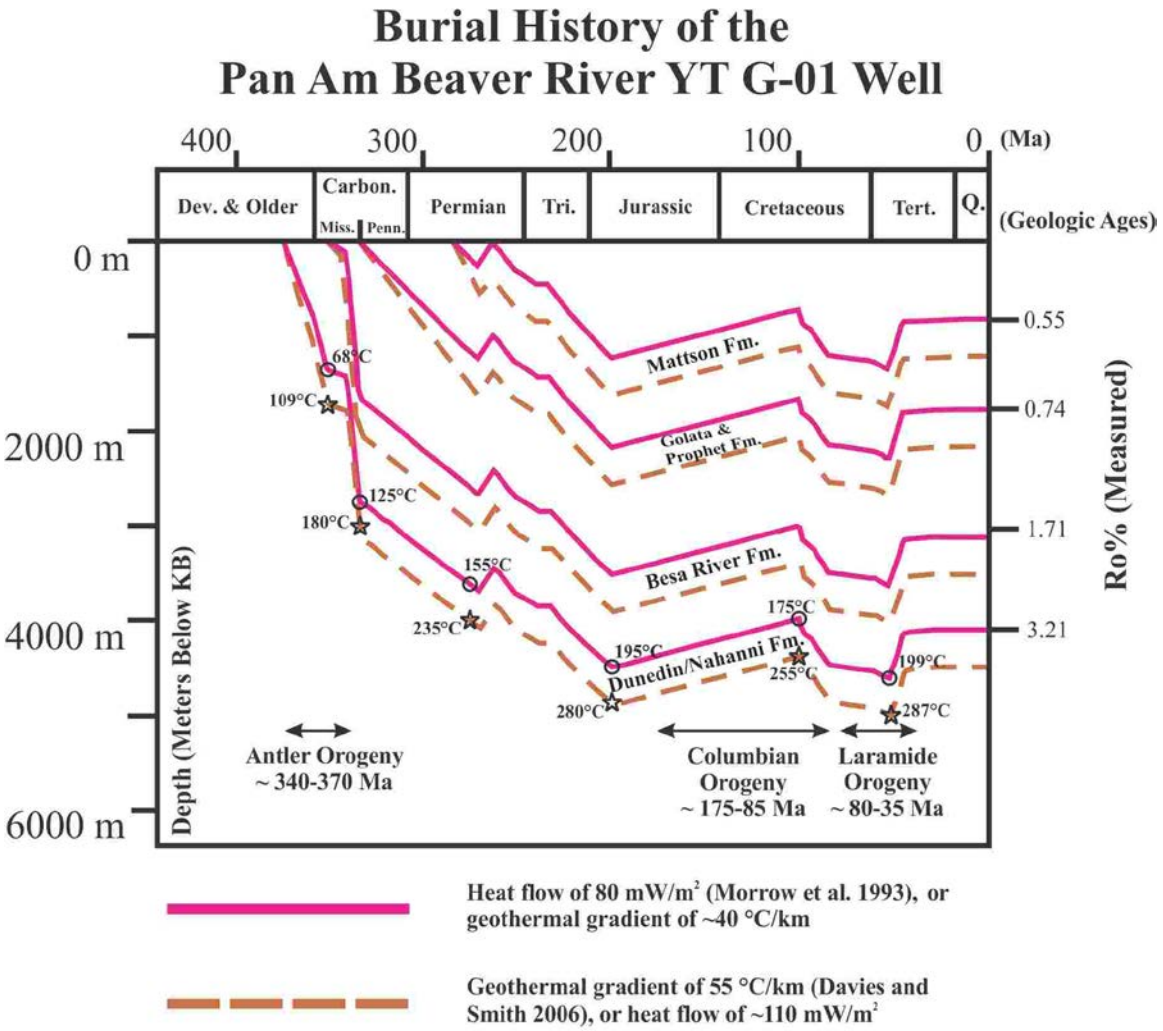

Figure 2.8: Burial history and organic maturation plot of the Pan Am Beaver River YT G-01 by Morrow et al. (1993; see Fig. 2.4 for the location of Pan Am Beaver River YT G-01), using the decompaction program of Osadetz and Mottershead (1992) based on vitrinite reflectances Ro% with EASY%Ro algorithm (Sweeney and Burnham 1990). The top of Devonian Dunedin/Nahanni Formation reached burial depth of 3500 m during Middle Permian. The corresponding geothermal temperature during Middle Permian is 155°C by calibrating the geothermal heat flow as 80 mW/m^2 (geothermal gradient of ~40 °C/km; Morrow et al. 1993), and 235°C by calibrating the geothermal gradient as 55 °C/km (heat flow of ~110 mW/m^2; Davies and Smith 2006). (original in color)

Devonian and Carboniferous formation tops through geological time were calculated by using the decompaction program of Osadetz and Mottershead (1992) based on vitrinite reflectances Ro% with EASY%Ro algorithm (Sweeney and Burnham 1990). The top of the Dunedin Formation and correlative Nahanni formation reached burial depth of 3500 m during Middle Permian. The corresponding geothermal temperature during Middle Permian is 155 °C by calibrating the geothermal heat flow as 80 mW/m^2 (geothermal gradient of ~40 °C/km; Morrow et al. 1993), and 235 °C by calibrating the geothermal gradient as 55 °C/km (heat flow of ~110 mW/m^2; Davies and Smith 2006).

Given that the Dunedin Formation and correlative Nahanni Formation are gas-bearing, and Middle Devonian marine shale is the possible source rock, peak gas-charge would have occurred during the Permian to Triassic (Morrow et al. 1993). If the source rock(s) were the younger Lower Devonian or early Paleozoic rocks in the Liard Basin, dry gas would have been generated before the Middle Permian. Morrow et al. (1993) suggested another possibility that the Stone and Dunedin formations were originally charged with oil, and oil cracked into gas during the Permian. However, no evidence of significant oil accumulation was found.

CHAPTER 3: Sedimentary Facies

3.1 Introduction

A facies is a body of rock defined by the association of sedimentary characteristics, such as lithology, texture, composition, sedimentary structures, fossil content and color (Tucker and Wright 1990). Primary lithofacies have a significant influence on the development of dolomite reservoirs. In geologic strata with good initial effective permeability and porosity, such as reefal buildups, fluid flow allows leaching of carbonate rocks and creates secondary porosity (Lonnee and Machel 2006).

Previous surface and subsurface sedimentologic studies by Nadjiwon (2001) identified eight facies in the Dunedin Formation in Northeast British Columbia. These include 1) dolomitic sandstone and siltstone, 2) mudstone and wackestone, 3) bioclastic wackestone and packstone, 4) bioclastic grainstone, 5) microbial mudstone and wackestone, 6) bioclastic floatstone, 7) bioclastic rudstone and bafflestone, and 8) amphiporid floatstone and rudstone.

In order to better document and interpret the sedimentologic attributes of the strata, and to correlate the sedimentologic and stratigraphic framework to the stratal dolomitization model, a comprehensive sedimentologic study were conducted. Twenty distinctive and representative depositional sedimentary facies were recognized from the cores recovered

in the study strata. Lithofacies occurrence, descriptions and interpreted depositional environments are described in this chapter.

Limestones are named by using the modified Dunham classification by Embry and Klovan (1971). The prefixes suggested by Embry and Klovan (1971) for describing the degree of dolomitization of limestone are outlined in Figure 3.1. Sedimentary bedding thickness measured from core photos are classified according to the classification by Demicco and Hardie (1994; Fig. 3.2). A summary of the lithofacies of the Stone and Dunedin formations is presented on Table 3.1 and Table 3.2. A stratigraphic cross-section of the studied 10 wells is presented in Figure 3.3. Figure numbers of core photos were marked on the cross-section.

3.2 Lithofacies of the Stone Formation

The Stone Formation is from ~ 200 to 290 m thick in the studied 10 wells. Cores of the Stone Formation were recovered from 6 of the 10 studied wells (Fig. 3.3). Seven distinctive and representative lithofacies have been recognized in 17 intervals from those 6 wells. These lithofacies include (i) mudstone to wackestone lithofacies (LF 1), (ii) laminated bioclastic packstone lithofacies (LF 2), (iii) bioclastic packstone to floatstone lithofacies (LF 3), (iv) coral-rich floatstone lithofacies (LF 4), (v) amphiporid floatstone lithofacies (LF 5), (vi) interbedded peloidal bioclastic packstone to grainstone lithofacies (LF 6), and (vii) clast-rich silty mudstone to silty mudstone lithofacies (LF 7). The petrographic and sedimentologic characteristics of these lithofacies, as well as

Dolomitization percentage/ dolomite percentage abundance	Prefix and modification of limestone names (names after Embry and Klovan 1971)
0 - 30 %	Limestone (e.g. mudstone)
31 - 60 %	Dolomitic Limestone (e.g. dolomitic mudstone)
61 - 90 %	Calcitic dolomite (e.g. calcitic dolomudstone)
91 - 100 %	Dolostone (e.g. dolomudstone)

Figure 3.1: Prefixes used for describing the dolomitized proportion of the limestones (dolomite mineralogical percentage abundance) in this study.

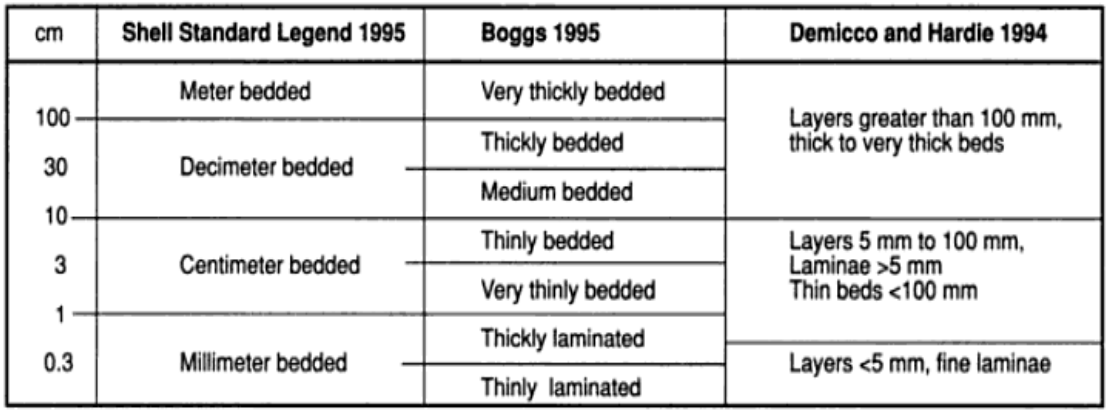

Figure 3.2: Bedding thickness classifications including Shell standard legend (1995), Boggs (1995), and Demicco and Hardie (1994). Classification from Demicco and Hardie (1994) is based on Paleozoic carbonate sedimentological studies and hence it is adapted in this study. Classification chart is from Flügel (2004).

Table 3.1: Summary of descriptions and interpreted depositional environments for the lithofacies in the Stone Formation

Lithofacies (Figure number)	Allochemical Components	Sedimentary Structures	Nature of Contact with Other Lithofacies	Interpreted Depositional Environments
Mudstone to wackestone lithofacies (LF 1) (Fig. 3.4A)	< 10 % bioclasts	Massive to faint laminated	- Overlain conformably by laminated bioclastic dolopackstone (LF 2) between 4036.9 and 4055 in c-54-K/94-N-16. - Overlain conformably by laminated bioclastic dolopackstone (LF 2) between 4040.0 and 4049.5 m in c-16-A/94-N-15.	Various - from peritidal to lagoonal
Laminated bioclastic packstone lithofacies (LF 2) (Figs. 3.4B & C)	~ 10 to 30 % bioclasts including peloids, ostracods and bivalves.	Fine laminated to thin bedded	- Conformably overlies dolomudstone to dolowackestone (LF 1) between 4036.9 and 4055 in c-54-K/94-N-16. - Conformably overlies dolomudstone to dolowackestone (LF 1) between 4040.0 and 4049.5 m in c-16-A/94-N-15.	Peritidal to restricted shallow marine
Bioclastic packstone to floatstone lithofacies (LF 3) (Figs. 3.4D & E)	~ 10 % marcofossil fragments; ~ 25 % peloids; ~ 20 % bioclasts; 2 pieces of bivalve fragment.	Massive to faint bedded	- Conformably interlayered with amphiporid dolofloatstone (LF 5) between 4007.8 and 4055.6 m in c-45-K/94-N-16. - Conformably interlayered with coral-rich dolofloatstone (LF 4) and overlain by amphiporid dolofloatstone (LF 5) between 4188.7 and 4206.6 m in b-19-K/94-N-16.	Lagoonal
Coral-rich floatstone lithofacies (LF 4) (Figs. 3.5A & B)	Up to 30 % ball-shaped colonial coral fragments; ~ 20 % bioclasts.	Massive	- Conformably interlayered with bioclastic dolopackstone to dolofloatstone (LF 3) and amphiporid dolofloatstone (LF 5) between 4188.7 and 4206.6 m in b-19-K/94-N-16.	Lagoonal

Table 3.1 (Continued): Summary of descriptions and interpreted depositional environments of lithofacies in the Stone Formation

Lithofacies (Figure number)	Allochemical Components	Sedimentary Structures	Nature of Contact with other lithofacies	Interpreted Depositional Environments
Amphiporid floatstone lithofacies (LF 5) (Figs. 3.5C & D)	~ 10 to up to 40 % amphiporids; up to 10 % macrofossil fragments; ~ 15 % bioclasts.	Massive to thick bedded	- Conformably interlayered with bioclastic dolopackstone to dolofloatstone (LF 3) between 4007.8 and 4055.6 m in c-45-K/94-N-16. - Overlies conformably over bioclastic dolopackstone to dolofloatstone (LF 3) and interlayered with coral-rich dolofloatstone (LF 4) between 4188.7 and 4206.6 m in b-19-K/94-N-16.	Lagoonal
Interbedded peloidal bioclastic packstone to grainstone lithofacies (LF 6) (Figs. 3.6A, B & C)	Packstone beds contain ~ 40 to 60 % peloids. Grainstone beds contain ~ 10 to 20 % peloids; > 70 % bioclasts.	Massive to faint thin bedded	- Conformably interlayered with crystalline dolomite in the 4 core intervals.	Peritidal to restricted shallow marine
Clast-rich silty mudstone to silty mudstone lithofacies (LF 7) (Figs. 3.7A, B & C)	~ 10 to 90 % sub-angular dolomudstone clasts.	Massive to faint bedded	- Overlain by silty to sandy mudstone (LF 8) in gradational to sharp contact at 1838.7 m in c-10-E/94-N-7. No evidence of subaerial exposure.	Peritidal

Table 3.2: Summary of descriptions and interpreted depositional environments of lithofacies in the Dunedin Formation

Lithofacies (Figure number)	Allochemical Components	Sedimentary Structures	Nature of Contact with other lithofacies	Interpreted Depositional Environments
Silty to sandy mudstone lithofacies (LF 8) (Figs. 3.7C; 3.8A)	~ 10 % silt and very fine quartz sand.	Massive	- Conformably overlies clast-rich silty dolomudstone to silty dolomudstone (LF 7) in gradational to sharp contact at 1838.7 m in c-10-E/94-N-7. No evidence of subaerial exposure.	Restricted shallow marine
Peloidal algal grainstone lithofacies (LF 9) (Figs. 3.8B, C & D)	~ 40 % peloids; ~ 10 % leaf-like phylloid algae and algal fragments; ~ 2 % gastropod.	Massive to fine laminated	- Conformably overlies and interlayered with silty to sandy mudstone to dolomitic mudstone (LF8) between ~ 1830 m and 1793 m in c-10-E/94-N-7. Silty charophytan calcitic dolowackestone to dolopackstone (LF 10) is also in the core interval.	lagoonal
Silty charophytan wackestone to packstone lithofacies (LF 10) (Figs. 3.9A & B)	~ 10 % charophyta oogonia and charophyta fragments; ~ 3 % ostracodes; ~ 1 % sub-rounded quartz silt.	Laminated to thin bedded	- Observed from 1 thin section made of a core chip collected in the lower Dunedin strata at 1802.3 m, where peloidal algal grainstone to dolomitic grainstone (LF 9) is the dominant lithofacies between ~ 1830 m and 1793 m in c-10-E/94-N-7. Silty to sandy mudstone to dolomitic mudstone (LF8) was also found in the same core interval.	Brackish water to peritidal
Echinoderm peloidal grainstone lithofacies (LF 11) (Figs. 3.10A, B & C)	~ 40 % echinoid plates; ~ 40 % peloids; ~ 10 % lime mud; ~ 4 % unidentified bioclasts; a piece of ~ 4 mm wide fragment of tubular coral and a very thin broken piece of trilobite? fragment in the studied sample.	Thin bedded to laminated	- Conformably interlayered with local unclassified dolopackstone and dolofloatstone to crystalline dolomite in all 3 studied core intervals.	Lagoonal

Table 3.2 (Continued): Summary of descriptions and interpreted depositional environments of lithofacies in the Dunedin Formation

Lithofacies (Figure number)	Allochemical Components	Sedimentary Structures	Nature of Contact with other lithofacies	Interpreted Depositional Environments
Amphiporid floatstone to rudstone lithofacies (LF 12) (Figs. 3.11A, B, C & D)	~ 15 % amphiporids less fossiliferous floatstone layers; locally > 65 % in more fossiliferous rudstone layers; Up to 10 % fragmented stromatoporoids scattered in both FSt & RSt layers.	Thin bedded	- Gradually changes to stromatoporoid bioclastic dolofloatstone (LF 13) in c-16-A/94-N-15.	Lagoon to back reef
Stromatoporoid bioclastic floatstone lithofacies (LF 13) (Figs. 3.12A & B)	~ 20 to 35 % irregular stromatoporoids; 10 % elongated amphiporids; up to 4 % delicated dendroid stromatoporoid Stachyodes sp.; up to 15 % rounded bioclasts	Massive to thick bedded	- Interbedded with crystalline dolomite in a-67-D /94-O-13. - Gradually changes from amphiporid floatstone to rudstone lithofacies (LF 12) in c-16-A/94-N-15.	Back reef to reef flat
Crinoidal packstone to grainstone lithofacies (LF 14) (Figs. 3.13A, B, C & D)	~ 50 % crinoid ossicles.	Massive to thick bedded	- Overlain by crystalline dolomite and interbedded with local thick beds of bioclastic dolofloatstone between 3934.8 and 3951.5 m in b-19-K/94-N-16.	Fore reef to fore slope

Table 3.2 (Continued): Summary of descriptions and interpreted depositional environments of lithofacies in the Dunedin Formation

Lithofacies (Figure number)	Allochemical Components	Sedimentary Structures	Nature of Contact with other lithofacies	Interpreted Depositional Environments
Bulbous stromatoporoid mudstone to floatstone lithofacies (LF 15) (Figs. 3.14A & B; 3.16)	~ 5 - 8 % bulbous stromatoporoid & stromatoporoid fragment in the less fossiliferous mudstone beds; ~ 15 to up to 40 % bulbous stromatoporoid & stromatoporoid fragment in the more fossiliferous floatstone beds; Up to 5 % dendroid stromatoporoid *Stachyodes* sp. was observed in both mudstone to floatstone beds.	Massive to thin bedded	- Overlain and interbedded with stromatoporoid dolobindstone (LF 17) between 3697.0 and 3715.3 m in c-54-K/94-N-16. - Interbedded with crystalline dolomite between 3617.8 and 3630.3 in c-54-K/94-N-16. - Interlayered with amphiporid dolobafflestone (LF 16), stromatoporoid dolobindstone (LF 17) and crystalline dolomite between 3808.2 and 3826.5 m in c-27-K/94-N-16.	Back reef to reef crest (and reef flank)
Amphiporid bafflestone lithofacies (LF 16) (Figs. 3.15; 3.16A & B)	> 50 % stromatoporoid *Amphipora*; ~ 5 to 20 % irregular stromatoporoid fragments	Thick bedded	- Interlayered with bulbous stromatoporoid dolomudstone to dolofloatstone (LF 15), stromatoporoid dolobindstone (LF 17) and crystalline dolomite between 3808.2 and 3826.5 m in c-27-K/94-N-16.	Back reef to reef crest (and reef flank)

Table 3.2 (Continued): Summary of descriptions and interpreted depositional environments of lithofacies in the Dunedin Formation

Lithofacies (Figure number)	Allochemical Components	Sedimentary Structures	Nature of Contact with other lithofacies	Interpreted Depositional Environments
Stromatoporoid bindstone lithofacies (LF 17) (Figs. 3.17A, B & C)	Platy to encrusting stromatoporoids from 3 ~ 6 cm thick and over 10 cm wide. Abundance cannot be accurately and precisely estimated.	Massive to thick bedded	- Overlies and interlayered with bulbous stromatoporoid dolomudstone to dolofloatstone (LF 15) between 3697.0 and 3715.3 m in c-54-K/94-N-16. - Interlayered with crystalline dolomite between 3527.0 and 3554.4 m in c-54-K/94-N-16. - Interlayered with bulbous stromatoporoid dolomudstone to dolofloatstone (LF 15), amphiporid dolobafflestone (LF 16) and crystalline dolomite between 3808.2 and 3826.5 m in c-27-K/94-N-16.	Back reef to reef crest (and reef flank)
Domal stromatoporoid framestone lithofacies (LF 18) (Figs. 3.18A & B; 3.19A)	Abundance of domal stromatoporoid cannot be accurately and precisely estimated. The matrix consists of ~ 98 % lime mud and ~ 2 % peloids.	Massive	- Interlayered with brachiopod packstone (LF 20) and crystalline dolomite between 2647.1 and 2662.3 m in b-21-G/94-O-6. - Overlain by clast-rich crystalline rock (LF 19) between 3650.0 and 3666.8 m in c-16-A/94-N-15.	Fore slope to slope
Clast-rich crystalline rock lithofacies (LF 19) (Figs. 3.19B & C)	~ 50 % to up to 80 % very poorly sorted bioclastic packstone clasts	Massive to thick bedded	- Overlain by the Besa River Formation between 3650.0 and 3666.8 m in c-16-A/94-N-15.	Fore slope to slope
Brachiopod packstone lithofacies (LF 20) (Figs. 3.20A & B)	~ 10 to up to 30 % fragments of robust brachiopod *Stringocephalus sp.*; up to 10% peloids	Massive	- Abrupt contact with the overlying Besa River Shale. - Comprises the uppermost ~ 4 m of the 26.9 m recovered cored interval between 3527.0 and 3554.4 m in c-54-K/94-N-16. Overlies ~ 1.5 m of poorly recovered stromatoporoid dolobindstone (LF 17). - Occurs as two local thick beds (~ 15 to 25 cm) in the uppermost 6 m of 16.8 m between 3650.0 and 3666.8 m, c-16-A/94-N-15.	Fore reef to fore slope

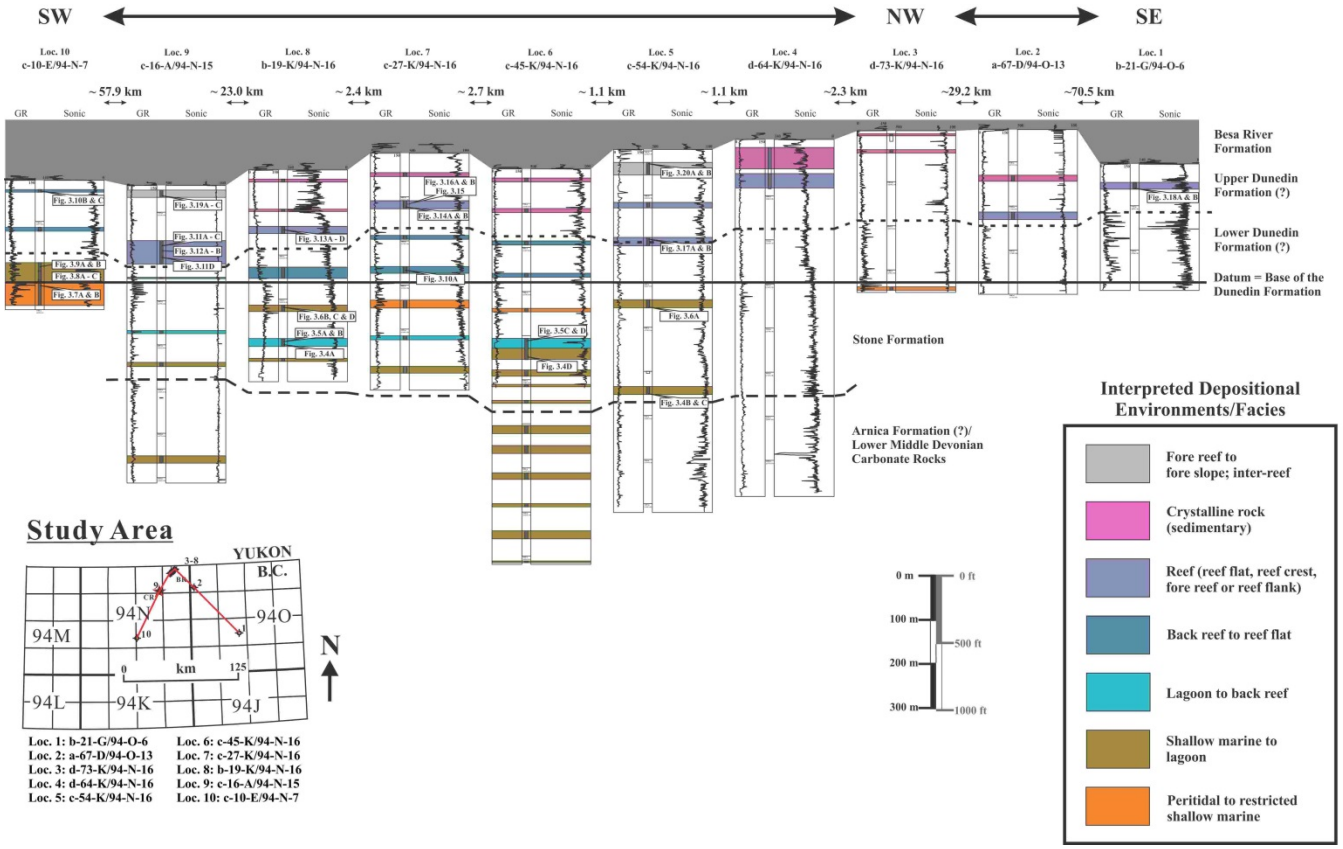

Figure 3.3: Stratigraphic cross-section of the Stone and Dunedin formations (including Lower Middle Devonian Arnica Formation?) constructed with gamma ray and sonic logs of the studied 10 wells. The base of the Dunedin Formation is used as the datum. Core and petrographic photos of different lithofacies are shown in figures from Fig 3.4 to Fig. 3.20. Figure numbers are marked next to the well logs. The distances (km) between the wells are marked between well logs. The horizontal scale is not in proportion. (original in color)

the interpretation of their depositional environments are given below.

Mudstone to wackestone lithofacies (LF 1)

Occurrence: mudstone to wackestone lithofacies (LF 1) was observed in 5 intervals of the Stone Formation between ~ 140 and 250 m below the Dunedin Formation in 4 wells (c-54-K/94-N-16, c-45-K/94-N-16, b-19-K/94-N-16 and c-16-A/94-N-15). All core samples of mudstone to wackestone lithofacies (LF 1) were found ~100 % dolomitized. Dolomudstone to dolowackestone (LF 1) comprises the lower ~3.6 m litho-unit of the 18.2 m core interval between 4036.9 and 4055 in c-54-K/94-N-16, where it is overlain conformably by laminated bioclastic dolopackstone (LF 2). In c-45-K/94-N-16, it comprises ~5 m of the 5.5 m recovered core between 4145.3 and 4150.8 m, and comprises ~2 m of the 2.2 m recovered core between 4111.8 and 4114.0 m. It comprises ~ 6 m of the 6.0 m recovered core from between 4233.5 and 4240.5 m in b-19-K/94-N-16. It comprises the lower ~ 5.5 m of the 9.5 m recovered core between 4040.0 and 4049.5 m in c-16-A/94-N-15, where it is overlain conformably by laminated bioclastic dolopackstone (LF 2).

Description: dolomudstone to dolowackestone (LF 1) is medium grey, massive to faint laminated with less than 10% bioclasts (Fig. 3.4A). Bioclasts were not observed in most of the core samples, polished core slabs and thin sections. No sedimentologic attribute was preserved due to fabric-destructive dolomitization.

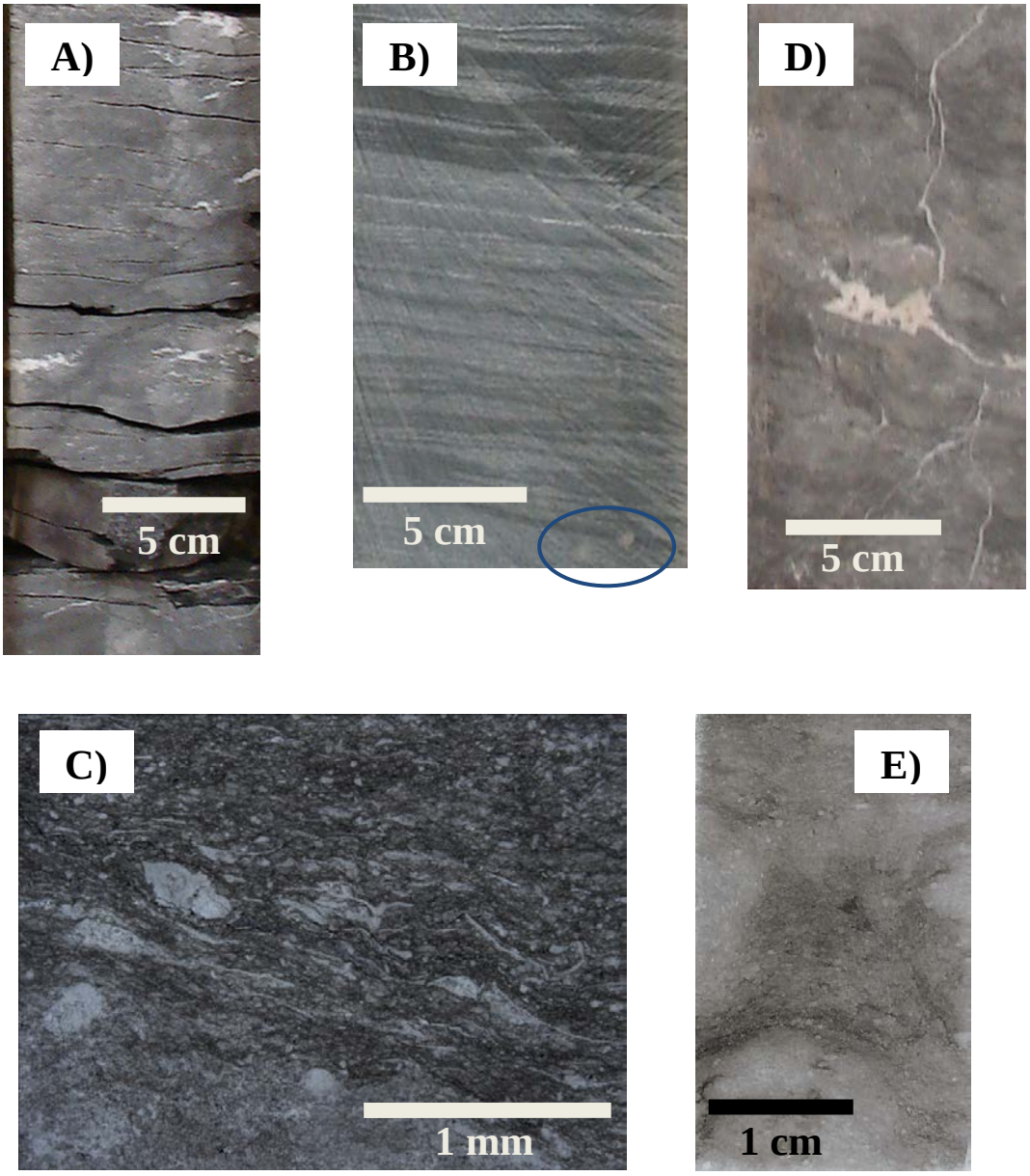

Figure 3.4A – E: Facies of the Stone Formation. A) Core photo of dolomudstone to dolowackestone. b-19-K/94-N-16, 4203.7 – 4203.9 m. B) Core photo of laminated bioclastic dolopackstone. Poorly preserved bioturbation possibly *Planolites* (circled) is rare to uncommon and is low in intensity. c-54-K/94-N-16, 4050.6 – 4050.8 m. The sub-vertical striations are resulted from core cutting. C) Thin section photomicrograph prepared from the sample in Fig. 3.4B. The dark-colored and light-colored dolomitic and limestone laminae in the photo correlates to the dark grey and medium grey laminae on core slab, respectively. D) Core photo of bioclastic dolopackstone to dolofloatstone. c-45-K/94-N-16, 4040.2 – 4040.4 m. E) Scanned image of a thin section made from the core slab in Fig. 3.4D. (original in color)

Interpretation: mudstone to wackestone lithofacies (LF 1) is one of the building blocks of the Stone Formation. It is widely observed between the lower ~ 100 to 200 m interval of the Stone Formation. It is summarized that the mudstone to wackestone lithofacies (LF 1) could have been deposited in a variety of shallow marine settings from peritidal to lagoonal facies. No other sedimentologic structure was found to sustain further interpretation.

Laminated bioclastic packstone lithofacies (LF 2)

Occurrence: laminated bioclastic packstone lithofacies (LF 2) was observed in 5 intervals of the Stone Formation between ~ 170 and 260 m below the Dunedin Formation in 4 wells (c-54-K/94-N-16, c-45-K/94-N-16, c-27-K/94-N-16 and c-16-A/94-N-15). All core samples of laminated bioclastic packstone lithofacies (LF 2) were found ~ 100 % dolomitized. The most representative cores of laminated bioclastic dolopackstone (LF 2) were recovered between 4036.9 and 4055.1 m in c-54-K/94-N-16, where it comprises ~14.6 m of the 18.2 m thick recovered core interval and overlies conformably over dolomudstone to dolowackestone (LF 1). It comprises ~ 13 m of the 14.5 m recovered core between 4078.6 and 4093.2 m in c-45-K/94-N-16, interlayered with crystalline dolomite. It is the dominant unit between 4184.4 and 4202.8 m in c-27-K/94-N-16 where it comprises ~ 16 m of the 18.4 m recovered core, with ~ 2 m of crystalline dolomite. It comprises the ~ 7 m of the 8.8 m recovered core between 4114.6 and 4123.4 m in c-27-K/94-N-16. It comprises ~ 4 m of the 9.5 m recovered core between 4040.5 and 4049.5 in c-16-A/94-N-15 and overlies conformably over

dolomudstone to dolowackestone (LF 1).

Description: laminated bioclastic dolopackstone (LF 2) is characterized by the mm-scale to cm-scale fine laminae to thin beds that resemble flaser to lenticular bedding structure (Fig. 3.4B). The bioclastic dolopackstone portion is light to medium grey and the laminae are medium to dark grey. The color variation appears related to the original abundance of lime mud in the matrix as well as the degree of dolomitization (Fig 3.4C). Horizontal burrows (*Planolites?*) were observed but rare. Intensity and diversity of bioturbation are both low in this lithofacies. Poorly preserved soft sediment deformation structure was observed in 2 thick beds in the core recovered between 4184.4 and 4202.8 m in c-27-K/ 94-N-16. The dolomitized packstone beds contain abundant framework grains including ~ 10 to 30 % bioclasts including peloids, ostracods and bivalves that are less than 0.05 mm in diameter with lime mud in the matrix (Fig. 3.4C). The matrix is dense and grain-to-grain contacts appear compacted. Other petrographic fabric was not preserved from fabric-destructive dolomitization.

Interpretation: the mm-scale to cm-scale flaser to lenticular bedding structure has been interpreted to represent fluctuation of hydraulic energy with strong tidal influence (Reineck and Wunderlich 1968). The flaser to lenticular bedding structure observed in this lithofacies, with low diversity of allochemical component, indicate that this lithofacies was deposited in peritidal to restricted shallow marine settings (Pratt et al. 1992; Jones and Desrochers 1992).

Bioclastic packstone to floatstone lithofacies (LF 3)

Occurrence: bioclastic packstone to floatstone lithofacies (LF 3) was observed in 2 intervals in the Stone Formation between ~ 125 and 175 m below the Dunedin Formation in 2 wells (c-45-K/94-N-16 and b-19-K/94-N-16). All core samples of bioclastic packstone to floatstone lithofacies (LF 3) were found ~ 100 % dolomitized. Approximately 47.8 m of core was recovered between 4007.8 and 4055.6 m in c-45-K/94-N-16. The upper ~ 15 m is dominantly crystalline calcite; the lower ~ 32 m consists of ~ 15 m of bioclastic dolopackstone to dolofloatstone (LF 3), ~ 3 m of amphiporid dolofloatstone (LF 5), and ~14 m of crystalline calcite and crystalline dolomite. Bioclastic dolopackstone to dolofloatstone (LF 3) comprises the lower ~ 9 m of the 17.9 m recovered core between 4188.7 and 4206.6 m in b-19-K/94-N-16, where it is interlayered with coral-rich dolofloatstone (LF 4) and overlain by amphiporid dolofloatstone (LF 5).

Description: bioclastic dolopackstone to dolofloatstone (LF 3) is medium grey and massive to faint bedded (Fig. 3.4D). Framework grains consist of ~ 10 % dolomitized unidentified marcofossil fragments that are ~ 2 mm in diameter (Fig. 3.4E), with ~ 25 % peloids, ~ 20 % bioclasts, ~ 45 % lime mud, and 2 pieces of bivalve fragment. All allochemical components are smaller than 0.1 mm in diameter. The matrix is dense and grain-to-grain contacts appear compacted. Other petrographic fabric was not preserved from fabric-destructive dolomitization.

Interpretation: bioclastic dolopackstone to dolofloatstone (LF 3) with abundant allochemical components and massive structure are common characteristics of carbonate rock in tropical carbonate platform settings. Fabric-destructive dolomitization hinders further analysis. Bioclastic dolopackstone to dolofloatstone is conformably interlayered with coral-rich dolofloatstone (LF 4) and overlain conformably by amphiporid dolofloatstone (LF 5) between 4188.7 and 4206.6 m in b-19-K 94-N-16, which amphiporid floatstone lithofacies (LF 5) is representative of lagoonal facies in the study strata. Bioclastic packstone to floatstone lithofacies (LF 3) is interpreted to have deposited in peritidal to restricted shallow marine and lagoonal environments (Pratt et al. 1992; Jones and Desrochers 1992).

Coral-rich floatstone lithofacies (LF 4)

Occurrence: coral-rich floatstone lithofacies (LF 4) was observed in 1 interval in the Stone Formation between ~ 140 and 160 m below the Dunedin in b-19-K/94-N-16. All core samples of coral-rich floatstone lithofacies (LF 4) were found ~ 100 % dolomitized. Coral-rich dolofloatstone (LF 4) comprises the upper 9 m of the 17.9 m recovered core between 4188.7 and 4206.6 m in b-19-K/94-N-16. It is conformably interlayered with bioclastic dolopackstone to dolofloatstone (LF 3) and amphiporid dolofloatstone (LF 5).

Description: coral-rich dolofloatstone (LF 4) is medium grey and massive (Fig. 3.5A). Macrofossil fragments include up to 30 % ball-shaped colonial coral fragments from 5 to 15 mm in diameter (*Syringopora* sp.? / *Acropora* sp.?). The matrix consists of ~ 50 %

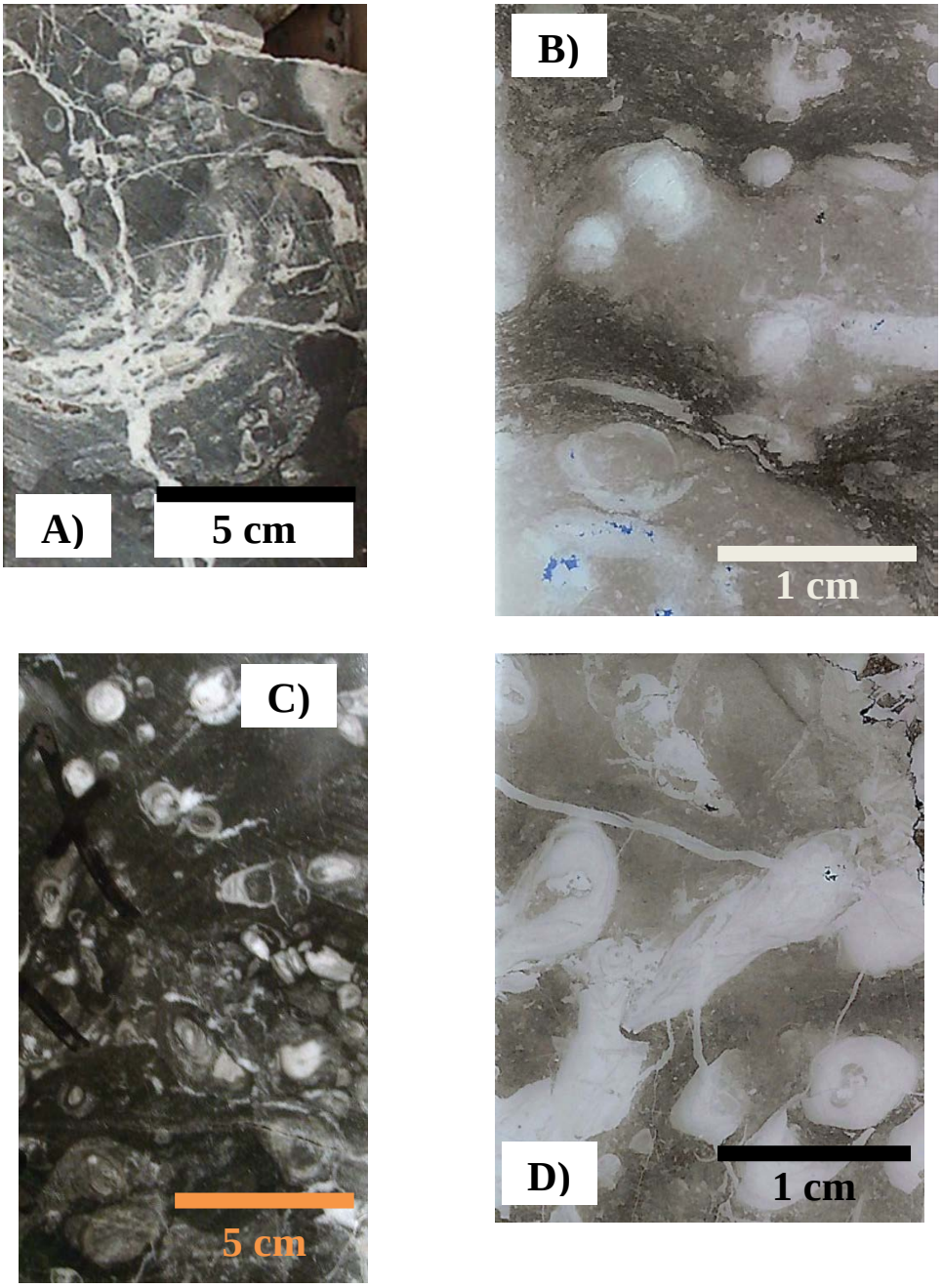

Figure 3.5A – D: Facies of the Stone Formation. A) Core photo of bioclastic coral fragment dolofloatstone. b-19-K/94-N-16, 4191.8 – 4192.0 m. B) Scanned image of a thin section prepared from the sample in Fig. 3.5A. C) Core photo of amphiporid dolofloatstone. c-45-K/94-N-16, 4038.2 – 4038.4 m. D) Scanned image of a thin section prepared from the sample in Fig. 3.5C. (original in color)

lime mud and ~ 20 % bioclasts including algal fragment, peloids and bivalve fragments from 0.1 to 2 mm in diameter (Fig. 3.5B). The matrix is dense and grain-to-grain contacts appear compacted. The petrographic fabric was not preserved due to dolomitization.

Interpretation: delicate, ball-shaped colonial corals (*Syringopora* sp.?/*Acropora* sp.?) have been interpreted to have developed in lagoonal environment (Vopni and Lerbekmo 1972; Stearn 1982). Fragments of colonial corals in this study were found in coral-rich floatstone lithofacies (LF 4) with peloids and bivalves in massive to thick bedded sedimentary structure. These indicate that coral-rich floatstone lithofacies (LF 4) could have been deposited in lagoonal settings.

Amphiporid floatstone lithofacies (LF 5)

Occurrence: amphiporid floatstone lithofacies (LF 5) was observed in 2 intervals in the Stone Formation between ~ 100 to 150 m below the Dunedin Formation in 2 wells (c-45-K/94-N-16 and b-19-K/94-N-16). All core samples of amphiporid floatstone lithofacies (LF 5) were found ~ 100 % dolomitized. Amphiporid dolofloatstone (LF 5) comprises ~ 3 m of litho-unit in the lower half of cored interval between 4007.8 and 4055.6 m in c-45-K/94-N-16, with ~ 15 m of bioclastic dolopackstone to dolofloatstone (LF 3) and ~14 m of crystalline calcite and crystalline dolomite. It comprises ~ 8 m of the upper interval of the 17.9 m recovered core between 4188.7 and 4206.6 m in b-19-K/94-N-16 overlying bioclastic dolopackstone to dolofloatstone (LF 3) and

interlayered with coral-rich dolofloatstone (LF 4).

Description: amphiporid dolofloatstone (LF 5) is medium grey and massive to thick bedded. It is defined by alternating amphiporid-rich (up to 40 %) and amphiporid-poor (~ 10 %) layers (Fig. 3.5C). The amphiporids are not in growth positions but rather scattered throughout the unit. Up to 10 % irregular stromatoporoid fragments are also present in the unit. The matrix contains ~ 15 % bioclasts that are from ~ 0.1 to 0.4 mm in diameter and ~ 30 to 70 % lime mud (Fig. 3.5D). The original texture has not been preserved from fabric-destructive dolomitization. Grain to grain contact appears very compacted (Fig. 3.5D).

Interpretation: amphiporids are abundant but do not appear to be in their growth positions as interpreted by Hladil (2007). They were found with irregular stromatoporoid fragments that are ~ 1 to 2 cm in diameter. The depositional environment is interpreted to be lagoonal to back reef settings where amphiporids and irregular stromatoporoid fragments are the dominant allochemical components, based on the quantitative paleontological study by Kobluk (1975) on Devonian reefal carbonate strata in Western Canada.

Interbedded peloidal bioclastic packstone to grainstone lithofacies (LF 6)

Occurrence: interbedded peloidal bioclastic packstone to grainstone lithofacies (LF 6) was observed in 4 intervals of the Stone Formation between ~ 40 to 100 m below the

Dunedin Formation in 4 wells (c-54-K/94-N-16, c-45-K/94-N-16, c-27-K/94-N-16 and b-19-K/94-N-16). All core samples of interbedded peloidal bioclastic packstone to grainstone lithofacies (LF 6) were found ~ 100 % dolomitized. Interbedded peloidal bioclastic dolopackstone to dolograinstone (LF 6) comprises ~ 14 m of the 18.2 m recovered core between 3837.2 and 3855.5 m in c-54-K/94-N-16. It comprises ~ 5 m of the 7.9 m recovered core between 3937.8 and 3945.7 m in c-45-K/94-N-16. It comprises ~ 6 m of the 18.2 m recovered core between 4033.5 and 4051.8 m in c-27-K/94-N-16. It comprises ~ 10 m of the 14.6 m recovered core between 4113.1 and 4127.7 m in b-19-K/94-N-16. In all 4 cored intervals, interbedded peloidal bioclastic dolopackstone to dolograinstone (LF 6) is interlayered with crystalline dolomite.

Description: the matrix of interbedded peloidal bioclastic dolopackstone to dolograinstone (LF 6) is medium grey and the dolomitized bioclasts appear ivory white in color (Figs. 3.6A and B). It is massive to faint thin bedded from ~ 2 to 10 mm thick and shows alternating peloid-rich packstone to grainstone beds and bioclast-rich grainstone beds (Fig. 3.6C). Petrographic studies observed that the packstone beds contain ~ 40 to 60 % peloids that are less than 0.4 mm in diameter and appear matrix to grain supported (Fig 3.6D). The bioclast-rich grainstone beds contain ~ 10 to 20 % peloids that are less than 0.4 mm in diameter, and over 70 % bioclasts from 2 to 10 mm in diameter. Grain-to-grain contact is compacted and dense. The gamma ray logs response of this facies is characterized by a left shift in API reading to approximately 30 to 60 API in the upper ~ 50 m of the Stone Formation, which can be used to differentiate interbedded peloidal bioclastic dolopackstone to dolograinstone (LF 6) from clast-rich

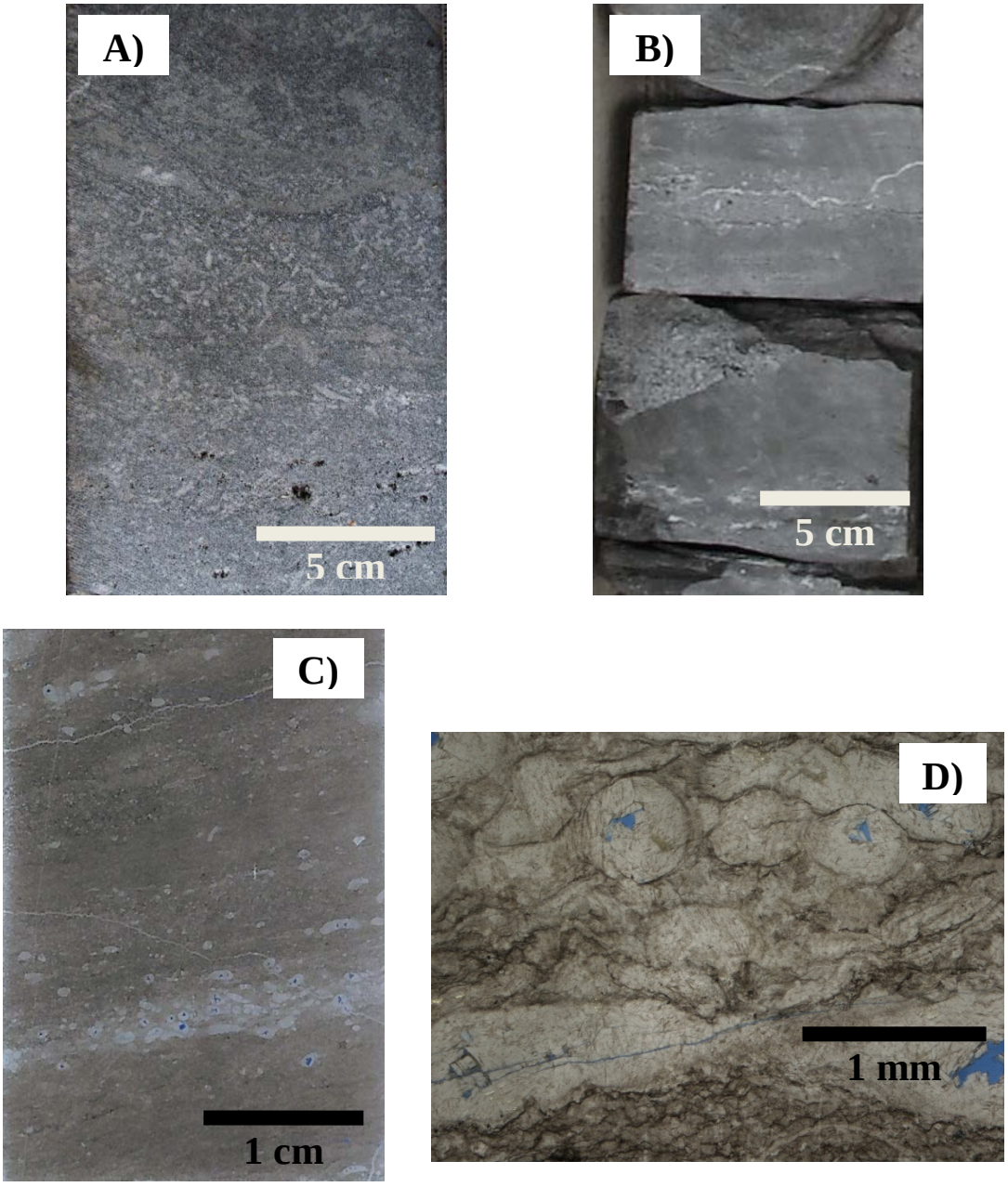

Figure 3.6A – D: Facies of the Stone Formation. A) Peloidal bioclastic dolopackstone. c-54-K/94-N-16, 3855.2 – 3855.3 m. B) Interbedded bivalve ostracod dolowackestone and dolopackstone with peloids and fragments of bivalve and ostracod. b-19-K/94-N-16, 4117.1 – 4117.3 m. C) Scanned image of a thin section of interbedded peloidal bioclastic dolopackstone to dolograinstone sampled at b-19-K/94-N-16, 4116.6 m. D) Representative photomicrograph of the thin section in Fig. 3.6C showing alternating dolopackstone and dolograinstone interbeds. Photomicrograph was taken by using the white card method. (original in color)

silty dolomudstone to silty dolomudstone (LF 7) in the upper ~ 0 to 60 m of the Stone Formation.

Interpretation: the thin planar bedding structure and abundance of peloids and ostracods may suggest that this lithofacies was deposited in a variety of peritidal to restricted shallow marine settings (Pratt et al. 1992; Jones and Desrochers 1992; Nadjiwon 2001). The absence of mudstone clast can be related to the distal depositional environment farther from the shore, or a lack of terrestrial sediment supply. No other distinctive petrological and sedimentologic features were observed and no further interpretation can be made.

Clast-rich silty mudstone to silty mudstone lithofacies (LF 7)

Occurrence: clast-rich silty mudstone to silty mudstone lithofacies (LF 7) was observed in 4 intervals of the Stone Formation between 0 and ~ 80 m immediately beneath the Dunedin Formation in 4 wells (d-73-K/94-N-16, c-45-K/94-N-16, c-27-K/94-N-16 and c-10-E/94-N-7). All core samples of clast-rich silty mudstone to silty mudstone lithofacies (LF 7) were found ~ 100 % dolomitized. Clast-rich silty dolomudstone is classified as containing ~ 50 % to up to 70 % dolomudstone clasts and ~ 30 % to 50 % dolomitized lime mud; silty dolomudstone is classified as containing ~ 10 % to up to 49 % dolomudstone clasts and ~ 51 % to 90 % dolomitized lime mud. Clast-rich silty dolomudstone to silty dolomudstone (LF 7) is overlain by the silty to sandy dolomitic mudstone (LF 8) of the lowermost Dunedin Formation at 1838.7 m in c-10-E/94-N-7,

which is the only observed direct contact between the Stone and Dunedin formations. This contact exhibits gradational to sharp lithologic and facies change but has no evidence of subaerial exposure. In c-27-K/94-N-16, clast-rich silty dolomudstone to silty dolomudstone (LF 7) occurs as ~ 2 m of poorly preserved clast-rich silty dolomudstone, and ~16 m of silty dolomudstone in the 18.2 m thick recovered cored interval between 4033.5 and 4051.8 m. Clast-rich silty dolomudstone to silty dolomudstone is the dominant lithofacies and best preserved in c-10-E/94-N-7 between 1838.7 and 1890.1 m. Clast-rich silty dolomudstone to silty dolomudstone (LF 7) occurs from silty dolomudstone in the lower ~ 20 m of the interval (between ~ 1870 and 1890 m), to clast-rich silty dolomudstone in the upper ~ 20 m of the interval (between 1838.7 to 1860 m).

Description: clast-rich silty dolomudstone to silty dolomudstone (LF 7) is grey to varied color and massive (Fig. 3.7A). No allochemical components and sedimentary structures were observed in the cores of clast-rich silty dolomudstone to silty dolomudstone (LF 7). No evidence of subaerial exposure was observed. Petrographic studies have identified the clasts as subangular dolomudstone clasts from 5 to 50 mm wide (Fig. 3.7B). The matrix of clast-rich silty dolomudstone to silty dolomudstone (LF 7) is mud-supported as observed in all 3 cored intervals, with up to 2 % quartz silt observed in 2 thin sections of clast-rich silty dolomudstone. Grain-to-grain contacts between clasts have not been observed. The log response of this facies is characterized by a major right shift by 40 API on a 0-150 API gamma log. Clast content decreases rapidly towards the Stone and Dunedin contact at1838.7 m in c-10-E 94-N-7 (Figs. 3.7A & C).

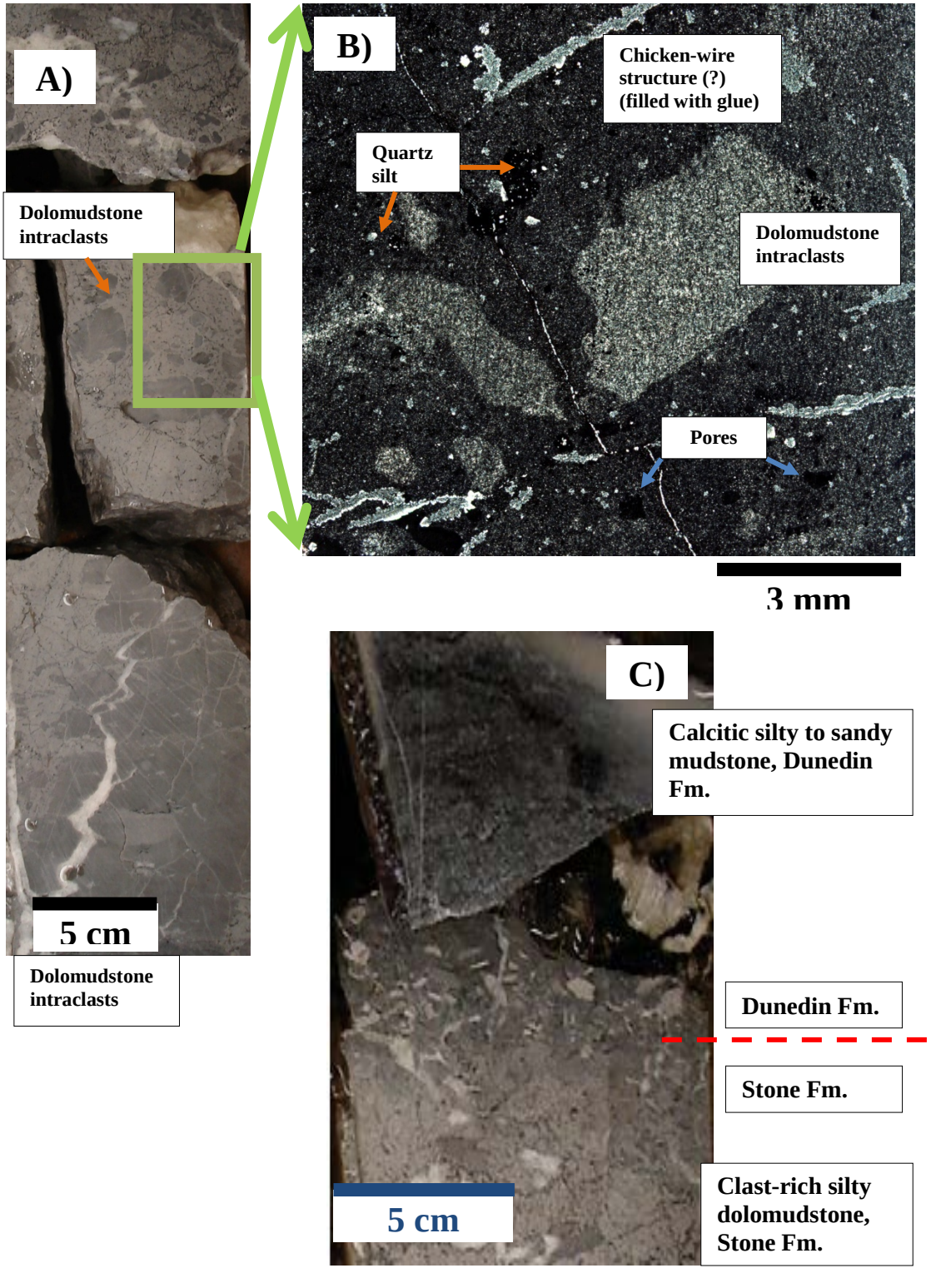
A)
Dolomudstone intraclasts
5 cm
Dolomudstone intraclasts
B)
Chicken-wire structure (?) (filled with glue)
Quartz silt
Dolomudstone intraclasts
Pores
3 mm
C)
Calcitic silty to sandy mudstone, Dunedin Fm.
Dunedin Fm.
Stone Fm.
Clast-rich silty dolomudstone, Stone Fm.
5 cm

Figure 3.7A – C: Facies of the Stone Formation. A) Core photo of clast-rich silty dolomudstone to silty dolomudstone. Photo of the recovered core slabs from the Stone Formation approximately 0.1 to 0.2 m below the Dunedin Formation. c-10-E/94-N-7, 1838.8 – 1839.0 m. Sub-rounded to sub-angular dolomitized limestone intraclasts are 5 to 50 mm wide. Shale extraclasts that are found in petrographic investigation cannot be clearly differentiated from limestone clasts in core slabs. The white coarsely crystalline cement is coarsely to very coarsely crystalline blocky calcite in a fracture. B) XPL petrographic microphotography of Fig. 3.7A at 1838.9 m. Dolomudstone clasts underwent greater degree of fabric-destructive dolomitization and resembles crystalline dolomite. The clasts are from 5 to 50 mm, sub-rounded to sub-angular. The dolomite texture of the dolomudstone clasts resembles finely crystalline dolomite, which is different from the dolomitized micritic texture in the matrix. Silt-size particles (quartz) are ~ 0.05 mm and sub-angular (orange arrows). The sub-horizontal striations appear to be chicken-wire structure that is filled with glue from thin section preparation. The sample was returned and thin section was prepared again; the quality was not improved. The sub-vertical fracture is likely to be resulted from sample preparation. Microphotography was taken by using the white card method outlined by Folk (1987). C) The contact between the Stone Formation and Dunedin Formation. Clast-rich silty dolomudstone of the Stone Formation (the lower core slab) and calcitic silty to sandy mudstone of the Dunedin Formation (the upper core slab) at c-10-E/94-N-7, 1838.6 – 1838.7 m. (original in color)

Interpretation: the dolomite crystals of the dolomudstone clasts are subhedral and 5 to 10 times bigger than the anhedral dolomite crystals in the matrix of the clast-rich silty dolomudstone to silty dolomudstone (LF 7). The sub-angular shape of these clasts indicate short distance of mechanical transportation. No evidence of subaerial exposure (e.g. caliche, desiccation cracks) was observed. However, quartz silt indicates terrestrial input. The absence of allochemical components suggest this lithofacies was possibly periodically exposed. The dolomudstone intraclasts indicate coastal reworking in a sediment-starved environment. Clast-rich silty mudstone to silty mudstone lithofacies (LF 7) has not been described and interpreted in detail in previous studies. The original observation in this study led to the interpretation that this facies was deposited in peritidal settings. The presence of quartz silt and absence of allochemical components

are interpreted to be influenced by a sea level drop caused by the middle Eifelian regression (Morrow 1978). The dolomudstone intraclasts indicate coastal reworking which is interpreted to have occurred during a depositional break.

3.3 Lithofacies of the Dunedin Formation

The Dunedin Formation is from ~ 210 to 330 m thick in the 10 studied wells. It can be informally divided into the ~ 40 to 160 m thick lower Dunedin Formation and the ~ 100 to 200 m thick upper Dunedin Formation for description purpose, based on the original lithofacies analysis in this study, aided by the gamma ray logs. Sixteen distinctive and representative lithofacies have been recognized in 29 cored intervals from the 10 wells that reached and cored parts of the Stone Formation.

These lithofacies include: (viii) silty to sandy mudstone (LF 8), (ix) peloidal algal grainstone (LF 9), (x) silty charophytan wackestone to packstone (LF 10), (xi) echinoderm peloidal grainstone (LF 11), (xii) amphiporid floatstone to rudstone (LF 12), (xiii) stromatoporoid bioclastic floatstone (LF 13), (xiv) crinoidal packstone to grainstone (LF 14), (xv) bulbous stromatoporoid mudstone to floatstone (LF 15), (xvi) amphiporid bafflestone (LF 16), (xvii) stromatoporoid bindstone (LF 17), (xviii) domal stromatoporoid framestone (LF 18), (xix) clast-rich crystalline rock (LF 19) and (xx) brachiopod packstone (LF 20). The term crystalline dolomite is used to described litho-units that appear crystalline, which the allochemical components and petrological features can no longer be identified due to fabric-destructive dolomitization.

Silty to sandy mudstone lithofacies (LF 8)

Occurrence: silty to sandy mudstone lithofacies (LF 8) was observed in 1 core interval in the lowest Dunedin Formation between ~ 1823 and 1835 m in c-10-E/94N7, where it comprises the lowest ~8 m interval of the Dunedin Formation immediately above the Stone Formation. The cored samples of silty to sandy mudstone lithofacies (LF 8) are from ~ 10 to 30 % dolomitized, while the underlying clast-rich silty dolomudstone to silty dolomudstone (LF 7) is ~ 100 % dolomitized. Sharp contact was observed between silty to sandy mudstone to dolomitic mudstone (LF 8) of the lowermost Dunedin Formation and clast-rich silty dolomudstone to silty dolomudstone (LF 7) of the Stone Formation at ~1838.7 m in c-10-E/94-N-7.

Description: silty to sandy mudstone to dolomitic mudstone (LF 8) is dark grey and massive (Fig. 3.7C). Petrographic studies show that silty to sandy mudstone to dolomitic mudstone (LF 8) consists of ~ 55 % micritized lime mud, ~ 30 % very finely crystalline calcite cement, ~ 10 % silt and very fine quartz sand that is ~ 0.1 mm in diameter, and less than 5 % bioclasts and peloids that are smaller than 0.3 mm (Fig. 3.8A). No evaporites or fenestral pores were observed. No lithic or carbonate clasts were observed in core samples.

Interpretation: the silt and fine quartz sand indicates that silty to sandy mudstone lithofacies (LF 8) was deposited in coastal to marginal margin environments with terrestrial input. The abundance of finely crystalline equant calcite cement, with no

evidence of subaerial exposure, indicate that this lithofacies was deposited in low energy settings and submerged at the time of deposition. This lithofacies is interpreted to represent restricted shallow marine settings (Pratt et al. 1992).

Peloidal algal grainstone lithofacies (LF 9)

Occurrence: peloidal algal grainstone lithofacies (LF 9) was observed in 3 intervals in the lowest Dunedin Formation in 3 wells, between ~ 8 and 45 m above the Stone Formation in 3 wells (c-27-K/94-N-16, b-19-K/94-N-16 and c-10-E/94-N-7). Dolomite content in this lithofacies is from ~ 10 to 50 % dolomite. Spatial and vertical variations cannot be indetermined based on 3 cores. Peloidal algal grainstone to dolomitic grainstone (LF 9) appears conformable with the underlying silty to sandy mudstone to dolomitic mudstone (LF 8). Approximately 6 m of discontinuous peloidal algal grainstone to dolomitic grainstone (LF 9) layers were recognized between 3957.3 and 3972.6 m (14.6 m core recovered) in c-27-K/94-N-16, interlayered with dominantly crystalline dolomite. Approximately 3 m of discontinuous peloidal algal grainstone to dolomitic grainstone (LF 9) core samples was recognized between 4027.7 and 4053.0 m (24.9 m core recovered) in b-19-K/94-N-16, interlayered with dominantly crystalline dolomite. Peloidal algal grainstone to dolomitic grainstone (LF 9) is best recovered from c-10-E/94-N-7 (~28 m/45.4 m recovered cores), between ~ 1793 m and 1830 m. It is found interlayered with and overlies silty to sandy mudstone to dolomitic mudstone (LF 8). Silty charophytan calcitic dolowackestone to dolopackstone (LF 10) was recognized from 1 thin section made from a core sample collected in the lower interval of the

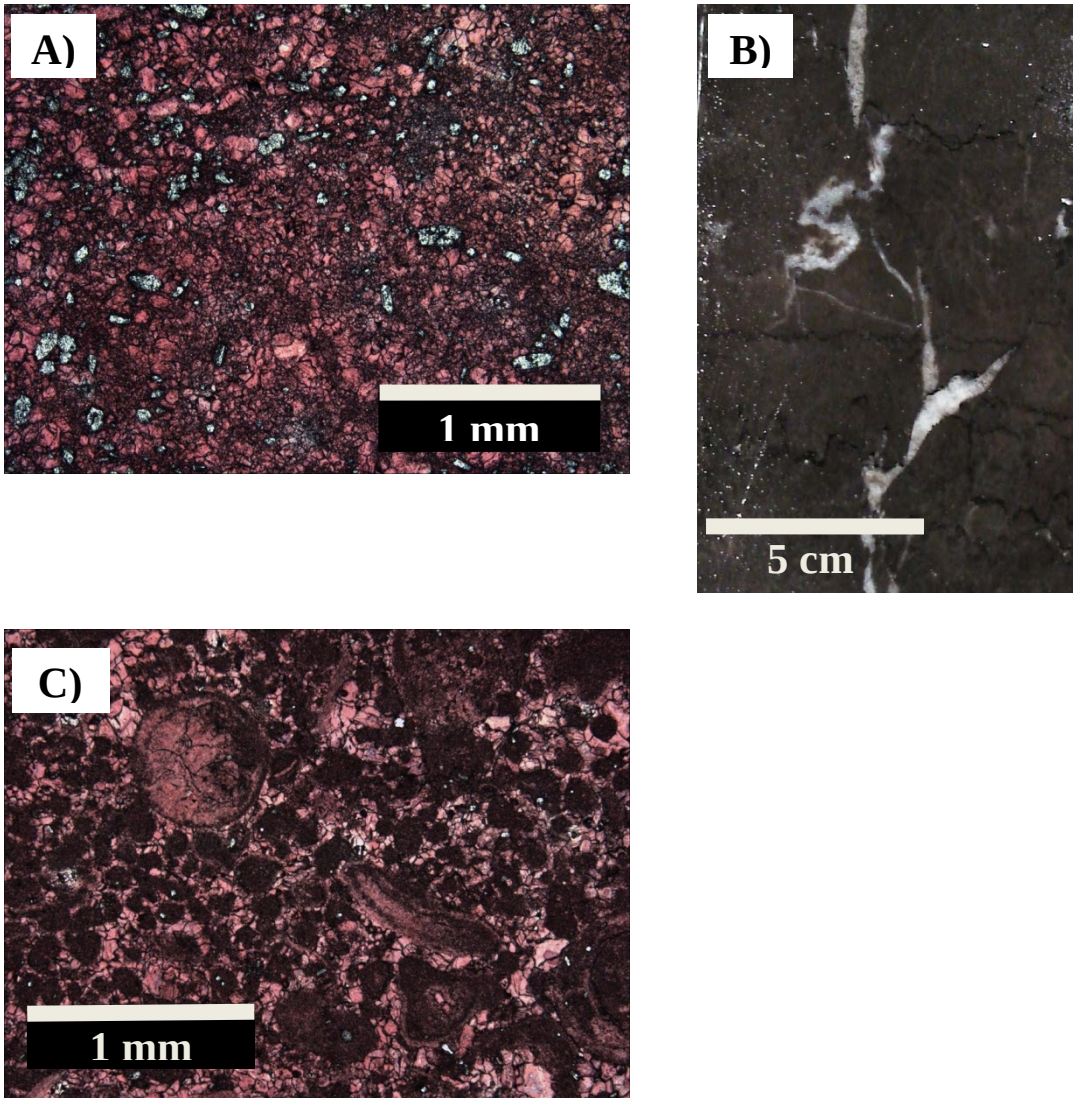

Figure 3.8A – C: Core and petrographic photos of samples from c-10-E/94-N-7. A) Silty to sandy mudstone. 1835.0 m. B) Masssive peloidal algal grainstone with fractures filled with calcite, 1814.3 – 1814.5 m. C) Representative photomicrograph of the peloidal algal grainstone in Fig. 3.8B. 1814.4 m. (original in color)

Dunedin Formation at 1802.3 m in c-10-E/94-N-7 where peloidal algal grainstone

lithofacies (LF 9) is the common litho-unit throughout the interval.

Description: peloidal algal grainstone to dolomitic grainstone (LF 9) is dark grey and massive to fine laminated (Fig. 3.8B). Petrographic studies show that peloidal algal grainstone to dolomitic grainstone (LF 9) contains ~ 48 % finely crystalline equant calcite cement, ~ 40 % peloids that are ~ 0.1 mm, ~ 10 % leaf-like phylloid algae and algal fragments that are up to 1 mm long, and ~ 2 % gastropod that are ~ 0.5 mm (Fig. 3.8C). The matrix of peloidal algal grainstone to dolomitic grainstone (LF 9) is cement supported. Grain to grain contact noticed in peloids are convex and concave.

Interpretation: the abundance of peloids, gastropods and phylloid green algae suggest that the depositional settings are possibly lagoonal settings with 1 – 5 m water depth, where phylloid green algae and gastropods were usually found (Jones and Desrochers 1992; Pratt et al. 1992). Peloidal algal grainstone lithofacies (LF 9) is closely associated with silty charophytan wackestone to packstone (LF 10) supports this interpretation.

Silty charophytan wackestone to packstone lithofacies (LF 10)

Occurrence: silty charophytan wackestone to packstone lithofacies (LF 10) was recognized from 1 thin section of core slab collected in the lower interval of the Dunedin Formation at 1802.3 m from c-10-E/94-N-7, approximately 36 m above the Stone Formation. Silty charophytan wackestone to packstone lithofacies (LF 10) is ~ 60 % dolomitized and thick bedded as observed from the one core slab sample. Identification of silty charophytan calcitic dolowackestone to dolopackstone (LF 10) in cores from the studied wells is impossible due to the particle size of the charophyta

oogonia in the studied core samples. Silty charophytan wackestone to packstone lithofacies (LF 10) is overlain by an interval of crystalline dolomite in erosional contact evident by a scour mark. It is interlayered with peloidal algal grainstone lithofacies (LF9) between ~ 1793 m and 1830 m in c-10-E/94-N-7, where silty to sandy mudstone lithofacies (LF 8) was also found. Occurrence and distribution of silty charophytan wackestone to packstone lithofacies (LF 10) across the study area cannot be further determined due to the difficulty in identification.

Description: silty charophytan calcitic dolowackestone to dolopackstone (LF 10) is light to medium grey and massive (Fig. 3.9A). Petrographic studies show that silty charophytan calcitic dolowackestone to dolopackstone (LF 10) consists of ~ 10 % charophyta oogonia and charophyta fragments that are from ~ 0.2 to 1 mm in diameter (Fig. 3.9B), ~ 3 % ostracodes that are ~ 0.1 to 0.5 mm long, and ~ 1 % sub-rounded quartz silt that is less than 0.1 mm in diameter.

Interpretation: the charophyta in Canada during the Devonian era comprises a group of non-marine green algae that have been interpreted to be the ancestry of plants which live in brackish water environments (Peck and Morales 1966; Burne et al. 1980). No remarkable sedimentary water depth indicator was observed. The co-existence of charophyta oogonia, ostracods and quartz silt are interpreted to represent brackish water to peritidal settings (Peck and Morales 1966; Pratt et al. 1992).

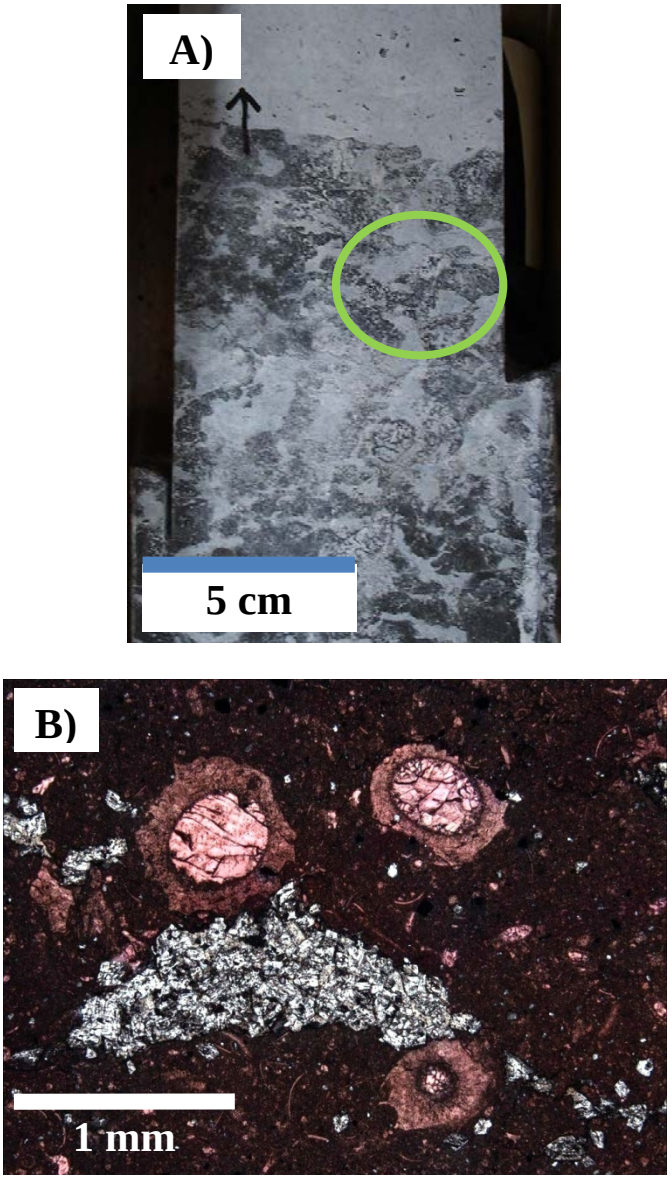

Figure 3.9A – B: Core and petrographic photos of samples from c-10-E/94-N-7. A) Silty charophytan calcitic dolowackestone to dolopackstone overlain by silty dolomite in erosional contact evidenced by a scour mark (circle) at 1802.3 m. Black arrow points up. B) Petrographic photo taken from a thin section of the core sample in Fig. 3.9A. Charophyta oogonia, ostracodes, lime mud and very finely to finely crystalline dolomite in the matrix. 1802.4 m. (original in color)

Echinoderm peloidal grainstone lithofacies (LF 11)

Occurrence: echinoderm peloidal grainstone lithofacies (LF 11) was observed in 3 intervals between ~ 10 to 20 m above the Stone Formation in 3 wells (c-27-K/94-N-16, b-19-K/94-N-16 and c-10-E/94-N-7). Echinoderm peloidal grainstone lithofacies (LF 11) can be divided into echinoderm peloidal grainstone (~ 5 to 10 % dolomite) and echinoderm peloidal dolograinstone (~ 90 % dolomite). Degree of dolomitization varies in the recovered cores. Echinoderm peloidal dolograinstone (LF 11) comprises ~ 12 m of the 14.2 m recovered core interval, and interbedded with ~ 1 m of crystalline dolomite and ~ 1 m unclassified dolofloatstone, between 3957.3 and 3972.6 m in c-27-K/94-N-16. Echinoderm peloidal dolograinstone (LF 11) comprises ~ 13 m of litho-unit in the ~ 24.9 m recovered core interval between 4027.7 and 4053.0 m in b-19-K/94-N-16, with the ~ 12 m of unclassified dolopackstones to crystalline dolomite. Echinoderm peloidal grainstone (LF 11) is abundant and best preserved in c-10-E/94-N-7, between 1712.7 and 1721.8 m, where it comprises ~ 8 m of the ~ 9.1 m recovered core interval, with minor packstones in conformable contact.

Description: echinoderm peloidal grainstone to dolograinstone (LF 11) is medium grey if dolomitized and dark grey if calcitic. The structure is massive to thin bedded (Fig 3.10A). Petrographic studies show that the framework grains consist of ~ 40 % echinoid plates that are from ~ 0.2 to 1 mm (Fig. 3.10B), ~ 40 % peloids that are typically smaller than 0.1 mm (Fig. 3.10C), ~ 10 % lime mud, a ~ 4 mm wide fragment of tubular coral that comprises ~ 6 % of the selected thin section, and ~ 4 % unidentified bioclasts that

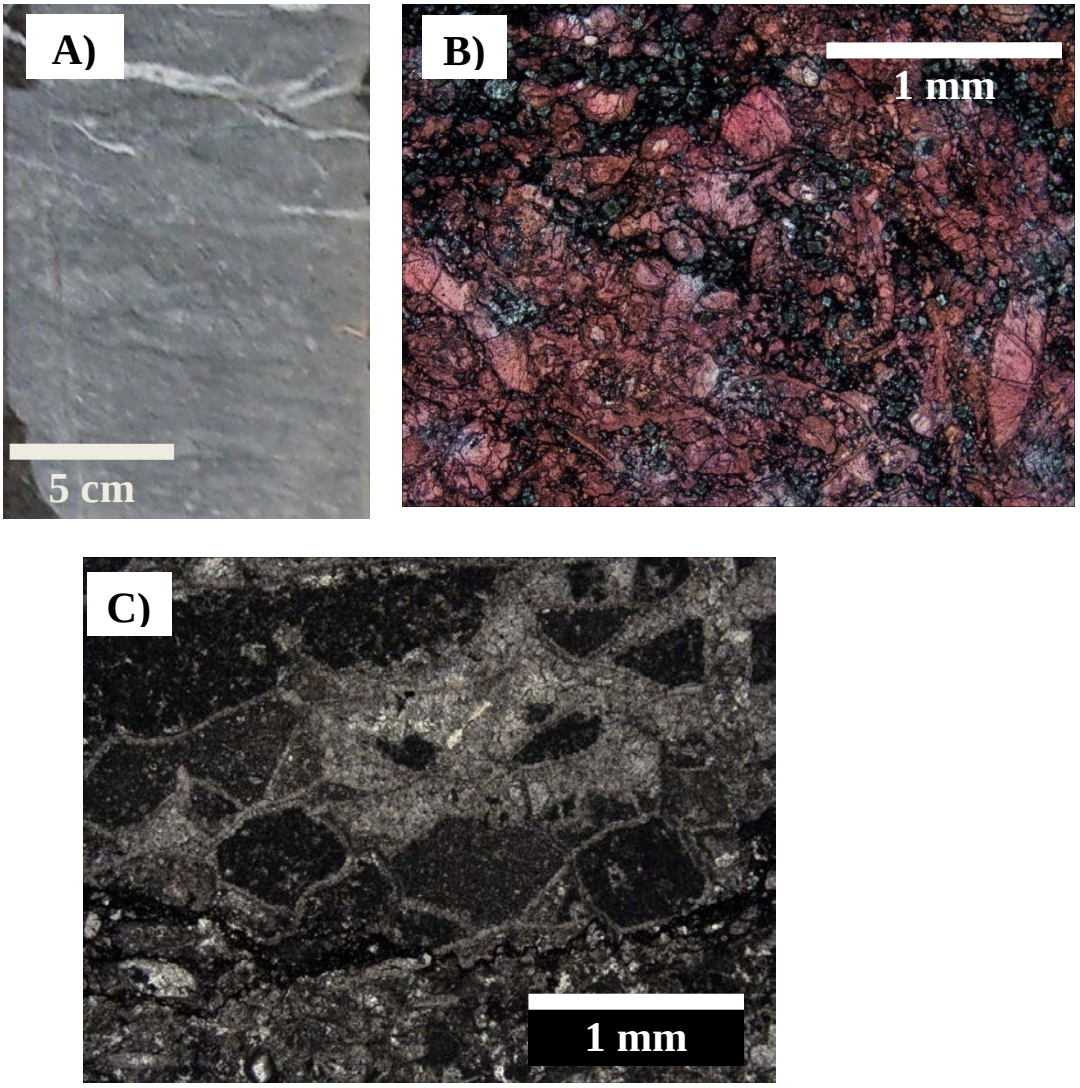

Figure 3.10A – C: Facies of the Dunedin Formation. A) Echinoderm peloidal dolograinstone. c-27-K/94-N-16, 3965.9 – 3966.1 m. B and C) Petrographic photos showing the stained and unstained side of a thin section of an echinoderm peloidal grainstone with ~ 4 mm wide fragment of tubular coral. c-10-E/94-N-7, 1630.4 m. In Fig. 3.10B, the lime mud has been replaced by very finely crystalline dolomite crystal. Some of the edges of the echinoderm plates appear pale pink. This is related to the fact that the echinoderm plates are not naturally oriented perfectly in the same direction, therefore staining can be uneven. This thin section has been stained and re-stained for 5 times and this is the most representative quality photo available. Alizarin red-S and K-ferricyanide solutions were used in staining. (original in color)

are less than 0.1 mm in diameter, and a very thin broken piece of trilobite? fragment. A piece of broken tubular coral fragment was found in petrographic investigation (Fig. 3.10C). The matrix is grain-supported and framework grains appear dense and compacted.

Interpretation: the abundance of echinderms and peloids in a massive to thin bedded structure may suggest lagoonal depositional settings (Jones and Desrochers 1992). The tubular coral is not in growth position and does not help to indicate depositional settings.

Amphiporid floatstone to rudstone lithofacies (LF 12)

Occurrence: amphiporid floatstone to rudstone lithofacies (LF 12) was observed in 1 interval in c-16-A/94-N-15, in the upper Dunedin Formation ~ 40 and 100 m above the Stone Formation, where the lower Dunedin Formation is the thinnest (< 40 m) among the 10 studied wells. All core samples of amphiporid floatstone to rudstone lithofacies (LF 12) were found ~ 100 % dolomitized. Amphiporid dolofloatstone to dolorudstone (LF 12) comprises ~ 15 m of the 16.5 m core interval between 3764.0 and 3818.0 m interval in c-16-A/94-N-15, with ~ 1.5 m crystalline dolomite. Amphiporid floatstone to rudstone lithofacies (LF 12) gradually shifts to stromatoporoid bioclastic floatstone lithofacies (LF 13) in the upper 37.5 m between 3764.0 and 3818.0 m in c-16-A/94-N-15.

Description: amphiporid dolofloatstone to dolorudstone (LF 12) is medium grey and

characterized by intimately less fossiliferous and more fossiliferous thin interbeds from 3 to 12 cm thick (Fig. 3.11A). These interbeds appear conformable and have no erosional scour or reactivation surface. The less fossiliferous floatstone layers contain ~ 15 % amphiporids and more fossiliferous rudstone layers contain locally over 65 % amphiporids in cm-scale thin beds (Fig. 3.11B). Up to 10 % fragmented stromatoporoids were found scattered in both floatstone and rudstone layers (Fig. 3.11C). The elongated amphiporids are from ~ 1 to 10 mm long and from ~ 1 to 3 mm in diameter. They appear broken and none of them are in growth position. Petrographic studies show that the matrix percentage varies from ~ 25 to 85 % among floatstone and rudstone thin beds. The matrix contains bioclasts and dolomitized lime mud in approximately in 3:2 ratio. The bioclasts are dominantly broken bivalves with rare echinoderm that are less than 0.1 mm in diameter. Both dolofloatstone and dolorudstone are matrix-supported to locally grain-supported. Framework grains appear dense and compacted.

Interpretation: amphiporids of the amphiporid floatstone to rudstone lithofacies (LF 12) do not appear in growth position as illustrated in the paleobiological study by Hladil (2007), but instead the amphiporids are aligned in less fossiliferous and more fossiliferous thin interbeds. These are interpreted to represent lagoon to back reef depositional environments in Middle Devonian by Kobluk (1975) and Bourque et al. (1986).

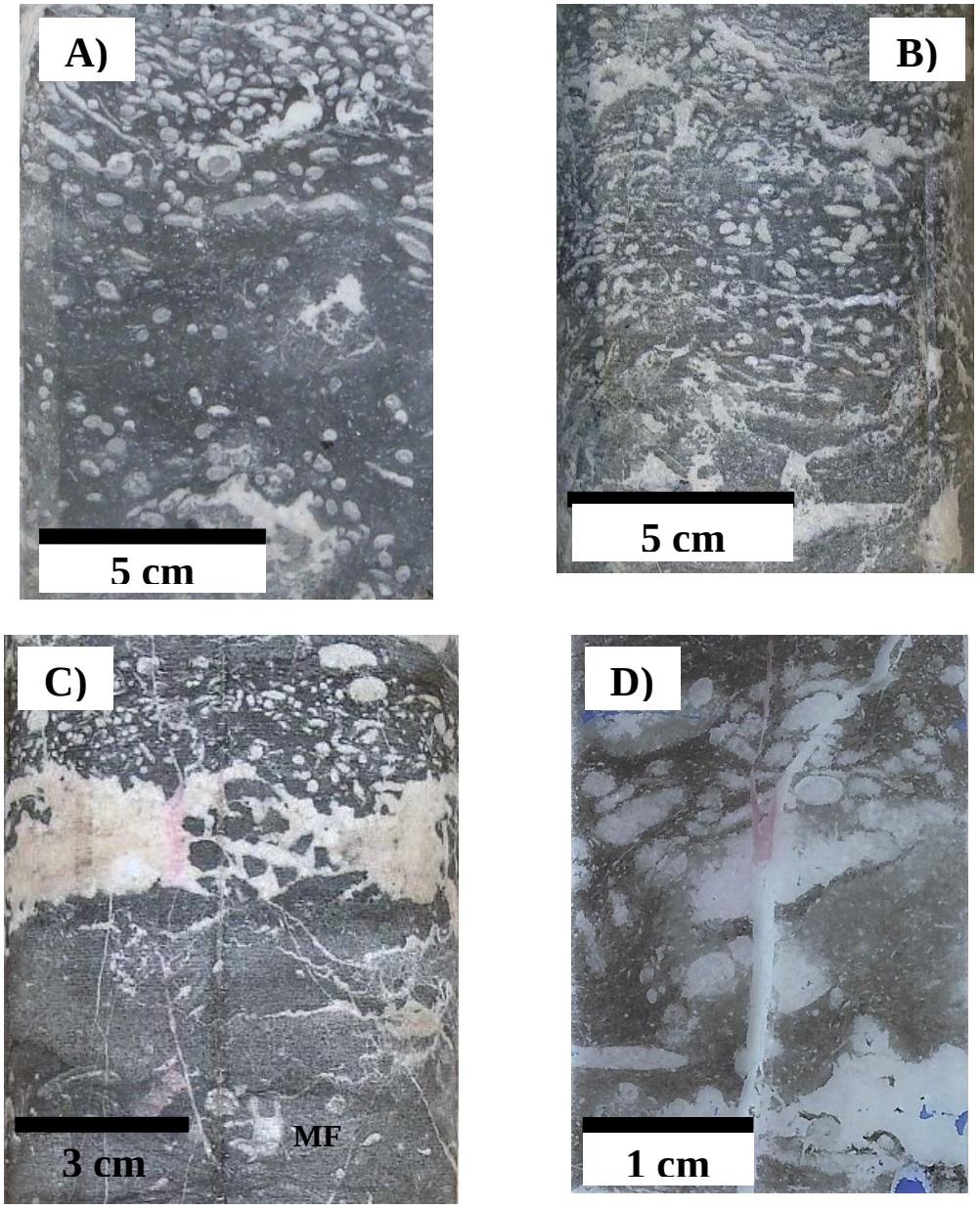

Figure 3.11A – D: Photos of a thin section and cores recovered from c-16-A/94-N-15. A) Amphiporid dolofloatstone to dolorudstone, 3777.9 – 3778.0 m. B) Amphiporid and bioclasts (stromatoporoids?) in amphiporid dolofloatstone to dolorudstone, 3766.7 – 3766.8 m. C) Amphiporid and macrofossil fragments (MF; stromatoporoids?) in amphiporid dolofloatstone to dolorudstone, 3765.5 – 3765.7 m. D) Scanned image of a thin section of amphiporid dolofloatstone to dolorudstone, 3801.2 m. The left half of this thin section had been stained with Alizarin red-S and K-ferricyanide solutions. (original in color)

Stromatoporoid bioclastic floatstone lithofacies (LF 13)

Occurrence: stromatoporoid bioclastic floatstone lithofacies (LF 13) was observed in 2 intervals in the upper Dunedin Formation in a-67-D /94-O-13 and c-16-A/94-N-15. These include one cored interval ~ 120 to 140 m above the Stone Formation from a-67-D/94-O-13, and one cored interval ~ 40 and 100 m above the Stone Formation from c-16-A/94-N-15. All core samples of stromatoporoid bioclastic floatstone lithofacies (LF 13) were found 100 % dolomitized. In a-67-D/94-O-13, stromatoporoid bioclastic dolofloatstone (LF 13) comprises about ~ 3 m of the 17.3-m recovered core between 5211.2 and 5229.5 m. It is typically 15 to 30 cm thick and interbedded with crystalline dolomite in this poorly recovered core interval. In c-16-A/94-N-15, stromatoporoid bioclastic dolofloatstone (LF 13) gradually changes from amphiporid dolofloatstone to dolorudstone (LF 12) in the upper 37.5 m of the 3764.0 ~ 3818.0 m interval in c-16-A/94-N-15.

Description: stromatoporoid bioclastic dolofloatstone (LF 13) is light to medium grey and massive to thick bedded (15 to over 50 cm thick). The dominant framework grains are ~ 20 to 35 % irregular stromatoporoids in different sizes and shapes from 2 cm to over 10 cm wide (Fig. 3.12A and B), with up to 10 % elongated amphiporids ~ 1 to 3 mm in diameter and ~ 1 to 10 mm long, up to 4 % delicated dendroid stromatoporoid *Stachyodes* sp. from 2 to 4 cm wide (Fig. 3.12A), and up to 15 % rounded bioclasts that are from 1 to 4 mm (Fig. 3.12B). Petrographic studies show that this lithofacies is made up of ~ 50 % framework grains and ~ 50 % matrix. The matrix contains ~30 %

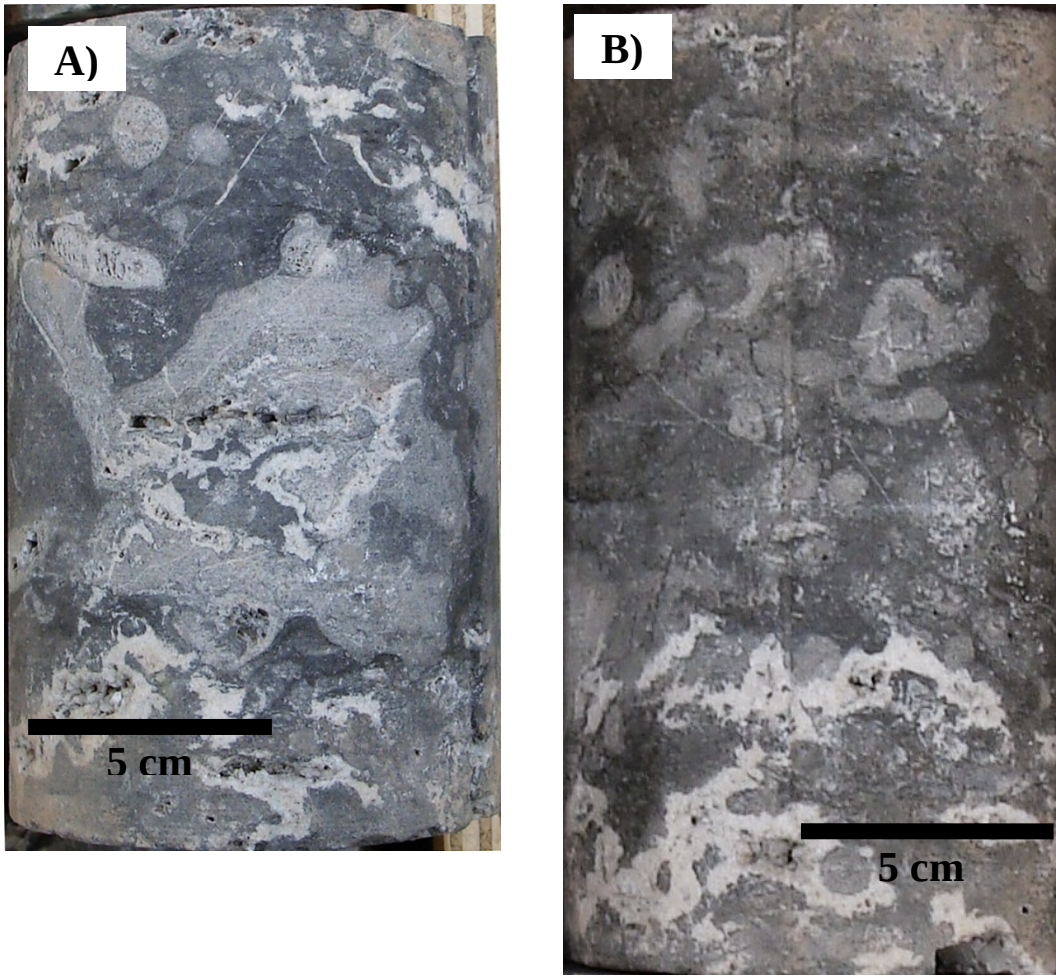

Figure 3.12A – B: Core photos. c-16-A/94-N-15. A) Stromatoporoid bioclastic dolofloatstone. Irregular to bulbous stromatoporoid with delicate dendroid stromatoporoid *Stachyodes sp.* and irregular stromatoporoids in the matrix, 3793.9 – 3794.2 m. B) Macrofossil fragments with delicate dendroid stromatoporoid *Stachyodes sp.* in stromatoporoid bioclastic dolofloatstone, 3795.9 – 3796.2 m. (original in color)

dolomitized lime mud and ~ 70 % bioclasts that are less than 0.1 mm. Grain to grain contact was not observed. Most of the petrographic fabirc were not preserved.

Interpretation: The irregular to bulbous growth form of the stromatoporoids observed in stromatoporoid bioclastic dolofloatstone (LF 13) has been interpreted to have developed in high energy back reef to reef flat environment (James and Bourque 1992). Up to 4%

dendroid stromatoporoid *Stachyodes* sp. *was* found in stromatoporoid bioclastic floatstone lithofacies (LF 13), which has been interpreted to have developed in back-reef (Kobluk 1975) to reef crest environments (Machel and Hunter 1994). In c-16-A/94-N-15, these dendroid stromatoporoids occur with abundant amphiporids. Base on the paleobiological interpretations in previous studies, stromatoporoid bioclastic floatstone lithofacies (LF 13) is interpreted to have deposited in back reef to reef flat settings.

Crinoidal packstone to grainstone lithofacies (LF 14)

Occurrence: crinoidal packstone to grainstone lithofacies (LF 14) was observed in 1 poorly recovered core interval from b-19-K/94N16, in the upper Dunedin Formation ~110 to 125 m above the Stone Formation. All core samples of crinoidal packstone to grainstone lithofacies (LF 14) were found 100 % dolomitized. Crinoidal dolopackstone to dolograinstone (LF 14) comprises the lower ~ 12 m of the 16.4 m recovered core interval, between ~ 3934.8 and 3951.5 m in b-19-K/94-N-16. The upper ~ 4 m cored interval consists of poorly recovered crystalline dolomite. Local thick beds of bioclastic dolofloatstone were observed in this interval.

Description: crinoidal dolopackstone to dolograinstone (LF 14) is light to medium grey, massive to thick bedded (Figs. 3.13A, B and C). Petrographic studies recognized ~50 % crinoid ossicles in a dolomitized finely crystalline matrix (Fig. 3.13D). Rounded crinoid ossicles are from 0.5 to 1 mm in diameter. The crinoid stems are in singular and star shape, instead of the distinctive twinned stem crinoid found in the previous study by

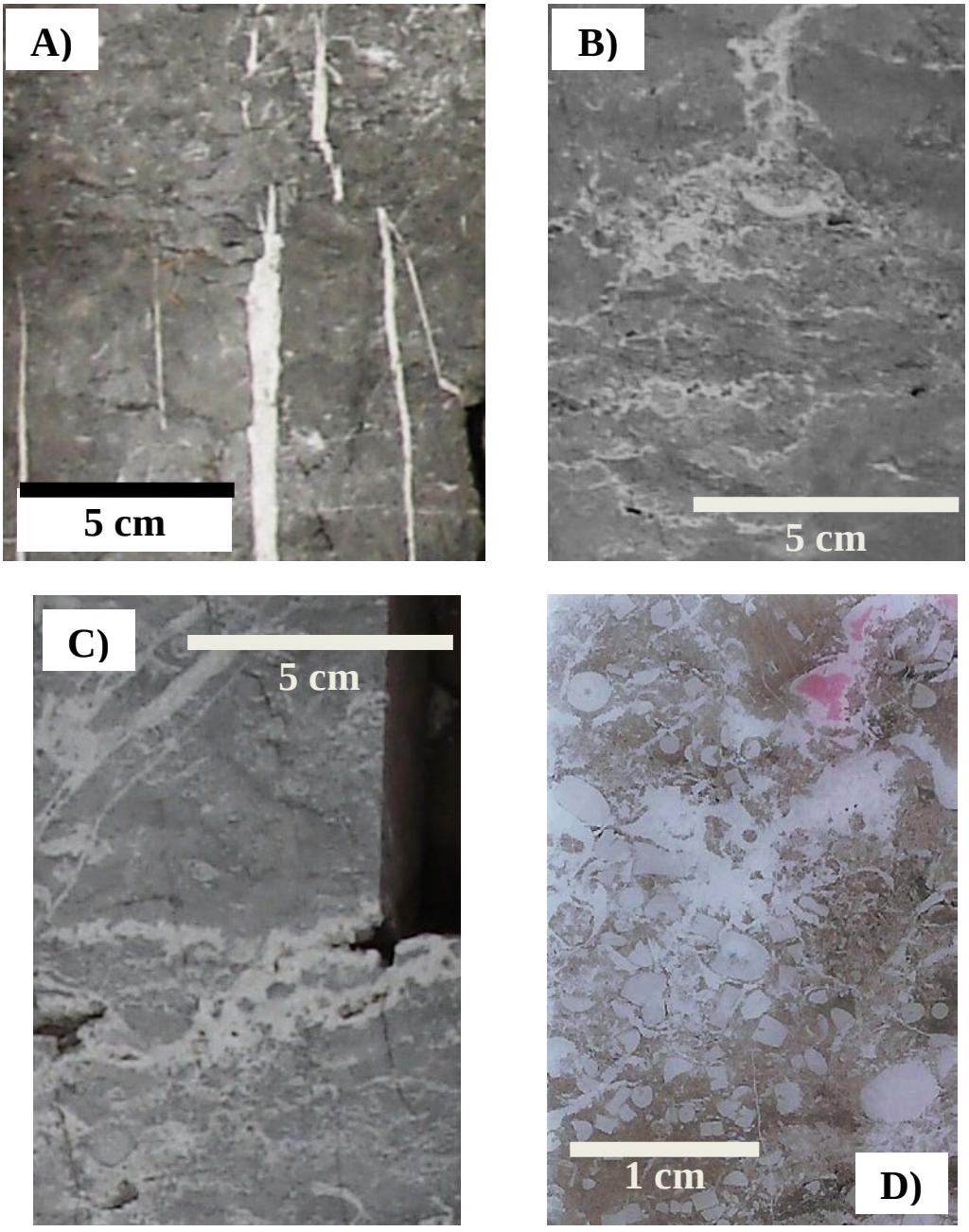

Figure 3.13A – D: Core photos of crinoidal dolopackstone to dolograinstone of the upper Dunedin Formation. Core samples recovered from b-19-K/94-N-16. A) 3942.9 – 3943.0 m; B) 3945.7 – 3945.8 m; C) 3941.1 – 3941.2 m; D) Scanned image of a thin section made of the core slab in Fig. 3.13C at 3941.1 m. The right half of this thin section had been stained with Alizarin red-S and K-ferricyanide solutions. (original in color)

Morrow (1978) in cutting samples. No direct grain-to-grain contact was observed.

Interpretation: Nadjiwon (2001) interpreted the crinoidal packstone to grainstone lithofacies (LF 14) as subtidal banks above fair weather wave base, where energy was not great enough to winnow the lime mud off the matrix. Gosselin et al. (1989) documented locally abundant crinoids and brachiopods in the Middle Devonian Slave Point Formation, which were interpreted as an open marine, off reef, mud-dominated environment. Similar interpretation was made by Machel and Hunter (1994). In this study, crinoidal packstone to grainstone lithofacies (LF 14) was found in a ~ 12 m interval from only one of the studied wells. It is a local facies that is overlain by crystalline dolomite. The stratigraphic position of the crinoidal packstone to grainstone lithofacies (LF 14) is at about the same stratigraphic level as the bulbous stromatoporoid mudstone to floatstone lithofacies (LF 15). It is suggested that crinoidal packstone to grainstone lithofacies (LF 14) was developed as local crinoid accumulation in back reef to reef flat settings rather than in open marine, off reef settings.

Bulbous stromatoporoid mudstone to floatstone lithofacies (LF 15)

Occurrence: bulbous stromatoporoid mudstone to floatstone lithofacies (LF15) was observed in 3 intervals in the upper Dunedin Formation between ~ 100 and 200 m above the Stone Formation in 2 wells (c-54-K/94-N-16 and c-27-K/94-N-16). All core samples of bulbous stromatoporoid mudstone to floatstone lithofacies (LF15) were found 100 % dolomitized. Bulbous stromatoporoid dolomudstone to dolofloatstone (LF 15) comprises

the lower 8.6 m in the 17.6 m recovered cored interval between 3697.0 and 3715.3 m in c-54-K/94-N-16, and interlayered with stromatoporoid dolobindstone (LF 17) in the upper 9 m. Approximately 6 m of bulbous stromatoporoid dolomudstone to dolofloatstone (LF 15) was observed in the 11.8 m recovered cored interval between 3617.8 and 3630.3 m in the same well, where it is interlayered with crystalline dolomite. In both intervals, bulbous stromatoporoid dolomudstone to dolofloatstone (LF 15) is in thick beds (~ 20 to 40 cm thick) of less fossiliferous dolomudstone and more fossiliferous dolofloatstone. In c-27-K/94-N-16, bulbous stromatoporoid dolomudstone to dolofloatstone (LF 15) comprises ~ 13 m of the 17.6 m recovered core, between 3808.2 and 3826.5 m, with two thick beds (~ 15 cm and ~25 cm respectively) of amphiporid dolobafflestone (LF 16), several thick beds (~ 15 cm thick) of stromatoporoid dolobindstone (LF 17), and ~ 4 m of crystalline dolomite.

Description: bulbous stromatoporoid dolomudstone to dolofloatstone (LF 15) is medium grey and thick bedded (Fig. 3.14A and B). It consists of alternating less fossiliferous mudstone and more fossiliferous floatstone thick beds (~ 20 to 40 cm thick), with no obvious contact or facies boundary. The less fossiliferous thick beds consist of ~ 5 to 8 % bulbous stromatoporoid and stromatoporoid fragment. The more fossiliferous thick beds consist of ~ 15 to up to 40 % bulbous stromatoporoid and stromatoporoid fragment. Up to 5 % dendroid stromatoporoid *Stachyodes* sp. was observed in both dolomudstone to dolofloatstone beds. These dendroid stromatoporoids appear very similar in growth form and size. Petrographic studies observed that the matrix of dolofloatstone beds contain ~ 60 to 70 % dolomitized lime mud and ~ 30 to 40 % unrecognized

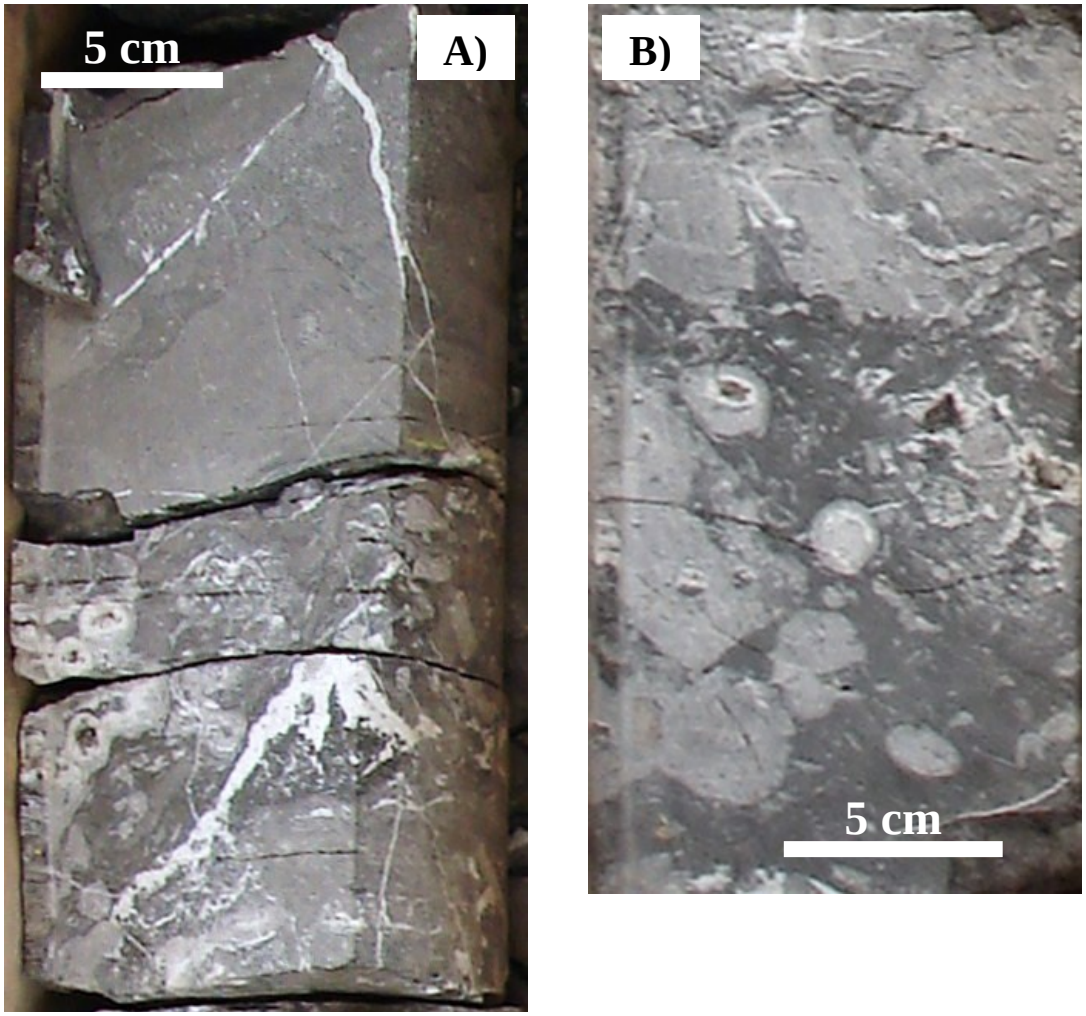

Figure 3.14A – B: Core photos. c-27-K/94-N-16. A) Bulbous stromatporoid dolomudstone to dolofloatstone. 3820.1 – 3820.0 m. B) Bulbous stromatporoid dolomudstone to dolofloatstone. 3813.1 – 3813.0 m. (original in color)

stromatoporoid fragments that are from 0.1 ~ 0.3 mm. Grain-to-grain contacts appear dense and compacted. Dolomudstone beds have not been sampled.

Interpretation: bulbous stromatoporoid dolomudstone to dolofloatstone (LF 15) has been interpreted to have deposited in back reef settings based on the bulbous stromatoporoid

morphology and dominance (James and Bourque 1992; Machel and Hunter 1994). Dendroid to bulbous stromatoporoid form have been interpreted to have developed in moderate energy reefal environments such as reef front, reef flat to back reef (James and Bourque 1992; Machel and Hunter 1994). Bulbous stromatoporoid dolomudstone to dolofloatstone (LF 15) is found in the same stratigraphic level with amphiporid dolobafflestone (LF 16), which amphiporid dolobafflestone (LF 16) is a strong indicator of lagoon to back reef environment. This further supports the interpretation.

Amphiporid bafflestone lithofacies (LF 16)

Occurrence: amphiporid bafflestone lithofacies (LF 16) was observed in 1 interval in the upper Dunedin Formation between 3808.2 and 3826.5 m in c-27-K/94-N-16, approximately 170 m above the Stone Formation and ~100 m below the Besa River Formation. All core samples of amphiporid bafflestone lithofacies (LF 16) were found 100 % dolomitized. Amphiporid dolobafflestone (LF 16) is a rare lithofacies. It occurs as several ~ 15 to 40 cm thick beds in the upper half of the 17.6 m recovered cored interval. Amphiporid dolobafflestone (LF 16) is conformably interlayered with bulbous stromatoporoid dolomudstone to dolofloatstone (LF 15; Fig. 3.15).

Description: amphiporid dolobafflestone (LF 16) is medium grey and massive (Fig. 3.16A). It consists of over 50 % stromatoporoid *Amphipora* in growth position from 2 to 7 mm in diameter and ~ 2 to 5 cm in height, and ~ 5 to 20 % irregular stromatoporoid fragments that are up to 3 cm in diameter. Amphiporid dolobafflestone (LF 16) typically

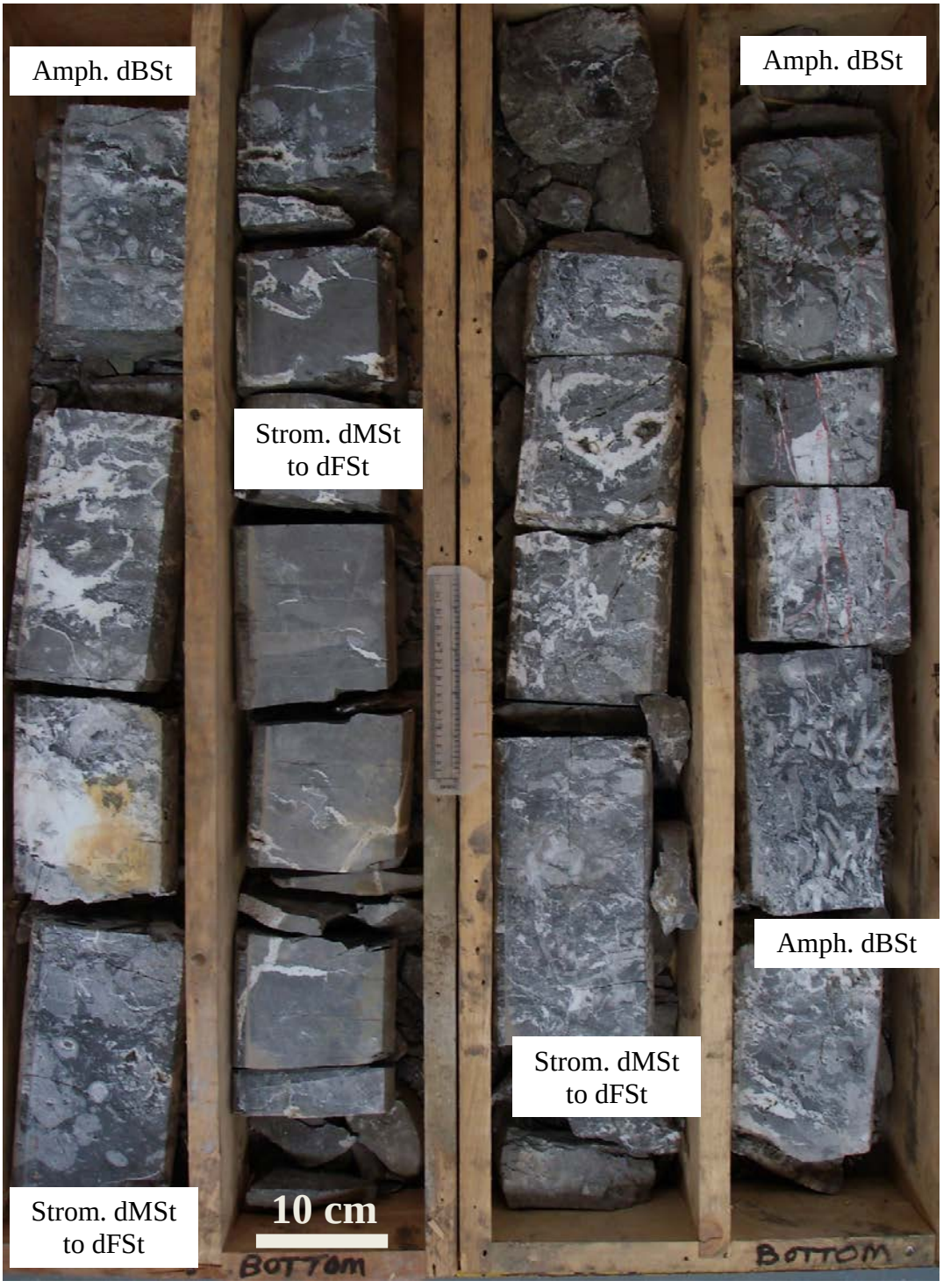

Figure 3.15: Core photo. c-27-K/94-N-16, 3813.1 – 3810.0 m. Interlayered bulbous stromatporoid dolomudstone to dolofloatstone (LF16) and amphiporid dolobafflestone (LF 18). (original in color)

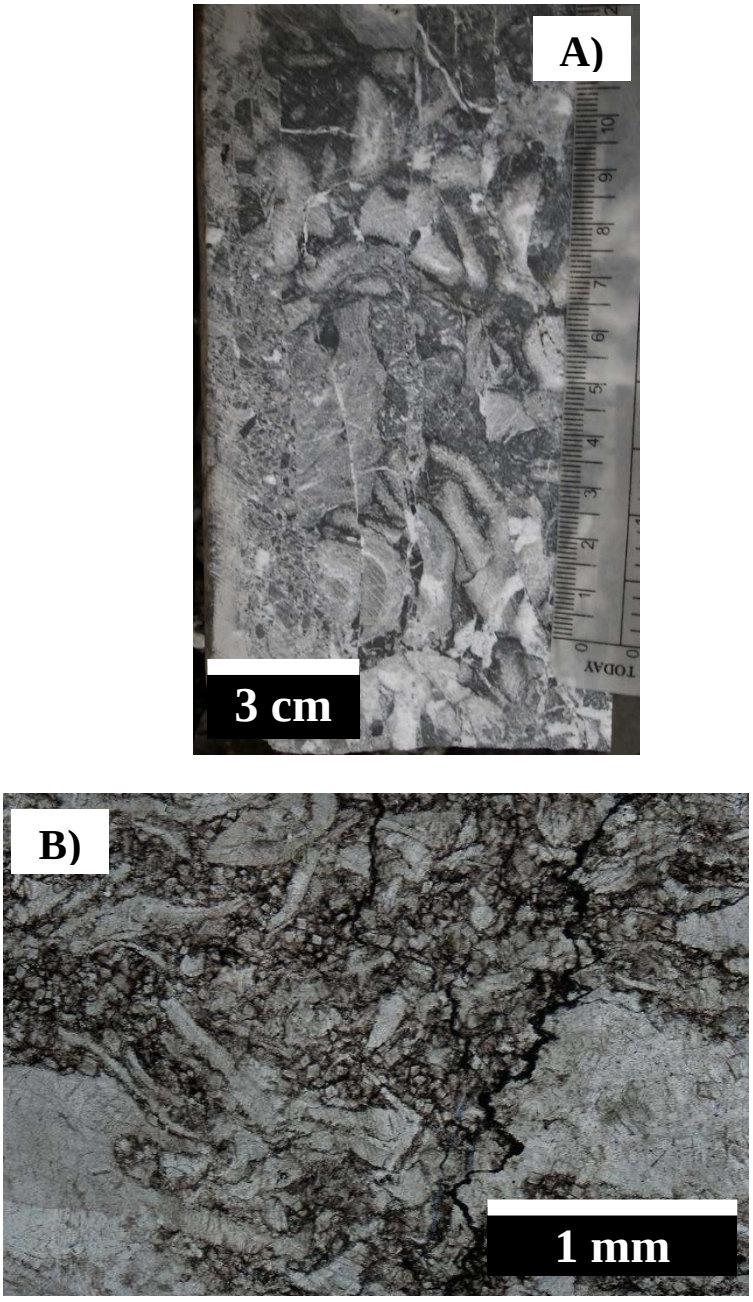

Figure 3.16A – B: Facies of the Dunedin Formation in c-27-K/94-N-16. A) Amphiporid dolobafflestone. Eifelian-Givetian stromatoporoid *Amphipora* in growth position as interpreted by Hladil (2007). 3810.7 – 3810.6 m. B) Petrographic photo taken from a thin section of the sample in Fig. 3.16A at 3810.7 m showing the matrix of amphiporid dolobafflestone. (original in color)

consists of ~ 30 to 50 % muddy matrix. Petrographic studies observed that the matrix contains ~ 70 % dolomitized lime mud, and ~ 30 % unrecognized bioclasts that are smaller than 0.2 mm (Fig. 3.16B). Grain-to-grain contacts appear dense and compacted.

Interpretation: amphiporid dolobafflestone (LF 16) is the only facies in this study which the amphiporids were found in growth position. Quantitative stromatoporoids paleobiological study in western Canada by Kobluk (1975) indicated that abundant amphiporids in growth position occurs predominantly in lagoonal environment, and with dendroid stromatoporoids in back-reef to marginal reef environments. Growth form and hydrodynamic interpretation by Hladil (2007) inferred that Eifelian-Givetian amphiporids were not strong enough to withstand in high energy reefal environments with their elongated narrow stems they exhibited, and suggested that amphiporid biota initiated in lagoonal facies and developed towards back reef. This facies is interpreted to be lagoon to back reef environments as evidential by the abundance of amphiporids in growth form (Kobluk 1975; Bourque et al. 1986; Hladil 2007).

Stromatoporoid bindstone lithofacies (LF 17)

Occurrence: stromatoporoid bindstone lithofacies (LF 17) was observed in 3 intervals in the upper Dunedin Formation in 2 wells (c-54-K 94-N-16 and c-27-K/94-N-16). All core samples of this lithofacies were found 100 % dolomitized. Stromatoporoid dolobindstone (LF 17) overlies and is interlayered with bulbous stromatoporoid dolomudstone to dolofloatstone (LF 15) and comprises ~ 7 m of the upper 9 m of the

17.6 m cored interval in the upper Dunedin Formation between 3697.0 and 3715.3 m in c-54-K/94-N-16, approximately 100 m above the Stone Formation and ~ 280 m below the Besa River Formation. Stromatoporoid dolobindstone (LF 17) occurs as two separated ~ 30 to 40 cm thick beds in the upper Dunedin Formation in the upper half of the 26.9 m recovered cored interval between 3527.0 and 3554.4 m in c-54-K/94-N-16, approximately 260 m above the Stone Formation and ~ 20 m below the Besa River Formation, where it is interlayered with crystalline dolomite. Stromatoporoid dolobindstone (LF 17) is interlayered with ~ 13 m of bulbous stromatoporoid dolomudstone to dolofloatstone (LF 15), two thick beds of amphiporid dolobafflestone (LF 16), and ~ 4 m of crystalline dolomite between 3808.2 and 3826.5 m in c-27-K/94-N-16.

Description: stromatoporoid bindstone lithofacies (LF 17) is characterized by distinctive beds of platy to encrusting stromatoporoids (Fig. 3.17A -C). It is light grey and 20 to 40 cm thick bedded. Stromatoporoid dolobindstone (LF 17) contain platy to encrusting stromatoporoids from 3 ~ 6 cm thick and over 10 cm wide (exceed core diameter). The abundance of the platy to encrusting stromatoporoids in stromatoporoid dolobindstone (LF 17) cannot be accurately and precisely estimated due to the randomness of stromatoporoid-lime mud interlayers. Internal organic structure of the platy to encrusting stromatoporoids has not been preserved. Petrographic studies revealed that nearly all of the textural details have been obliterated by dolomitization.

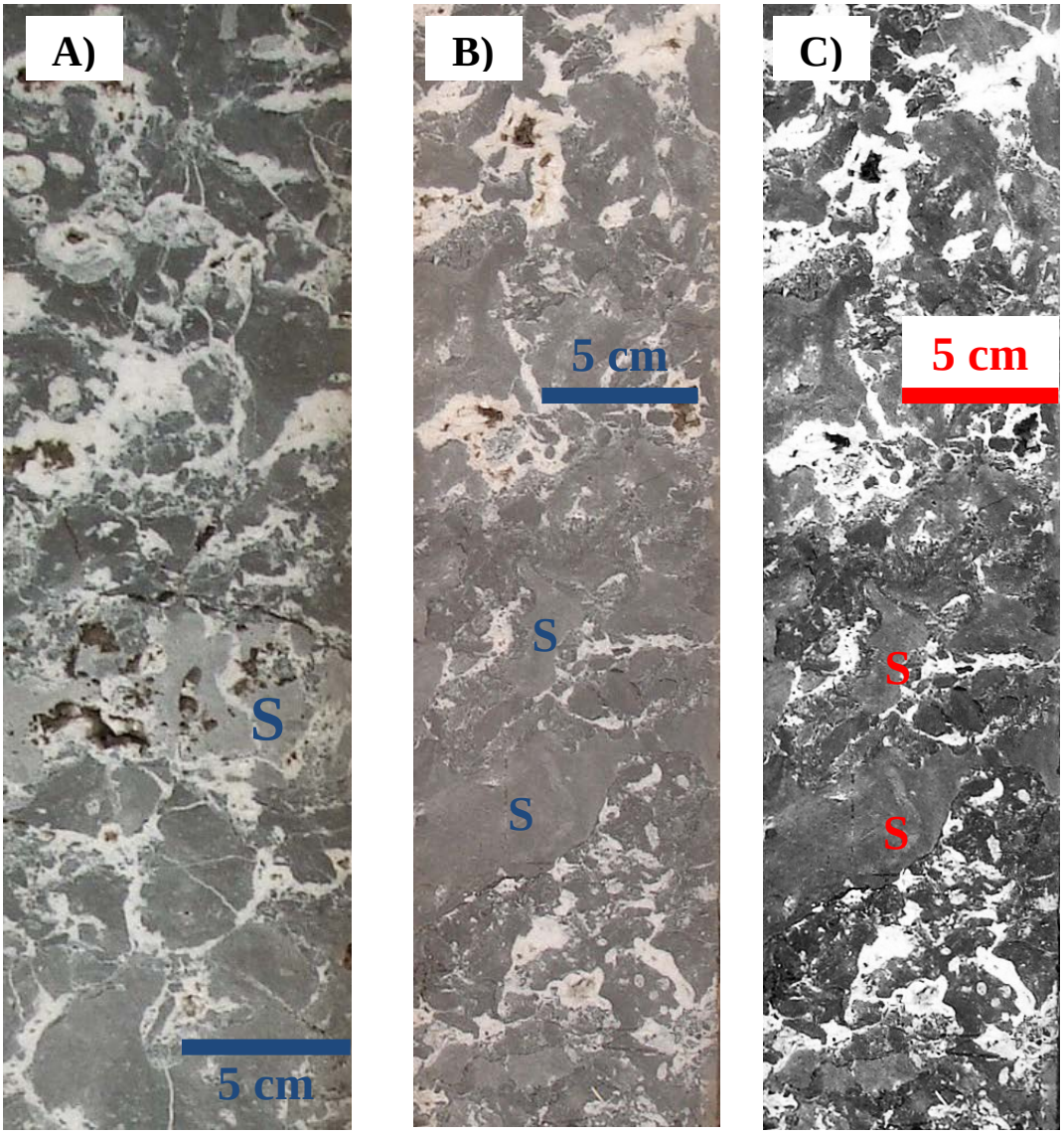

Figure 3.17A – C: Core photos from c-54-K/94-N-16. Encrusting stromatoporoids are marked with "S". A) Stromatoporoid dolobindstone, 3703.8 m – 3704.1 m (lower portion) with interbedded bulbous stromatoporoid dolomudstone to dolofloatstone, 3703.6 – 3703.8 m (upper portion). Color of this photo was adjusted towards black and white. B) stromatoporoid dolobindstone, 3702.2 – 3702.6 m (lower portion) with interbedded bulbous stromatoporoid dolomudstone to dolofloatstone, 3702.0 – 3702.2 m. C) High contrast image of Fig. 3.17B showing the growth form of the encrusting stromatoporoids (S) in stromatoporoid dolobindstone. (original in color)

Interpretation: stromatoporoid bindstone lithofacies (LF 17) is a rare lithofacies in the

Dunedin Formation and occurs in discontinued thick beds in between bulbous

stromatoporoid mudstone to floatstone lithofacies (LF 15) and amphiporid bafflestone lithofacies (LF 16). Although the growth forms of platy to encrusting stromatoporoid in stromatoporoid dolobindstone (LF 17) have been interpreted to represent stromatoporoids in high energy, wave-dominated reef crest to reef front environments (James and Bourque 1992), the rare occurrence of stromatoporoid bindstone lithofacies (LF 17) as discontinued thick beds with bulbous stromatoporoid mudstone to floatstone lithofacies (LF 15) and amphiporid bafflestone lithofacies (LF 16) indicates the depositional environment is likely to be lagoon to back reef in which the whole package was deposited.

Domal stromatoporoid framestone lithofacies (LF 18)

Occurrence: domal stromatoporoid framestone lithofacies (LF 18) was observed in 2 intervals in the upper Dunedin Formation in 2 wells (b-21-G/94-O-6 and c-16-A/94-N-15). Core samples of both undolomitized and 100% dolomitized domal stromatoporoid framestone lithofacies (LF 18) were observed in separated wells. Domal stromatoporoid doloframestone (LF 18) comprises ~ 12 m of the 15.2 m core recovered between 2647.1 and 2662.3 m in the easternmost well b-21-G/94-O-6, approximately 210 m above the Stone Formation and ~ 50 m below the Besa River Formation, where it is interlayered conformably with brachiopod packstone (LF 20) and crystalline dolomite. Domal stromatoporoid doloframestone (LF 18) occurs as a ~ 40 cm thick bed between 3650.0 and 3666.8 m in c-16-A/94-N-15, approximately 260 m above the Stone Formation and ~ 15 m below the Besa River Formation, where it is overlain by

clast-rich crystalline rock (LF 19).

Description: domal stromatoporoid doloframestone (LF 18) is medium to dark grey and thick layered (Fig. 3.18A). It consists of dominantly domal stromatoporoid in enveloping growth position with dolomitized lime mud in between the allochemical component (Fig. 3.18B). The domal stromatoporoids are from ~ 5 cm to up to 40 cm in height (Fig. 3.19A), with their widths exceed the core width (> 11 cm). Petrographic studies show that the matrix of domal stromatoporoid doloframestone (LF 18) consists of ~ 98 % lime mud and ~ 2 % peloids. Grain-to-grain contact has not been observed.

Interpretation: domal stromatoporoids in enveloping form and growth position have been interpreted to have developed in fore slope to slope depositional environments below wave base, or in back reef environment where sedimentation rate is high (James and Bourque 1992; Machel and Hunter 1994). The ~ 98 % lime mud percent abundance in the matrix indicates that this lithofacies was more likely to have deposited in fore slope to slope environments than in shallow back reef environment, where biota development is restricted by the lack of sunlight in deeper water environment and lime mud is the dominant allochemical component.

Clast-rich crystalline rock lithofacies (LF 19)

Occurrence: clast-rich crystalline rock lithofacies (LF 19) was observed in 1 interval in the upper Dunedin Formation in c-16-A/94-N-15, where it is directly overlain by the

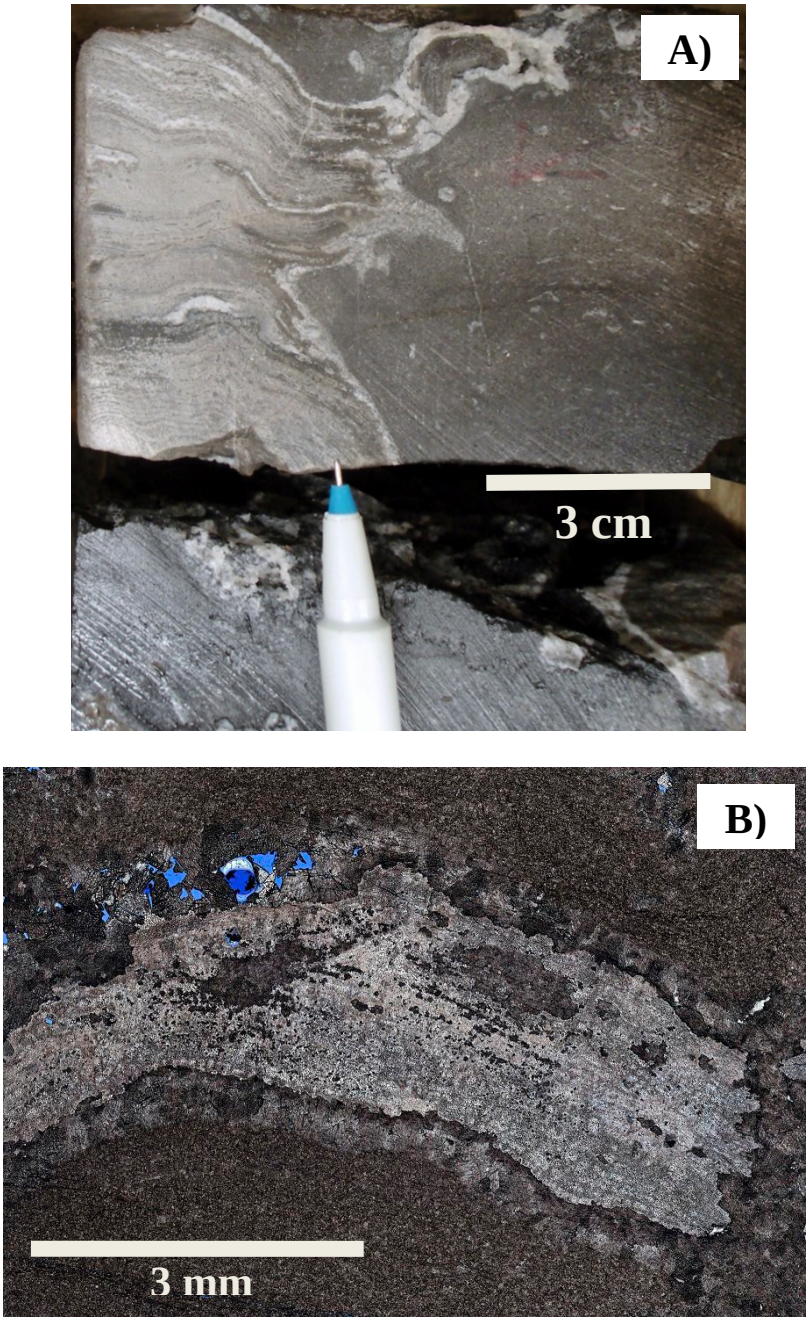

Figure 3.18A – B: Facies of the Dunedin Formation. A) Stromatoporoid doloframestone with a lamellar stromatoporoid. This growth structure has been interpreted to represent stromatoporoid in high energy, wave-dominated environment (James and Bourque 1992). b-21-G/94-O-6, 2657.8 m. B) Petrographic photo taken from a thin section of the sample in Fig. 3.18A. Photo was taken by using the white card method outlined by Folk (1987). No fossil fragments were observed in the matrix. (original in color)

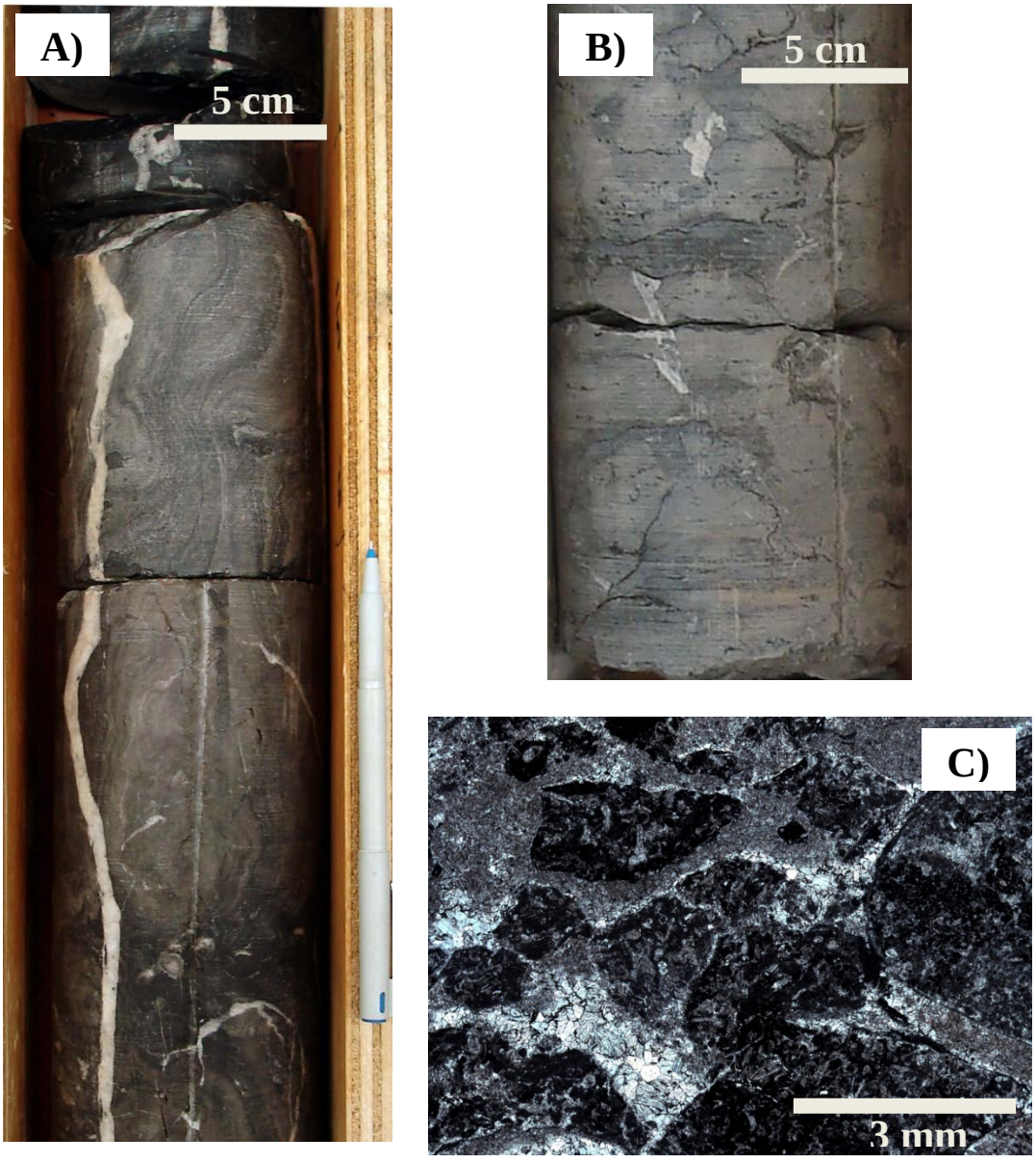

Figure 3.19A – C: Facies of the Dunedin Formation. A) Domal stromatoporoid doloframestone with a domal stromatoporoid which appears in growth position. 3663.4 – 3663.8 m. B) Clast-rich crystalline rock. 3664.9 – 3665.1 m. C) PPL petrographic photo taken from a thin section of the sample in Fig. 3.19B. The extraclasts are angular to rounded, laminated to massive shell fragment bioclasts packstone clasts. The matrix is cemented by finely crystalline equant and blocky calcite cements. The bright spots are finely crystalline blocky cement which has a very high transparency when compared to the finely crystalline equant calcite cement as well as the packstone clasts. Unstained side of the thin section is shown for better clarity. (original in color)

Besa River Formation, approximately 200 m above the Stone Formation. Clast-rich crystalline rock (LF 19) is ~ 100% limestone and comprises the uppermost ~ 6 m of the cored interval between 3650.0 and 3666.8 m in c-16-A/94-N-15.

Description: clast-rich crystalline rock (LF 19) is light grey and massive (Fig. 3.19B). No sedimentary structure and allochemical component can be observed in the polished core slabs due to previous chemical flushing(?) or staining (?). Petrographic study found clast-rich crystalline rock consist of 50 % to up to 80 % micritized bioclastic packstone clasts from 1 mm to up to 15 mm in diameter (Fig. 3.19C). These bioclastic packstone clasts are held together by very finely to finely crystalline equant calcite cement. Lime mud is almost absent (< 1 %). They are angular to sub-rounded, very poorly sorted, with massive to faint laminated bedding structure, and contain unrecognizable bioclasts that are < 0.1 mm. All of the bioclastic packstone clasts appear very similar regardless of their shapes. No other type of clast was observed. Grain-to-grain contacts between these bioclastic packstone clasts cannot be determined due to the nature of cementation.

Interpretation: the angular to sub-rounded shape and very poor sorting nature of the bioclastic packstone clasts indicate mechanical breaking down of pre-existing carbonate rocks, further transportation, and certain degree of marine reworking. No lime mud was observed and all the clasts were cemented by very finely to finely crystalline equant calcite cement. These suggest that sedimentation took place in very low energy and deep water marine environment, possibly below storm wave base where lime mud supply was very limited and biota rarely developed (Coniglio and Dix 1992). The bioclastic

packstone clasts contain abundant lime mud and up to 30 % bioclasts, which is unlikely to have deposited in deep water environment, therefore these bioclastic packstone clasts are interpreted to be extraclasts. Clast-rich crystalline rock lithofacies (LF 19) is interpreted to have deposited in fore slope to slope facies.

Brachiopod packstone lithofacies (LF 20)

Occurrence: brachiopod packstone lithofacies (LF 20) was observed in 2 intervals of the upper Dunedin Formation in 2 wells (c-54-K/94-N-16 and d-16-A/94-N-15). Core samples of brachiopod packstone lithofacies (LF 20) is ~ 100% dolomitized. Brachiopod dolopackstone (LF 20) comprises the uppermost ~ 4 m litho-unit of the 26.9 m recovered cored interval between 3527.0 and 3554.4 m in c-54-K/94-N-16, approximately 260 m above the Stone Formation and ~ 10 m below the Besa River Formation, where it overlies ~ 1.5 m of poorly recovered stromatoporoid dolobindstone (LF 17). Brachiopod dolopackstone (LF 20) occurs as two local thick beds (~ 15 to 25 cm) in the uppermost 6 m between 3650.0 and 3666.8 m in d-16-A/94-N-15, between ~ 215 m above the Stone Formation and ~ 10 m below the Besa River Formation.

Description: brachiopod dolopackstone (LF 20) is light and contains ~ 10 to up to 30 % fragments of robust brachiopod *Stringocephalus* sp. from 1 to up to 5 mm long (Fig. 3.20A), which is characterized by its thick punctate shell and brachial valves (Fig. 3.20B; Crickmay 1960; Braun et al. 1988). Up to 10% peloids that are < 0.1 mm in diameter

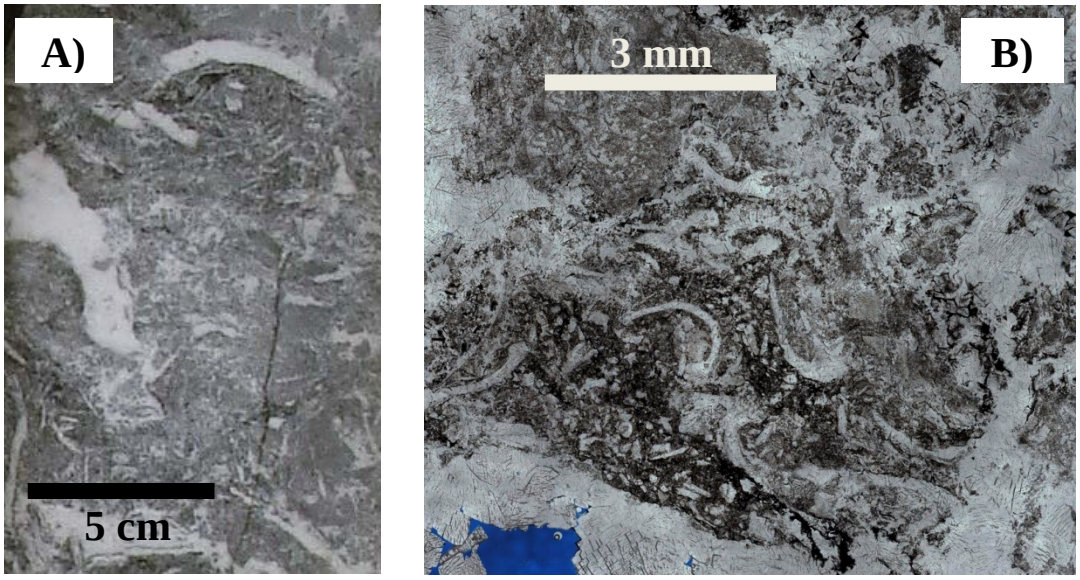

Figure 3.20A – B: Facies of the Dunedin Formation. A) Brachiopod bioclastic dolowackestone. c-54-K/94-N-16, 3527.0 – 3528.1 m. B) Petrographic photo of the sample in Fig. 3.20A at ~ 3527.0 m. Photo was taken by using the white card method outlined by Folk (1987). (original in color)

were observed. The matrix appears mud-supported. Grain-to-grain contacts were not preserved due to fabric-destructive dolomitization.

Interpretation: Givetian brachiopod *Stringocephalus* sp. is known to be common in reefal to reef edge environments (Crickmay 1960; Braun et al. 1989; Machel and Hunter 1994). These brachiopods were found broken and not in growth position in both studied core intervals in c-54-K/94-N-16 and d-16-A/94-N-15. This indicates that brachiopod packstone (LF 20) was deposited in high energy environment. Brachiopod packstone lithofacies (LF 20) has been interpreted to have deposited in fore reef to fore slope or reef flat settings by Nadjiwon (2001). The stratigraphic position where brachiopod packstone lithofacies (LF 20) is found further supports previous interpretations.

3.4 Summary

The lower to middle Stone Formation comprises of a subtle vertical facies transition from intertidal mudstones to lagoonal wackestones and amphiporid floatstone (Fig. 3.3). The upper Stone Formation in c-10-E/94-N-7 comprises of dominantly clast-rich silty dolomudstone to silty dolomudstone (LF 7; Fig. 3.3), which is interpreted to have deposited in peritidal settings and represent the middle Chinchaga depositional break caused by the middle Eifelian regression (Morrow 1978). Clast-rich silty dolomudstone to silty dolomudstone (LF 7) is sharply overlain by the silty to sandy mudstone (LF 8) of the lowermost Dunedin Formation, which is characterized by abundant finely crystalline equant calcite cement and lime mud of restricted shallow marine settings. The middle to upper Stone Formation comprises of a shallowing upward facies succession and the middle Chinchaga depositional break is represented by the clast-rich silty mudstone to silty mudstone lithofacies (LF 7) of peritidal origin in the study area. The deposition of the silty to sandy mudstone (LF 8) marks the end of the middle Chinchaga depositional break.

The Dunedin Formation comprises of a vertical facies transition from mudstones of restricted shallow marine origin, to reefal floatstones and boundstones, and to clast-bearing crystalline rock of slope facies (Fig. 3.3). These are interpreted to be a deepening upward sequence.

CHAPTER 4: Diagenesis

4.1 Introduction

The diagenesis of sediments is defined as all of the processes that affect sediments from immediately after deposition to metamorphism at elevated temperatures and pressure (Tucker 1981). Diagenetic processes in carbonate rocks may include mechanical and chemical compaction, cementation, dissolution, dolomitization and recrystallization. These processes result in modifications to the texture, mineralogy, chemistry and porosity of carbonate rocks (Tucker and Wright 1990).

Nineteen diagenetic phases were identified from the Stone and Dunedin formations during core examination and petrographic studies. A paragenetic sequence of these phases was defined based on their cross cutting relationships (Fig. 4.1). These diagenetic phases are further classified and characterized into 3 diagenetic settings (Machel 1999): near-surface, shallow burial, intermediate burial and deep burial settings (Fig. 4.2). These 3 settings are best elaborated by Lonnee (2005) as the following: “Near-surface diagenetic settings are defined as those within the first few meters of burial, where the pores are filled with interstitial fluids. Shallow burial diagenetic settings are similar to the near-surface diagenetic settings except that physical compression takes place and pore fluids can be altered or mixed with other diagenetic fluids. The lower boundary of the shallow burial diagenetic setting is placed at roughly 600 – 1000 m of burial, where chemical compaction takes place and stylolites develops which postdates earlier

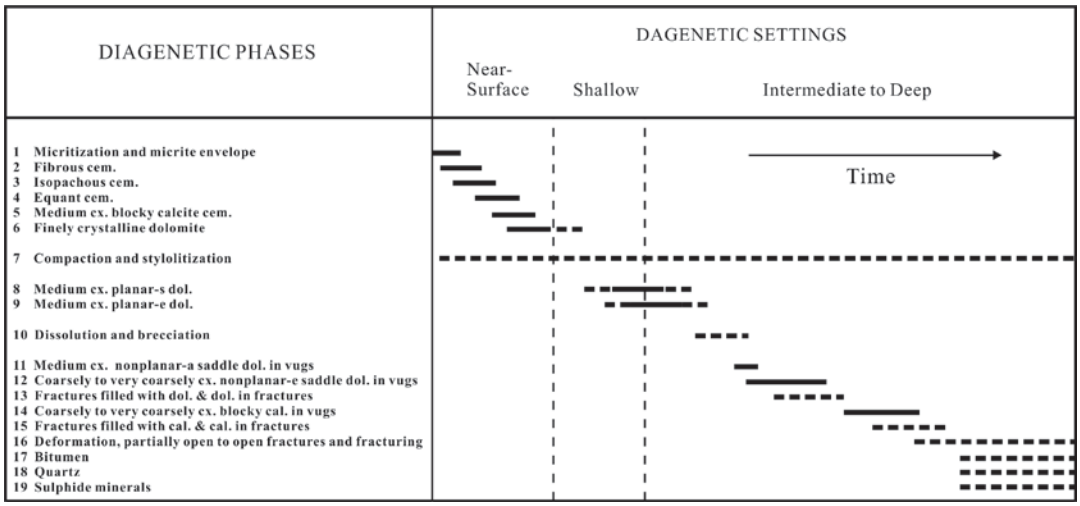

Figure 4.1: Diagenetic phases identified in the Stone and Dunedin formations during core examination and petrographic studies. Abbreviations: cem. = cement; cx. = crystalline; dol. = dolomite; cal. = calcite.

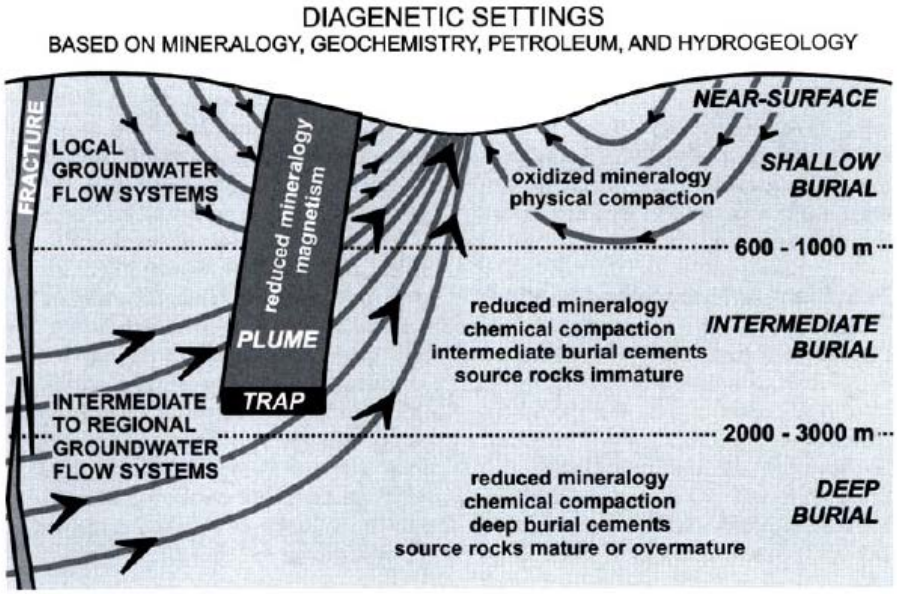

Figure 4.2: Classification of diagenetic settings on the basis on mieralogy, petrology, hydrogeochemistry, and hydrogeology. The depth limits separating the burial diagenetic settings are approximate and based on geologic phenomena that are easily recognizable. Near-surface settings may be meteoric, brackish, marine, or hypersaline (from Machel 1999; 2005).

developed diagenetic phases. Intermediate and deep burial diagenetic settings represent the zones of intense chemical compaction, cementation and dissolution. The limit between intermediate and deep burial diagenetic setting is defined relative to the top of the liquid oil window in hydrocarbon source rocks."

Six types of dolomite cement were observed and classified by their petrographic attributes (Fig. 4.3) which are to be discussed in this chapter. The luminescent brightness of different types of calcite and dolomite cements were documented, compared and described in a similar way to the study by Frank et al. (1982; Fig. 4.4).

Unlike the core-based sedimentological description in Chapter 3, diagenetic phases and their descriptions of this study are based on the 28 thin sections prepared from core samples from the Stone Formation and 90 thin sections prepared from the cores samples from the Dunedin Formation. All of which are from the 10 studied wells within the study area that is over 100 km wide and two formations that are over 400 m thick if combined. Therefore descriptions on diagenetic phases are descriptive rather than quantitative in order to avoid bias. The exception applies to coarsely to very coarsely crystalline nonplanar-e saddle dolomite in vugs (CSD) because the percentage abundance of CSD can be estimated by point counting on core photos.

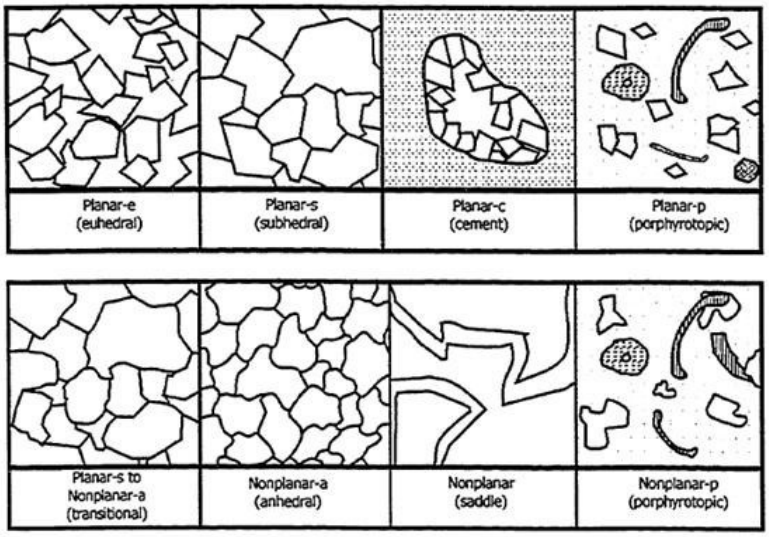

Figure 4.3: Textural classification of dolomite from Gregg and Sibley (1984), and Sibley and Gregg (1987). This diagram is from Wright (2001).

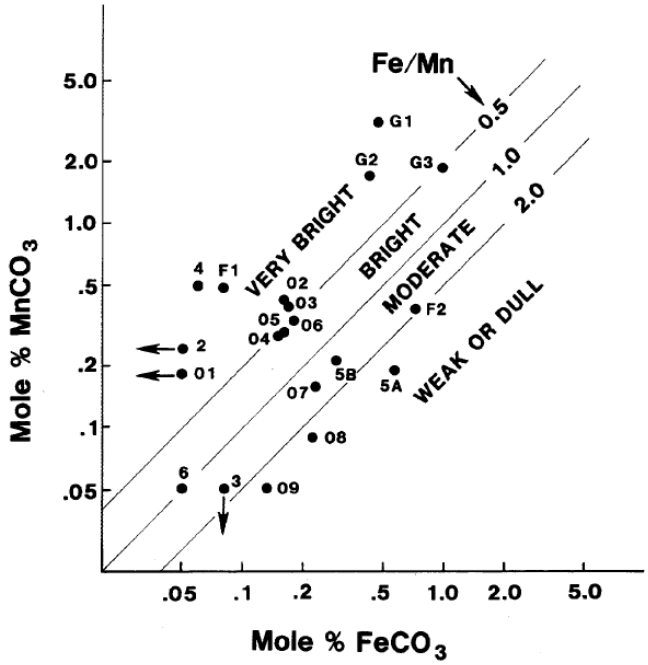

Figure 4.4: Relationship between concentration of $FeCO_3$ and $MnCO_3$ (mole %) and luminescence in calcite cements. Similar principle applies to dolomite. Original data (data points shown in the diagram) and diagram are from Frank et al. (1982).

4.2 Diagenetic phases

4.2.1 Near-surface diagenesis

A stratigraphic cross-section with the distribution of core sample and thin sections prepared is presented in Fig. 4.5. The arrows on the left of the cored intervals indicate that thin section(s) had been prepared from the cores recovered. Sample numbers were marked next to the arrows. Cores that are limestone to calcitic dolomite (0 to 90 % dolomite) are colored in blue; cores that are dolostone (91 to 100 % dolomite) are colored in purple.

Micritization and micrite envelope: Micritization widely occurs in peloids and lime mud. Micrite cement is ~ 5 to 10 μm (Figs. 4.6A and B). Micritie envelope is a very thin rim of micrite cement from ~ 10 to 30 μm thick that develops on fossil fragments. Micritization and micrite envelopes were observed in all 9 thin sections prepared from cores of the Dunedin Formation from the limestone to calcitic dolomite intervals in c-10-E/94-N-7 and c-16-A/94-N-15.

Fibrous cement: Fibrous cement is typically elongated and ~ 10 to 20 μm long and ~10 μm wide (Figs. 4.6A and B). Fibrous cement postdates micrite envelope. Fibrous cement was observed in 7 out of 9 thin sections prepared from cores of the Dunedin

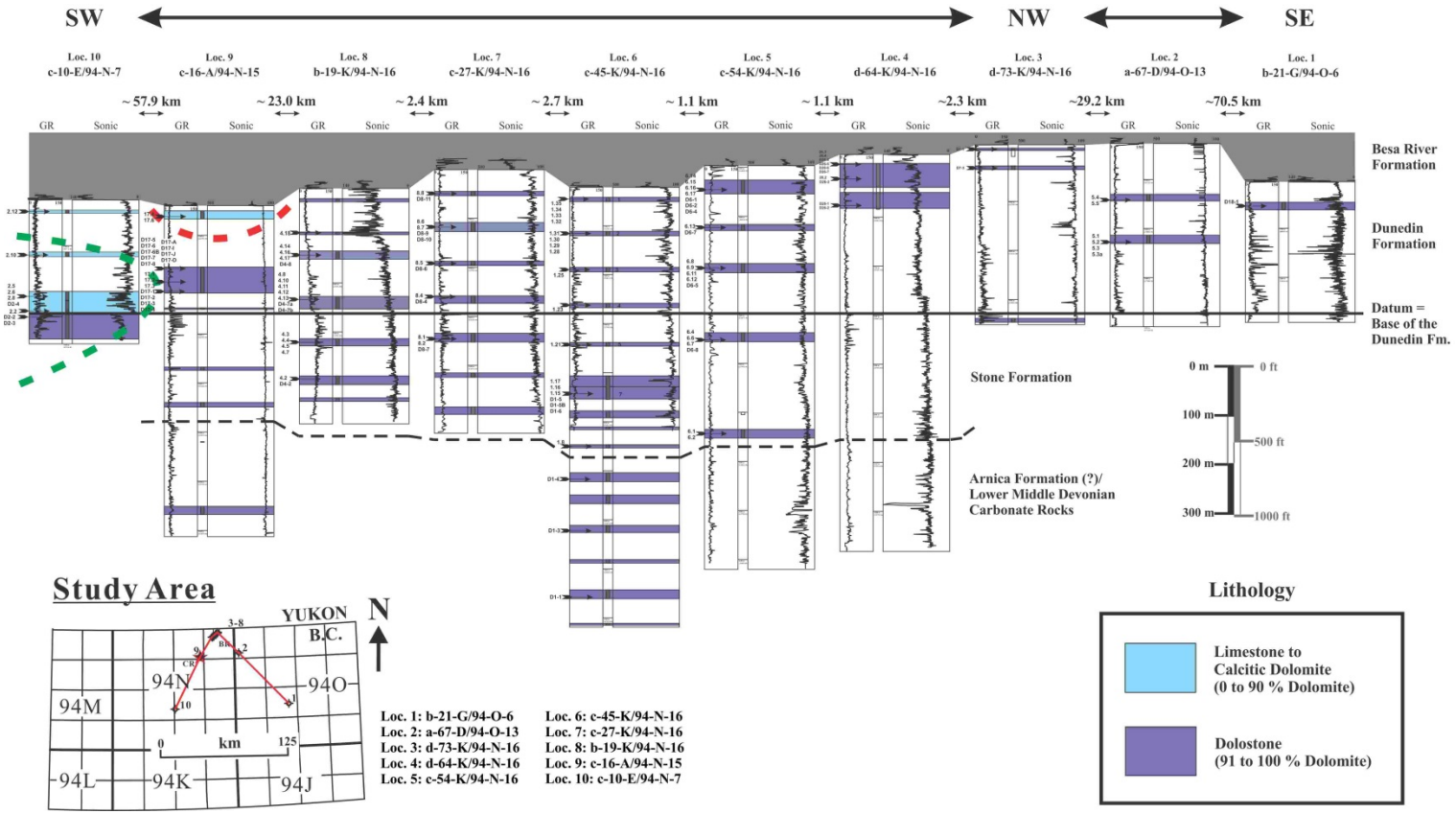

Figure 4.5: Stratigraphic cross-section of the Stone and Dunedin formations (including Lower Middle Devonian Arnica Formation?) constructed with gamma ray and sonic logs of the studied 10 wells. Cores that are limestone and calcitic dolomite (0 to 90 % dolomite) are colored in blue. Cores that are dolostone (91 to 100 % dolomite) are colored in purple. The base of the Dunedin Formation is used as the datum. The red dotted line (upper left) circles the interval where FCD was not observed. The green dotted line (upper left) circles the interval where MCD-1 was not observed. The horizontal scale of this cross-section is not in proportion. (original in color)

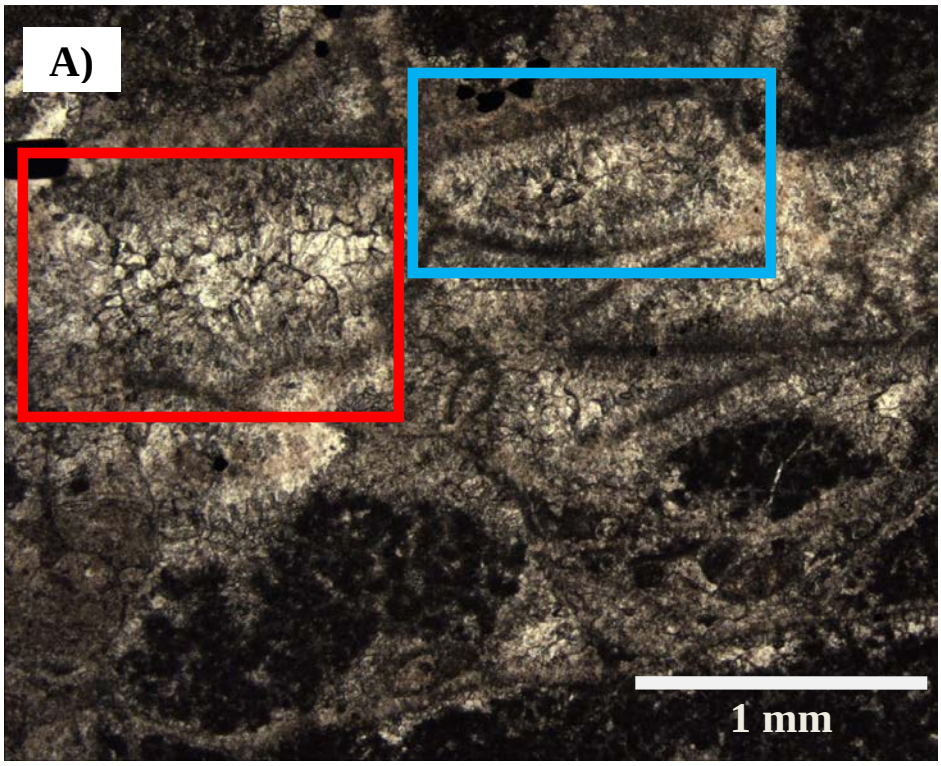
A)
1 mm

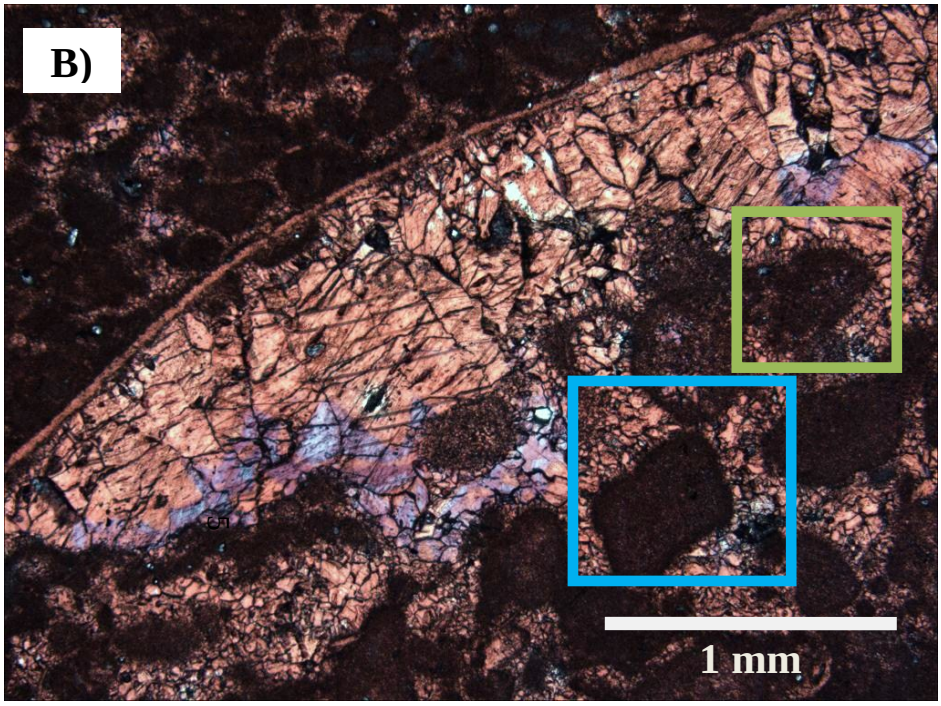
B)
1 mm

Figure 4.6A – B: Submarine to subsurface diagenetic features in limestone: A) photomicrograph of an unstained thin section showing a colonial coral fragment in peloidal grainstone. Blue square: micrite envelope around the tube of the colonial coral fragment and very finely crystalline isopachous cement around and within a tube of the colonial coral fragment. Red square: equant cement inside the tube of a colonial coral fragment. c-10-E/94-N-7, 1630.4 m. B) Photomicrograph of an unstained thin section showing a peloid grainstone and which comprises a shell fragment. Green square: micritized peloids; micrite envelopes are well-developed around the peloids; fibrous cement at the tip of a peloid. Blue square: Equant cement is well-developed in the interparticle pores. Medium crystalline blocky calcite cement in the now cemented shelter pore. Medium crystalline blocky calcite cement also shows gradational blue to purple stain. c-10-E/94-N-7, 1810.9 m. (original in color)

Formation from the limestone to calcitic dolomite intervals in c-10-E/94-N-7 and c-16-A/94-N-15.

Isopachous cement: Isopachous cement is typically elongated and ~ 20 to 40 µm long and ~10 µm wide (Figs. 4.6 and B). Isopachous cement postdates micrite envelopes and fibrous cement. Isopachous cement was observed in 7 out of 9 thin sections prepared from cores of the Dunedin Formation from the limestone to calcitic dolomite intervals in c-10-E/94-N-7 and c-16-A/94-N-15.

Equant cement: Equant cement is typically rounded and in polygonal shape and from ~ 20 to 100 µm in size (Figs. 4.6A and B). Equant cement is well developed around skeletal grains, and in primary fenestral, interparticle and shelter pores. Equant cement postdates isopachous cement. Equant cement was observed in all 9 thin sections

prepared from cores of the Dunedin Formation from the limestone to calcitic dolomite intervals in c-10-E/94-N-7 and c-16-A/94-N-15.

4.2.2 Shallow burial diagenesis

Medium crystalline blocky calcite cement: Medium crystalline blocky calcite cement is blocky, subhedral to euhedral, and ~ 50 to up to 200 µm in diameter (Fig. 4.6B). Medium crystalline blocky calcite cement appears blue to purple in a few stained limestone samples. This indicates that medium crystalline blocky calcite cement was precipitated from fluid(s) with elevated Fe^{2+} in composition and which suggests anoxic settings. Medium crystalline blocky calcite cement postdates equant cement and other near-surface diagenetic phases. Under cathodoluminescence, blocky cement is non-luminescent. Medium crystalline blocky calcite cement was observed in all 9 thin sections prepared from cores of the Dunedin Formation from the limestone to calcitic dolomite intervals in c-10-E/94-N-7 and c-16-A/94-N-15.

Finely crystalline dolomite(s) (FCD): FCD appears grey and occurs as patches in core samples (Fig. 4.7A). For geochemical studies and comparison, FCD samples were divided into 2 categories based on the lithological units where they were collected: FCD in limestone to calcitic dolomite and FCD in dolostone. However, FCD in both categories exhibit uniform petrographic features: they are white to brownish white (Figs.

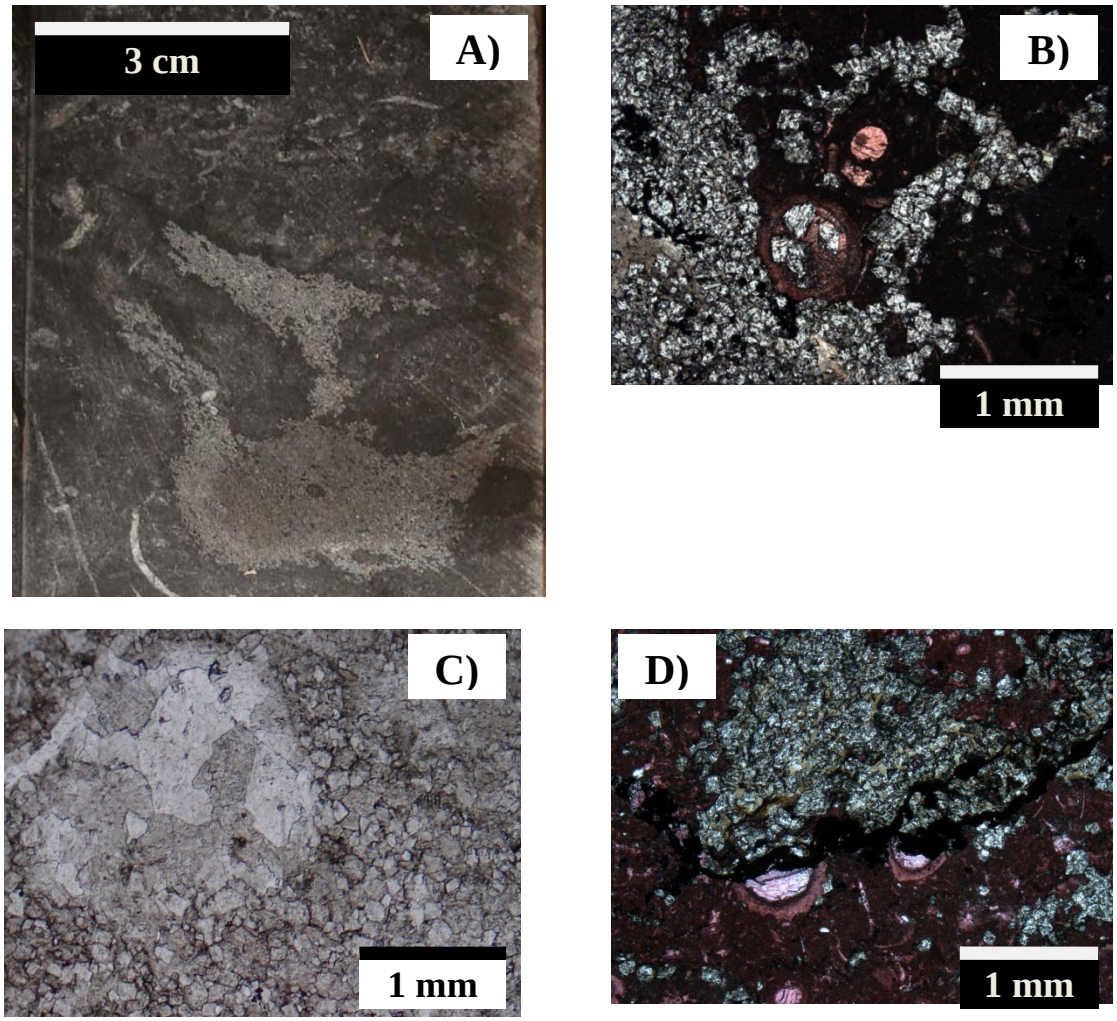

Figure 4.7A – D: Finely crystalline dolomite(s). A) Finely crystalline dolomite in limestone to calcitic dolomite (FCD in limestone to calcitic dolomite) on the polished surface of a limestone core. c-10-E/94-N-7, 1720.4 – 1720.3 m. B) Thin section photomicrograph of finely crystalline dolomite in limestone to calcitic dolomite (FCD in limestone to calcitic dolomite). c-10-E/94-N-7, 1802.4 m. C) Thin section photomicrograph of finely crystalline dolomite in dolostone (FCD in dolostone). b-19-K/94-N-16, 4034.0 m. D) Photomicrograph showing horizontal stylolites wrap around FCD in limestone to calcitic dolomite. c-10-E/94-N-7, 1802.4 m. (original in color)

4.7B and C), subhedral, exhibits planar extinction, and from 10 to 50 µm in diameter. Under cathodoluminescence, FCD exhibits weak to very weak luminescence. FCD postdates medium crystalline blocky calcite. In one thin section sample from c-10-E/94-N-7, 1802.4 m, FCD is wrapped by a mm-thick, low amplitude stylolites (Fig. 4.7D). FCD was observed in nearly all of the thin sections prepared from limestone to calcitic dolomite and dolostone core samples from the Stone and Dunedin formations, except for the thin sections of the cores from the uppermost limestone to calcitic dolomite core interval in c-16-A/94-N-15 (Fig. 4.5).

Compaction and stylolitization: Compaction of sedimentary rocks occurs upon deposition continues throughout the burial history (Choquette and James 1987). Stylolites develop from pressure solution in which is resulted from burial compaction and compression (Dunnington 1967). Stylolitization starts from about 300 to 500 m, becomes significant beyond >1000 m, and continues throughout burial history. Stylolites in horizontal form can be logically interpreted as a product of burial compaction, or compaction from atop (Choquette and James 1987). On the other hand, stylolites in vertical form can be interpreted as a product of horizontal to sub-horizontal compression, presumably through local structural development or regional tectonic events (Qing 1991). In this study, stylolites are not classified into horizontal or vertical stylolites. It is because this is a core-based study which observations were made from ~11 cm-wide core samples. Any high amplitude stylolites could be mistaken as vertical stylolites. Stylolites was observed in a sample of calcitic dolomite in c-10-E/94-N-7

(Fig. 4.7D), which a stylolites wraps the FCD. Stylolites postdates multiple diagenetic features but it is also postdated by the same diagenetic features. This is possible because stylolitization occurs in a continuous fashion. Stylolites were observed in almost all limestone to calcitic dolomite and dolostone core samples and thin sections that were prepared from those core samples.

Medium crystalline planar-s dolomite (MCD-1): MCD-1 appears medium grey in core samples and brownish white in 30 µm-thick thin section (Figs. 4.8A and B). It is subhedral and ~ 50 to 120 µm in diameter. Under cathodoluminescence, MCD-1 exhibits weak to moderate luminescence (Fig. 4.8C). MCD-1 postdates FCD. MCD-1 was observed in most of the thin sections except those from the cored intervals in the Stone Formation and lower interval of the Dunedin Formation in c-10-E/94-N-7 (Fig. 4.5).

4.2.3 Intermediate to deep burial diagenesis

Medium crystalline planar-e dolomite (MCD-2): MCD-2 is light grey in core samples and light grey in 30 µm-thick thin section (Figs. 4.9A and B). It is euhedral and exhibits planar extinction, from ~ 50 to 200 µm in diameter (Fig. 4.9C). Under cathodoluminescence, MCD-2 exhibits moderate luminescence (Fig. 4.9D). MCD-2 postdates MCD-1 as seen in Fig. 4.8B. MCD-2 was observed in nearly half of the thin

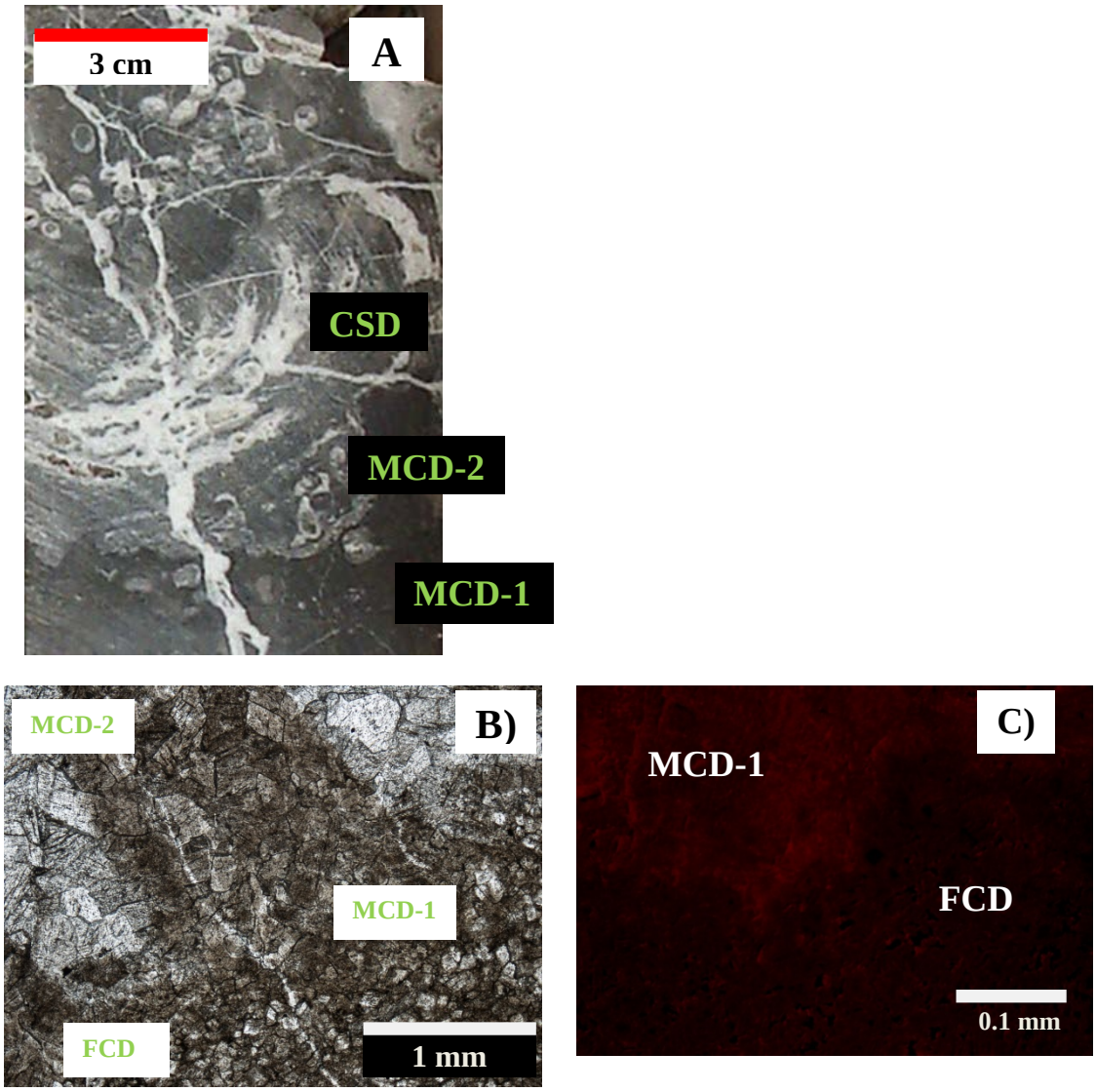

Figure 4.8A – C: Medium crystalline dolomites. A) Core photo showing medium crystalline planar-s dolomite (MCD-1; medium grey), medium crystalline planar-e dolomite (MCD-2; light grey) and coarsely to very coarsely crystalline nonplanar-e saddle dolomite in vugs (CSD; white). b-19-K/94-N-16, 4191.8 – 4192.0 m. B) Photomicrograph of a 100 um-thick thin section showing finely crystalline dolomite in dolostone (FCD in dolostone), MCD-1 (brown) and MCD-2 (white). c-54-K/94-N-16, 3697.9 m. C) The same sample in Fig. 4.8A. Photomicrograph of FCD in dolostone and MCD-1 under cathodoluminescence. FCD in dolostone exhibits weak to almost no luminescence; MCD-1 exhibits weak to moderate luminescence. (original in color)

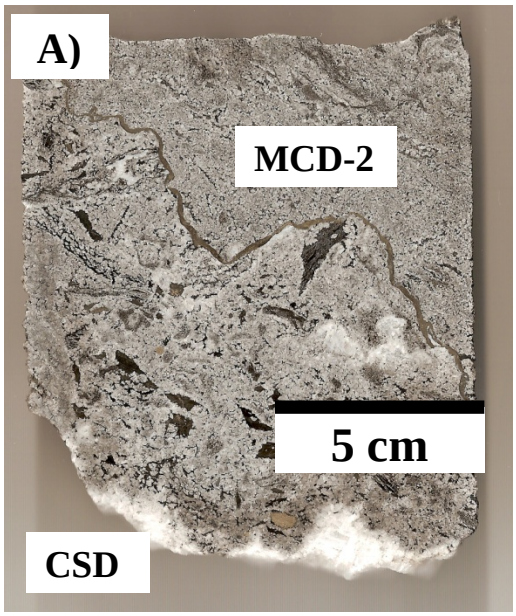
A)
MCD-2
5 cm
CSD

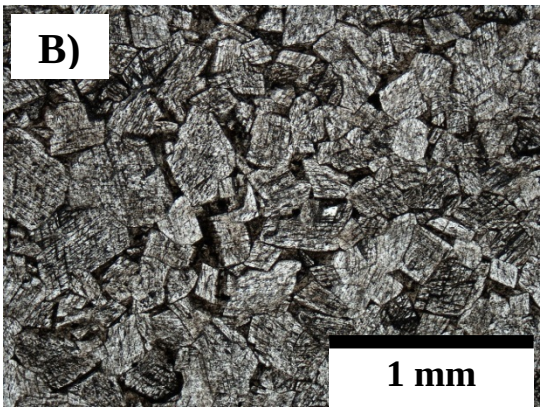
B)
1 mm

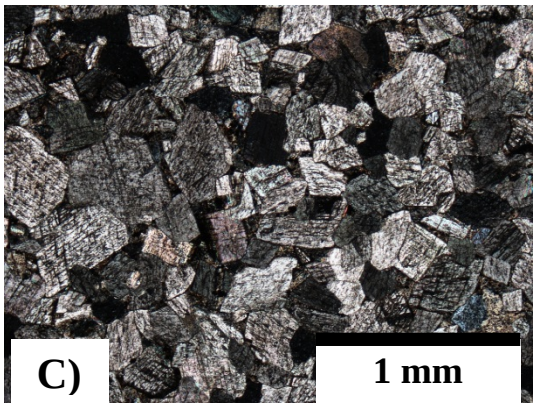
C)
1 mm

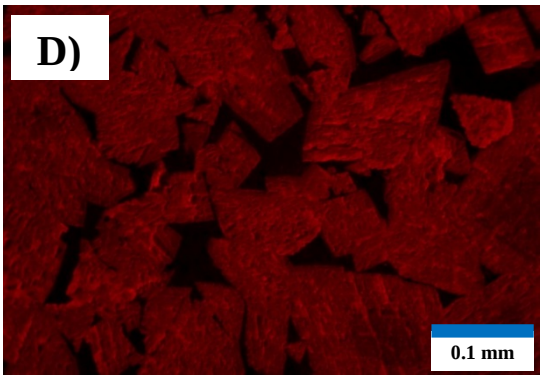
D)
0.1 mm

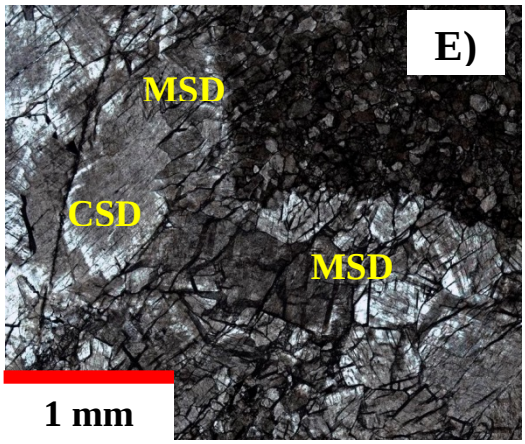
E)
MSD
CSD
MSD
1 mm

Figure 4.9A – E: Medium crystalline planar-e dolomite. A) A core that is comprised of dominantly medium crystalline planar-e dolomite (MCD-2; light grey). d-16-A/94-N-15, 3781.8 m. B to D) Photomicrograph of MCD-2 from a sample in c-54-K/94-N-16, 3846.1 m. B) Taken under plane-polarized light (PPL); C) Taken under cross-polarized light (XPL); D) Taken under cathodoluminescence. MCD-2 exhibits moderate luminescence. This image is best seen in digital copy. E) Medium crystalline nonplanar-a saddle dolomite in vugs (MSD) and coarsely to very coarsely crystalline nonplanar-e saddle dolomite in vugs (CSD). A 100-µm thick, doubly polished thin section is used for demonstration because MSD stands out in photomicrograph as the thin section is thicker and is better polished. c-45-K/94-N-16, 4324.1 m. (original in color)

sections prepared from dolostone cores from the Stone and Dunedin formations (Fig. 4.5). It is also commonly associated with CSD.

Dissolution and brecciation: Dissolution and brecciation, and their classifications, patterns and possible processes, were documented by Nadjiwon (2001) and published by Davies and Smith (2006). Features of dissolution and brecciation postdates MSD-2 and appear have developed contemporaneously with MSD and CSD, or immediately after CSD. Dissolution and brecciation are not in the scope of this study due to budget consideration, availability of analytical facilities, and most importantly the investigation cannot generate critical result on linking the timing of dolomitization to tectonic development, as well as supporting the sedimentological analysis of the Stone and Dunedin formations, which are the focuses of this thesis.

Medium crystalline nonplanar-a saddle dolomite in vugs (MSD): MSD is white in 30 µm-thick thin section and light grey in 100 µm-thick thin section which the photomicrograph was taken in Fig. 4.9E. MSD is anhedral, exhibit weak undulose extinction, and ~ 50 to 200 µm in diameter. Under cathodoluminescence, MSD exhibits bright luminescence. MSD postdates MCD-2. MSD appears to precipitate just before CSD and MSD resembles chill margin in extrusive volcanic rocks. MSD was only observed in several very polished thin section samples. It cannot be identified in core samples but it is closely associated with CSD (Fig. 4.9E). Therefore the distribution of MSD is not reported in order to avoid bias.

Coarsely to very coarsely crystalline nonplanar-e saddle dolomite in vugs (CSD): CSD is white in 30 µm-thick thin section, euhedral, exhibits undulose extinction, and ~0.2 to up to 2 cm in diameter (Figs. 4.10A and B). Under cathodoluminescence CSD exhibits bright to very bright luminescence and shows compositional zoning (Figs. 4.10C and D). CSD postdates MSD and MCD-2. CSD was observed exclusively in thin sections prepared from the cores of dolostone, which CSD was observed in almost all of them. CSD comprises over 20% of the lithological units in the middle to upper middle strata of the Dunedin Formation based on point counting on core photos (Fig. 4.11; see Methodology in Chapter 1). The lower limit where CSD comprises of 1% of the lithological units is marked by a green dotted line.

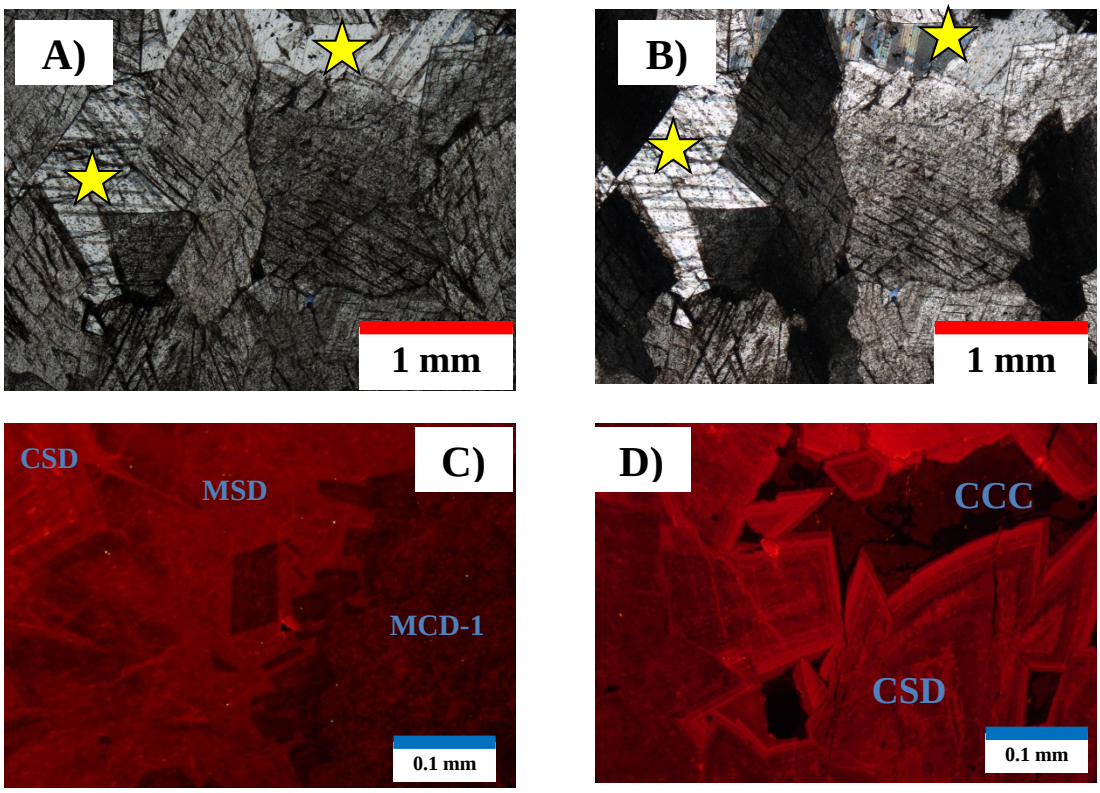

Figure 4.10A – D: Photomicrographs of diagenetic phases. Medium crystalline planar-s dolomite (MCD-1), medium crystalline nonplanar-a saddle dolomite in vugs (MSD), coarsely to very coarsely crystalline nonplanar-e saddle dolomite in vugs (CSD) and coarsely to very coarsely crystalline blocky calcite in vugs (CCC). c-45-K/94-N-16, 4324.1 m. A) Photomicrograph of CSD and CCC taken under Plane-polarized light (PPL). B) Photomicrograph of CSD and CCC under cross-polarized light (XPL). C – D) Photomicrographs taken under cathodoluminescence. C) MCD-1 exhibits weak to moderate luminescence; MSD exhibits bright luminescence; and CSD exhibits bright to very bright luminescence. D) CSD exhibits bright to very bright luminescence; CCC exhibits weak to moderate luminescence. These images are best seen in digital copy. (original in color)

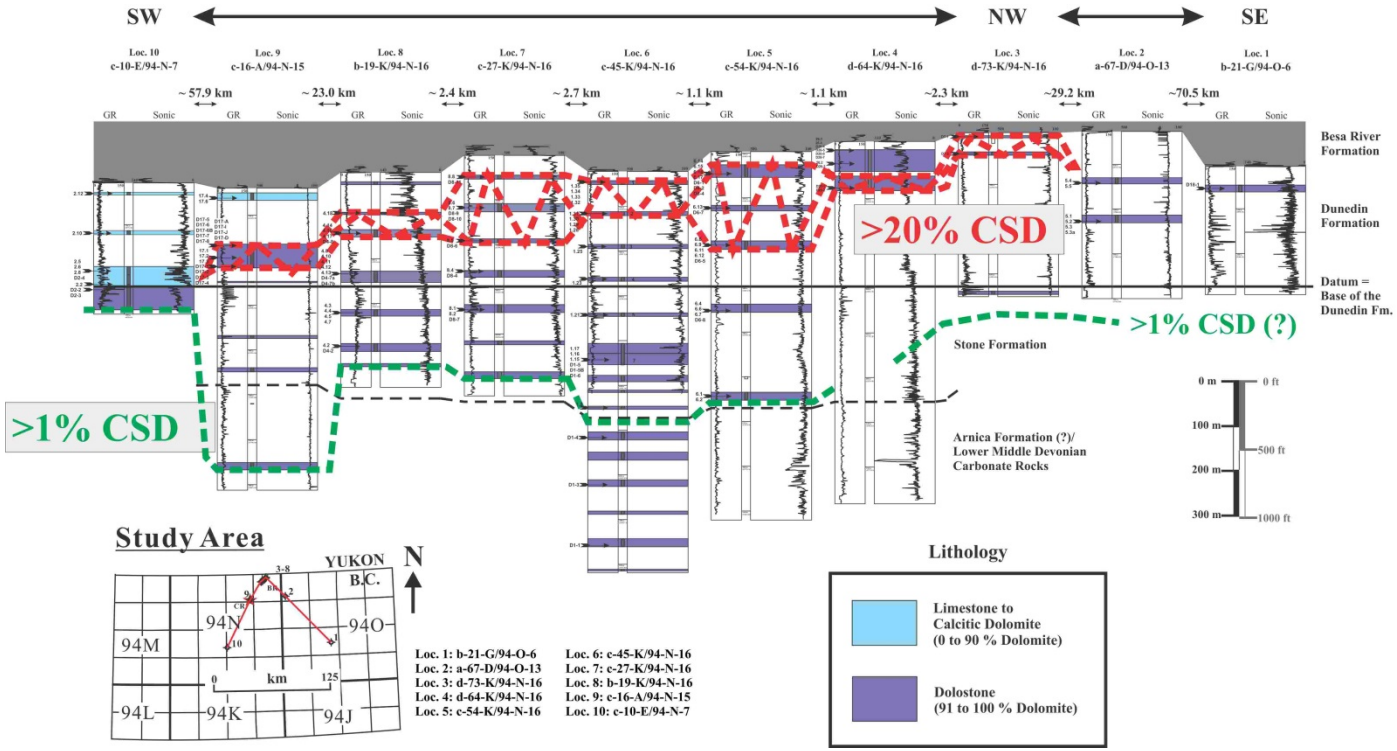

Figure 4.11: Stratigraphic cross-section of the Stone and Dunedin formations (including Lower Middle Devonian Arnica Formation?) constructed with gamma ray and sonic logs of the studied 10 wells. Cores that are limestone and calcitic dolomite (0 to 90 % dolomite) are colored in blue. Cores that are dolostone (91 to 100 % dolomite) are colored in purple. The base of the Dunedin Formation is used as the datum. The red dotted line highlights the interval where CSD comprises >20% of the lithological unit. The green dotted line marks the boundary where CSD comprises >1% of the lithological unit. The horizontal scale of this cross-section is not in proportion. (original in color)

Fractures filled with dolomite (FD) and dolomite in fractures (DIF): FD are typically 15 to 90 cm long and 1 to 20 mm wide (Fig. 4.12A). DIF is white in 30 µm-thick thin section (Fig. 4.12B), fine to coarsely crystalline, anhedral to euhedral, and ~ 50 to 1000 µm in diameter, all of which depend on the fracture width where DIF was precipitated. Undulose extinction in DIF was rarely observed. Under cathodoluminescence, DIF exhibits bright luminescence (Figs. 4.13A and B). FD postdate MSD and MCD-2. FD appear to have developed contemporaneously with or immediately after CSD (Figs. 4.13A and B). FD were typically observed in cores where CSD is abundant.

Coarsely to very coarsely crystalline blocky calcite in vugs (CCC): CCC is translucent in 30 µm-thick thin section (Fig. 4.14A), blocky, euhedral and from ~ 0.2 to up to 2 cm in diameter. Under cathodoluminescence, CCC exhibits weak to moderate luminescence (Fig. 4.14B). CCC postdates CSD and FD (Figs. 4.14C and D). CCC was observed in almost all cored intervals and some of the thin sections from the limestone to calcitic dolomite and dolostone core samples from the Stone and Dunedin formations. CCC was typically observed in the vuggy and intercrystalline pores.

Fractures filled with calcite (FC) and calcite in fractures (CIF): FC are typically 15 to 90 cm long and 1 to 15 mm wide (Fig. 4.14C and D). CIF is translucent in 30 µm-thick thin section, fine to coarsely crystalline, anhedral to euhedral, and ~ 50 to 1000 µm in

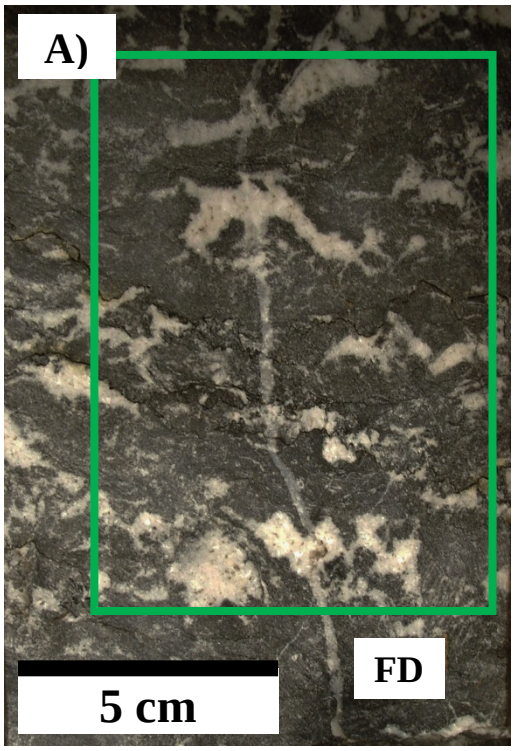

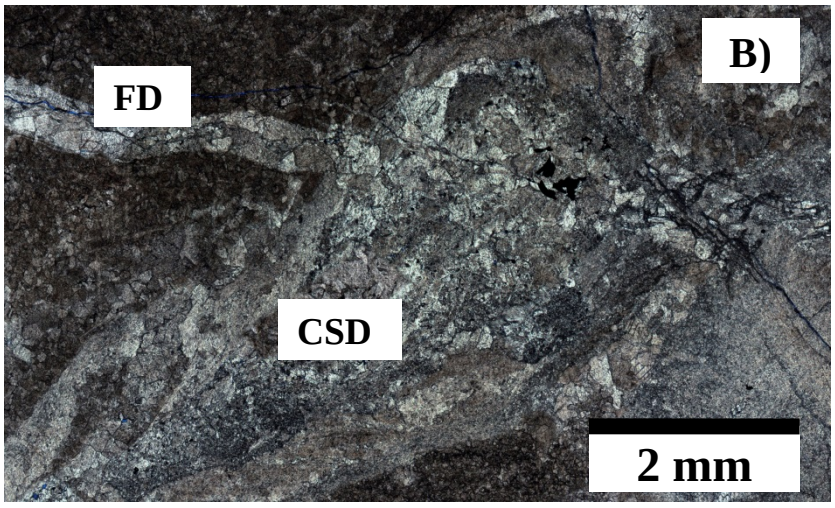

Figure 4.12A – B: Fractures filled with dolomite (FD). A) A fracture filled with dolomite (FD) cuts through coarsely to very coarsely crystalline nonplanar-e saddle dolomite in vugs (CSD). A network of stylolites postdates the same FD. c-54-K/94-N-16, 3867.7 – 3867.5 m. B) Photomicrograph of CSD in a moldic pore that resembles a dissolved amphipora. A FD cuts into the CSD. c-45-K/94-N-16, 4038.3. (original in color)

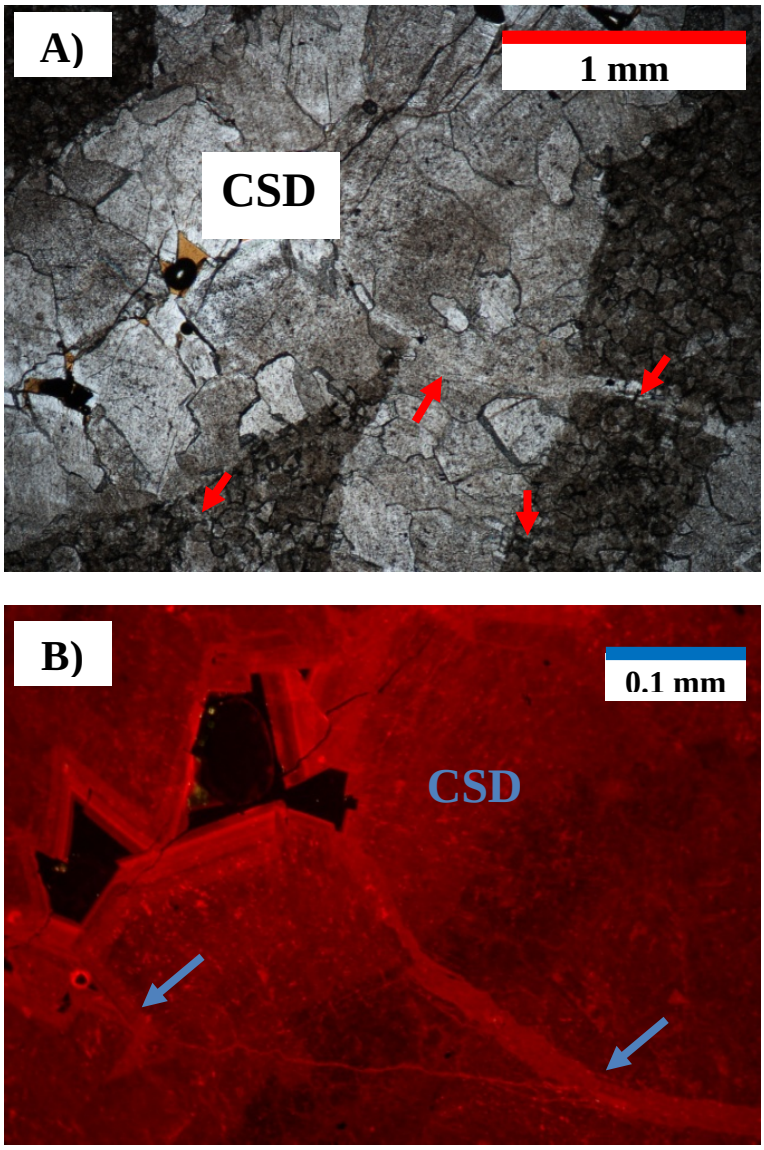

Figure 4.13A – B: Diagenetic phases. A) Photomicrograph of coarsely to very coarsely crystalline nonplanar-e saddle dolomite in vugs (CSD) being cut by two fractures filled with dolomite (FD; red arrows). The matrix is medium crystalline planar-s dolomite (MCD-1). d-16-A/94-N-15, 3810.9 m. B) Photomicrograph of the same thin section sample in Fig. 4.13A under cathodoluminescence. MCD-1 exhibits moderate luminescence. CSD exhibits bright to very bright luminescence. Within the two FD (blue arrows), the dolomite in fracture (DIF) shows bright luminescence. The narrower FD in the lower half of the photomicrograph overlaps both the CSD and the wider FD. (original in color)

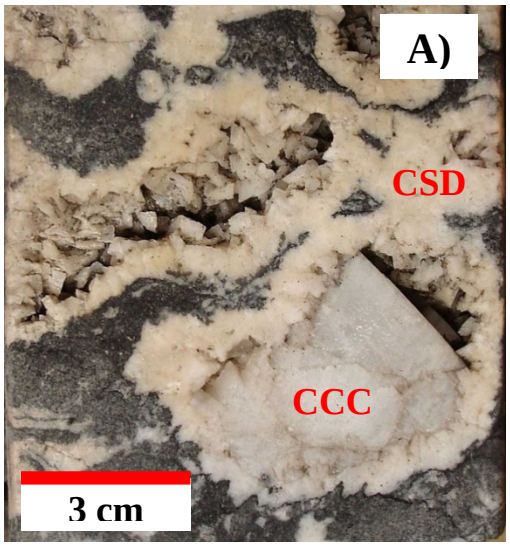
A)
CSD
CCC
3 cm

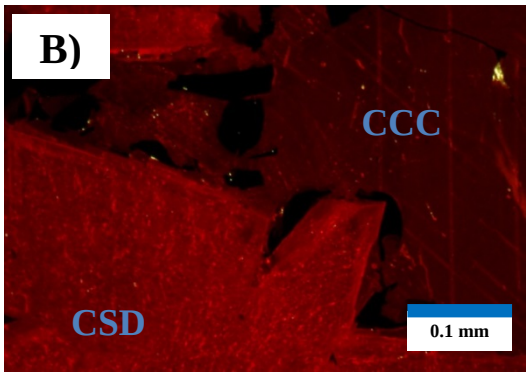
B)
CCC
CSD
0.1 mm

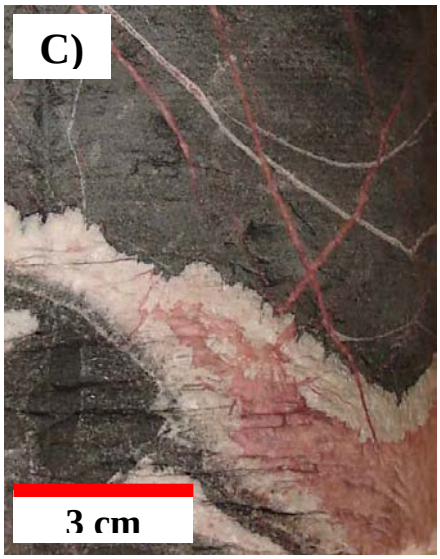
C)
3 cm

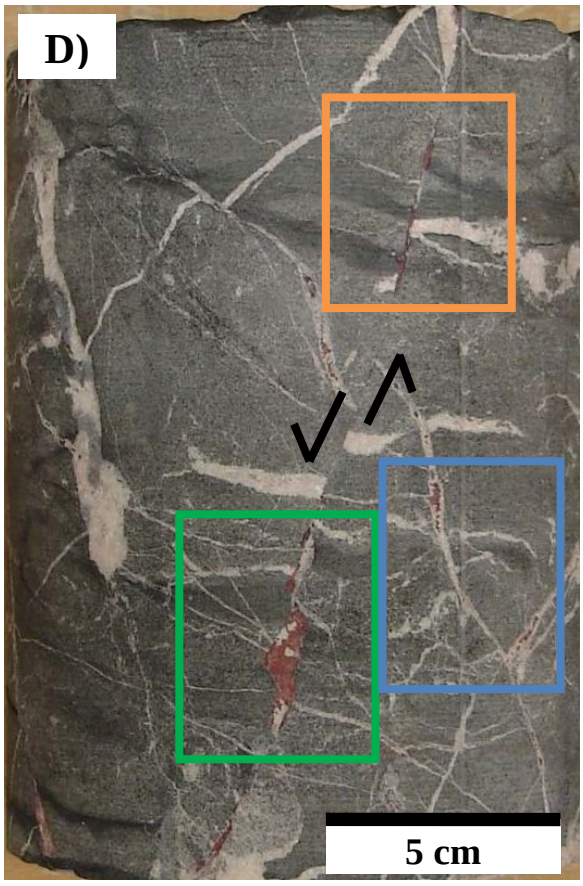
D)
5 cm

Figure 4.14A – D: Diagenetic phases. A) Core photo of coarsely to very coarsely crystalline nonplanar-e saddle dolomite in vugs (CSD) and coarsely to very coarsely crystalline blocky calcite in vugs (CCC). d-73-K/94-N-16, 3783.6 – 3783.7 m. B) Photomicrograph taken under cathodoluminescence. CSD exhibits bright to very bright luminescence; CCC exhibits weak to moderate luminescence. The opaque crystals are sphalerite. d-16-A/94-N-15, 3779.4 m. C) CSD and CCC. Fractures filled with dolomite (FD) were vertically displaced by Fractures filled with calcite (FC) (upper half of the photo). Also FC cut into CSD and appear cutting into CCC. d-16-A/94-N-15, 3768.1 – 3768.2 m. D) Coarsely to very coarsely crystalline nonplanar-e saddle dolomite in vugs (CSD) is vertically displaced (the arrows indicate the direction of displacement). CCC appears both vertically displaced (in green rectangle) and cemented along a vertical joint (in orange rectangle). Calcite cement also occurs within a FD (in blue rectangle). d-16-A/94-N-15, 3811.8 – 3812.1 m. (original in color)

diameter, all of which depend on the fracture width where CIF was precipitated. CIF exhibits weak luminescence. FC postdate CSD and FD. FC appear to have developed contemporaneously with or immediately after CCC. FC were typically observed in where CCC is abundant.

Deformation, partially open to open fractures (POF) and fracturing: Deformational structures were observed in cores and thin section prepared from cores. CSD and FD were displaced along fractures (Figs. 4.15A and B). Some styolites were found vertically aligned along a fracture (Figs. 4.15A and B). In one thin section sample from d-64-K/94-N-16, 3570.5 m, a stylolites was vertically displaced along a fracture. POF were commonly observed in the cores of the Stone and Dunedin formations. The length and width of the fractures varied from milometers to centimeters. Fractures resulted

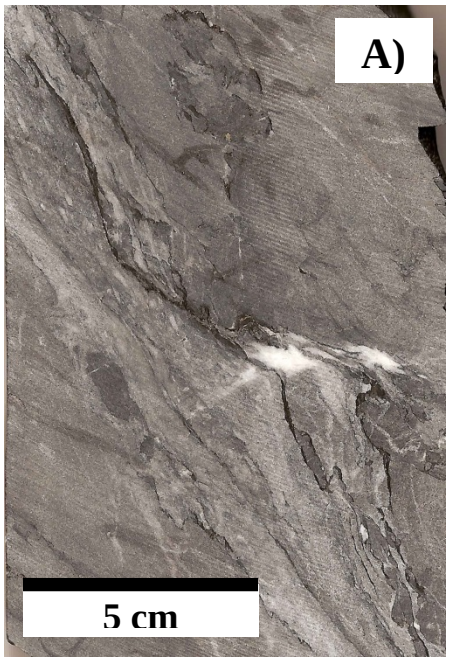
A)
5 cm

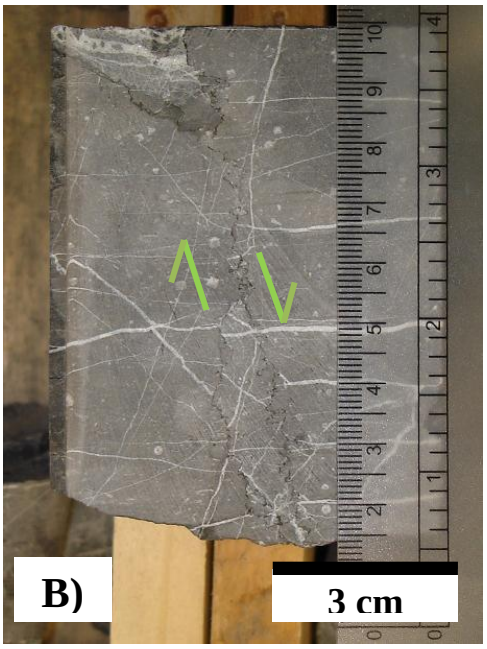
B)
3 cm

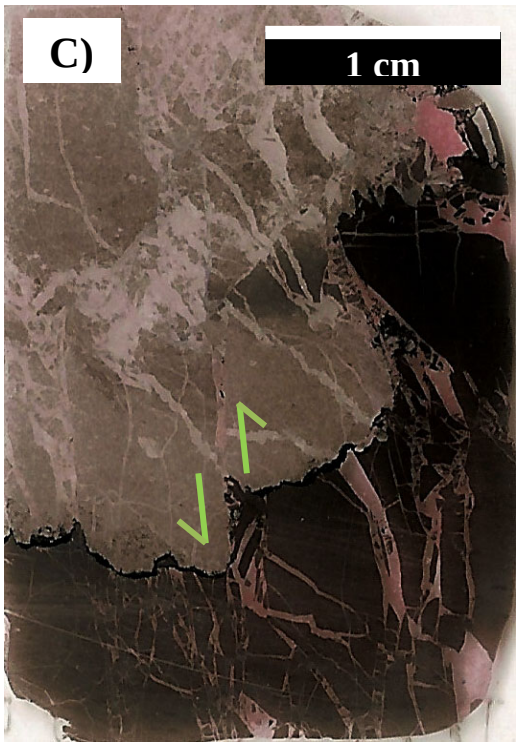
C)
1 cm

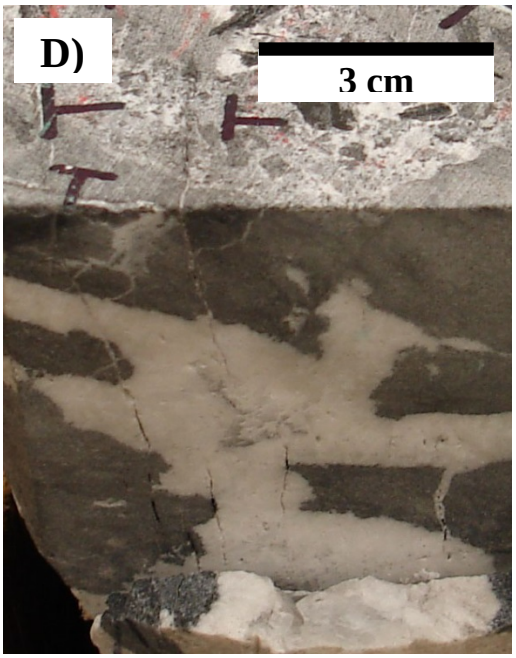
D)
3 cm

Figure 4.15A – D: Deformation structures. A) Vertical stylolites postdate coarsely to very coarsely crystalline nonplanar-e saddle dolomite in vugs (CSD). a-67-D/94-O-13, 5139.1 – 5139.3 m. B) Displacement of fractures fill with dolomite (FD) along a slickenline. Vertical stylolites were observed along the slickenline. c-45-K/94-N-16, 4324.0 – 4324.2 m. C) Scanned image of a stained thin section image showing a vertical displacement and which postdates horizontal stylolites, CSD and coarsely to very coarsely crystalline blocky calcite in vugs (CCC). The arrows indicate the direction of displacement. The horizontal stylolites postdates CSD and CCC. d-64-K/94-N-16, 3570.5 m. D) Partially to completely open fractures (POF). POF postdate CSD. d-16-A/94-N-15, 3766.3 – 3766.5 m. (original in color)

from core recovering and laboratory examination cannot be differentiated from fractures resulted from structural events. However, it was observed that almost all POF postdate CSD and CCC in the Stone and Dunedin formations (Fig. 4.15D). Moreover, the vitrinite reflectance study by Morrow et al. (1993) indicated that the Stone and Dunedin formations were progressively buried shortly after deposition. Major burial event occurred at the end of Devonian to early Mississippian during the Antler Orogeny. The first major structural folding occurred after the deposition of Mississippian Mattson Formation (Fig. 4.16). The strata have been deformed over 3 stages (F1 to F3; Fig. 4.16), in which the F1 folding postdates the deposition of Mississippian Mattson Formation. This suggests that the F1 occurred after the Middle Mississippian. The F1 folding was followed by the F2 faulting and F3 faulting (Fig. 4.16). The folded blocks were further displaced and split into thrust sheets during the F2 faulting. This is followed by the F3 thrusting that created a kilometer-scale reverse fault that cut both F1 fold and F2 thrust sheets. Two fracture development patterns during stage 1 and 2 were

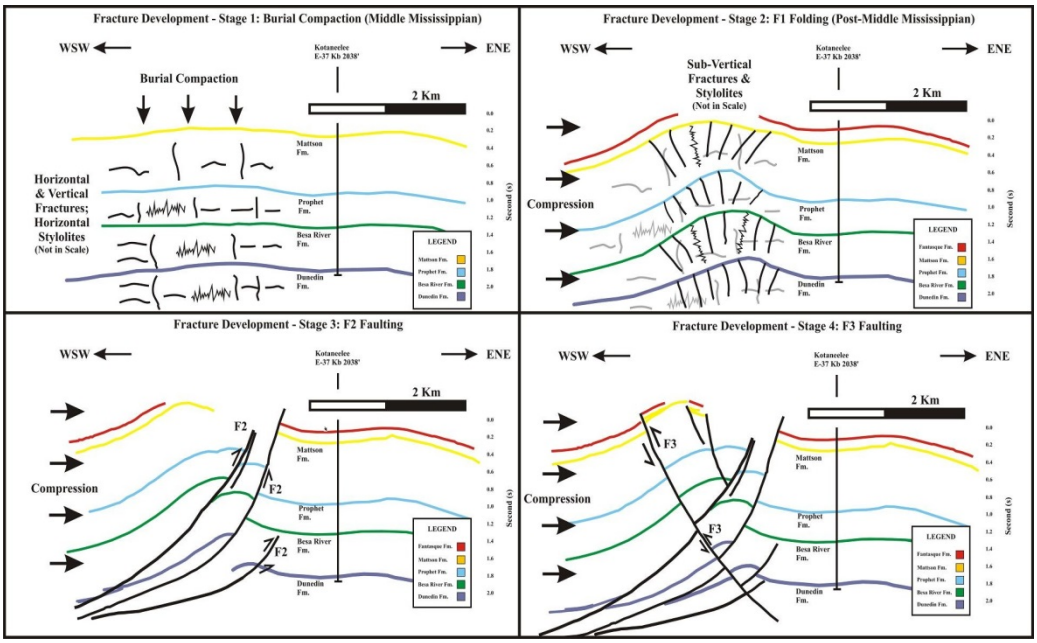

Figure 4.16: A schematic diagram illustrating the structural deformation of the Devonian and Mississippian strata near the Beaver River gas field and adjacent area in NE British Columbia and SE Yukon. This illustration is based on the seismic profile published by the Government of Yukon, Oil and Gas Resources Branch (2001). Structural deformation and fracture development developed over 4 stages (Stage 1 to 4) with 3 major structural deformations (F1 to F3 from Stage 2 through 4). (original in color)

sketched based on the possible stress orientation as indicated by the seismic profile and stratal deformation style (Fig. 4.16). Fracture development over stage 3 and 4 can be resulted from thrusting, faulting and possibly transform displacement, these are far more complicated than the deformation and fracturing pattern resulted during stage 1 and 2, which cannot be deducted from a single one-dimension seismic profile.

Bitumen: Bitumen is not included in this research due to poorly defined cross-cutting relationship, which cannot lead to critical interpretation. Bitumen is common and it was

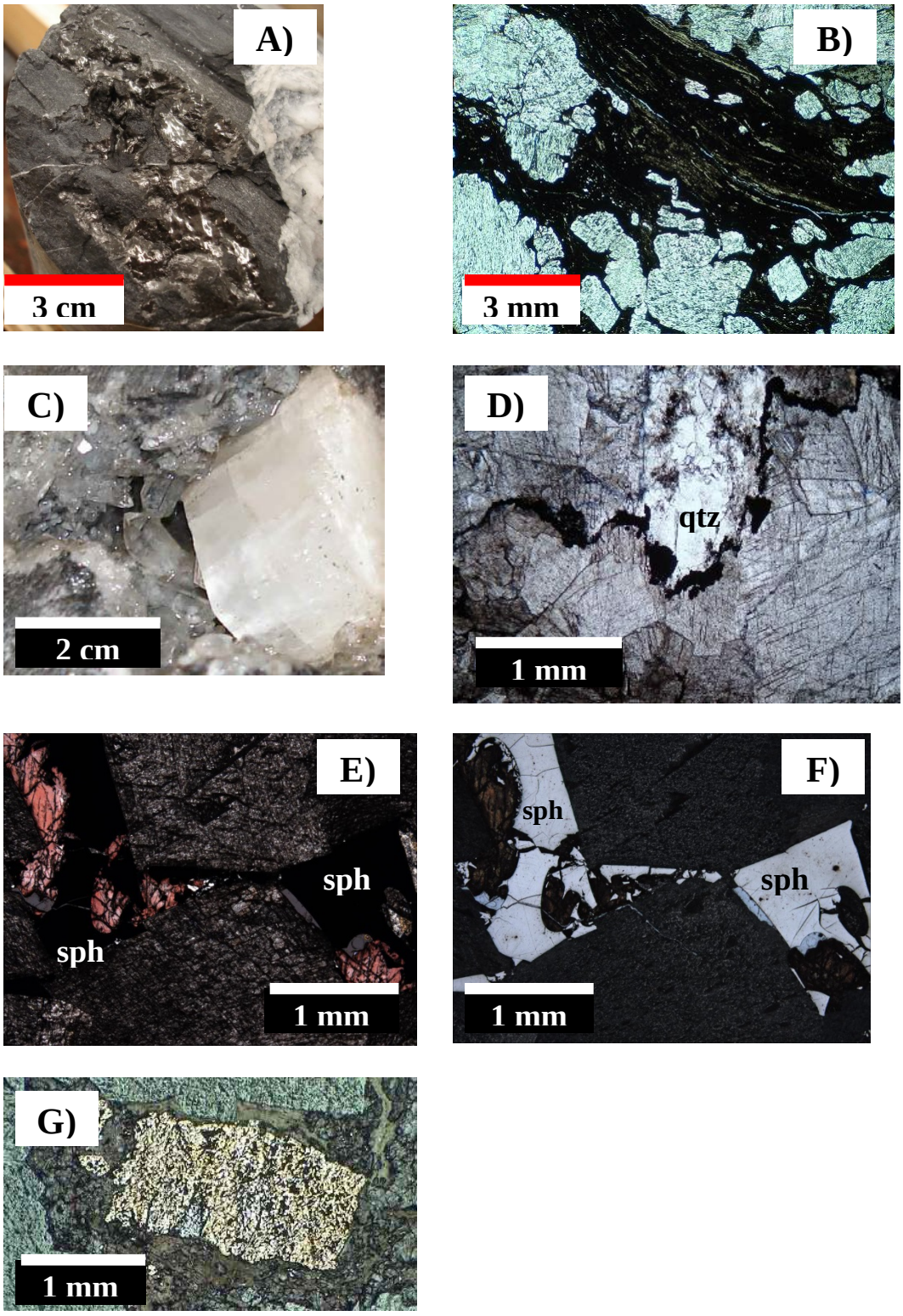

Figure 4.17A – G: Diagenetic phases. A) Bitumen on the surface of a core sample. c-16-A/94-N-15, 3765.2 – 3765.4 m. B) Photomicrograph taken under plane polarized light

(PPL) in high power showing bitumen within the intercrystalline pores among MCD-2. b-19-K/94-N-16, 4119.9 m. C) A quartz prism in a vug which postdates coarsely to very coarsely crystalline blocky calcite in vugs (CCC). c-54-K/94-N-16, 3697.8 m. D) The same sample in Fig. 4.17C. Photomicrograph of a quartz cement crystal being wrapped by high amphitude stylolites in coarsely to very coarsely crystalline nonplanar-e saddle dolomite in vugs (CSD). This thin section was collected from a rock chip hence the orientation of the stylolites is not known. E and F) Photomicrographs showing sphalerite in the intercrystalline pores among CCC. Sphalerite is opaque under plane-polarized light (PPL) and has very low reflectance under reflected light. d-64-K/94-N-16, 3574.2 m. E) Photomicrograph taken under PPL. F) Photomicrograph taken under reflected light. G) Photomicrograph of a cubic, euhedral pyrite within the intercrystalline pores among MCD-2. b-19-K/94-N-16, 4116.6 m. (original in color)

observed mostly in dolostone core samples as seams and rarely as ~ 1 mm thick layers (Figs. 4.17A and B). It postdates CCC.

Quartz: Quartz has been studied but not included in this thesis due to the poorly defined cross-cutting relationship among quartz and other diagenetic phases. Quartz appears as very coarsely crystalline prisms (~ 0.1 to 0.3 cm in diameter and ~ 0.1 to 2 cm long) in hand samples (Fig. 4.17C). In thin sections (Fig. 4.17D), quartz is translucent, euhedral, and from 100 μm to 1 mm. Quartz postdates CCC.

Sulphide minerals: Sphalerite and pyrite are excluded in this research due to poorly defined cross-cutting relationships, which cannot lead to critical interpretation. Sphalerite and pyrite were observed in cores and thin sections (Figs. 4.17E, F & G).

CHAPTER 5: Geochemistry

5.1 Stable oxygen and carbon isotopes

5.1.1 Rationale and application

Isotopes of an element have the same number of protons but different number of neutrons. Due to this difference, atoms of a particular element have similar, though not identical chemical properties but different masses. This difference also results in isotopic exchange and isotopic fractionation, which occur during phase transformation, mineral precipitation and diagenetic reactions (Land et al. 1975). Variation in isotopic compositions of minerals is resulted from these processes (Anderson and Arthur 1983).

Fractionation factors (α) determine the amount of fractionation or the partial separation of isotopes during physical or chemical processes that take place for a given reaction between two phases, assuming the reaction reaches the equilibrium. These factors are dependent on temperature, and approach unity at high temperatures (Morse and Mackenzie 1990). The fractionation factor can be determined at any given temperature by the following equation:

$$10^3 \ln \alpha (C\text{-}D) = A (10^6 T^2) + B \qquad (5.1)$$

Where A and B are constants that have been determined for a particular mineral-water or mineral-mineral system; C and D are the phases in which fractionation is occurring, and T is the absolute temperature.

Oxygen has 2 main isotopes: ^{16}O and ^{18}O. The $\delta^{18}O$ ($^{18}O/^{16}O$) isotope value of carbonate minerals are controlled primarily by the temperature and isotopic composition of the precipitating fluids (Land 1980; Tucker and Wright 1990). Factors that control the oxygen isotopic fractionation of carbonate minerals include (Brand and Veizer 1981; Anderson and Arthur 1983):

1) The isotopic composition of the diagenetic fluids. Meteoric fluids (e.g. rainwater), whose source is evaporated seawater, is typically depleted in ^{18}O relative to coeval marine water. This is due to the preferred incorporation of the light ^{16}O isotope in rainwater during evaporation.

2) Water-Rock interaction. In burial environment, fluids of elevated temperature react with carbonate rocks and become enriched in heavier oxygen isotope. The carbonate rocks will become enriched in lighter oxygen isotope, in another word, depleted in ^{18}O (Clayton et al. 1966).

3) Water-rock ratio. Water-rock interaction is controlled by the volume of water that was involved in the reaction. If the volume of water is significantly larger than the mass of carbonate rocks, input of ^{18}O from the carbonate rocks in the system will be lessen, hence no significant ^{18}O isotopes will enter the system. If the mass of the carbonate rocks is significantly larger than the volume of water, the effect of water-rock interaction is limited.

4) The fractionation factor. Fractionation factor is determined primarily by the temperature at which precipitation occurs.

5) Altitude, latitude, and seasonal variations. These affect the ^{18}O composition of meteoric and marine water due to the difference in evaporation rate in equatorial, semi-arid, arid, temperate and polar regions over the 4 seasons.

6) Secular variations in seawater isotopic composition. The pattern was discussed by Veizer et al. (1999).

7) Biological fractionation or vital effects. These refer to the vital selection of isotopes during plant or animal metabolism. For example, some organisms, such as crinoids and rugose corals, produce carbonate that is not in isotopic equilibrium with seawater.

Carbon has 2 main isotopes: ^{12}C and ^{13}C. Fractionation between $^{13}C/^{12}C$ and temperature gradient and $\delta^{13}C$ ($^{13}C/^{12}C$) is strongly influenced by the carbon isotopic composition of precursor carbonate minerals (the host limestone) and input of organic CO_2 (Allen and Wiggins 1993). Given the fluid-rock ratio is large enough, the carbon isotopic composition of precursor carbonate minerals can be reset by fluid. The depletion in carbon isotope suggests possible input of organic carbon into carbonate minerals through organic CO_2 during the cannibalization of organic matter (CH_2O; James and Choquette 1990), sulfate (SO_4) reduction (Machel 1987), oil degradation (Machel 1987) or kerogen

decarboxylation (Allen and Wiggins 1993). These processes typically precipitate calcite and dolomite that yield $\delta^{13}C$ from -15 to -5 ‰ V-PDB, to just 1 to 2 ‰ V-PDB slightly more depleted than the original limestone, depending on the ratio between organic CO_2 input and host limestone contribution (Allen and Wiggins 1993). Fermentation of organic matter during methanogenesis which generates CH_4 from organic matter typically precipitates calcite and dolomite that yield $\delta^{13}C$ = +5 to +20 ‰ V-PDB (Irwin et al. 1977). Methane oxidation and thermal sulfate reduction typically precipitate calcite and dolomite that yield $\delta^{13}C$ less than -25 ‰ V-PDB (Allan and Wiggins 1993).

5.1.2 Analytical results

Eighty six samples of diagenetic phases were sampled from cores from 9 wells recovered from the Stone and Dunedin formations and sent for oxygen and carbon stable isotopes analyzes. Core intervals that were sampled for oxygen and carbon isotope analyzes were marked on stratigraphic cross-section in Fig. 5.1. The results were summarized in Table 5.1. A cross-plot is presented in Figure 5.2. The following describes the statistics of the results:

- Five limestones (bulk samples) have $\delta^{18}O$ values from -12.03 to -10.05 ‰ V-PDB, $\delta^{13}C$ values from -2.74 to 0.89 ‰ V-PDB, with the mean $\delta^{18}O$ = -11.04 ‰ V-PDB and $\delta^{13}C$ = -1.95 ‰ V-PDB.
- Three samples of finely crystalline dolomite in limestone to calcitic dolomite

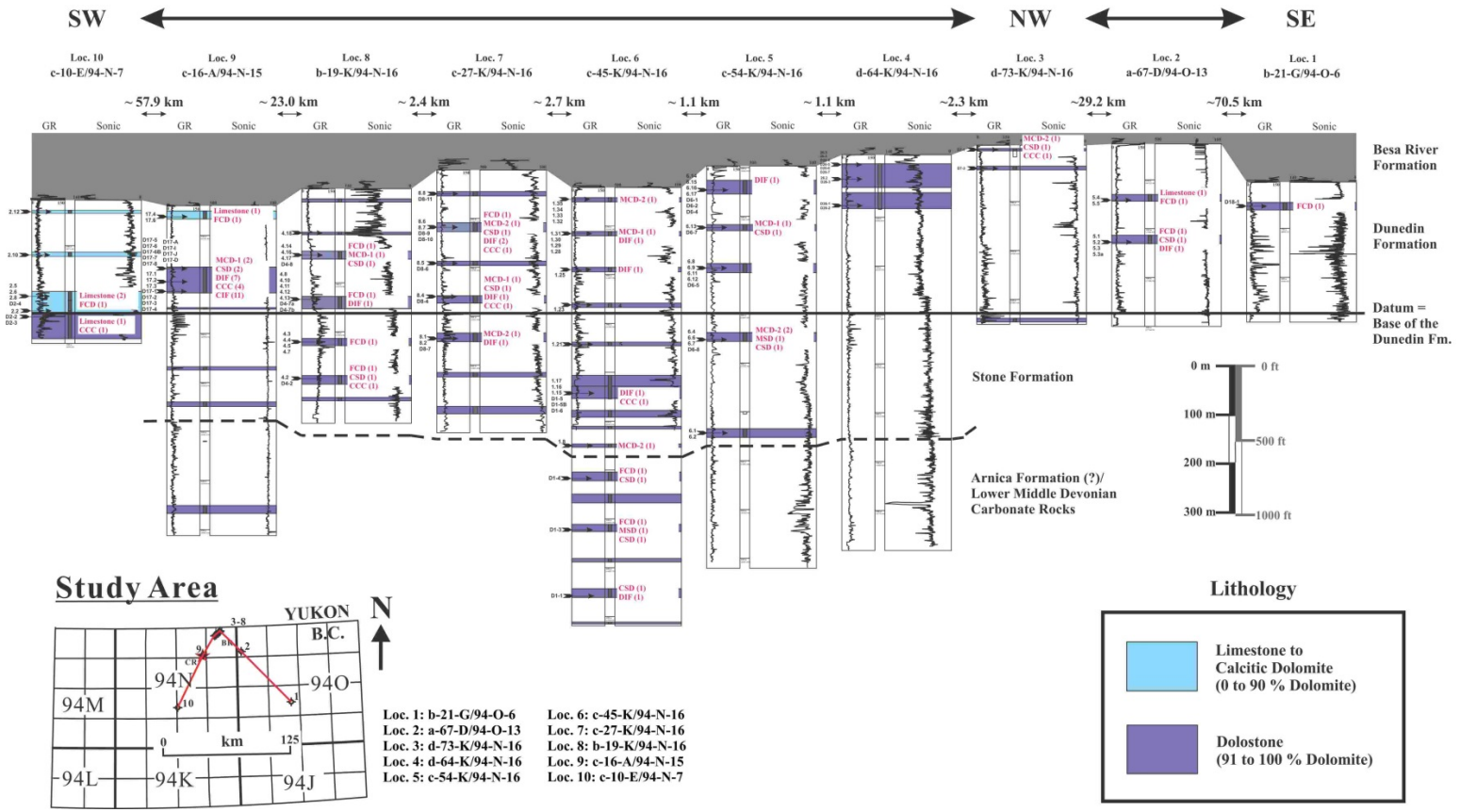

Figure 5.1: The stratigraphic cross-section used for sampling for stable oxygen and carbon isotopes analyzes. The white labels marked the intervals which samples of diagenetic phases were taken as well as the numbers of sample taken. Diagenetic phases include finely crystalline dolomite(s) (FCD), medium crystalline planar-s dolomite (MCD-1), medium crystalline planar-e dolomite (MCD-2), medium crystalline nonplanar-a saddle dolomite in vugs (MSD), coarsely to very coarsely crystalline nonplanar-e saddle dolomite in vugs (CSD), dolomite in fractures (DIF), coarsely to very coarsely crystalline blocky calcite in vugs (CCC), and calcite in fractures (CIF). (original in color)

Table 5.1: Summary of stable oxygen and carbon isotopes analytical result for samples from the Stone and Dunedin formations.

Sample/Diagenetic Phase (Number of Sample)	$\delta^{18}O$ (Mean; ‰, V-PDB)	$\delta^{13}C$ (Mean; ‰, V-PDB)
Limestones (allochemical components with various types of very finely to finely crystalline calcite cements; n = 5)	-11.04	-1.95
Finely crystalline dolomite (FCD; n = 12)	-10.42	-1.64
FCD in limestone to calcitic dolomite (n = 3)	-10.15	-1.11
FCD in dolostone (n = 9)	-10.51	-1.81
Medium crystalline dolomites (MCD's; n = 13)	-10.84	-1.79
Medium crystalline planar-s dolomite (MCD-1; n = 6)	-10.89	-1.73
Medium crystalline planar-e dolomite (MCD-2; n = 7)	-10.80	-1.84
Nonplanar saddle dolomites in vugs (SD's; n = 15)	-12.28	-2.90
Medium crystalline nonplanar-a saddle dolomite in vugs (MSD; n = 2)	-12.32	-2.75
Coarsely to very coarsely crystalline nonplanar-e saddle dolomite in vugs (CSD; n = 13)	-12.26	-3.06
Dolomite in fractures (DIF; n = 18)	-11.68	-2.73
Coarsely to very coarsely crystalline blocky calcite in vugs (CCC; n = 10)	-13.26	-6.95
Calcite in fractures (CIF; n = 13)	-12.87	-6.58

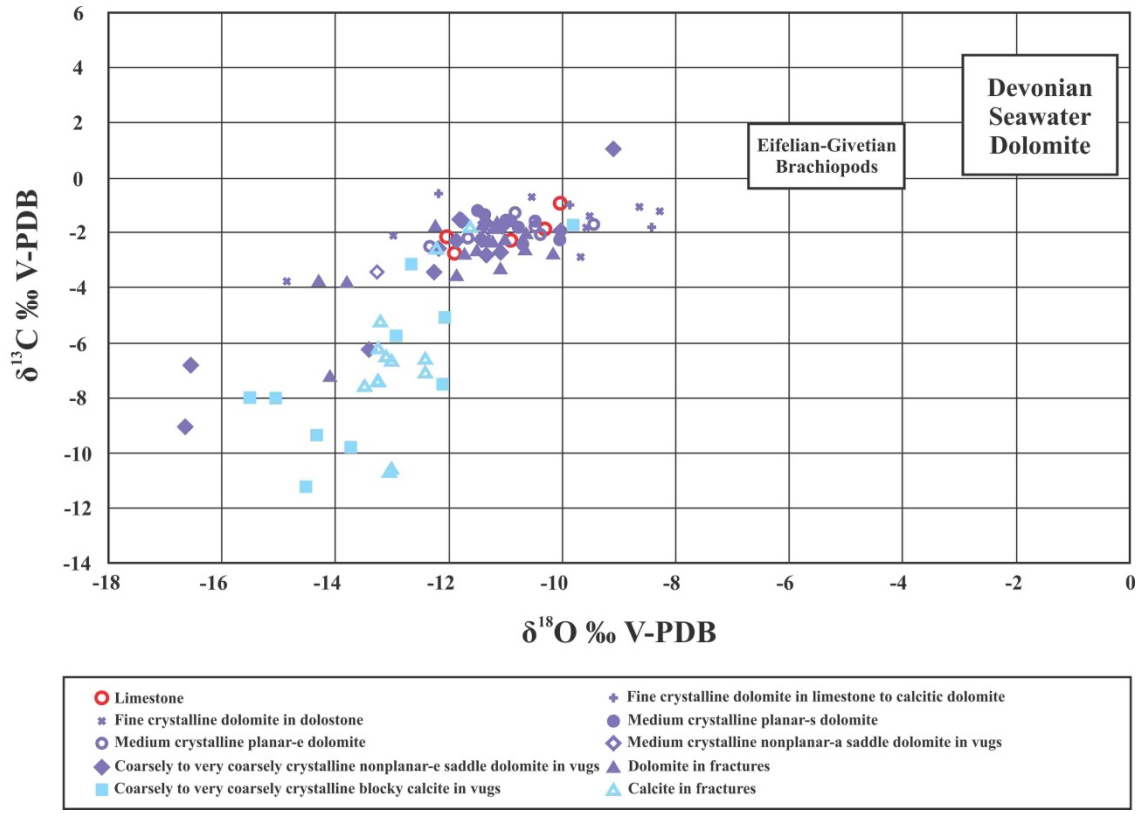

Figure 5.2: A cross-plot of oxygen versus carbon isotope for various diagenetic phases in the Stone and Dunedin formations. These phases include: finely crystalline dolomite in limestone to calcitic dolomite (FCD in limestone to calcitic dolomite), finely crystalline dolomite in dolostone (FCD in dolostone), medium crystalline planar-s dolomite (MCD-1), medium crystalline planar-e dolomite (MCD-2), medium crystalline nonplanar-a saddle dolomite in vugs (MSD), coarsely to very coarsely crystalline nonplanar-e saddle dolomite in vugs (CSD), dolomite in fractures (DIF), coarsely to very coarsely crystalline blocky calcite in vugs (CCC), and calcite in fractures (CIF). The range for the Eifelian to Givetian brachiopods is from Veizer (1999). The $\delta^{18}O$ values are from -6.69 to -3.99 ‰ V-PDB and the $\delta^{13}C$ values are from -0.36 to 1.99 ‰ V-PDB. This range represents the average values from numerous studies. The field for Middle Devonian seawater dolomite of -2.93 to -0.20 ‰ V-PDB is calculated by using the equation from Land (Equation 6.3; 1983) with the range of Eifelian to Givetian seawater = -5.79 to -3.05 ‰ V-SMOW and temperature = 20 °C. (original in color)

(FCD in limestone to calcitic dolomite) have $\delta^{18}O$ values from –12.17 to -8.42 ‰ V-PDB, $\delta^{13}C$ values from -1.79 to -0.57 ‰ V-PDB, with the mean $\delta^{18}O$ = -10.15 ‰ V-PDB and $\delta^{13}C$ = -1.11 ‰ V-PDB.

- Nine samples of finely crystalline dolomite in dolostone (FCD in dolostone) have $\delta^{18}O$ values from –14.87 to -8.28 ‰ V-PDB, $\delta^{13}C$ values from -3.75 to -0.69 ‰ V-PDB, with the mean $\delta^{18}O$ = -10.51 ‰ V-PDB and $\delta^{13}C$ = -1.81 ‰ V-PDB.
- Six samples of medium crystalline planar-s dolomite (MCD-1) have $\delta^{18}O$ values from –11.51 to -10.03 ‰ V-PDB, $\delta^{13}C$ values from -2.40 to -1.19 ‰ V-PDB, with the mean $\delta^{18}O$ = -10.89 ‰ V-PDB and $\delta^{13}C$ = -1.73 ‰ V-PDB.
- Seven samples of medium crystalline planar-e dolomite (MCD-2) have $\delta^{18}O$ values from –12.33 to -9.44 ‰ V-PDB, $\delta^{13}C$ values from -2.49 to -1.26 ‰ V-PDB, with the mean $\delta^{18}O$ = -10.80 ‰ V-PDB and $\delta^{13}C$ = -1.84 ‰ V-PDB.
- Two samples of medium crystalline nonplanar-a saddle dolomite in vugs (MSD) have $\delta^{18}O$ values from –13.25 to -11.39 ‰ V-PDB, $\delta^{13}C$ values from -3.40 to -2.09 ‰ V-PDB (Fig 5.1), with the mean $\delta^{18}O$ = -12.32 ‰ V-PDB and $\delta^{13}C$ = -2.75 ‰ V-PDB.
- Thirteen samples of coarsely to very coarsely crystalline nonplanar-e saddle dolomite in vugs (CSD) have $\delta^{18}O$ values from –16.63 to –9.09 ‰ V-PDB, $\delta^{13}C$ values from -9.02 to +1.05 ‰ V-PDB, with the mean $\delta^{18}O$ = -12.26 ‰ V-PDB and $\delta^{13}C$ = -3.06 ‰ V-PDB.
- Eighteen samples of dolomite in fractures (DIF) have $\delta^{18}O$ values from –14.28 to -10.16 ‰ V-PDB, $\delta^{13}C$ values from -7.17 to -1.54 ‰ V-PDB, with the mean $\delta^{18}O$ = -11.68 ‰ V-PDB and $\delta^{13}C$ = -2.73 ‰ V-PDB.

- Ten samples of coarsely to very coarsely crystalline blocky calcite in vugs (CCC) have $\delta^{18}O$ values from –15.50 to -9.80 ‰ V-PDB, $\delta^{13}C$ values from -11.23 to -1.71 ‰ V-PDB, with the mean $\delta^{18}O$ = -13.26 ‰ V-PDB and $\delta^{13}C$ = -6.95 ‰ V-PDB.
- Thirteen samples of calcite in fractures (CIF) have $\delta^{18}O$ values from –13.49 to -11.61 ‰ V-PDB, $\delta^{13}C$ values from -10.63 to -1.74 ‰ V-PDB, with the mean $\delta^{18}O$ = -12.87 ‰ V-PDB and $\delta^{13}C$ = -6.58 ‰ V-PDB.

5.2 Radiogenic strontium isotopic ratio

5.2.1 Rationale and application

$^{87}Sr/^{86}Sr$ isotope ratio is analyzed for carbonate minerals studies. ^{87}Sr is generated naturally by the radioactive decay of ^{87}Rb, while ^{86}Sr naturally exists (Faure 1986). Strontium (^{87}Sr and ^{86}Sr) can be incorporated into the structures of carbonate minerals but Rb cannot. Strontium is inherited into the carbonate minerals from the precipitating fluid without fractionation (Veizer 1983). Unlike stable oxygen and carbon isotopes, $^{87}Sr/^{86}Sr$ ratio is not fractionated by pressure, temperature and microbial processes (Faure and Powell 1972). $^{87}Sr/^{86}Sr$ ratio of a fluid can be elevated through fluid-mineral interaction especially with Rb-rich minerals such as feldspars, which are abundant in clastic sediments and basement rocks (Mountjoy et al. 1992). The $^{87}Sr/^{86}Sr$ isotope ratio of the carbonate minerals do not change significantly over time because the concentration of Rb in the minerals is close to none and if there is no additional ^{87}Sr

being put into the system (Faure 1986). Therefore, marine carbonate minerals that have not been alterated or recrystallized should record the strontium isotopic composition of the diagenetic fluid(s) that precipitated them. Similarly, in burial settings, carbonate minerals acquire their strontium signatures from the diagenetic fluid(s) that precipitated them. The isotopic composition of these fluids is controlled by the initial strontium composition and ratio, and prior interaction with different rocks. These give $^{87}Sr/^{86}Sr$ ratio a good index to deduce the composition and compositional changes of the fluid(s) which carbonate minerals precipitated from (Cavell and Machel 1997; Machel and Cavell 1999; Lonnee and Machel 2006).

5.2.2 Analytical results

Forty-one samples of diagenetic phases were sampled from cores from 9 wells recovered from the Stone and Dunedin formations and sent for $^{87}Sr/^{86}Sr$ isotope ratio analyze. Core intervals that were sampled for strontium isotope analyzes were marked on stratigraphic cross-section in Fig. 5.3. The results were summarized in Table 5.2. A cross-plot is presented in Figure 5.4. The following describes the statistics of the results:

- Three samples of FCD in limestone to calcitic dolomite have $^{87}Sr/^{86}Sr$ ratios from 0.70897 to 0.71365 with a mean of 0.71070.

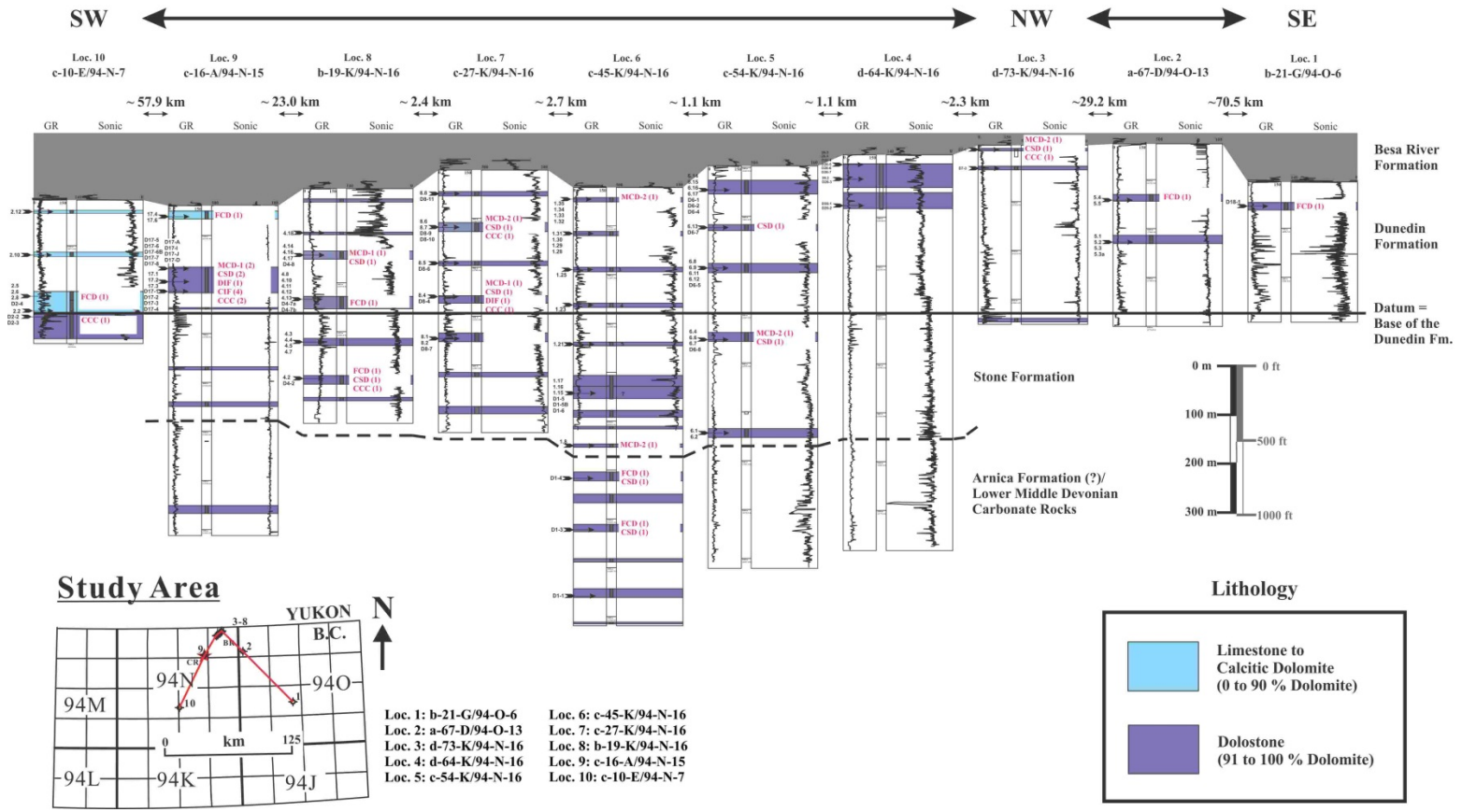

Figure 5.3: The stratigraphic cross-section used for sampling for radiogenic strontium isotope analyzes. The white labels marked the intervals which samples of diagenetic phases were taken as well as the numbers of sample taken. Diagenetic phases include finely crystalline dolomite(s) (FCD), medium crystalline planar-s dolomite (MCD-1), medium crystalline planar-e dolomite (MCD-2), medium crystalline nonplanar-a saddle dolomite in vugs (MSD), coarsely to very coarsely crystalline nonplanar-e saddle dolomite in vugs (CSD), dolomite in fractures (DIF), coarsely to very coarsely crystalline blocky calcite in vugs (CCC), and calcite in fractures (CIF). (original in color)

Table 5.2: Summary of radiogenic strontium $^{87}Sr/^{86}Sr$ isotopic ratio analytical result for samples from the Stone and Dunedin formations.

Diagenetic Phases (Number of Sample)	Mean $^{87}Sr/^{86}Sr$ Isotopic Ratio
Finely crystalline dolomite (FCD; n = 8)	0.71072
FCD in limestone to calcitic dolomite (n = 3)	0.71070
FCD in dolostone (n = 5)	0.71073
Medium crystalline dolomites (MCD's; n = 9)	0.71015
Medium crystalline planar-s dolomite (MCD-1; n = 4)	0.71008
Medium crystalline planar-e dolomite (MCD-2; n = 5)	0.71021
Nonplanar saddle dolomite in vugs (SD's; n = 11)	0.71147
Coarsely to very coarsely crystalline nonplanar-e saddle dolomite in vugs (CSD; n = 11)	0.71147
Dolomite in fractures (DIF; n = 2)	0.71112
Coarsely to very coarsely crystalline blocky calcite in vugs (CCC; n = 7)	0.71187
Calcite in fractures (CIF; n = 4)	0.71608

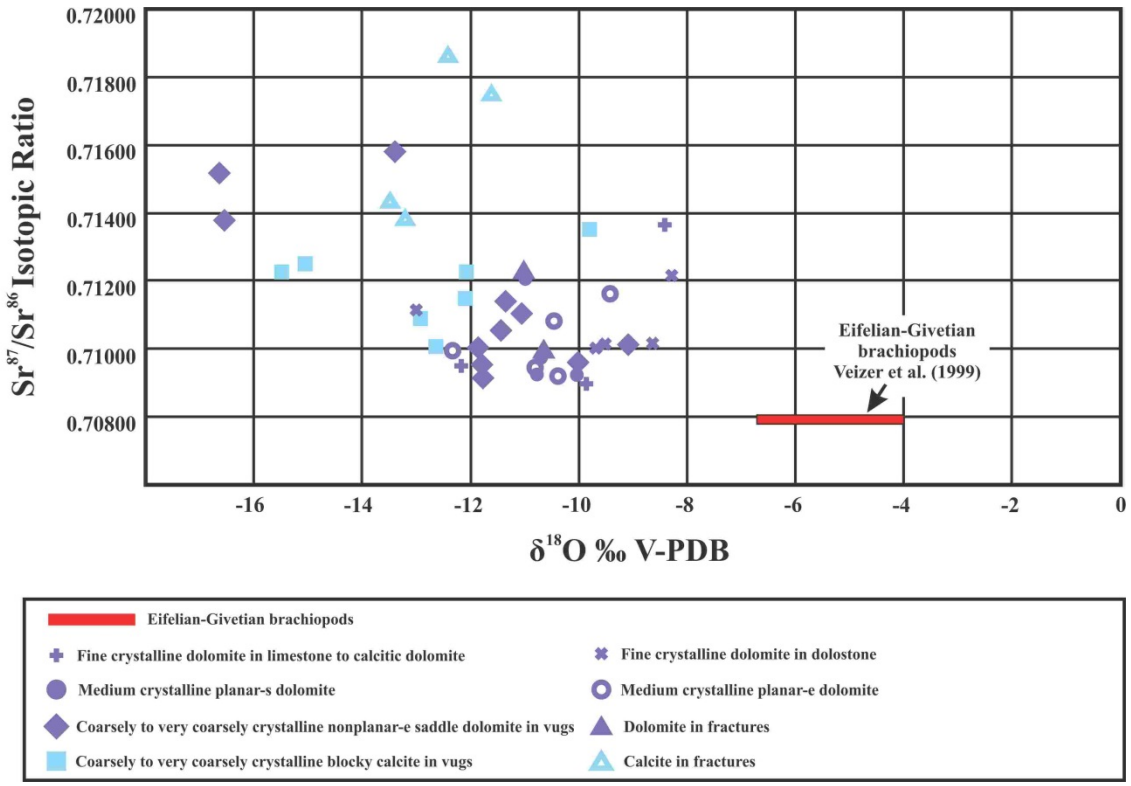

Figure 5.4: A cross-plot of stable oxygen isotope values versus radiogenic strontium $^{87}Sr/^{86}Sr$ ratios of various diagenetic calcite and dolomite phases in the Stone and Dunedin formations. These phases include: finely crystalline dolomite in limestone to calcitic dolomite (FCD in limestone to calcitic dolomite), finely crystalline dolomite in dolostone (FCD in dolostone), medium crystalline planar-s dolomite (MCD-1), medium crystalline planar-e dolomite (MCD-2), coarsely to very coarsely crystalline nonplanar-e saddle dolomite in vugs (CSD), dolomite in fractures (DIF), coarsely to very coarsely crystalline blocky calcite in vugs (CCC), and calcite in fractures (CIF). Fractionation of strontium is insignificant in carbonate minerals (and brachiopod shells). The $^{87}Sr/^{86}Sr$ ratio for Middle Devonian seawater is adapted from 0.70779 to 0.70804 which is adopted from Veizer et al. (1999). (original in color)

- Five samples of FCD in dolostone have $^{87}Sr/^{86}Sr$ ratios from 0.71001 to 0.71218 with a mean of 0.71073.
- Four samples of MCD-1 have $^{87}Sr/^{86}Sr$ ratios from 0.70922 to 0.71210 with a mean of 0.71008.
- Five samples of MCD-2 have $^{87}Sr/^{86}Sr$ ratios from 0.70919 to 0.71161 with a mean of 0.71021.
- Eleven samples of CSD have $^{87}Sr/^{86}Sr$ ratios from 0.70914 to 0.71582 with a mean of 0.71147.
- Two samples of DIF have $^{87}Sr/^{86}Sr$ ratios from 0.70995 to 0.71228 with a mean of 0.71112.
- Seven samples of CCC have $^{87}Sr/^{86}Sr$ ratios from 0.71009 to 0.71354 with a mean of 0.71187.
- Four samples of CIF have $^{87}Sr/^{86}Sr$ ratios from 0.71384 to 0.71862 with a mean of 0.71608.

5.3 Fluid inclusion petrography and microthermometry

5.3.1 Introduction

Fluid Inclusion studies are conducted in 2 steps. Step 1 is the fluid inclusion petrographic studies; step 2 is the fluid inclusion microthermometric studies. Fluid inclusion petrographic studies identify the types and occurrences of fluid inclusion in diagenetic phases. Eighteen 100-μm-thick thin sections were prepared from core samples recovered

from 8 wells were studied and fluid inclusions were characterized (Fig. 5.5). Five diagenetic phases were chosen to for fluid inclusion petrographic and microthermometric analysis. These include the 1) MSD, 2) CSD, 3) DIF, 4) CCC, and 5) CIF. These 5 diagenetic phases were chosen because the first three dolomite phases (MSD, CSD and DIF) precipitated during or immediately after fabric-destructive dolomitization. The CCC and possibly CIF immediately postdated the MSD, CSD and DIF. This put time constraints on the precipitation of the dolomite cements.

Occurrence, distribution, abundance, size and vapor-liquid ratio of different types of fluid inclusion were documented. Abundance of different types of fluid inclusion is classified into rare, uncommon, common and abundant in this study. Rare indicates that a specific type of fluid inclusion is rarely observed and only found locally in a few crystals and samples. Uncommon indicates that a specific type of fluid inclusion was found in most of the samples, but not most of the crystals. Common indicates that a specific type of fluid inclusion was found in most of the samples and crystals. Abundant indicates that a specific type of fluid inclusion was found almost in every sample and crystal. The term "locally" is also adopted here, which indicates that a specific type of inclusion is only found in a few samples or even a few crystals within a sample. This scheme is aimed to classify fluid inclusions in a descriptive manner because no quantitative method can be used to estimate the relative abundance of different types of fluid inclusion.

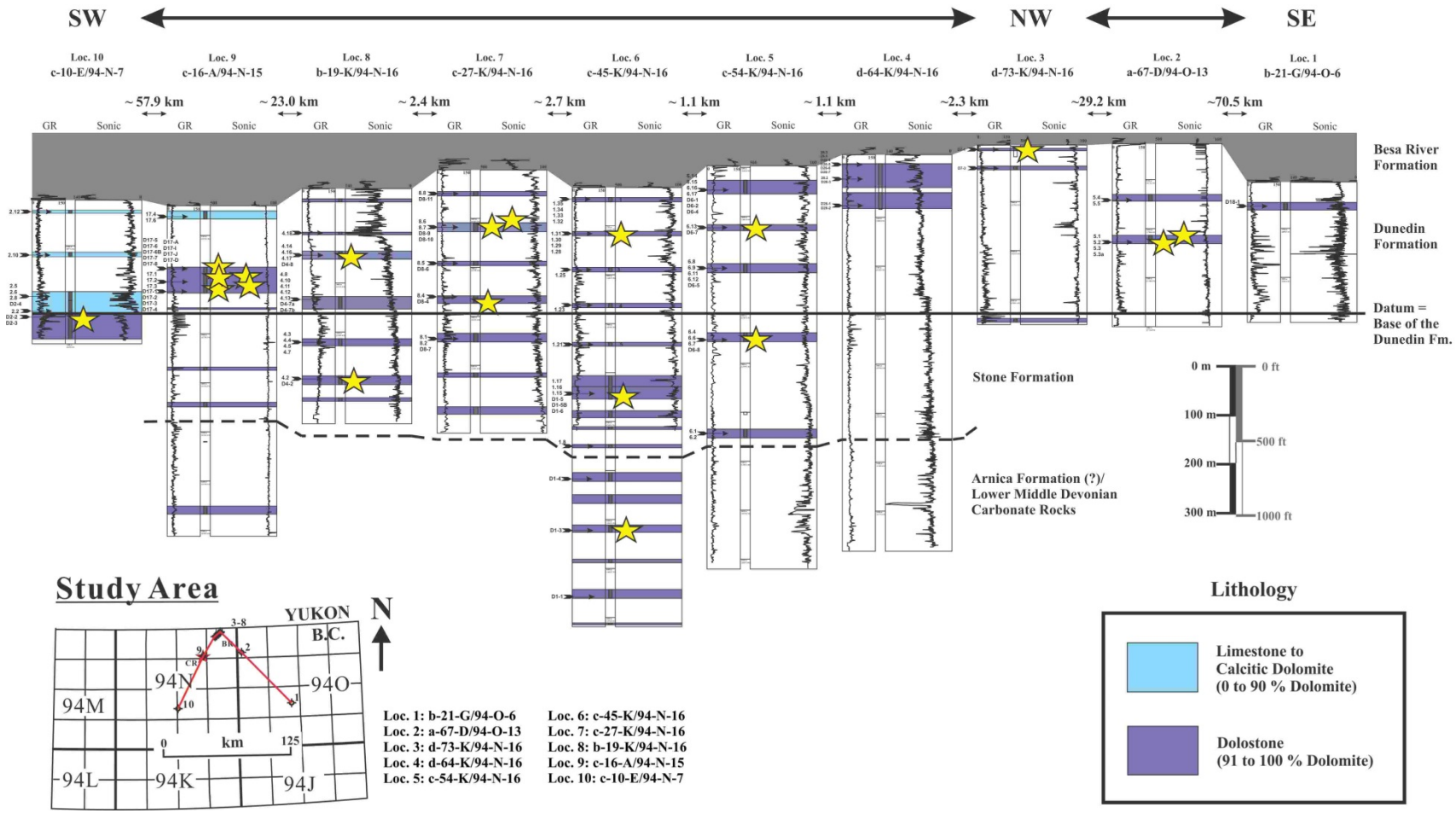

Figure 5.5: The stratigraphic cross-section used for sampling for fluid inclusion analysis. The stars mark where the samples were chosen for fluid inclusion studies. (original in color)

Fluid inclusions can be interpreted as primary to pseudo-primary inclusions and secondary inclusions (Roedder 1984; Goldstein 2003). Primary to pseudo-primary inclusions are fluid inclusions that were trapped during mineral precipitation. Secondary inclusions are fluid inclusions that were trapped or injected into the mineral after it precipitated. Petrographic observation and interpretation are summarized in Table 5.3 and discussed in this chapter.

Fluid inclusion microthermometric studies measure the homogenization, first melting, second melting and last melting temperatures of the selected fluid inclusions in diagenetic phases. Homogenization temperature of the entrapped inclusions in different diagenetic phases (e.g. dolomite and calcite cements) reflects the thermal condition of precipitation, which can be correlated to the geothermal gradient (Morrow et al. 1993; Davies and Smith 2006). Homogenization temperature measurements can also be used with analytical oxygen isotope values to calculate the oxygen isotopic composition of the diagenetic fluid (Friedman and O'Neil 1977). Moreover, the NaCl-$CaCl_2$ molecular ratio and salinity (NaCl weight percentage) of the diagenetic fluid (s) can also be calculated from the measured hydrohalite melting temperature ($T_{m\text{-}HH}$) and/or ice melting temperature ($T_{m\text{-}ice}$; Chi and Ni 2007). The formulas and in-house program used for calculation are discussed in the later part of this chapter.

New discovery was made during the fluid inclusion studies. Carbonic inclusions were identified in coarsely to very coarsely crystalline blocky calcite in vugs (CCC) and calcite in fractures (CIF). Similar inclusion(s) was documented and interpreted by

Table 5.3: Petrographic summary of the fluid inclusions in the selected diagenetic phases.

Diagenetic Phase	Fluid Inclusion Types	Occurrence (Number of Inclusions)	Size (µm)	Vapor (%)	Abundance	Interpretation
Medium crystalline nonplanar-a saddle dolomite in vugs (MSD)	Aqueous; biphase (H_2O; liquid + vapor)	Clusters (8 – 20+)	~ 0.5 – 2	~5 %	Uncommon	Primary to pseudo-primary inclusions
	Aqueous; biphase (H_2O; liquid + vapor)	Randomly distributed to isolated (1)	2 – 6	~5 %	Rare	Primary to pseudo-primary inclusions
	Aqueous; biphase (H_2O; liquid + vapor)	Trails (4 – 10+)	~0.5 – 2	~5 %	Uncommon	Secondary inclusions
Coarsely to very coarsely crystalline nonplanar-e saddle dolomite in vugs (CSD)	Aqueous; biphase (H_2O; liquid + vapor)	Randomly distributed to clusters (5 – 10+)	~0.5 – 3	5–7 %	Abundant	Primary to pseudo-primary inclusions
	Aqueous; biphase (H_2O; liquid + vapor)	Randomly distributed (2 – 4)	3 – 8	5–7 %	Uncommon	Primary to pseudo-primary inclusions
	Aqueous; biphase (H_2O; liquid + vapor)	Isolated to randomly distributed (1)	4 – 8	5–7 %	Rare to uncommon	Primary to pseudo-primary inclusions
	Aqueous; biphase (H_2O; liquid + vapor)	Trails (5–20+)	< 1 – 3	5–7 %	Common	Secondary inclusions
Dolomite in fractures (DIF)	Aqueous; biphase (H_2O; liquid + vapor)	Randomly distributed to clusters (5–10)	~0.5 – 2	5–7 %	Uncommon	Primary to pseudo-primary inclusions
	Aqueous; biphase (H_2O; liquid + vapor)	Isolated to randomly distributed (1)	3 – 7	5–7 %	Rare	Primary to pseudo-primary inclusions
	Aqueous; biphase (H_2O; liquid + vapor)	Trails (5–10+)	~0.5 – 2	5–7 %	Uncommon	Secondary inclusions

Table 5.3 (continued): Petrographic summary of the fluid inclusions in the selected diagenetic phases.

Diagenetic Phase	Fluid Inclusion Types	Occurrence (Number of Inclusions)	Size (µm)	Vapor (%)	Abundance	Interpretation
Coarsely to very coarsely crystalline blocky calcite in vugs (CCC)	Aqueous; biphase (H_2O; liquid + vapor)	Clusters (5 –15)	4 – 20	6–7 %	Common	Primary to pseudo-primary inclusions
	Aqueous; biphase (H_2O; liquid + vapor)	Isolated to randomly distributed (1)	5 – 20	6–7 %	Common to abundant	Primary to pseudo-primary inclusions
	Aqueous; biphase (H_2O; liquid + vapor)	Trails (8–20)	2 – 5	6–7 %	Abundant	Secondary inclusions
	Carbonic inclusion; (vapor only?)	Trails (4–15)	2– 6	Vapor only?	Locally uncommon	Secondary inclusions
	Carbonic inclusion; (vapor only?)	Randomly distributed to isolated (1–6)	6 – 30	Vapor only?	Locally uncommon	Pseudo-secondary inclusions
Calcite in fractures (CIF)	Aqueous; biphase (H_2O; liquid + vapor)	Random (5–10)	~0.5 – 3	6–7 %	Uncommon	Primary to pseudo-primary inclusions
	Aqueous; biphase (H_2O; liquid + vapor)	Isolated to randomly distributed (1– 6)	5 – 20	6–7 %	Uncommon	Primary to pseudo-primary inclusions
	Aqueous; biphase (H_2O; liquid + vapor)	Trails (8–20)	2 – 5	6–7 %	Common	Secondary inclusions
	Carbonic inclusion; (vapor only?)	Randomly distributed to isolated (1– 6)	6 – 30	Vapor only?	Locally uncommon	Pseudo-secondary inclusions
	Carbonic inclusion; (vapor only?)	Trails (4–10)	6 – 20	Vapor only?	Abundant in 2 samples; not observed in all others.	Secondary inclusions

Schaefer (2002) on the Bushy Park carbonate-hosted Pb-Zn deposit in South Africa. To the best of the author's knowledge and search effort, there is very little material on carbonic inclusions in the Middle Devonian carbonate rocks in western Canada.

5.3.2 Fluid inclusion petrography

Medium crystalline nonplanar-a saddle dolomite in vugs (MSD)

Observation: fluid inclusions observed in MSD include 1) uncommon aqueous biphase (~95% liquid and ~5% vapor) inclusions from ~0.5 to 2 μm in size. They occur in clusters of 8 – 20+ (Fig. 5.6A); 2) rare aqueous biphase (~95% liquid and ~5% vapor) fluid inclusions from 2 – 6 μm in size are found randomly distributed or isolated (Fig. 5.6A); and 3) uncommon aqueous biphase (~95% liquid and ~5% vapor) inclusions from ~0.5 to 2 μm in size which occur in trails of 4 – 10+ inclusions (Fig. 5.6B).

Interpretation: Interpretations were made and based on the logic discussed by Roedder (1984). 1) Aqueous biphase (L-V) inclusions in clusters are considered as primary to pseudo-primary inclusions if they occur in the cores or along growth zones of MSD, which indicate that they formed during mineral growth. 2) Randomly distributed or isolated aqueous biphase (L-V) inclusions are considered as primary to pseudo-secondary inclusions if they occur in the cores or along growth zones of MSD. 3) Aqueous biphase (L-V) inclusions in trails or along healed fractures that cut across the

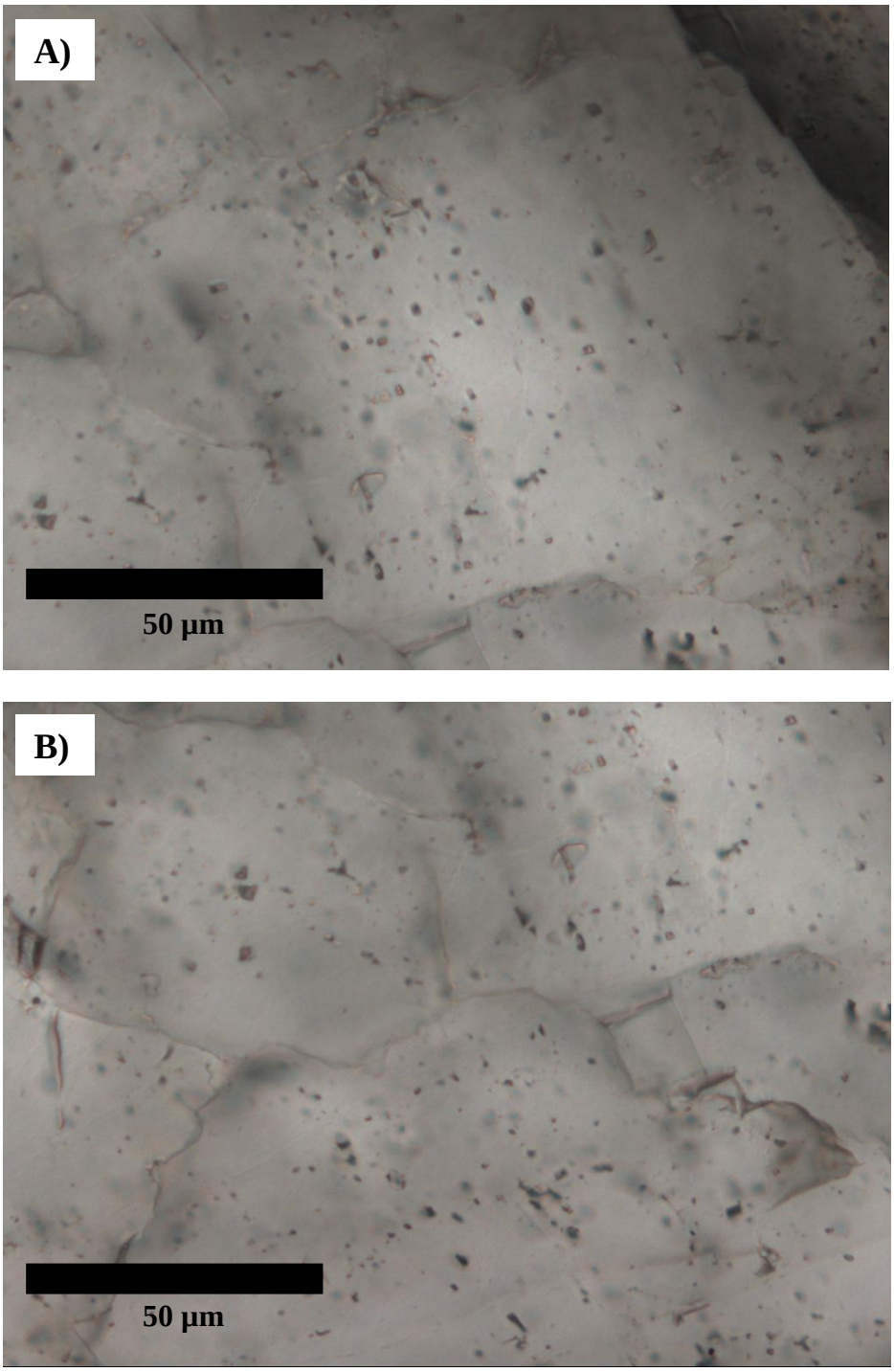

Figure 5.6A – B: Fluid inclusions in medium crystalline nonplanar-a saddle dolomite in vugs (MSD). A) Aqueous biphase (liquid + vapor) inclusions in clusters and randomly distributed. c-45-K/94-N-16, 4324.1 m. B) Aqueous biphase (liquid + vapor) inclusions in trails. c-45-K/94-N-16, 4324.1 m. (original in color)

mineral growth zones are considered as secondary inclusions. It is because if patterns of the fractures or trails do not match with the growth patterns of the host MSD, the fluid inclusions that were trapped inside are not likely to have trapped during mineral growth.

Coarsely to very coarsely crystalline nonplanar-e saddle dolomite in vugs (CSD)

Observation: fluid inclusions observed in CSD include 1) abundant aqueous biphase (~93 – 95% liquid and ~5 – 7 % vapor) inclusions from ~0.5 to 3 μm in size. They are randomly distributed in groups of 5 – 10+, and resemble clusters (Fig. 5.7A). 2) Uncommon aqueous biphase (~93 – 95 % liquid and ~5 – 7 % vapor) inclusions from 3 to 8 μm in size are found randomly distributed in three dimensions in groups of 2 – 4 (Fig. 5.7B). 3) Rare to uncommon, isolated to randomly distributed aqueous biphase (~93 – 95 % liquid and ~5 – 7 % vapor) inclusions from 4 to 8 μm (Figs. 5.7A, B and C). And 4) common aqueous biphase (~93 – 95 % liquid and ~5 – 7 % vapor) inclusions from <1 – 3 μm in size that occur in trails of 5 – 20+ (Fig. 5.7D).

Interpretation: Interpretations were made and based on the logic discussed by Roedder (1984). 1) Aqueous biphases (L-V) inclusions that are randomly distributed and resemble clusters are considered as primary to pseudo-secondary inclusions if they occur in the cores or along growth zones of CSD, which indicate that they formed during mineral growth. 2) Randomly distributed aqueous biphase (L-V) inclusions are considered as primary to pseudo-primary inclusions if they occur in the cores or along growth zones of

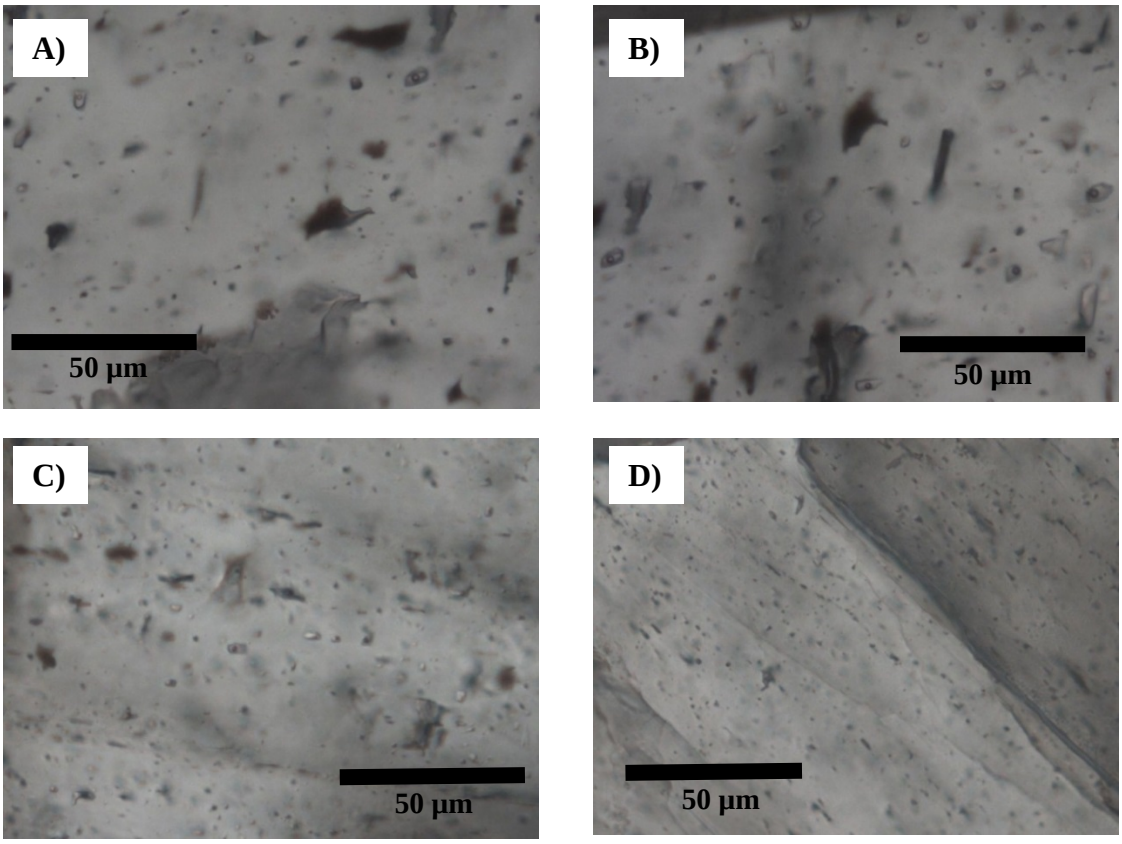

Figure 5.7A – D: Fluid inclusions in coarsely to very coarsely crystalline nonplanar-e saddle dolomite in vugs (CSD). A) Randomly distributed aqueous biphase (liquid + vapor) inclusions. c-54-K/94-N-16, 3851.6 m. B) Randomly distributed to isolated aqueous biphase (liquid + vapor) inclusions. c-54-K/94-N-16, 3851.6 m. C) Isolated aqueous biphase (liquid + vapor) inclusion in dolomite. c-54-K/94-N-16, 3851.6 m. D) Aqueous biphase (liquid + vapor) fluid inclusions in trails in dolomite. d-16-A/94-N-15, 3816.8 m. (original in color)

CSD. 3) Isolated to randomly distributed aqueous biphase (L-V) inclusions are considered as primary to pseudo-primary inclusions if they occur in the cores or along

growth zones of CSD. And 4) aqueous biphase (L-V) inclusions in trails or along healed fractures that cut across the mineral growth zones are considered as secondary inclusions. It is because if patterns of the fractures or trails do not match with the growth patterns of the host CSD, the fluid inclusions that were trapped inside are not likely to have trapped during mineral growth.

Dolomite in fractures (DIF)

Observation: fluid inclusions observed in DIF include 1) uncommon aqueous biphase (~93 – 95 % liquid and ~5 – 7 % vapor) inclusions. The inclusions are from ~0.5 to 2 μm in size and randomly distributed in groups of 5 – 10, and some of them resemble clusters (Figs. 5.8A and B). 2) Rare isolated to randomly distributed aqueous biphase (~93 – 95 % liquid and ~5 – 7 % vapor) inclusions from 3 to 7 μm (Fig. 5.8C). And 3) uncommon aqueous biphase (~93 – 95 % liquid and ~5 – 7 % vapor) inclusions in trails from ~0.5 to 2 μm of 5 – 10+ (Figs. 5.8A).

Interpretation: Interpretations were made and based on the logic discussed by Roedder (1984). 1) Randomly distributed aqueous biphases (L-V) inclusions (some that resemble clusters) are considered as primary to pseudo-primary inclusions if they occur in the cores or along growth zones of DIF. 2) Isolated to randomly distributed aqueous biphases (L-V) inclusions are considered as primary to pseudo-primary inclusions if they occur in the cores or along growth zones of DIF. 3) Aqueous biphases (L-V) inclusions

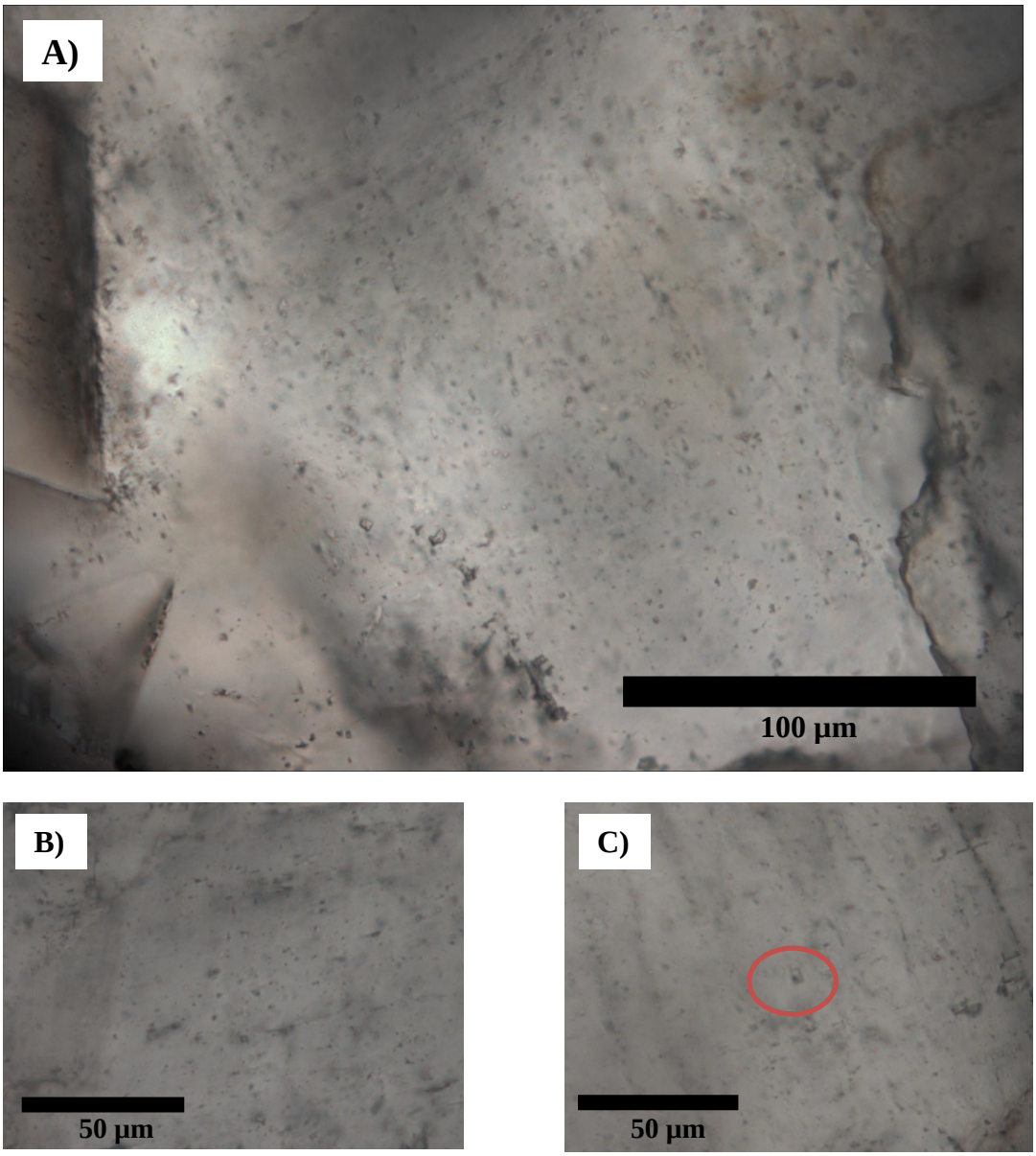

Figure 5.8A – C: Fluid inclusions in dolomite in fractures (DIF). A) Randomly distributed aqueous biphase (liquid + vapor) inclusions and aqueous biphase (liquid + vapor) inclusions in trail in medium crystalline nonplanar-c dolomite in fractures. c-45-K/94-N-16, 3716.7 m. B) Randomly distributed aqueous biphase (liquid + vapor) inclusions in groups of 5 to 10. d-16-A/94-N-15, 3810.9 m. C) Isolated to randomly distributed aqueous biphase (liquid + vapor) inclusion (circle). (original in color)

in trails that appear entrapping along healed fractures are considered as secondary inclusions. It is because if patterns of the fractures or trails do not match with the growth patterns of the host DIF, the fluid inclusions that were trapped inside are not likely to have trapped during mineral growth.

Coarsely to very coarsely crystalline blocky calcite in vugs (CCC)

Observation: fluid inclusions observed in CCC include 1) common biphase (~93 – 95 % liquid and ~ 6 – 7 % vapor) inclusions from 4 to 20 μm in size and occur in clusters in groups of 5 –15 (Fig. 5.9A). 2) Common to abundant inclusions from 5 to 20 μm in size are found isolated to randomly distributed in three dimensions in groups of 2 to 6 inclusions (Figs. 5.9B, E and F). 3) Abundant biphases (~95% liquid and 6 – 7 % vapor) inclusions from 2 to 5 μm in size that occur in trails of 8 – 20 (Figs. 5.9B and C). 4) Locally uncommon carbonic (vapor only?) inclusions from 2 to 6 μm in size were found and occur in trails of 4 – 15 (Figs. 5.9C, D and E). And 5) locally uncommon randomly distributed to isolated carbonic (vapor only?) inclusions from 6 – 30 μm (Figs. 5.9E and F).

Interpretation: Interpretations were made and based on the logic discussed by Roedder (1984). 1) Aqueous biphases (L-V) inclusions inclusions in clusters are considered as primary to pseudo-secondary inclusions if they occur in the cores or along growth zones of CSD, which indicate that they formed during mineral growth. 2) Isolated to randomly

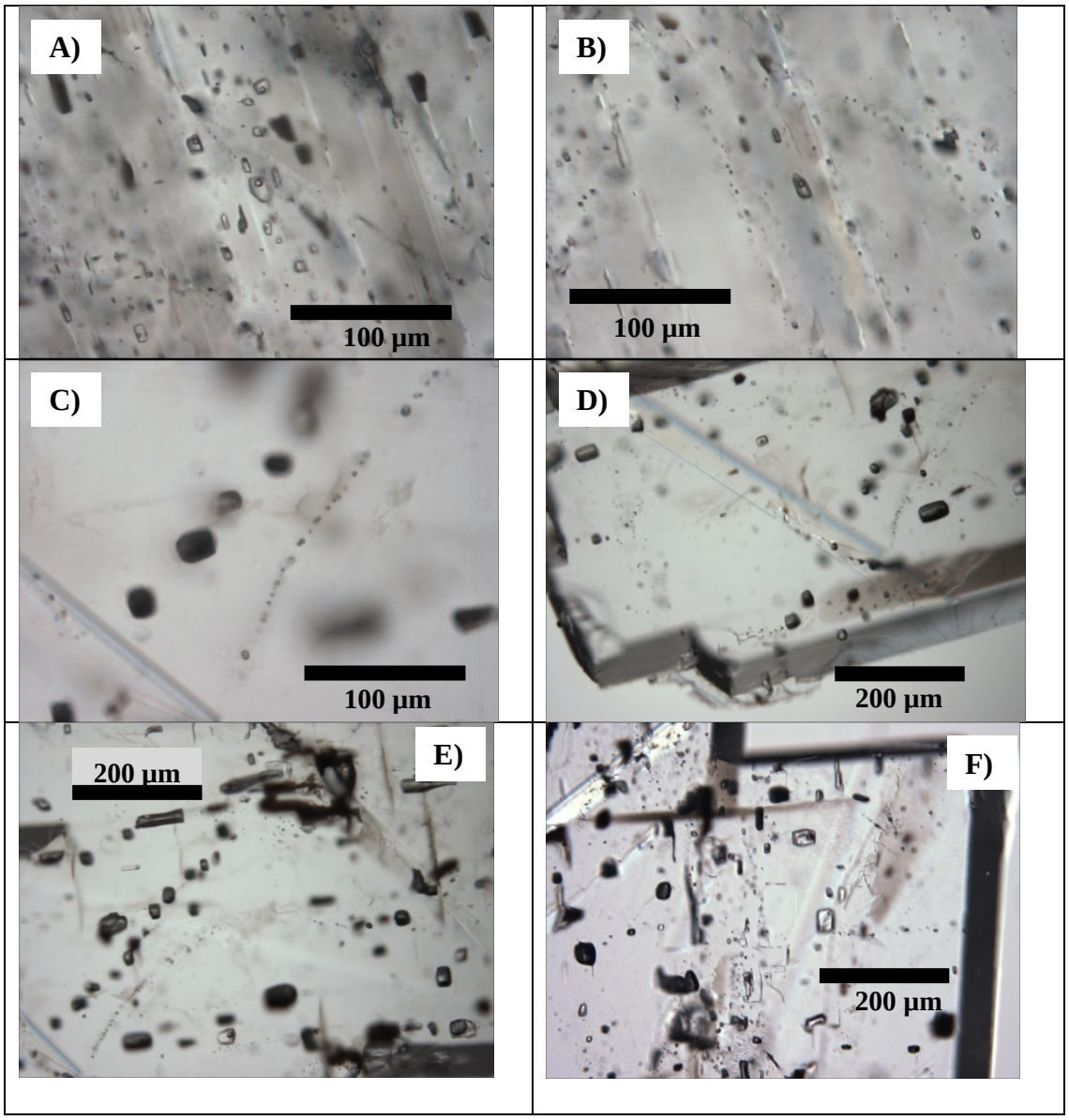

Figure 5.9A – F: Fluid inclusions in coarsely to very coarsely crystalline blocky calcite in vugs (CCC). A) A cluster of aqueous biphase (liquid + vapor) inclusions. c-27-K/94-N-16, 3958.4 m. B) Randomly distributed aqueous biphase (liquid + vapor) inclusions, and aqueous biphase (liquid + vapor) inclusions in trails. c-27-K/94-N-16, 3958.4 m. C) Carbonic (vapor only?) inclusions in trails. d-73-K/94-N-16, 3783.6 m. D) Carbonic (vapor only?) inclusions in trails, and a few randomly distributed carbonic (vapor only?) inclusions. d-73-K/94-N-16, 3783.6 m. E) Carbonic (vapor only?) inclusions in trails and a few of them appear randomly distributed. d-73-K/94-N-16, 3783.6 m. F) Randomly distributed aqueous biphase (liquid + vapor) and carbonic inclusions (vapor only?; dark colored). d-73-K/94-N-16, 3783.6 m. (original in color)

distributed aqueous biphases (L-V) inclusions are considered as primary to pseudo-primary inclusions if they occur in the cores or along growth zones of CCC. 3) Aqueous biphases (L-V) inclusions in trails that that cut across the mineral growth zones are considered as secondary inclusions. It is because if patterns of the trails do not match with the growth patterns of the host CCC, the fluid inclusions that were trapped inside are not likely to have trapped during mineral growth. 4) Carbonic (vapor only?) inclusions in trails that appear entrapping along healed fractures are considered as secondary inclusions. It is because if patterns of the fractures or trails do not match with the growth patterns of the host CCC, the fluid inclusions that were trapped inside are not likely to have trapped during mineral growth. 5) Randomly distributed to isolated carbonic (vapor only?) inclusions are considered as pseudo-secondary inclusions if they do not occur in the cores or along growth zones of CCC.

Calcite in fractures (CIF)

Observation: fluid inclusions observed in CIF include: 1) uncommon biphase (~93 – 95 % liquid and 6 – 7 % vapor) inclusions from ~0.5 – 3 μm in size. They are randomly distributed in groups of 5 to 10 (Fig. 5.10A). 2) Uncommon aqueous biphase (~93 – 95 % liquid and 6 – 7 % vapor) inclusions from 5 – 20 μm in size are found isolated to randomly distributed in three dimensions in groups of 1 – 6 inclusions (Figs. 5.10A and B). 3) Common aqueous biphase (~93 – 94 % liquid and 6 – 7 % vapor) inclusions from 2 – 5 μm in size that occur in trails in groups of 8 ~ 20 (Fig. 5.10A). 4) Locally

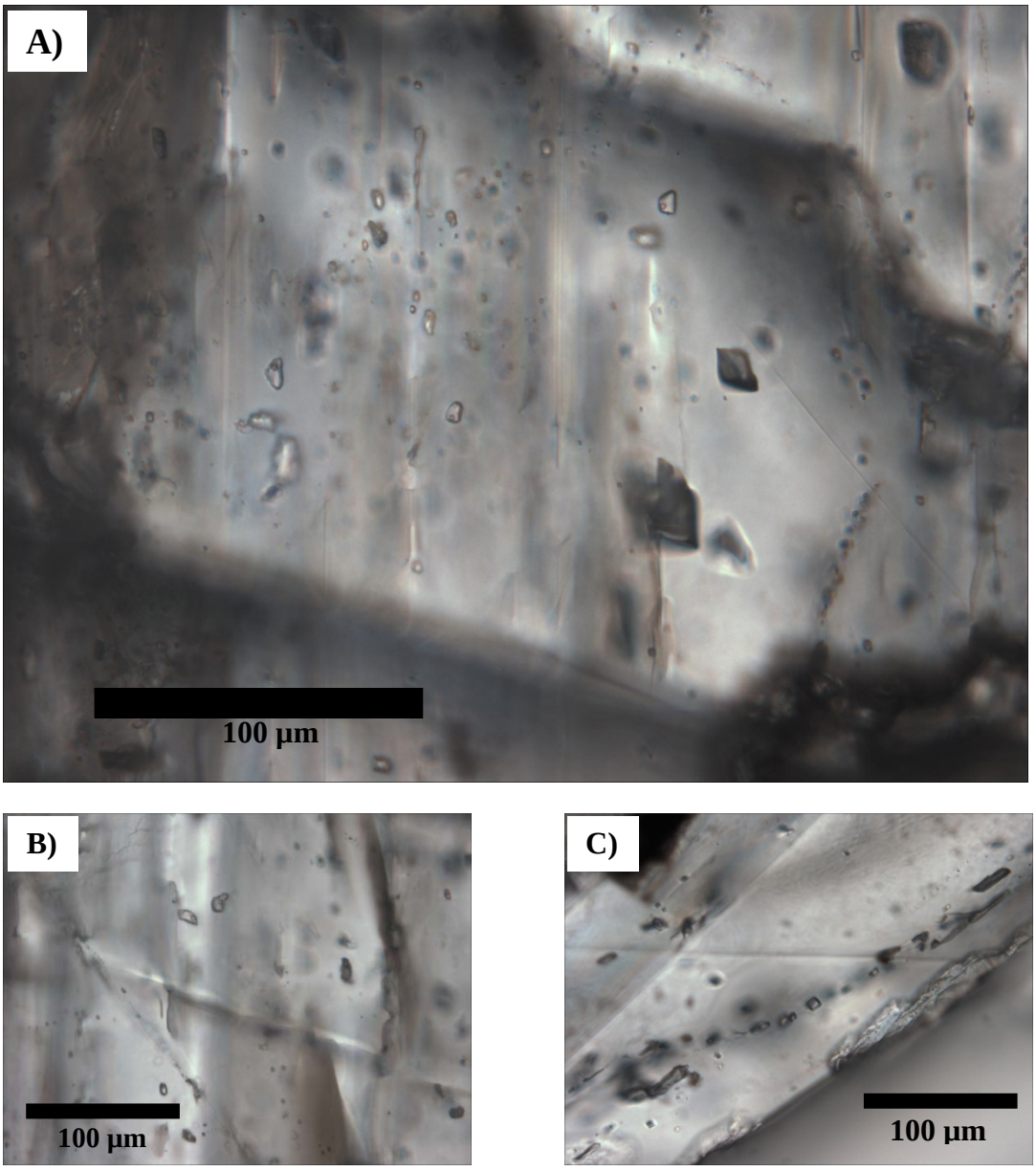

Figure 5.10A – C: Fluid inclusions in calcite in fractures (CIF). A) Randomly distributed aqueous biphase (liquid + vapor) inclusions, randomly distributed to isolated carbonic (vapor only?) inclusions (the nearly opaque inclusions). d-16-A/94-N-15, 3768.1 m. B) Randomly distributed aqueous biphase (liquid + vapor) inclusions. d-16-A/94-N-15, 3768.1 m. C) Carbonic (vapor only?) inclusions in a trail. d-16-A/ 94-N-15, 3768.1 m. (original in color)

uncommon randomly distributed to isolated gas (carbonic?) inclusions from 6 – 30 µm (Fig. 5.10A). And 5) common gas (carbonic?) inclusions of 6 – 20 µm were found in 2 samples that occur in trails of 2 – 10 (Fig. 5.10C).

Interpretation: Interpretations were made and based on the logic discussed by Roedder (1984). 1) Randomly distributed aqueous biphase (L-V) inclusions are considered as primary to pseudo-primary inclusions if they occur in the cores or along growth zones of CIF, which indicate that they formed during mineral growth. 2) Isolated to randomly distributed aqueous biphase (L-V) inclusions are considered as primary to pseudo-primary inclusions if they occur in the cores or along growth zones of CIF. 3) Aqueous biphase (L-V) inclusions in trails that cut across the mineral growth zones are considered as secondary inclusions. It is because if patterns of the trails do not match with the growth patterns of the host CIF, the fluid inclusions that were trapped inside are not likely to have trapped during mineral growth. 4) Randomly distributed to isolated carbonic (vapor only?) inclusions are considered as pseudo-secondary inclusions if they do not occur in the cores or along growth zones of CIF. 5) Carbonic (vapor only?) inclusions in trails that appear entrapping along healed fractures are considered as secondary inclusions. It is because if patterns of the fractures or trails do not match with the growth patterns of the host CIF, the fluid inclusions that were trapped inside are not likely to have trapped during mineral growth.

5.3.3 Fluid inclusion microthermometry

The “fluid inclusion assemblage” (FIA) concept of Goldstein and Reynolds (1994) was applied in this study. Fluid inclusions that 1) are associated spatially (e.g., within a cluster, or along a trail in a crystal, or randomly distributed in 3-D that resemble a group), 2) are in similar size, and 3) show similar liquid:vapor ratio are treated as an entity or FIA. Isolated inclusions that are in the neighborhood of each others were compared as if they belong to a cluster, but they are reported as separated FIAs (Chi. per. comm.). Most if not all of the measured temperature data were recorded. Fluid inclusion stretching that would produce elevated homogenization temperature measurements was taken into consideration.

An FIA represents one data point in reporting results, regardless of the number of inclusions measured in the FIA. Fluid inclusions in a cluster or along a trail are considered to be an FIA. Randomly distributed fluid inclusions that are spatially very close to each other were treated as an FIA. Isolated fluid inclusions were also treated like FIAs and represent one data point. This way of data reporting can help to avoid statistical bias caused by large number of measurements from populated fluid inclusion groups (e.g., a cluster of inclusions with fifteen fluid inclusions), because 15 measurements from a cluster with 15 inclusions will statistically outweigh a singular measurement from an isolated fluid inclusion. Therefore the mean is biased and inclined to the mean of that cluster (Chi per. comm.). The mean homogenization temperature of a sample is

calculated by adding-up the mean homogenization temperatures of each FIA and divided by the number of FIAs. The NaCl-$CaCl_2$ molecular ratio and salinity of the diagenetic fluid (s) were calculated by measuring the hydrohalite melting temperature ($T_{m\text{-}HH}$) and/or ice melting temperature ($T_{m\text{-}ice}$) from fluid inclusions then inputting the temperature measurements into the program written by Chi and Ni (2007). The two equations used by the program are:

$$y = (a+bx)^{-1/c} \qquad (5.2)$$

X_{NaCl} is calculated from $T_{m\text{-}HH}$; where y is X_{NaCl}, x is $T_{m\text{-}HH}$, a = 0.33124402, b = -0.031518028, and c = 0.22932736; and

$$y = (a + bx + cx^2)^{-1} \qquad (5.3)$$

$T_{m\text{-}ice}$ is used as the maximum possible $T_{m\text{-}HH}$ to calculate the maximum value of X_{NaCl} when only $T_{m\text{-}ice}$ can be measured and $T_{m\text{-}HH}$ is not known; where y is sailinity, x is $T_{m\text{-}HH}$ a = 0.057184817, b = 0.00078565757, and c = 5.7262766E-6.

Medium crystalline nonplanar-a saddle dolomite in vugs (MSD)

Aqueous biphase (L-V) inclusions in clusters and randomly distributed aqueous biphase (L-V) inclusions in MSD were analyzed from 2 samples. Data is summarized in Table 5.4 and Fig. 5.11. The measured inclusions are considered to be primary to pseudo-secondary inclusions, which provide information on a minimum entrapment temperature, fluid composition and salinity of the diagenetic fluid. Homogenization temperatures measured are from 177 to 207 ºC (FIA = 11). Mean homogenization temperature is 193 °C (FIA = 11). One measured first melting temperature is -56 °C (FIA = 1); hydrohalite

Table 5.4: Summary of fluid inclusion microthermometric data: biphase aqueous (liquid + vapor) inclusions in medium crystalline nonplanar-a saddle dolomite in vugs (MSD).

Diagenetic Phase	Well ID/ Depth/ Sample Number	Size (μm)	Vapor (%)	Tm-first (mean °C; FIAs)	Tm-HH (mean °C; FIAs)	Tm-H_2O (mean range °C; FIAs)	Tm-H_2O (mean °C; FIAs)	Th (mean range °C; FIAs)	Th (mean °C; FIAs)	XNaCl (mean; FIAs)	Salinity (mean wt. %; FIAs)
MSD	c-45-K/94-N-16 4324.1 m D1-3	3 – 5	5 – 7	-56 (1)	-24 (1)	-13.5 (1)	-13.5 (1)	183 – 207 (6)	197 (6)	0.7 (1)	17.2 (1)
	c-54-K/94-N-16 3851.6 m D6-8	3 – 7	5 – 6	-	-	-	-	177 – 193 (5)	187 (5)	-	-
	Summary	3 – 7	5 – 7	-56 (1)	-24 (1)	-13.5 (1)	-13.5 (1)	177 – 207 (11)	193 (11)	0.7 (1)	17.2 (1)

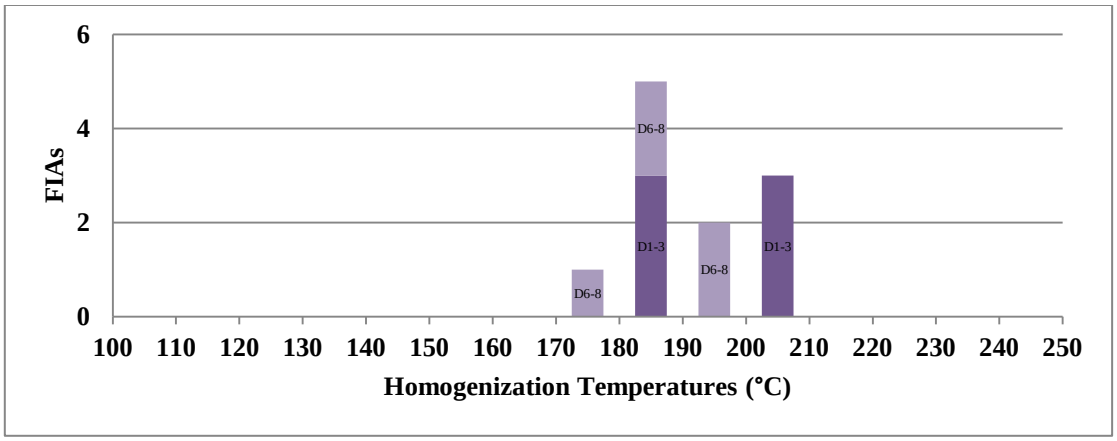

Figure 5.11: A bar plot of fluid inclusion microthermometric data of aqueous biphase (liquid + vapor) inclusions measured from medium crystalline nonplanar-a saddle dolomite in vugs (MSD). Homogenization temperatures for 11 FIAs from 2 samples. (original in color)

melting temperature is -24 °C (FIA = 1); final melting temperature is -13.5 °C (FIA = 1). The calculated $X_{NaCl/(NaCl+CaCl2)}$ is 0.7 (FIA = 1) and salinity is 17.2 wt.% $NaCl+CaCl_2$ (FIA = 1).

Coarsely to very coarsely crystalline nonplanar-e saddle dolomite in vugs (CSD)

Randomly distributed and isolated aqueous biphase (L-V) inclusions, and aqueous biphase (L-V) inclusions in clusters in CSD were analyzed from 11 samples (Tables 5.5 and Figs. 5.12A – E). Homogenization temperatures are from 170 to 231 ºC (FIA = 61). Mean homogenization temperature is 198 °C (FIA = 61). First melting temperatures are from -56 to -55 °C (mean = -55°C; FIA = 25). Hydrohalite melting temperatures are from -26 to -24 °C (mean = -25 °C; FIA = 32). Final melting temperatures are from -19.8

to -12.2 °C (mean = -16.3 °C; FIA = 27). The calculated mean $X_{NaCl/(NaCl+CaCl2)}$ is 0.6 (FIA = 32) and mean salinity is 19.3 wt.% $NaCl+CaCl_2$ (FIA = 27).

Dolomite in fractures (DIF)

Randomly distributed and isolated aqueous biphase (L-V) inclusions in DIF in 6 samples were analyzed. Data is summarized in Table 5.6 and Figs. 5.13A – E. Homogenization temperatures are from 161 to 224 ºC (FIA = 39). Mean homogenization temperature is 195°C (FIA = 39). Mean first melting temperature is -55 °C (FIA = 8). Mean hydrohalite melting temperature is -24 °C (FIA = 4). Mean final melting temperature is -15.3 °C (FIA = 2). Calculated mean $X_{NaCl/(NaCl+CaCl2)}$ is 0.7 (FIA = 4) and mean salinity is 18.6 wt.% $NaCl+CaCl_2$ (FIA = 2).

Coarsely to very coarsely crystalline blocky calcite in vugs (CCC)

Aqueous biphase (L-V) inclusions in clusters, randomly distributed or isolated, and carbonic (vapor only?) inclusions in trails (Figs. 5.14A – H), and randomly distributed carbonic (vapor only?) inclusions in CCC were analyzed. For aqueous biphase (L-V) inclusions, eight samples were analyzed and data is summarized in Table 5.7 and Figs 5.15A – E. For carbonic (vapor only?) inclusions, five samples were analyzed and data is summarized in Table 5.8 and Figs. 5.16A – C.

Table 5.5: Summary of fluid inclusion microthermometric data: biphase aqueous (liquid + vapor) inclusions in coarsely to very coarsely crystalline nonplanar-e saddle dolomite in vugs (CSD).

Diagenetic Phase	Well ID/ Depth/ Sample Number	Size (μm)	Vapor (%)	Tm-first (mean °C; FIAs)	Tm-HH (mean °C; FIAs)	Tm-H_2O (range °C; FIAs)	Tm-H_2O (mean °C; FIAs)	Th (mean range °C; FIAs)	Th (mean °C; FIAs)	XNaCl (mean; FIAs)	Salinity (mean wt. %; FIAs)
CSD	c-45-K/94-N-16 4324.1 m D1-3	3 – 15	5 – 7	-55 (1)	-25 (2)	-16.0 – -14.0 (2)	-15.0 (2)	186 – 217 (8)	199 (8)	0.6 (2)	18.5 (2)
	b-19-K/94-N-16 4192.9 m D4-2	2 – 8	6 – 10	-56 (6)	-25 (5)	-18.7 – -14.8 (6)	-16.6 (6)	170 – 221 (10)	194 (10)	0.6 (5)	19.5 (6)
	b-19-K/94-N-16 3947.1 m D4-8	2 – 9	6	-	-24 (2)	-14.9 (1)	-14.9 (1)	174 – 197 (4)	186 (4)	0.7 (2)	18.3 (1)
	a-67-D/94-O-13 5221.3 m 5.2	2 – 6	5	-56 (1)	-25 (1)	-16.9 – -17.1 (1)	-17.0 (1)	195 (1)	195 (1)	0.6 (1)	19.7 (1)
	c-54-K/94-N-16 3620.1 m D6-7	2 – 7	5	-55 (3)	-24 (4)	-17.7 – -15.2 (4)	-16.1 (4)	175 – 185 (4)	180 (4)	0.7 (4)	19.1 (4)
	c-54-K/94-N-16 3851.6 m D6-8	3 – 11	5 – 6	-55 (4)	-25 (4)	-17.3 – -15.5 (3)	-16.2 (3)	170 – 208 (13)	182 (13)	0.6 (4)	19.1 (3)
	d-73-K/94-N-16 3783.6 m D7-1	3 – 12	5 – 7	-56 (3)	-26 (6)	-19.2 – -12.2 (5)	15.5 (5)	176 – 231 (6)	194 (6)	0.5 (6)	18.4 (5)
	c-27-K/94-N-16 3958.4 m D8-4	2 – 8	5 – 7	-55 (2)	-26 (2)	-19.8 (2)	-19.8 (2)	173 – 216 (3)	209 (3)	0.6 (2)	21.9 (2)
	c-27-K/94-N-16 3815.3 m D8-10	3 – 8	5 – 7	-55 (1)	-24 (2)	-	-	187 – 224 (5)	211 (5)	-0.7 (2)	-
	d-16-A/94-N-15 3816.8 m D17-3	2 – 7	5 – 6	-56 (3)	-25 (3)	-16.1 – -16.0 (2)	-16.1 (2)	189 – 207 (6)	199 (6)	-0.6 (3)	-19.3 (2)
	d-16-A/94-N-15 3764.3 m D17-8	3 – 6	5 – 7	-55 (1)	-25 (1)	-16.8 – -17.0 (2)	-16.9 (1)	209 (1)	209 (1)	0.6 (1)	19.6 (1)
	Summary	2 – 15	5 – 10	-55 (25)	-25 (32)	-19.8 – -12.2 (27)	-16.3 (27)	170 – 231 (61)	198 (61)	0.6 (32)	19.3 (27)

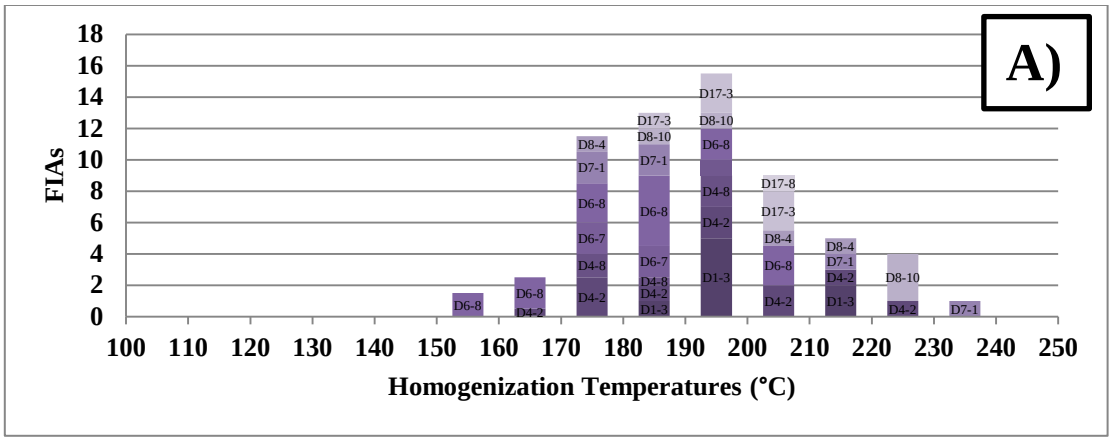
A)
FIAs
Homogenization Temperatures (°C)
100 110 120 130 140 150 160 170 180 190 200 210 220 230 240 250
0 2 4 6 8 10 12 14 16 18

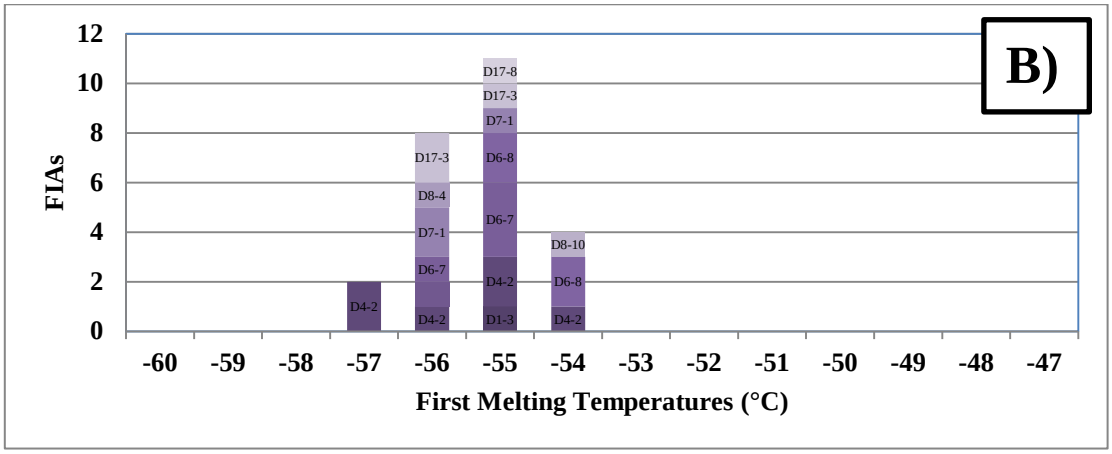
B)
FIAs
First Melting Temperatures (°C)
-60 -59 -58 -57 -56 -55 -54 -53 -52 -51 -50 -49 -48 -47
0 2 4 6 8 10 12

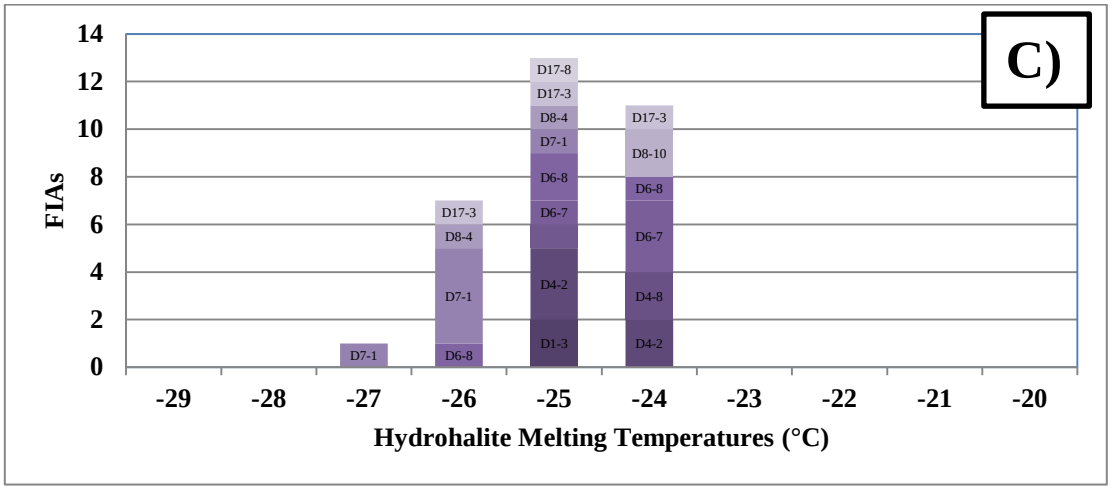
C)
FIAs
Hydrohalite Melting Temperatures (°C)
-29 -28 -27 -26 -25 -24 -23 -22 -21 -20
0 2 4 6 8 10 12 14

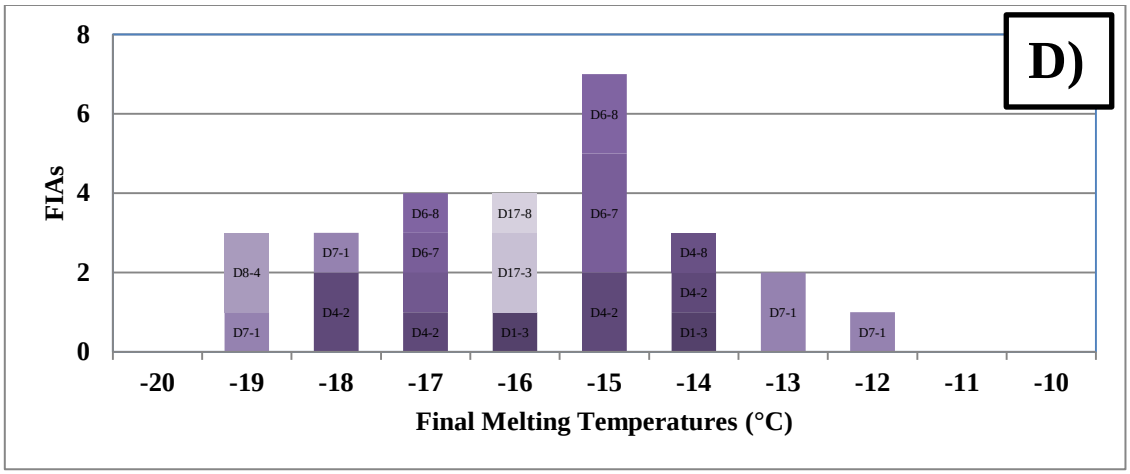

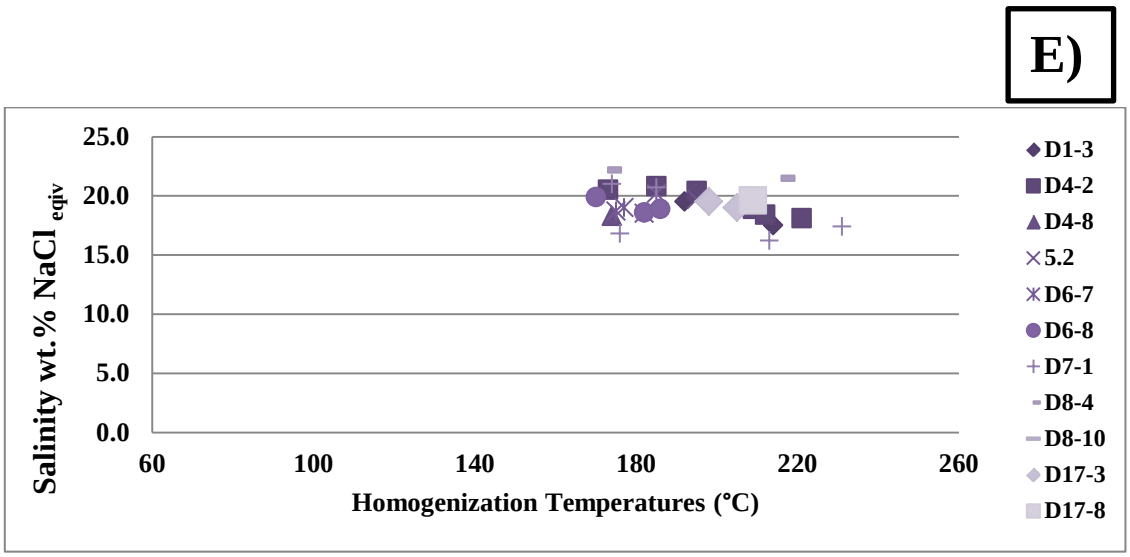

Figure 5.12A – E: Bar plots of fluid inclusion microthermometric data of aqueous biphase (liquid + vapor) inclusions measured from coarsely to very coarsely crystalline nonplanar-e saddle dolomite in vugs (CSD). A) Homogenization temperatures of 61 FIAs from 11 samples. B) First melting temperatures of 25 FIAs from 10 samples. C) Hydrohalite melting temperatures of 32 FIAs from 11 samples. D) Final melting temperatures of 27 FIAs from 10 samples. E) Cross-plot of homogenization temperatures and salinities of 27 FIAs from 11 samples. (original in color)

Table 5.6: Summary of fluid inclusion microthermometric data: biphase aqueous (liquid + vapor) inclusions in dolomite in fractures (DIF).

Diagenetic Phase	Well ID/ Depth/ Sample Number	Size (µm)	Vapor (%)	Tm-first (mean °C; FIAs)	Tm-HH (mean °C; FIAs)	Tm-H_2O (range °C; FIAs)	Tm-H_2O (mean °C; FIAs)	Th (mean range °C; FIAs)	Th (mean °C; FIAs)	XNaCl (mean; FIAs)	Salinity (mean wt. %; FIAs)
DIF	c-45-K/94-N-16 3716.7 m 1.30	3 – 6	6	-	-24 (1)	-14.5 (1)	-14.5 (1)	173 – 224 (15)	201 (15)	0.7 (1)	18.0 (1)
	b-19-K/94-N-16 3947.1 m D4-8	6 – 8	6 – 7	-55 (2)	-24 (1)	-	-	174 – 200 (5)	192 (5)	0.7 (1)	-
	a-67-D/94-O-13 5225.1 m 5.1	4	6	-	-	-	-	184 – 187 (2)	186 (2)	-	-
	c-54-K/94-N-16 3851.6 m D6-8	4 – 7	6 – 7	-55 (3)	-25 (2)	-16.0 (1)	-16.0 (1)	161 – 217 (8)	189 (8)	0.7 (2)	19.1 (1)
	c-27-K/94-N-16 3821.7 m 8.6	2 – 11	6	-55 (1)	-	-	-	176 – 206 (4)	186 (4)	-	-
	d-16-A/94-N-15 3810.9 m D17-2	2 – 5	6 – 7	-55 (2)	-	-	-	184 – 213 (5)	198 (5)	-	-
	Summary	2 – 11	6 – 7	-55 (8)	-24 (4)	-15.3 (2)	-15.3 (2)	161 – 224 (39)	195 (39)	0.7 (4)	18.6 (2)

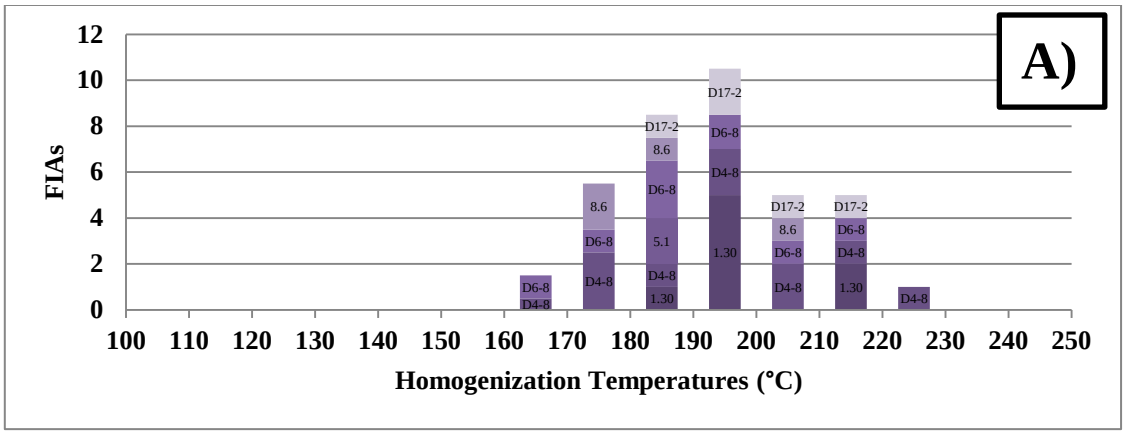
A)
FIAs
12
10
8
6
4
2
0
100 110 120 130 140 150 160 170 180 190 200 210 220 230 240 250
Homogenization Temperatures (°C)
D6-8
D4-8
8.6
D6-8
D4-8
D17-2
8.6
D6-8
5.1
D4-8
1.30
D17-2
D6-8
D4-8
1.30
D17-2
8.6
D6-8
D4-8
D17-2
D6-8
D4-8
1.30
D4-8

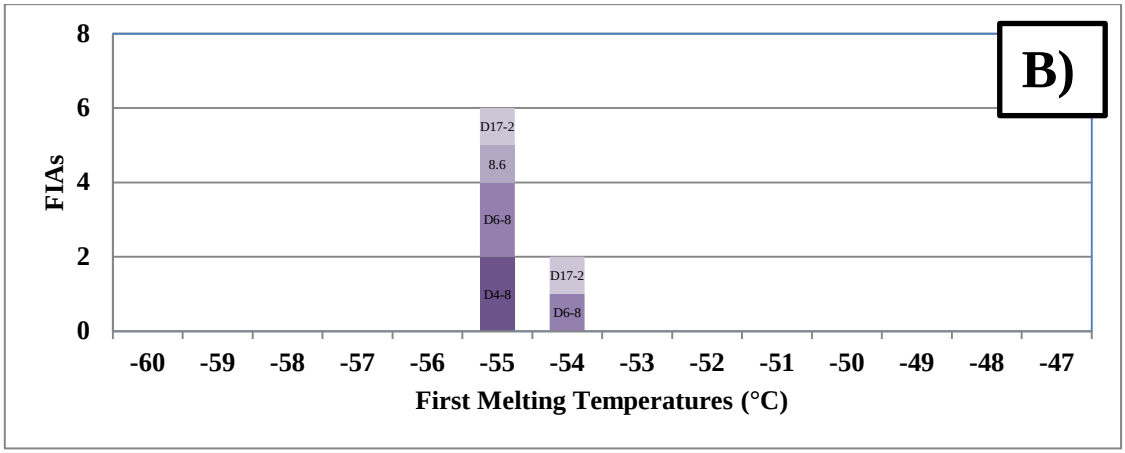
B)
FIAs
8
6
4
2
0
-60 -59 -58 -57 -56 -55 -54 -53 -52 -51 -50 -49 -48 -47
First Melting Temperatures (°C)
D17-2
8.6
D6-8
D4-8
D17-2
D6-8

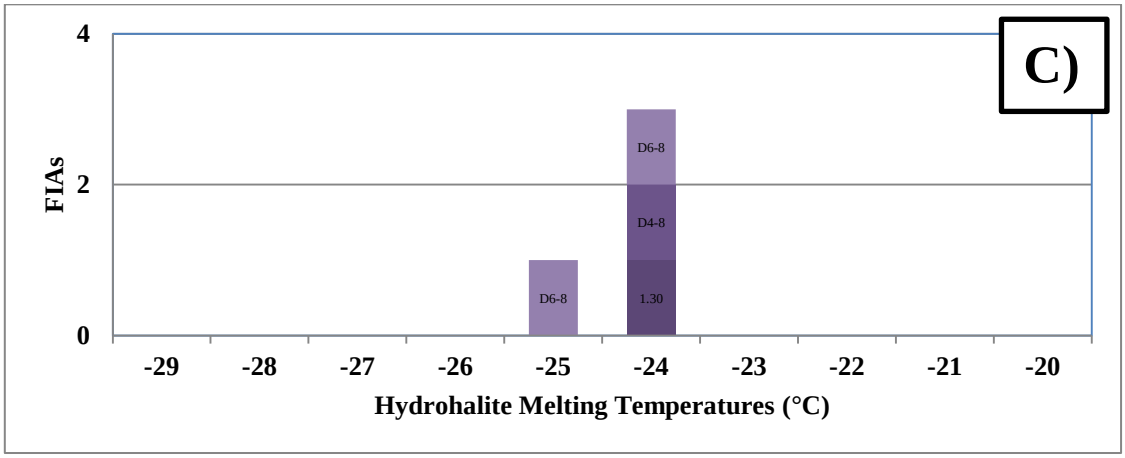
C)
FIAs
4
2
0
-29 -28 -27 -26 -25 -24 -23 -22 -21 -20
Hydrohalite Melting Temperatures (°C)
D6-8
D6-8
D4-8
1.30

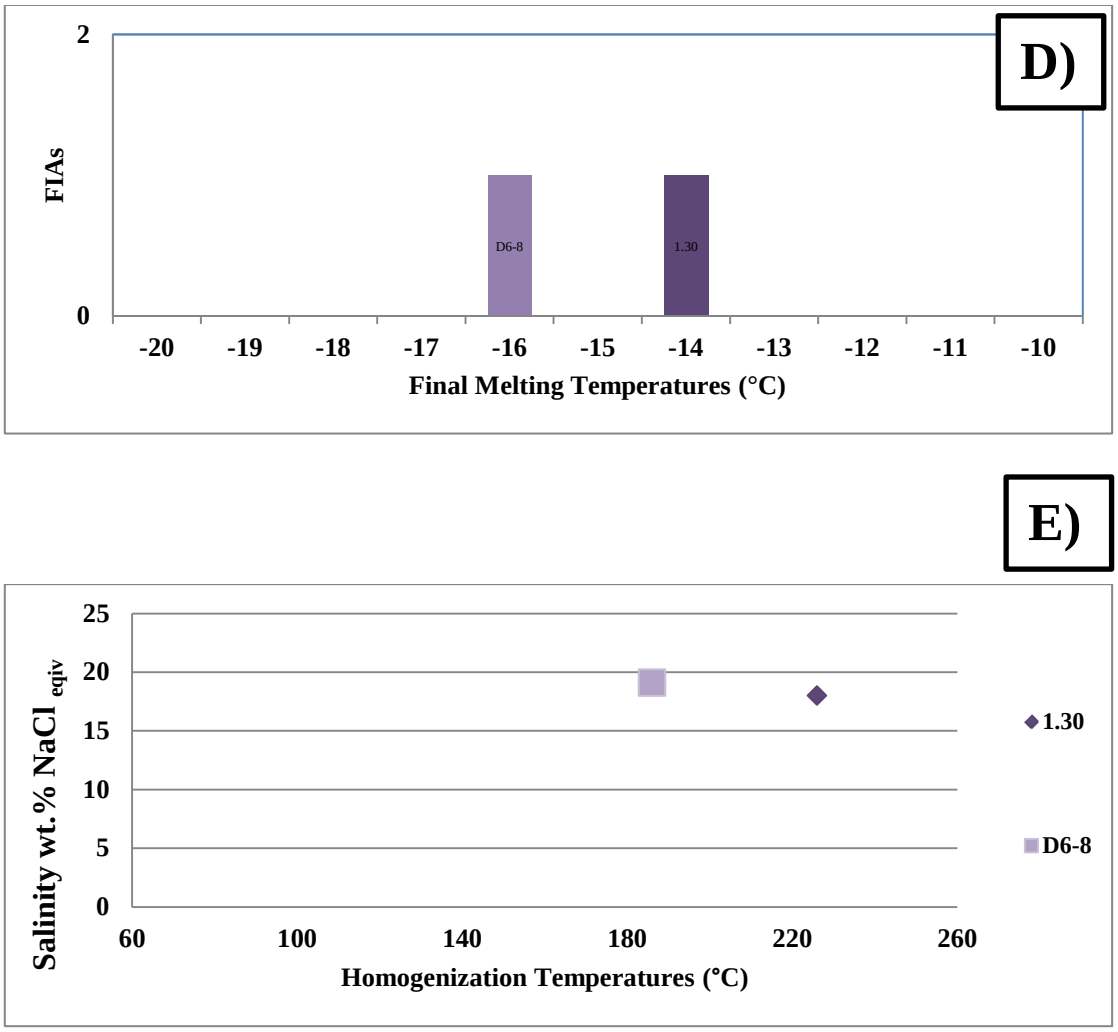

Figure 5.13A – E: Bar plots of the fluid inclusion microthermometric data of aqueous biphase (liquid + vapor) inclusions measured from dolomite in fractures (DIF). A) Homogenization temperatures of 39 FIAs from 4 samples. B) First melting temperatures of 8 FIAs from 4 samples. C) Hydrohalite melting temperatures of 4 FIAs from 3 samples. D) Final melting temperature of 2 FIAs from 2 samples. E) Cross-plot of homogenization temperatures and salinities of 2 FIAs from 2 samples. (original in color)

Aqueous biphase (L-V) inclusions: Measured homogenization temperatures are from 138 to 209 ºC (FIA = 50). Mean homogenization temperature is 179°C (FIA = 50). Mean first melting temperature measured is -53°C (FIA = 26). Mean hydrohalite melting temperature is -23°C (FIA = 39). Mean final melting temperature is -14.8°C (FIA = 36). The calculated mean $X_{NaCl/(NaCl+CaCl2)}$ is 0.8 (FIA = 39) and mean salinity is 18.0 wt.% $NaCl+CaCl_2$ (FIA = 36).

Carbonic (vapor only?) inclusions: Homogenization temperatures (solid + liquid + vapor → vapor, or liquid + vapor → vapor) were measured from randomly distributed or isolated carbonic (vapor only?) inclusions, and carbonic (vapor only?) inclusions in trails. Homogenization temperatures measured from randomly distributed or isolated carbonic (vapor only?) inclusions are from –53.8 to –51.4 °C (mean = -52.7 °C; FIA = 5). Homogenization temperatures measured from carbonic (vapor only?) inclusions in trails are from –56.0 to –52.4 °C (mean = -53.9 °C; FIA = 9). Mean homogenization temperature of all carbonic (vapor only?) inclusions measured is -53.5 °C (FIA = 14).

Calcite in fractures (CIF)

Randomly distributed and isolated aqueous biphase (L-V) inclusions, and carbonic (vapor only?) inclusions in trails and randomly distributed carbonic (vapor only?) inclusions in CIF were analyzed. For aqueous biphase (L-V) inclusions, three samples were analyzed and data is summarized in Table 5.9 and Figs 5.17A – E. For carbonic

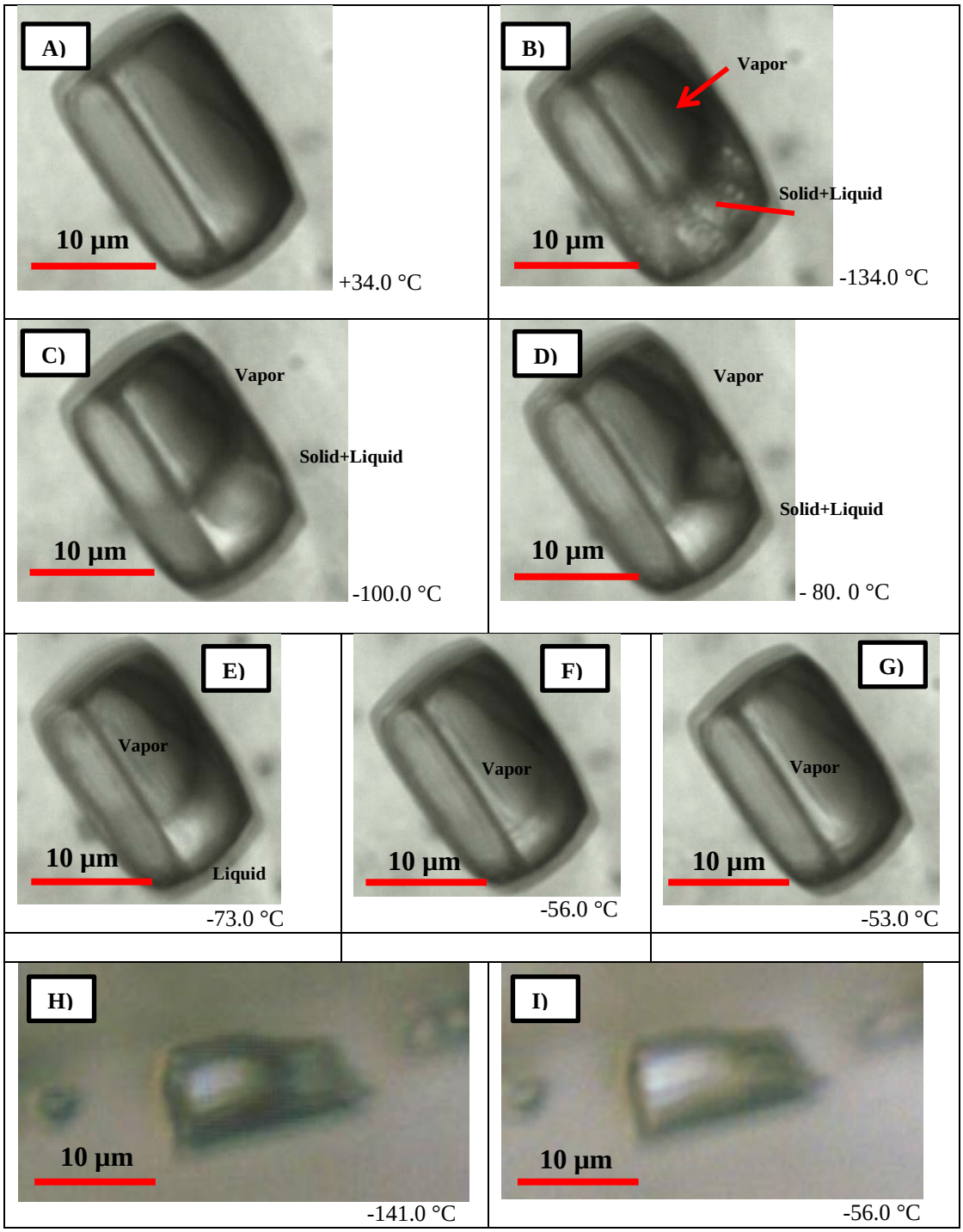
A)
10 µm
+34.0 °C
B)
Vapor
Solid+Liquid
10 µm
-134.0 °C
C)
Vapor
Solid+Liquid
10 µm
-100.0 °C
D)
Vapor
Solid+Liquid
10 µm
- 80. 0 °C
E)
Vapor
10 µm
Liquid
-73.0 °C
F)
Vapor
10 µm
-56.0 °C
G)
Vapor
10 µm
-53.0 °C
H)
10 µm
-141.0 °C
I)
10 µm
-56.0 °C

Figure 5.14A – I: Photomicrographs of two carbonic inclusions. A – G) A carbonic inclusion in coarsely to very coarsely crystalline blocky calcite in vugs (CCC). Sample is from d-73-K/94-N-16, 3783.6 m. A) At +34.0 °C, carbonic inclusion appeared to comprise of ~100% vapor(?). B) At -134.0 °C, vapor, solid and liquid phases were observed within the carbonic inclusion. C) Starting at approximately -100 °C, the solid phase started to thaw. D) At -80.0 °C, the solid phase and started to move in the liquid. E) At -73.0 °C, the solid phase was melt. F) At -56.0 °C, vapor and liquid homogenize into vapor(?). G) At approximately -53.0 °C, vapor and liquid were homogenized. H and I) A carbonic inclusion in calcite in fractures (CIF). Sample is from d-16-A/94-N-15, 3768.1 m. G) A carbonic inclusion at -141.0 °C and H) The same inclusion in Fig. 5.13G at -56.0 °C, which the liquid and vapor homogenized into vapor. (original in color)

Table 5.7: Summary of fluid inclusion microthermometric data: biphase aqueous inclusions (liquid + vapor) in the coarsely to very coarsely crystalline blocky calcite in vugs (CCC).

Diagenetic Phase	Well ID/ Depth/ Sample Number	Size (μm)	Vapor (%)	Tm-first (mean °C; FIAs)	Tm-HH (mean °C; FIAs)	Tm-H_2O (range °C; FIAs)	Tm-H_2O (mean °C; FIAs)	Th (mean range °C; FIAs)	Th (mean °C; FIAs)	XNaCl (mean; FIAs)	Salinity (mean wt. %; FIAs)
CCC	c-45-K/94-N-16 4026.3 m 1-5B	4 – 7	5 – 7	-54 (3)	-25 (5)	-14.2 (1)	-14.2 (1)	144 – 179 (5)	167 (5)	0.6 (5)	17.7 (1)
	c-10-E/94-N-7 1823.0 m D2-3	7 – 20	4 – 6	-52 (4)	-23 (6)	-13.7 – -11.2 (6)	-12.8 (6)	141 – 185 (8)	165 (8)	0.8 (6)	16.6 (6)
	b-19-K/94-N-16 4192.9 m D4-2	10 – 28	4 – 6	-54 (6)	-24 (8)	-17.5 – -13.5 (9)	-16.0 (9)	138 – 209 (11)	176 (11)	0.7 (8)	19.1 (9)
	a-67-D/94-O-13 5221.3 m 5.2	2 – 8	5	-54 (2)	-24 (2)	-14.6 (1)	-14.6 (1)	185 – 188 (3)	187 (3)	0.8 (2)	18.0 (1)
	d-73-K/94-N-16 3783.6 m D7-1	15 – 23	4 – 6	-50 (4)	-21 (4)	-12.0 – -10.7 (4)	-11.2 (4)	174 – 208 (6)	185 (6)	1.0 (4)	15.2 (4)
	c-27-K/94-N-16 3958.4 m D8-4	6 – 48	4 – 6	-54 (2)	-25 (2)	-19.3 – -18.0 (3)	-18.6 (3)	185 – 199 (5)	190 (5)	0.7 (2)	20.6 (3)
	c-27-K/94-N-16 3815.3 m D8-10	5 – 9	6	-53 (3)	-24 (4)	-169 – -12.9 (4)	-14.9 (4)	164 – 195 (4)	182 (4)	0.8 (4)	18.2 (4)
	d-16-A/94-N-15 3764.3 m D17-8	10 – 33	5 – 10	-53 (2)	-23 (8)	-17.5 – -13.3 (8)	-15.4 (8)	166 – 196 (8)	186 (8)	0.8 (8)	18.6 (8)
	Summary	2 – 33	4 – 10	-53 (26)	-23 (39)	-19.3 – -11.2 (36)	-14.8 (36)	138 – 209 (50)	179 (50)	0.8 (39)	18.0 (36)

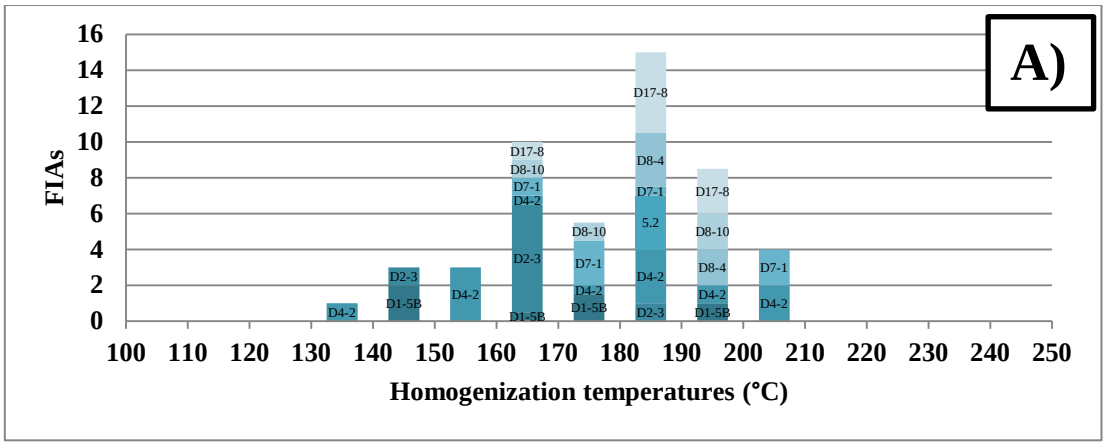
A)
FIAs
Homogenization temperatures (°C)

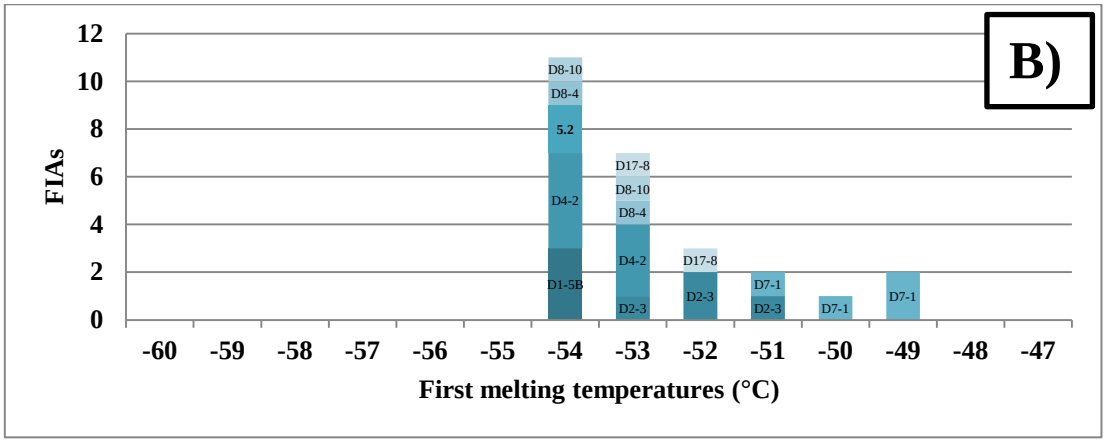
B)
FIAs
First melting temperatures (°C)

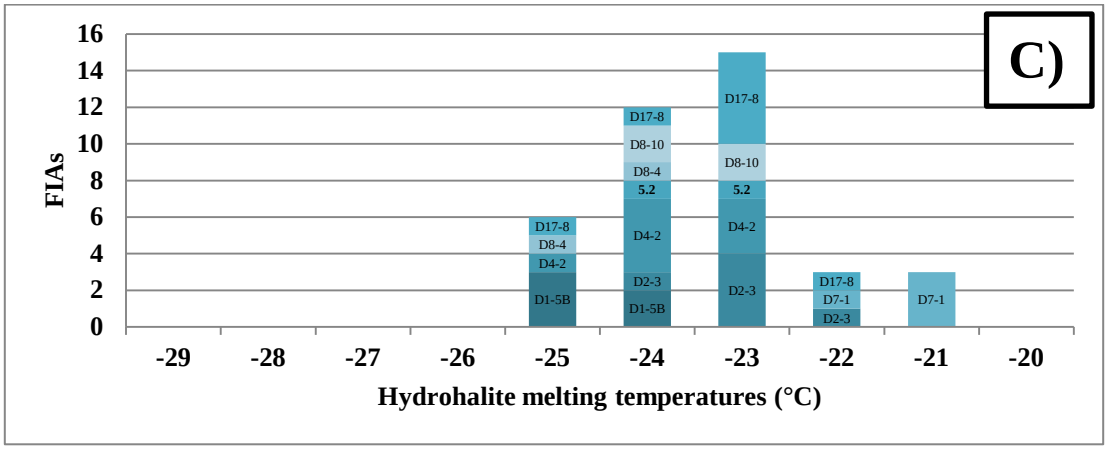
C)
FIAs
Hydrohalite melting temperatures (°C)

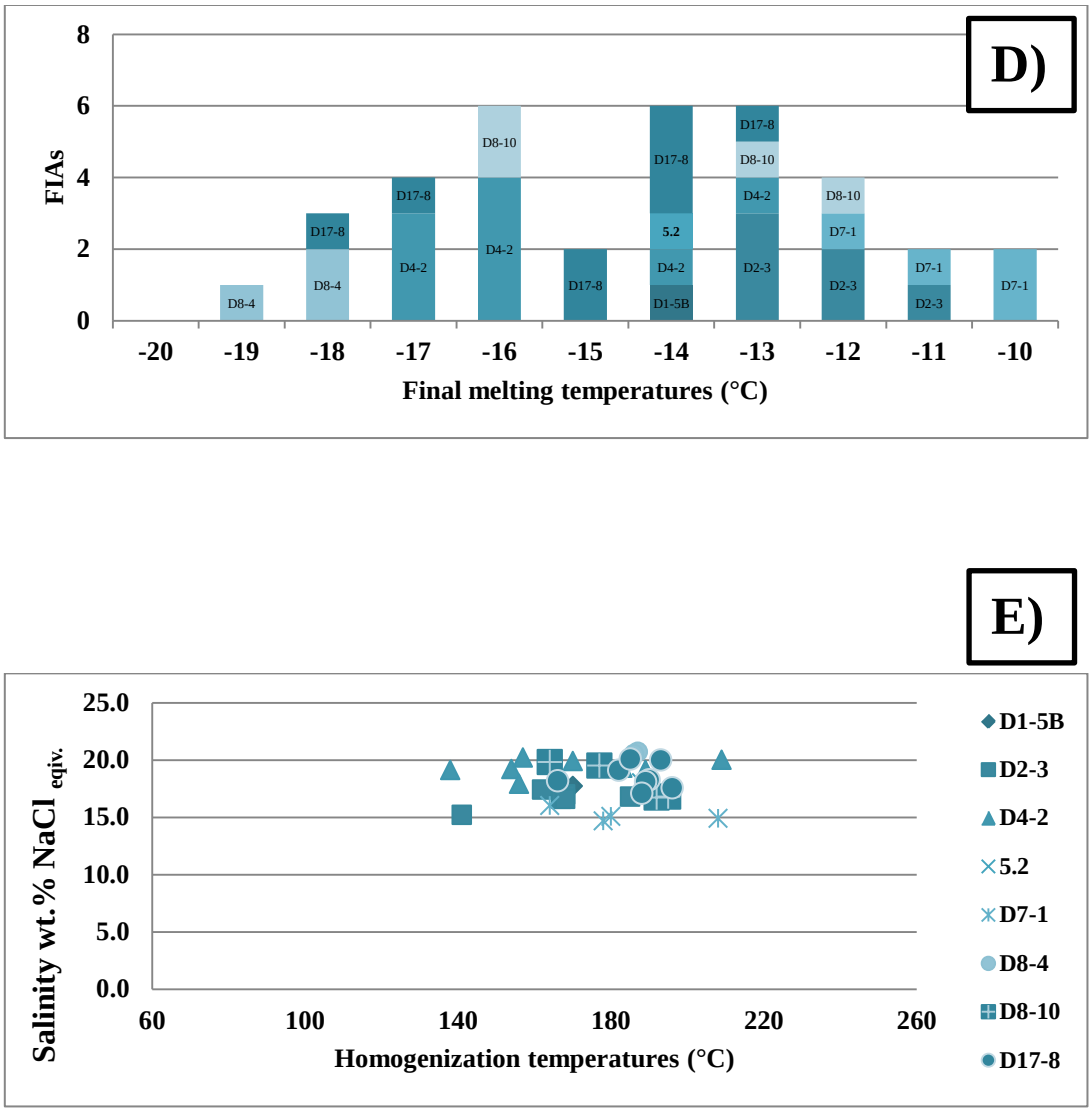

Figure 5.15A – E: Bar plots of the fluid inclusion microthermometric data of aqueous biphase (liquid + vapor) inclusions measured from coarsely to very coarsely crystalline blocky calcite in vugs (CCC). A) Homogenization temperatures of 50 FIAs from 8 samples. B) First melting temperatures of 26 FIAs from 8 samples. C) Hydrohalite melting temperatures of 39 FIAs from 8 samples. D) Final melting temperatures of 36 FIAs from 8 samples. E) Cross-plot of homogenization temperatures and salinities of 36 FIAs from 8 samples. (original in color)

Table 5.8: Summary of fluid inclusion microthermometric data: carbonic (vapor only?) inclusions in the coarsely to very coarsely crystalline blocky calcite in vugs (CCC)

Diagenetic Phase	Well ID/ Depth/ Sample Number	Size (µm)	Vapor (%)	Th (mean range °C; FIAs)	Th (mean °C; FIAs)
CCC	b-19-K/94-N-16 4192.9 m D4-2				
	Random /Isolated	16	~100	-53.1 (1)	-53.1 (1)
	Trails	11 – 36	~100	-56.0 – -52.5 (3)	-54.2 (3)
	a-67-D/94-O-13 5221.3 m 5.2				
	Random /Isolated	9	~100	-52.1 (1)	-52.1 (1)
	Trails	-	-	-	-
	d-73-K/94-N-16 3783.6 m D7-1				
	Random /Isolated	21 – 31	~100	-53.8 – -51.4 (2)	-52.6 (2)
	Trails	10 – 21	~100	-53.2 – -52.7 (2)	-53.0 (2)
	c-27-K/94-N-16 3958.4 m D8-4				
	Random /Isolated	-	-	-	-
	Trails	16	~100	-54.7 (1)	-54.7 (1)
	c-27-K/94-N-16 3815.3 m D8-10				
	Random /Isolated	8	~100	-53.0 (1)	-53.0 (1)
	Trails	8 – 10	~100	-54.7 – -52.4 (3)	-53.9 (3)
	Random /Isolated	8 – 31	~100	-53.8 – -51.4 (5)	-52.7 (5)
	Trails	8 – 36	~100	-56.0 – -52.4 (9)	-53.9 (9)
	Summary	8 – 36	~100	-56.0 – -51.4 (14)	-53.5 (14)

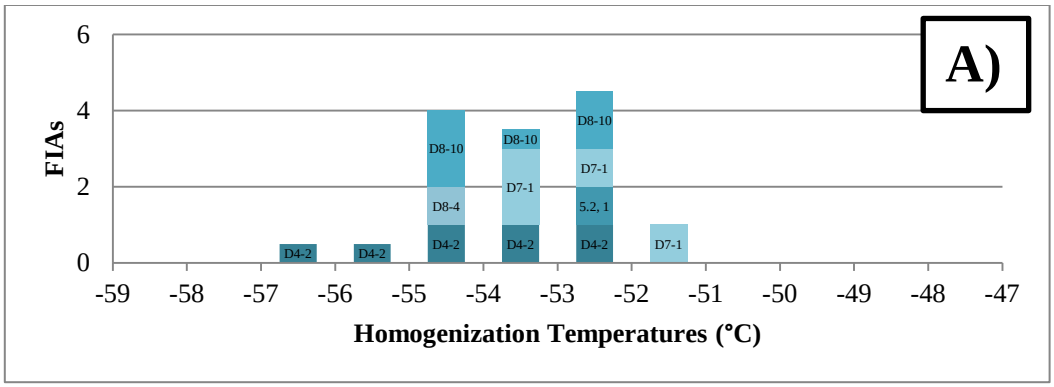
A)
FIAs
6
4
2
0
D4-2
D4-2
D8-10
D8-4
D4-2
D8-10
D7-1
D4-2
D8-10
D7-1
5.2, 1
D4-2
D7-1
-59 -58 -57 -56 -55 -54 -53 -52 -51 -50 -49 -48 -47
Homogenization Temperatures (°C)

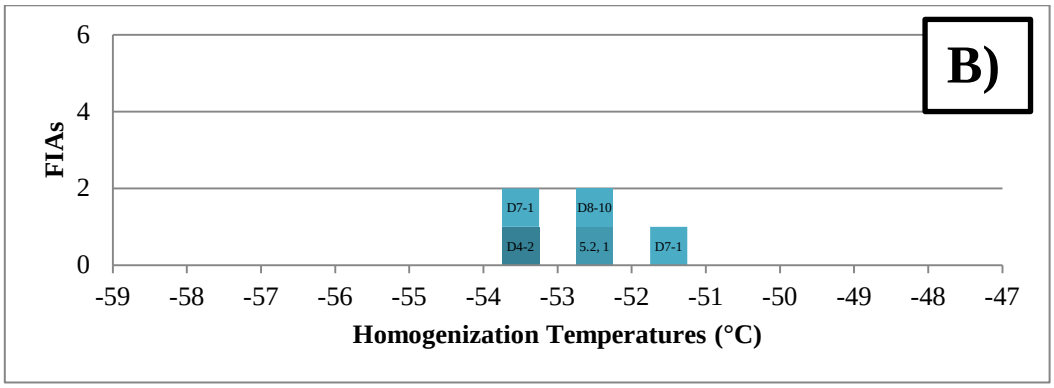
B)
FIAs
6
4
2
0
D7-1
D4-2
D8-10
5.2, 1
D7-1
-59 -58 -57 -56 -55 -54 -53 -52 -51 -50 -49 -48 -47
Homogenization Temperatures (°C)

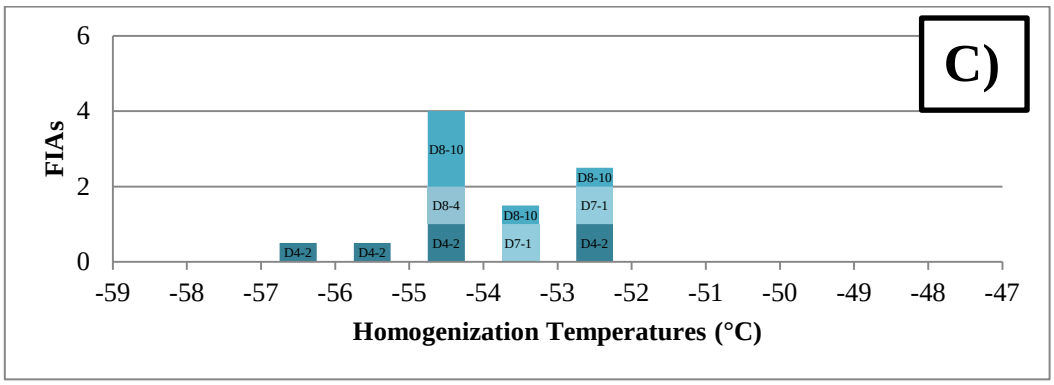
C)
FIAs
6
4
2
0
D4-2
D4-2
D8-10
D8-4
D4-2
D8-10
D7-1
D8-10
D7-1
D4-2
-59 -58 -57 -56 -55 -54 -53 -52 -51 -50 -49 -48 -47
Homogenization Temperatures (°C)

Figure 5.16A – C: Bar plots of the homogenization temperatures of carbonic (vapor only?) inclusions measured from coarsely to very coarsely crystalline blocky calcite in vugs (CCC). A) Homogenization temperatures measured from randomly distributed or isolated carbonic (vapor only?) inclusions from 14 FIAs in 5 samples. B) Homogenization temperatures measured from randomly distributed or isolated carbonic (vapor only?) inclusions from 5 FIAs in 4 samples. C) Homogenization temperatures measured from carbonic (vapor only?) inclusions in trails from 9 FIAs in 4 samples. (original in color)

(vapor only?) inclusions, two samples were analyzed and data is summarized in Table 5.10 and Figs. 5.18A – C. Aqueous biphase (L-V) inclusions: Homogenization temperatures are from 172 to 194 ºC (FIA = 11). Mean homogenization temperature is 183°C (FIA = 11). Mean first melting temperature is -52 °C (FIA = 8). Mean hydrohalite melting temperature is -24 °C (FIA = 11). Mean final melting temperature is -16.6 °C (FIA = 9). The calculated mean $X_{NaCl/(NaCl+CaCl2)}$ is 0.7 (FIA = 11) and mean salinity is 19.4 wt.% NaCl+$CaCl_2$ (FIA = 9). Carbonic (vapor only?) inclusions: Homogenization temperatures (solid + liquid + vapor → vapor, or liquid + vapor → vapor) were measured from randomly distributed or isolated carbonic (vapor only?) inclusions, carbonic (vapor only?) inclusions in clusters, and carbonic (vapor only?) inclusions in trails. Homogenization temperatures measured from carbonic (vapor only?) inclusions that are randomly distributed, isolated or in clusters are from -58.7 to -49.5 °C (mean = -55.0 °C; FIA = 12). Homogenization temperatures measured from carbonic (vapor only?) inclusions in trails are from –56.8 to –54.2 °C (mean = -54.4 °C; FIA = 3). Mean homogenization temperature of all carbonic (vapor only?) inclusions measured is -55.1 °C (FIA = 15).

Table 5.9: Summary of fluid inclusion microthermometric data: biphase aqueous (liquid + vapor) inclusions in calcite in fractures (CIF).

Diagenetic Phase	Well ID/ Depth/ Sample Number	Size (μm)	Vapor (%)	Tm-first (mean °C; FIAs)	Tm-HH (mean °C; FIAs)	Tm-H_2O (range °C; FIAs)	Tm-H_2O (mean °C; FIAs)	Th (mean range °C; FIAs)	Th (mean °C; FIAs)	XNaCl (mean; FIAs)	Salinity (mean wt. %; FIAs)
CIF	d-16-A/94-N-15 3768.1 m D17-1	5 – 8	6	-49 (1)	-24 (2)	-16.0 – -11.9 (2)	-14.0 (2)	174 – 180 (2)	177 (2)	0.8 (2)	17.5 (2)
	d-16-A/94-N-15 3816.8 m D17-3	7 – 18	5 – 6	-53 (6)	-24 (7)	-20.8 – -15.1 (5)	-17.8 (5)	176 – 194 (7)	187 (7)	0.7 (7)	20.2 (5)
	d-16-A/94-N-15 3769.1 m D17-J	13 – 15	6	-52 (1)	-24 (2)	-16. 3 – -16.1 (2)	-16.2 (2)	172 – 175 (2)	174 (2)	0.8 (2)	19.3 (2)
	Summary	5 – 18	5 – 6	-52 (8)	-24 (11)	-20.8 – -11.9 (9)	-16.6 (9)	172 – 194 (11)	183 (11)	0.7 (11)	19.4 (9)

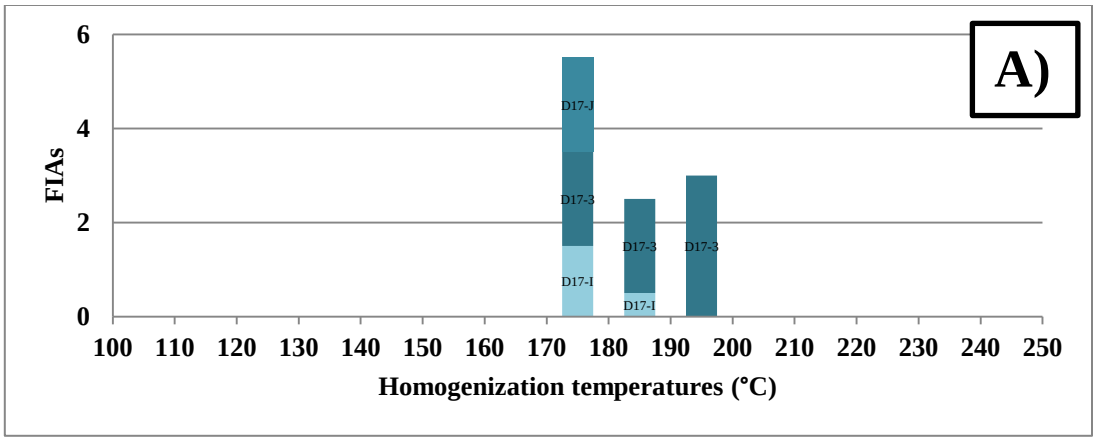
A)
FIAs
0
2
4
6
D17-I
D17-3
D17-3
D17-3
D17-I
D17-I
100 110 120 130 140 150 160 170 180 190 200 210 220 230 240 250
Homogenization temperatures (°C)

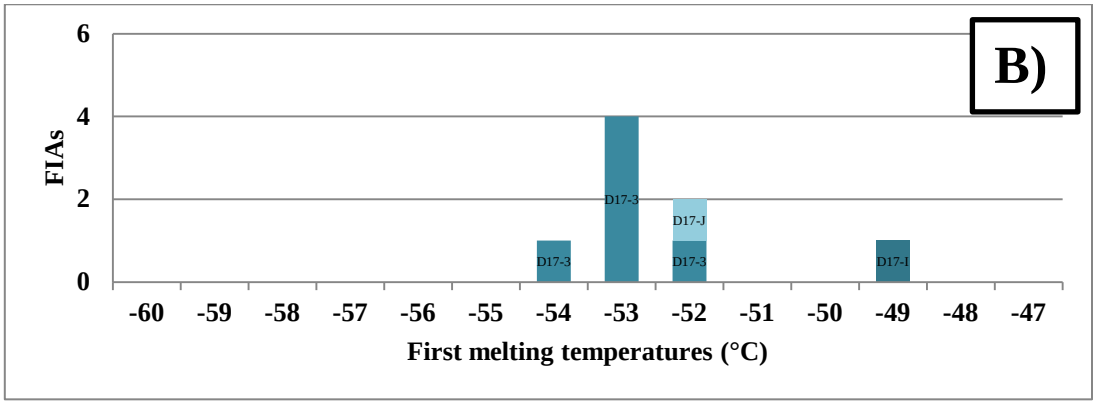
B)
FIAs
0
2
4
6
D17-3
D17-3
D17-J
D17-3
D17-I
-60 -59 -58 -57 -56 -55 -54 -53 -52 -51 -50 -49 -48 -47
First melting temperatures (°C)

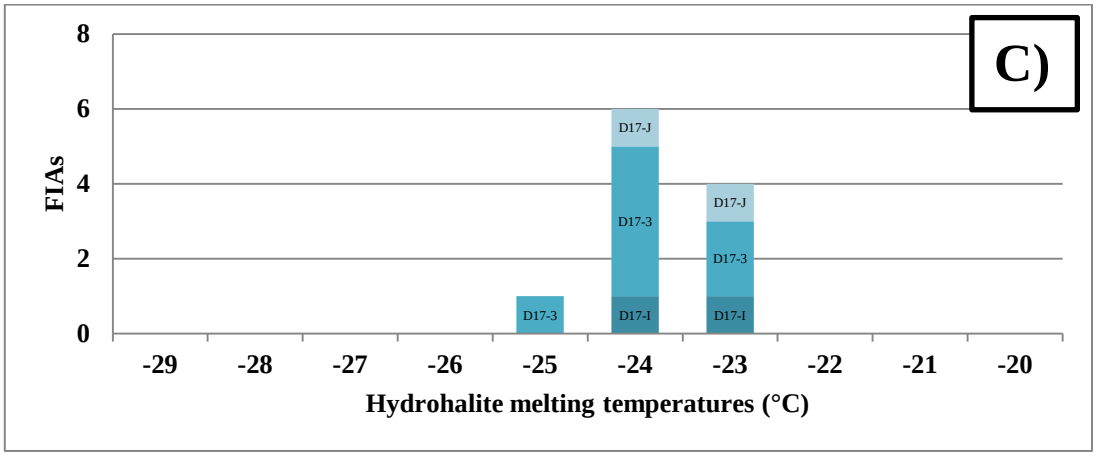
C)
FIAs
0
2
4
6
8
D17-3
D17-J
D17-3
D17-I
D17-J
D17-3
D17-I
-29 -28 -27 -26 -25 -24 -23 -22 -21 -20
Hydrohalite melting temperatures (°C)

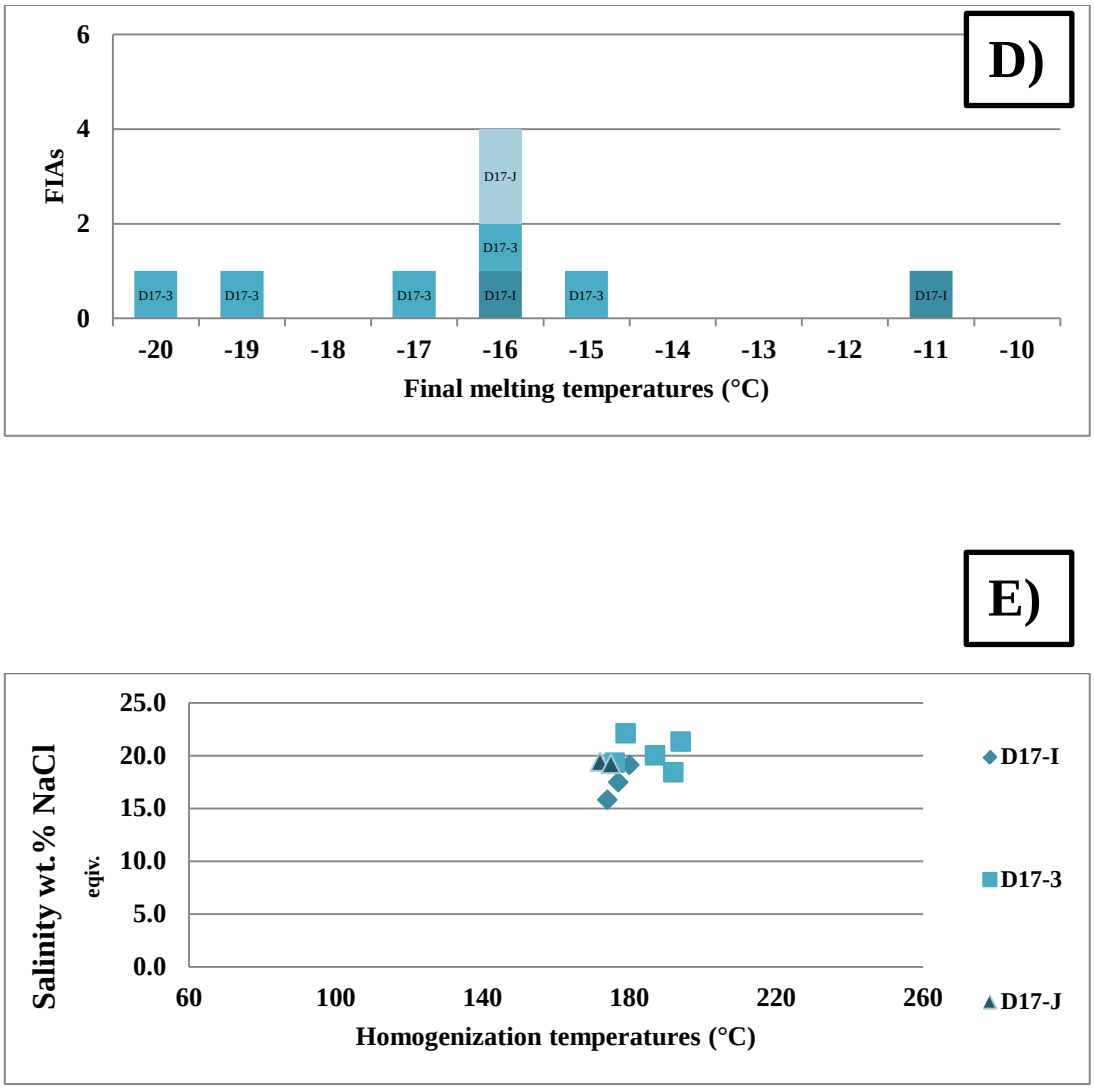

Figure 5.17A – E: Bar plots of the fluid inclusion microthermometric data of aqueous biphase (liquid + vapor) inclusions measured from calcite in fractures (CIF). A) Homogenization temperatures of 11 FIAs from 3 samples. B) First melting temperatures of 8 FIAs from 3 samples. C) Hydrohalite melting temperatures of 11 FIAs from 3 samples. D) Final melting temperatures of 11 FIAs from 3 samples. E) Cross-plot of homogenization temperatures and salinities of 9 FIAs from 3 samples. (original in color)

Table 5.10: Summary of fluid inclusion microthermometric data: carbonic (vapor only?) inclusions in calcite in fractures (CIF).

Diagenetic Phase	Well ID/ Depth/ Sample Number	Size (μm)	Vapor (%)	Th (mean range °C; FIAs)	Th (mean °C; FIAs)
CIF	d-16-A/94-N-15 3768.1 m D17-1				
	Random/clusters/Isolated	10 – 20	~100	-56.5 – -49.5 (5)	-52.3 (5)
	Trails	10	~100	-54.2 (1)	-54.2 (1)
	d-16-A/94-N-15 3769.1 m D17-J				
	Random/clusters/Isolated	6 – 23	~100	-58.7 – -51.9 (7)	-56.9 (7)
	Trails	7 – 14	~100	-56.8 – -55.3 (2)	-56.1 (2)
	Random/clusters/Isolated	6 – 23	~100	-58.7 – -49.5 (12)	-55.0 (12)
	Trails	7 – 14	~100	-56.8 – -54.2 (3)	-55.4 (3)
	Summary	6 – 23	~100	-58.7 – -49.5 (15)	-55.1 (15)

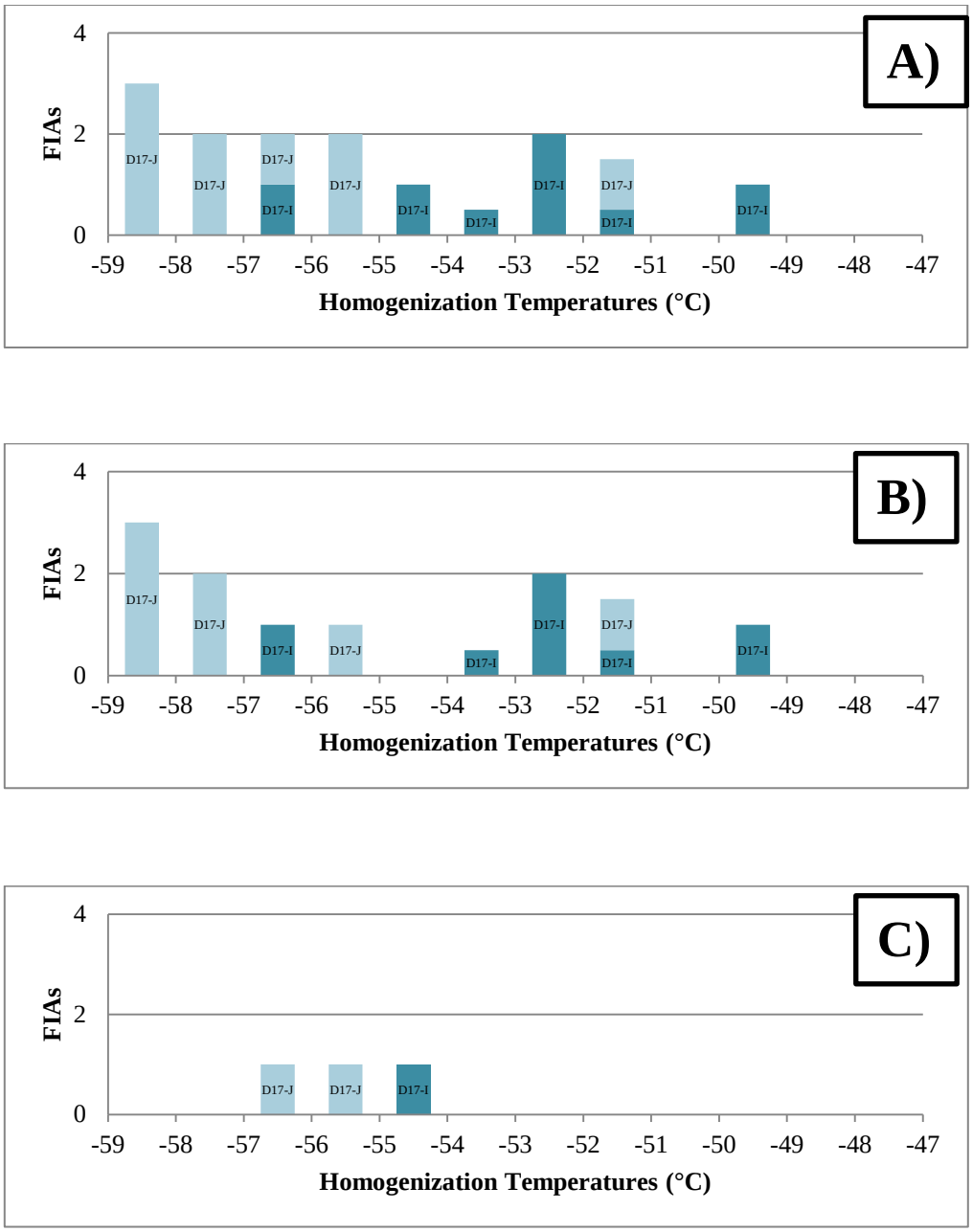

Figure 5.18A – C: Bar plots of the homogenization temperatures of carbonic (vapor only?) inclusions measured from calcite in fractures (CIF). A) Homogenization temperatures measured from randomly distributed or isolated carbonic (vapor only?) inclusions from 15 FIAs in 2 samples. B) Homogenization temperatures measured from randomly distributed or isolated carbonic (vapor only?) inclusions from 12 FIAs in 2 samples. C) Homogenization temperatures measured from carbonic (vapor only?) inclusions in trails from 3 FIAs in 2 samples. (original in color)

CHAPTER 6: Discussion and Interpretation

6.1 Discussion

Petrographic observations and geochemical analytical results for various diagenetic phases are discussed. A cross-plot of the analytical results of stable oxygen and carbon isotope values for various diagenetic phases is presented in Fig. 6.1. A cross-plot of the analytical results of stable oxygen isotope value and radiogenic strontium $^{87}Sr/^{86}Sr$ isotopic ratio for different diagenetic phases is presented in Fig. 6.2. Diagenetic phases that developed contemporaneously or immediately after one another and have very close geochemical analytical results were paired up and discussed. The reasons are to facilitate discussion and condense the text portion of this thesis.

6.1.1 Finely crystalline dolomite(s) (FCDs)

FCD in limestone to calcitic dolomite and FCD in dolostone exhibit similar crystal size and petrographic properties. FCD was observed in almost all of the studied cores. Both FCDs in limestone to calcitic dolomite and FCD in dolostone have very similar stable oxygen and carbon isotope results (Fig. 6.3). These indicate that deep burial dolomitization processes did not greatly altered the stable oxygen and carbon isotope values of FCD in dolostone. However, it is still possible that FCD in limestone to calcitic dolomite and FCD in dolostone could have been altered during the precipitation

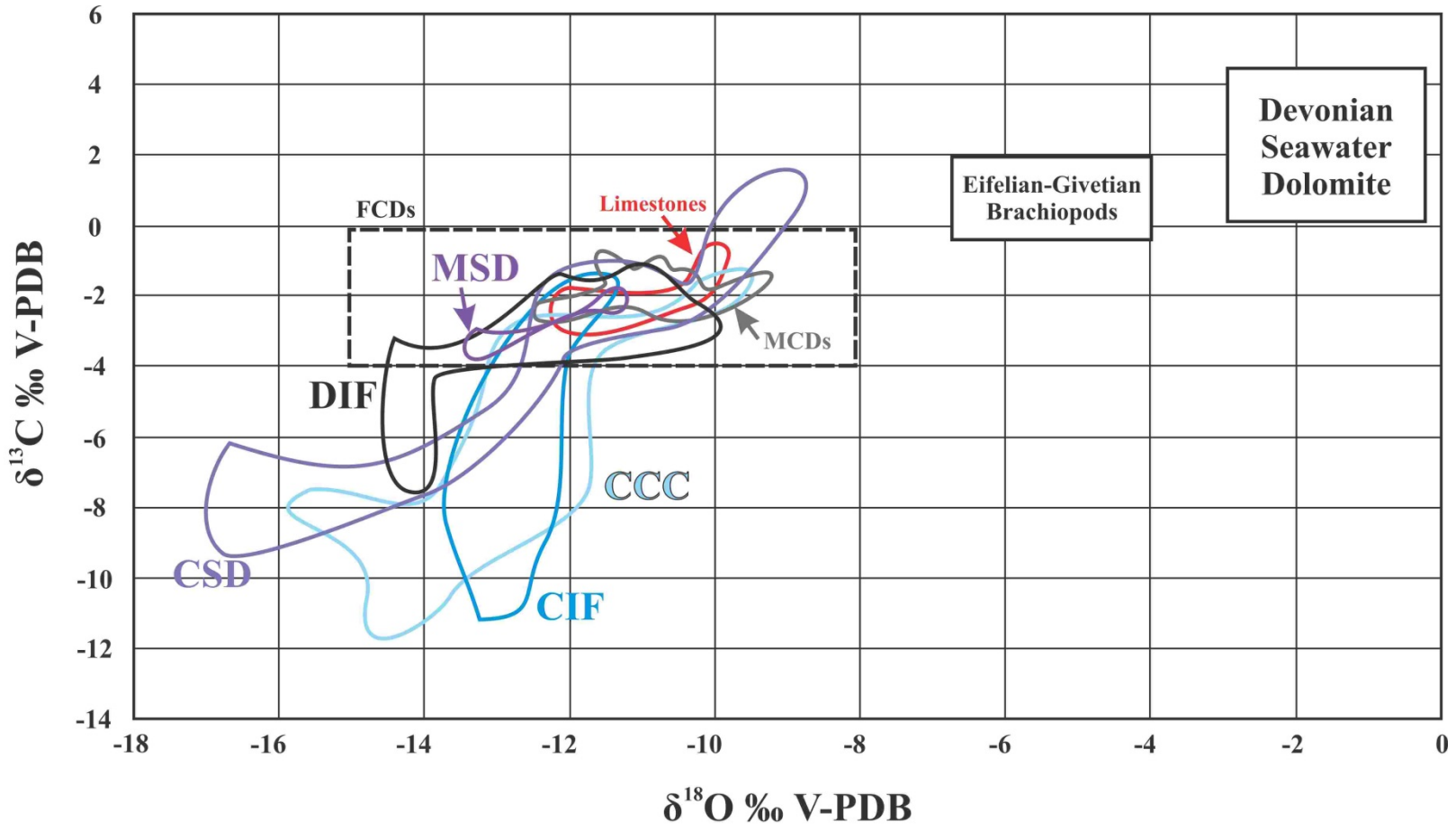
Devonian
Seawater
Dolomite
Eifelian-Givetian
Brachiopods
FCDs
Limestones
MSD
MCDs
DIF
CCC
CSD
CIF
δ13C ‰ V-PDB
δ18O ‰ V-PDB
6
4
2
0
-2
-4
-6
-8
-10
-12
-14
-18
-16
-14
-12
-10
-8
-6
-4
-2
0

Figure 6.1: A cross-plot of stable oxygen versus carbon isotope values for various diagenetic phases in the Stone and Dunedin formations. These phases include: finely crystalline dolomite in limestone to calcitic dolomite (FCD in limestone to calcitic dolomite), finely crystalline dolomite in dolostone (FCD in dolostone), medium crystalline planar-s dolomite (MCD-1), medium crystalline planar-e dolomite (MCD-2), medium crystalline nonplanar-a saddle dolomite in vugs (MSD), coarsely to very coarsely crystalline nonplanar-e saddle dolomite in vugs (CSD), dolomite in fractures (DIF), coarsely to very coarsely crystalline blocky calcite in vugs (CCC), and calcite in fractures (CIF). The range for the Eifelian to Givetian brachiopods is from Veizer (1999). The $\delta^{18}O$ values are from -6.69 to -3.99 ‰ V-PDB and the $\delta^{13}C$ values are from -0.36 to 1.99 ‰ V-PDB. This range represents the average values from numerous studies. The field for Middle Devonian seawater dolomite of -2.93 to -0.20 ‰ V-PDB is from Land (1983) with the range of Eifelian to Givetian seawater = -3.05 to -5.79 ‰ V-SMOW and temperature = 20 °C. (original in color)

of CCC and CIF. FCDs from both limestone to calcitic dolomite and dolostone have a mean $\delta^{18}O$ value of -10.42 ‰ V-PDB from 12 samples (Fig. 6.3). This is 7 ‰ more depleted in the stable oxygen isotope value when compared to the calculated value of any dolomite precipitated from the Middle Devonian seawater, which is -3 ‰ V-SMOW (Land 1983). This supports the possibility that FCDs might have been altered during the precipitation of CCC and CIF in deep burial settings.

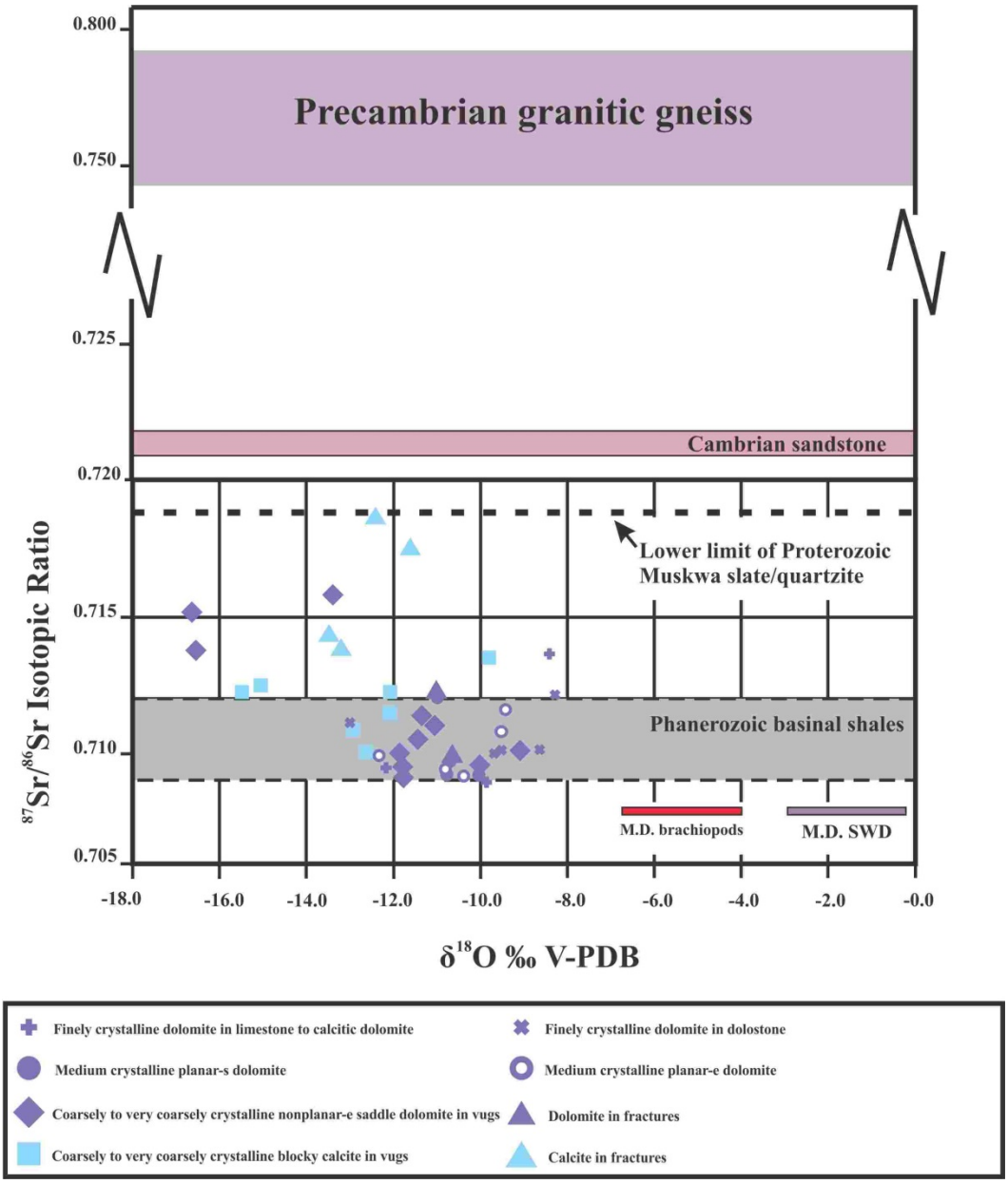

Figure 6.2: Comparison of $^{87}Sr/^{86}Sr$ isotope ratios of various diagenetic phases in the Stone and Dunedin formations. The ranges of $^{87}Sr/^{86}Sr$ ratios for Phanerozoic basinal shales, Cambrian sandstone, Precambrian granitic gneiss, and the lower limit of $^{87}Sr/^{86}Sr$ ratio for Proterozoic Muskwa slate/quartzite are adapted from Cavell and Machel (1997) and Machel and Cavell (1999) for comparison. $^{87}Sr/^{86}Sr$ ratios of Eifelian and Givetian brachiopods (0.70779 to 0.70804) is from Veizer et al. (1999). Middle Devonian seawater dolomite is estimated to have approximately the same $^{87}Sr/^{86}Sr$ ratios as Eifelian and Givetian brachiopods because strontium fractionation is dominantly controlled by the parent diagenetic fluid composition. (original in color)

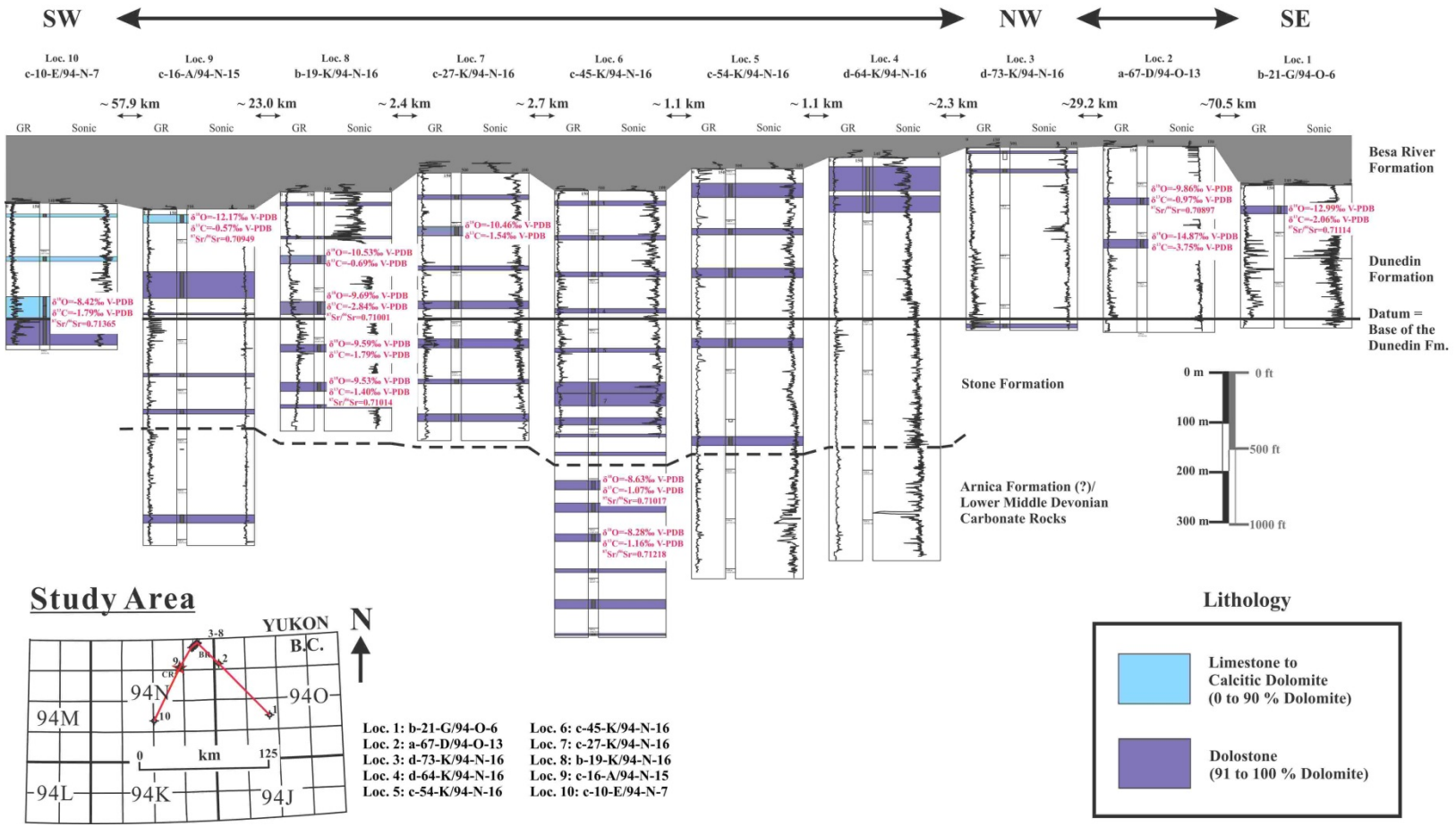

Figure 6.3: A stratigraphic cross-section showing the spatial variation in geochemical analytical results for finely crystalline dolomite in limestone to calcitic dolomite (FCD in limestone to calcitic dolomite) and finely crystalline dolomite in dolostone (FCD in dolostone) (original in color)

For the stable carbon isotope, one FCD in limestone to calcitic dolomite from the fore reef to slope facies has $\delta^{13}C$ = -0.57 ‰ V-PDB (Fig. 6.3). Other FCD samples from the lagoonal facies have a mean $\delta^{13}C$ value of ~1.6 ‰ V-PDB. However, this trend is not apparent.

Analytical results of the FCD from two different lithological units overlap in the $\delta^{18}O$-$^{87}Sr/^{86}Sr$ cross-plot (Fig. 6.2). They are average ~0.004 slightly enriched in radiogenic ^{87}Sr when compared to the Middle Devonian seawater dolomite. Spatial variation in radiogenic strontium $^{87}Sr/^{86}Sr$ isotopic ratio is insignificant.

6.1.2 Medium crystalline dolomites (MCDs)

Both MCD-1 and MCD-2 were postdated by MSD and CSD. In core samples, patches of MCD-2 typically occur as alteration halos around CSD. In petrographic studies, MCD-1 has slightly smaller average crystal size and typically in subhedral shape. In contrast, MCD-2 has slightly bigger crystal size and typically in euhedral shape.

MCD-1 and MCD-2 have very similar stable oxygen and carbon isotope values especially in the upper Stone and Dunedin formations (Fig. 6.4), where CSD comprises >20 % of the lithological units. Variations were observed at the lowest Stone Formation ($\delta^{18}O$ = -9.44 ‰ V-PDB and $\delta^{13}C$ = -1.66 ‰ V-PDB) as well as at the uppermost

Dunedin Formation ($\delta^{18}O$ = -12.33 ‰ V-PDB and $\delta^{13}C$ = -2.49 ‰ V-PDB). The $\delta^{13}C$ values are slightly varied.

MCD-1 and MCD-2 have radiogenic $^{87}Sr/^{86}Sr$ isotopic ratios between 0.70919 and 0.71210 and overlap in the $\delta^{18}O$-$^{87}Sr/^{86}Sr$ cross-plot (Fig. 6.2). They are ~ 0.001 to 0.004 slightly enriched in $^{87}Sr/^{86}Sr$ isotopic ratio when compared to the Middle Devonian seawater dolomite. Spatial variation of radiogenic $^{87}Sr/^{86}Sr$ isotopic ratios is insignificant.

6.1.3 Medium crystalline nonplanar-a saddle dolomite in vugs (MSD) and coarsely to very coarsely crystalline nonplanar-e saddle dolomite in vugs (CSD)

Petrographic studies observed that CSD was precipitated immediately after MSD. MSD appears to be a less developed diagenetic phase of CSD. Two samples of MSD were analyzed (Fig. 6.1). CSD from the same core interval were also sampled for comparison. One sample of MSD (c-45-K/94-N-16, 4324.1 m) has $\delta^{18}O$ = -13.25 ‰ V-PDB and $\delta^{13}C$ = -3.40 ‰ V-PDB. The CSD from the same sample has $\delta^{18}O$ = -16.55 and $\delta^{13}C$ = -6.79 ‰ V-PDB. Another sample of MSD (c-54-K/94-N-16, 3851.6 m) has $\delta^{18}O$ = -11.39 ‰ V-PDB and $\delta^{13}C$ = -2.09 ‰ V-PDB. The CSD from the same sample has $\delta^{18}O$ = -11.87 ‰ V-PDB and $\delta^{13}C$ = -2.28 ‰ V- PDB. These similar results indicate that MSD and CSD were possibly precipitated from diagenetic fluid(s) with similar oxygen isotopic

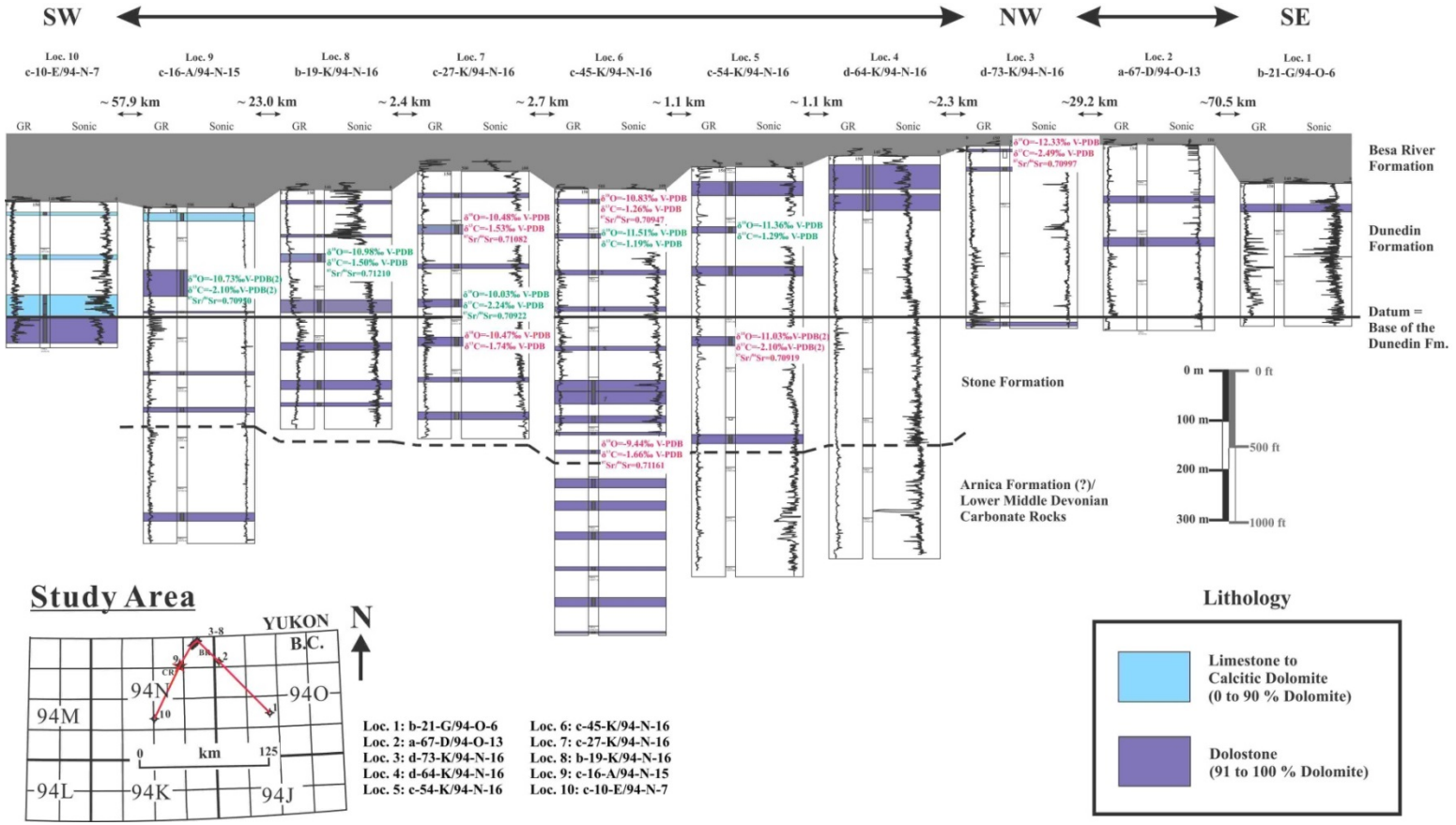

Figure 6.4: A stratigraphic cross-section showing the spatial variation in geochemical analytical results for medium crystalline planar-s dolomite (MCD-1; red) and medium crystalline planar-e dolomite (MCD-2; green). If two or more samples were analyzed from a cored interval, the mean value(s) among the samples from that particular cored interval is reported with the numbers of sample (n) being indicated. (original in color)

composition and under similar temperature condition.

Mean homogenization temperature measured in the primary to pseudo-primary aqueous biphase (L-V) fluid inclusions in MSD from c-45-K/94-N-16, 4324.1 m is 197 °C (FIA = 6); mean homogenization temperature for the CSD from the same sample is 199 °C (FIA = 8). Mean homogenization temperature measured in the primary to pseudo-primary aqueous biphase (L-V) fluid inclusions in MSD from c-54-K/94-N-16, 3851.6 m is 187 °C (FIA = 5); mean homogenization temperature for the CSD from the same sample is 182 °C (FIA = 13).

For the sample from c-54-K/94-N-16, 3851.6 m, MSD and CSD have almost the same oxygen and carbon isotope values and homogenization temperatures for their primary to pseudo-primary aqueous biphase (L-V) fluid inclusions. The primary to pseudo-primary aqueous biphase (L-V) fluid inclusions in MSD and CSD from c-45-K/94-N-16, 4324.1 m have very close homogenization temperatures. However, the 3 ‰ V-PDB difference for both the oxygen and carbon isotope values cannot be accounted for.

6.1.4 Coarsely to very coarsely crystalline nonplanar-e saddle dolomite in vugs (CSD) and dolomite in fractures (DIF)

Petrographic studies in Chapter 4 showed that DIF were precipitated along fractures contemporaneously or immediately after CSD. Samples of CSD and DIF from the Stone

Formation (extending into the Arnica? Formation) are slightly depleted in stable oxygen isotope values than samples from the Dunedin Formation by 2 to 3 ‰ V-PDB (Figs. 6.5 and 6.6).

Radiogenic $^{87}Sr/^{86}Sr$ isotopic ratios of CSD and DIF overlap in an area in the $\delta^{18}O$-$^{87}Sr/^{86}Sr$ cross-plot (Fig. 6.2), except for 3 samples of CSD from the Stone Formation (extending into the Arnica? Formation) in 2 wells (c-45-K/94-N-16 and b-19-K/94-N-16) with elevated $^{87}Sr/^{86}Sr$ isotopic ratio and more depleted $\delta^{18}O$ isotope values (Fig. 6.5). Radiogenic $^{87}Sr/^{86}Sr$ isotopic ratios of CSD are 0.001 to 0.008 more enriched in $^{87}Sr/^{86}Sr$ ratios when compared to the Middle Devonian seawater dolomite (Fig. 6.2). Eight samples of CSD fall into the experimental range of Phanerozoic basinal shales while 3 samples are in between the experimental range of Phanerozoic basinal shales and lower limit of Proterozoic Muskwa slate/quartzite. They are 0.002 to 0.004 more enriched in $^{87}Sr/^{86}Sr$ isotopic ratios when compared to the Middle Devonian seawater dolomite. One DIF has $^{87}Sr/^{86}Sr$ isotopic ratio falls into the experimental range of Phanerozoic basinal shales; another DIF sample has $^{87}Sr/^{86}Sr$ isotopic ratio slightly above the experimental range of Phanerozoic basinal shales.

Mean homogenization temperature measured from the primary to pseudo-primary aqueous biphase (L-V) fluid inclusions in CSD is 198 °C (FIA = 61). Mean homogenization temperature measured from the primary to pseudo-primary aqueous biphase (L-V) fluid inclusions in DIF is 195 °C (FIA = 39). This is a strong indicator which CSD and DIF were precipitated under similar geothermal condition.

Spatial variation of homogenization temperatures for both CSD and DIF is not prominent across the Stone and Dunedin formations in a stratigraphic framework (approximately ±13 °C and ±9 °C respectively; Fig. 6.5 and 6.6). However, the primary to pseudo-primary aqueous biphase (L-V) fluid inclusions in the CSD sample from a-67-D/94-O-13, 5221.3 m have a representative homogenization temperature of 195 °C (FIA= 1); a mean homogenization temperature of 186 °C (FIA = 2) was measured in the primary to pseudo-primary aqueous biphase (L-V) fluid inclusions in a DIF sample from a-67-D/94-O-13, 5225.1 m. The present burial depths of these two samples (a-67-D/94-O-13, 5221.3 m & 5225.1 m) are ~1200 m deeper than the majority of the CSD and DIF samples. Given the regional geothermal gradient is from ~ 40 °C/km to up to 55 °C/km during orogenic events (Morrow et al. 1993; Davies and Smith 2006), the homogenization temperatures measured in primary to pseudo-primary aqueous biphase (L-V) fluid inclusions in these two CSD and DIF samples indicate that they were likely to have precipitated in a similar geothermal setting and at approximately the same burial depth with the rest of the CSD and DIF samples.

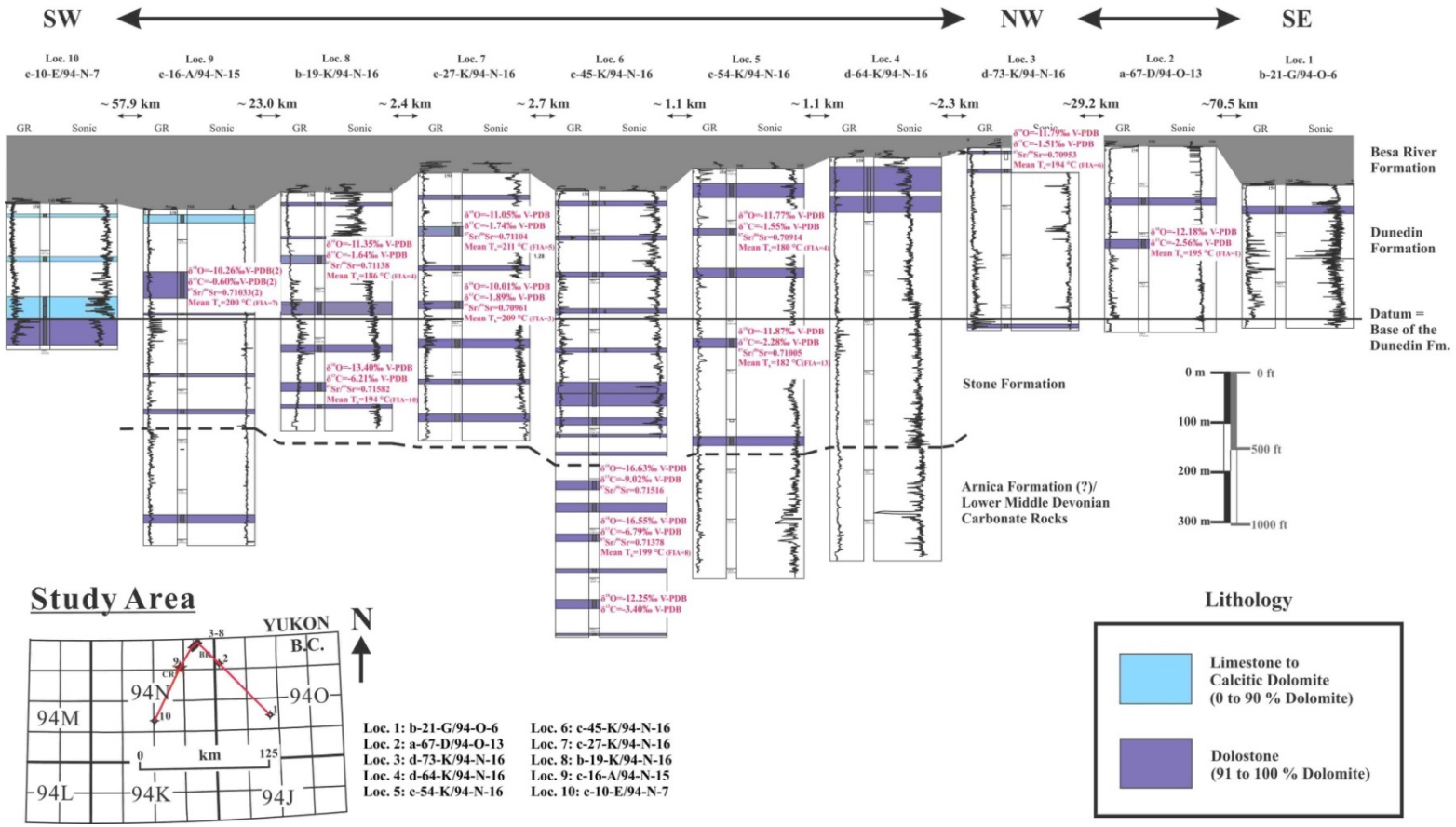

Figure 6.5: A stratigraphic cross-section showing the spatial variation in geochemical analytical results for coarsely to very coarsely crystalline nonplanar-e saddle dolomite in vugs (CSD). If two or more samples were analyzed from a cored interval, the mean value(s) among the samples from that particular cored interval is reported with the numbers of sample (n) being indicated. (original in color)

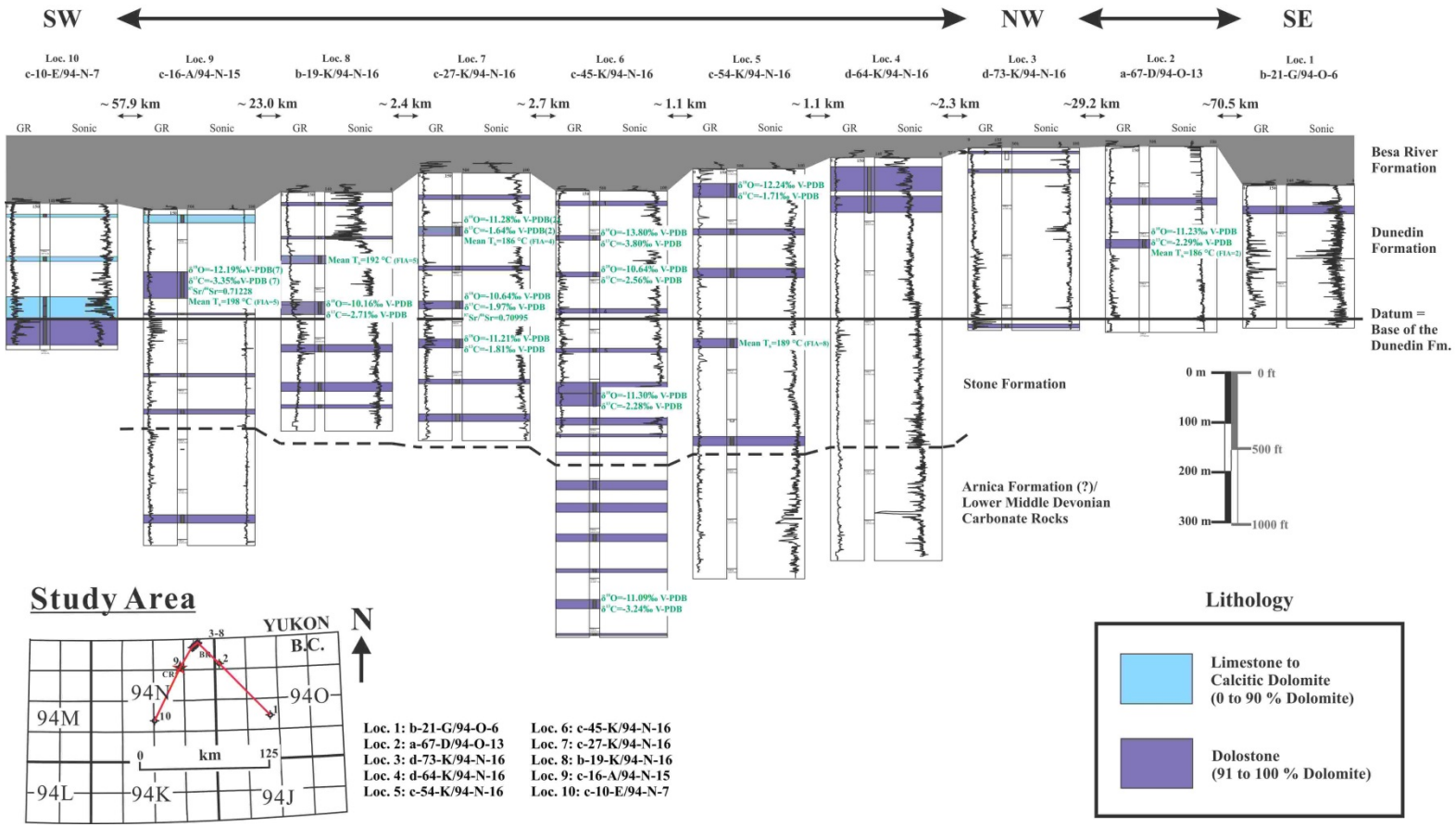

Figure 6.6: A stratigraphic cross-section showing the spatial variation in geochemical analytical results for dolomite in fractures (DIF). If two or more samples were analyzed from a cored interval, the mean value(s) among the samples from that particular cored interval is reported with the numbers of sample (n) being indicated. (original in color)

A cross-plot of $\delta^{18}O$ values and homogenization temperatures measured from the primary to pseudo-primary aqueous biphase (L-V) fluid inclusions in CSD and DIF is presented in Fig. 6.7. The dolomite-water fractionation equilibrium lines were drawn based on the formula by Land (1983), which is used to estimate and compare the V-SMOW values of the diagenetic fluid(s). The formula is given by:

$$10^3 \ln\alpha_{\text{dolomite-water}} = (3.2 \times 10^6)\, T^{-2} - 3.3 \qquad (6.1)$$

where T is temperature in Kelvins.

CSD has $\delta^{18}O$ V-SMOW values from ~ 0 to +12 ‰ V-SMOW. DIF has $\delta^{18}O$ V-SMOW values from ~ +4 to +11 ‰ V-SMOW and that falls within the fluid $\delta^{18}O$ range of CSD. The majority of the $\delta^{18}O$ V-SMOW values for CSD and DIF fall within and above the $\delta^{18}O$ V-SMOW values of evaporated Middle Devonian Seawater (Knauth and Beeunas 1986). This is can be interpreted as hydrothermal alteration which fluid with the oxygen isotopic composition of evaporated Middle Devonian Seawater was heated and circulate through the Middle Devonian Strata (Nadjiwon 2001).

6.1.5 Coarsely to very coarsely crystalline blocky calcite in vugs (CCC) and calcite in fractures (CIF)

Petrographic studies in Chapter 4 showed that CIF were precipitated along fractures contemporaneously or immediately after CCC. The $\delta^{18}O$ values of CCC varied from

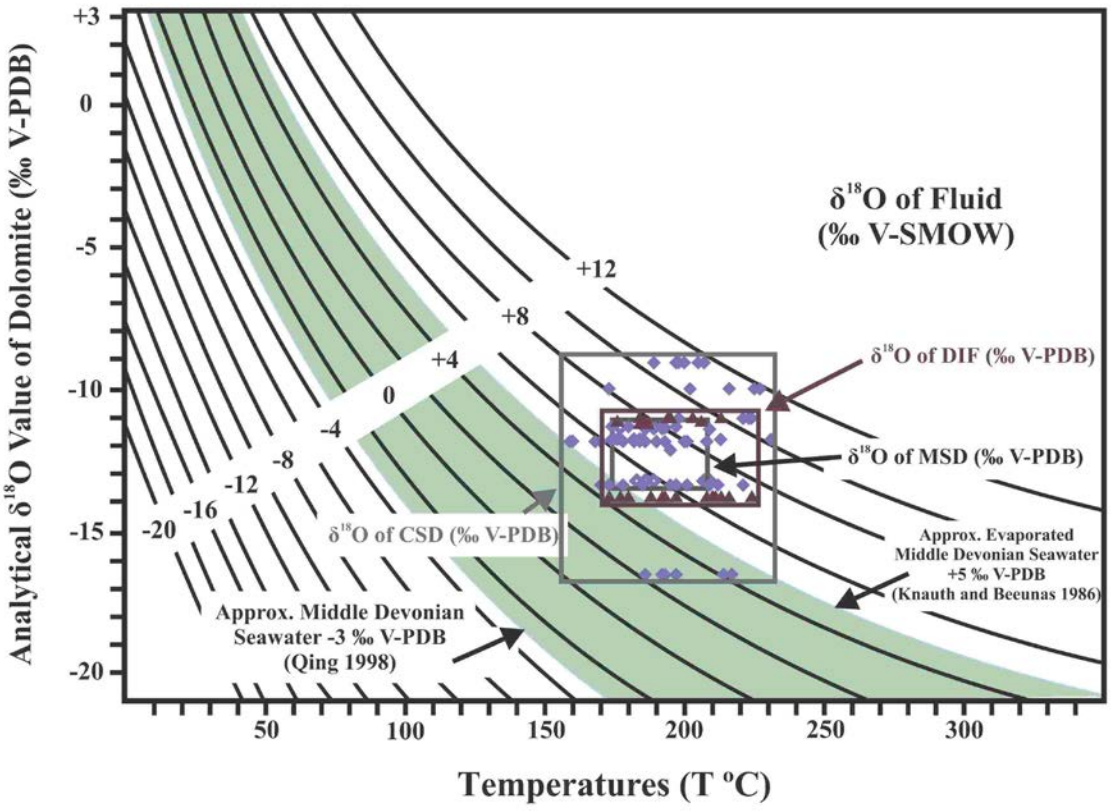

Figure 6.7: A cross-plot of homogenization temperatures versus oxygen isotope values for MSD, CSD and DIF. Equilibrium lines are from the dolomite-water fractionation equation by Land (1983). Approximated $\delta^{18}O$ isotope value of Middle Devonian Seawater of -3 ‰ V-SMOW is from Qing (1998). Approximated upper limit of evaporated Middle Devonian Seawater of +5 ‰ V-SMOW is from Knauth and Beeunas (1986). (original in color)

-15.05 ‰ V-PDB in the uppermost Dunedin Formation in the eastern d-73-K/94-N-16 (Fig. 6.8), to -9.80 ‰ V-PDB in the upper Dunedin Formation in c-27-K/94-N-16. The $\delta^{13}C$ values varied from -11.23 to -1.71 ‰ V-PDB. All thirteen samples of CIF were collected from the lower Dunedin interval in c-16-A/94-N-15 and have a mean $\delta^{18}O$

value of -12.87 ‰ V-PDB and mean $\delta^{13}C$ value of -6.58 ‰ V-PDB (Fig. 6.8). Four CCC samples from the same interval have a mean $\delta^{18}O$ value of -13.90 ‰ V-PDB and mean $\delta^{13}C$ value of -8.05 ‰ V-PDB.

Seven samples of CCC have radiogenic $^{87}Sr/^{86}Sr$ isotopic ratios between 0.71009 and 0.71354 and a mean radiogenic $^{87}Sr/^{86}Sr$ isotopic ratio of 0.71187 (Fig. 6.2). Four samples of CIF from the lower Dunedin interval in c-16-A/94-N-15 have radiogenic $^{87}Sr/^{86}Sr$ isotopic ratios between 0.71384 and 0.71862 and a mean $^{87}Sr/^{86}Sr$ isotopic ratio of 0.71608. One CCC sample from the lower Dunedin interval in c-16-A/94-N-15 has radiogenic $^{87}Sr/^{86}Sr$ isotopic ratio = 0.71226. Radiogenic $^{87}Sr/^{86}Sr$ ratios of CCC are 0.002 to 0.006 more enriched in $^{87}Sr/^{86}Sr$ isotopic ratios when compared to the Eifelian and Givetian brachiopods (Fig. 6.2). Three samples of CCC have $^{87}Sr/^{86}Sr$ isotopic ratios in the experimental range of Phanerozoic basinal shales and 4 samples are slightly above it. Radiogenic $^{87}Sr/^{86}Sr$ isotopic ratios of CIF are 0.006 to 0.010 more enriched in $^{87}Sr/^{86}Sr$ ratios when compared to the Eifelian and Givetian brachiopods. Four CIF samples have $^{87}Sr/^{86}Sr$ isotopic ratios above the experimental range of Phanerozoic basinal shales and approach the range of Proterozoic slate and Cambrian sandstone.

Mean homogenization temperature measured from the primary to pseudo-primary aqueous biphase (L-V) fluid inclusions in CCC is 179 °C (FIA = 50). Mean homogenization temperature measured from the primary to pseudo-primary aqueous biphase (L-V) fluid inclusions in CIF from the lower Dunedin interval in c-16-A/94-N-15 is 183 °C (FIA = 11). Mean homogenization temperature measured from the primary

to pseudo-primary aqueous biphase (L-V) fluid inclusions in CCC from the same interval is 186 °C (FIA = 8). This indicates that CCC and CIF were precipitated in very similar geothermal setting.

Spatial variation of homogenization temperatures for both CCC and CIF is not prominent across the Stone and Dunedin formations in a stratigraphic framework (approximately ±14 °C and ±9 °C respectively; Fig. 6.8). However, the primary to pseudo-primary aqueous biphase (L-V) fluid inclusions in the CCC sample from a-67-D/94-O-13, 5221.3 m have a mean homogenization temperature of 187 °C (FIA = 3), in which the present burial depth of the sample (a-67-D/94-O-13, 5221.3 m) is ~1200 m deeper than the majority of the CCC samples. Furthermore, the primary to pseudo-primary aqueous biphase (L-V) fluid inclusions in the CCC sample from c-10-E/94-N-7, 1823.0 m have a mean homogenization temperature of 165 °C (FIA = 8), in which the present burial depth of the sample is ~1900 m shallower than the majority of the CCC samples. Given the regional geothermal gradient is from ~ 40°C/km to up to 55 °C/km during orogenic events (Morrow et al. 1993; Davies and Smith 2006), the homogenization temperatures measured in primary to pseudo-primary aqueous biphase (L-V) fluid inclusions in these two CCC samples indicate that they were likely to have precipitated in a similar geothermal setting and at approximately the same burial depth with the rest of the CCC.

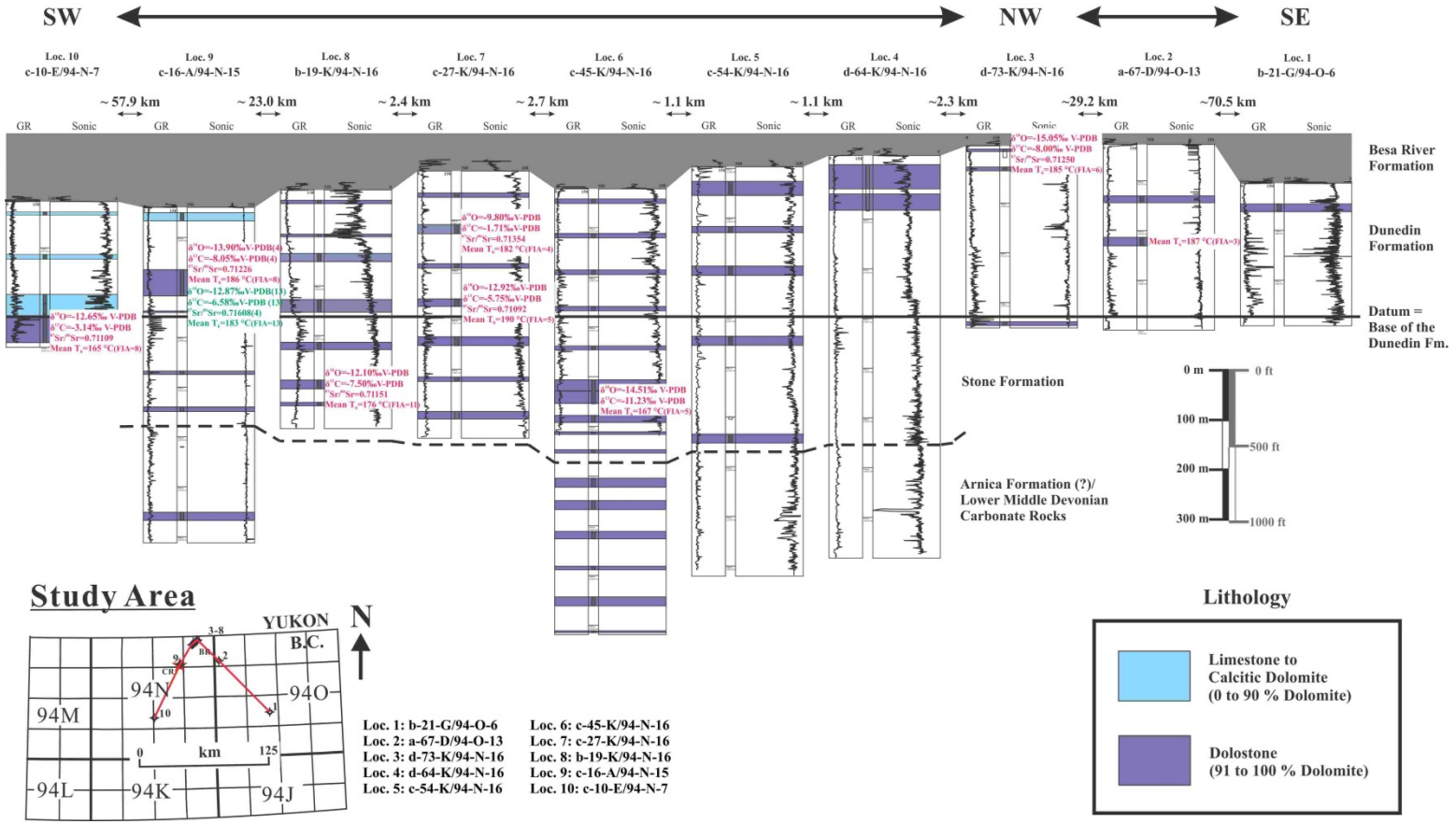

Figure 6.8: A stratigraphic cross-section showing the spatial variation in geochemical analytical results for coarsely to very coarsely crystalline blocky calcite in vugs (CCC; red) and calcite in fractures (CIF; green). If two or more samples were analyzed from a cored interval, mean value(s) among the samples from that particular cored interval is reported with the number of sample (n) being indicated. (original in color)

A cross-plot of $\delta^{18}O$ values and homogenization temperatures measured from the primary to pseudo-primary aqueous biphase (L-V) fluid inclusions in CCC and CIF is presented in Fig. 6.9. The calcite-water fractionation equilibrium lines were drawn based on the formula by Friedman and O'Neil (1977), which is used to estimate and compare the V-SMOW values of the diagenetic fluid(s). The formula is given by:

$$10^3 \ln\alpha_{\text{calcite-water}} = (2.78 \times 10^6)\, T^{-2} - 2.89 \qquad (6.2)$$

where T is temperature in Kelvins.

CCC has $\delta^{18}O$ (‰ V-SMOW) values from ~ 0 to +10 ‰ V-SMOW with the majority of the values fall within +2 to +6 ‰ V-SMOW. CIF falls within the fluid $\delta^{18}O$ range of CCC and has $\delta^{18}O$ V-SMOW values from ~ +4 to +6 ‰ V-SMOW. The majority of the $\delta^{18}O$ V-SMOW values for CCC and CIF fall within the range of evaporated Middle Devonian Seawater (Knauth and Beeunas 1986). This is cross-checked by the calculated salinity of 18.0 wt. % NaCl (FIA = 36) from the primary to pseudo-primary aqueous biphase (L-V) fluid inclusions in CCC.

Fluid inclusion petrographic and microthermometric studies have discovered carbonic (vapor only?) inclusions in a few samples of CCC and CIF. The carbonic (vapor only?) inclusions in CCC have mean homogenization temperature at -53.5 °C (FIA = 14); the carbonic (vapor only?) inclusions in CIF have a mean homogenization temperature of -55.1 °C (FIA = 15). The melting temperature of the solid observed in one of the fluid inclusions is ~ 74 °C (Fig. 5.14), but the melting process was rarely observed in most of

the carbonic (vapor only?) inclusions due to technical difficulties. However, these measurements still fit the properties of carbon dioxide (CO_2) which has a melting point (solid → liquid) of -78 °C and a boiling point (liquid → vapor) of -57 °C under atmospheric pressure. It is possible that the carbonic (vapor only?) inclusions are CO_2-dominated and belong to a CO_2-(CH_4-volatiles) fluid system (Zhang and Frantz 1992).

The presence of CO_2-dominated carbonic (vapor only?) inclusions also account for the varied $\delta^{13}C$ values (from -11.23 to -1.71 ‰ V-PDB). The CO_2-dominated carbonic (vapor only?) inclusions were considered as pseudo-secondary to secondary inclusions based on their petrographic occurrences and distribution. There might already have carbon input into diagenetic processes during the precipitation of CCC and CIF. The CO_2-dominated carbonic (vapor only?) inclusions were observed in 5 samples of CCC (b-19-K/94-N-16, 4192.9 m; a-67-D/94-O-13, 5221.3 m; d-73-K/94-N-16, 3783.6 m; c-27-K/94-N-16, 3958.4 m; & c-27-K/94-N-16, 3815.3 m) and 3 samples of CIF (d-16-A/94-N-15, 3768.1 m; d-16-A/94-N-15, 3816.8 m; & d-16-A/94-N-15, 3769.1 m). Four of the above CCC samples have $\delta^{13}C$ values from -8.00 to -1.71 ‰ V-PDB, which fall into the less depleted end of the $\delta^{13}C$ values among all CCC samples. Three of the above CIF samples have $\delta^{13}C$ values from 5.19 to 7.52 ‰ V-PDB, which are closed to the

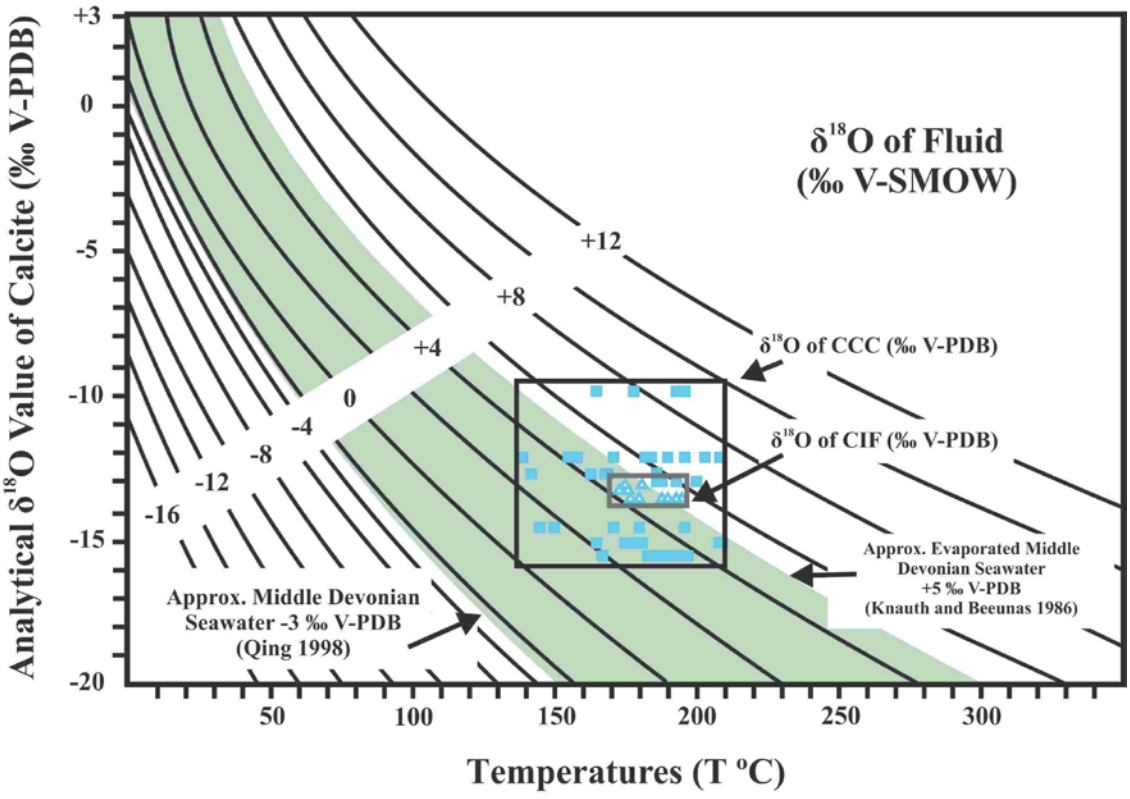

Figure 6.9: A cross-plot of homogenization temperatures versus oxygen isotope values for CCC and CIF. Equilibrium lines are from the calcite-water fractionation equation by Friedman and O'Neil (1977). Approximated $\delta^{18}O$ isotope value of Middle Devonian Seawater of -3 ‰ V-SMOW is from Qing (1998). Approximated upper limit of evaporated Middle Devonian Seawater of +5 ‰ V-SMOW is from Knauth and Beeunas 1986). (original in color)

$\delta^{13}C$ values among all CIF samples. The correlation between the presence of CO_2-dominated carbonic (vapor only?) inclusions and depletion in stable carbon $\delta^{13}C$ is not strong.

6.2 New insights into the relative timing of coarsely crystalline saddle dolomite and calcite precipitation (CSD and CCC)

6.2.1 Fractures and regional structural evolution

Petrographic studies and geochemical analysis indicated that DIF were precipitated along fractures contemporaneously or immediately after CSD; CIF were precipitated along fractures contemporaneously or immediately after CCC. Fracture analysis was conducted on DIF, CIF and POF. The results were inconclusive. However, based on core observations and petrographic studies (see Chapters 3 and 4), it is suggested that most of the structural deformation features e.g. stylolites (vertical stylolites?), joints and fractures postdate CSD, DIF, CCC and CIF.

If CSD, DIF, CCC and DIF postdate orogenic events (The Antler, Columbian or Laramide Orogeny) and structural deformations, they would imprint or cross cut structural deformation features. This was rarely observed except for soft sediment deformation structures.

6.2.2 Fluid inclusion microthermometry

The uncorrected mean homogenization temperature measured from the primary to pseudo-primary aqueous biphase (L-V) fluid inclusions in CSD is 198 °C (FIA = 61). Mean homogenization temperature measured from the primary to pseudo-primary aqueous biphase (L-V) fluid inclusions in DIF is 195 °C (FIA = 39). The range for the measured homogenization temperatures are approximately ±13 °C and ±9 °C respectively. Given the regional geothermal gradient is from ~ 40 °C/km to up to 55 °C/km during orogenic events (Morrow et al. 1993; Davies and Smith 2006), and a mean surface temperature of 25 °C, this will give an estimated burial depth of ~ 4.5 to 5 km for CSD and DIF for their time of precipitation in burial setting, or ~ 3 km during orogenic events. The pressure-temperature-fluid composition corrected range for the homogenization temperature is approximately ± 5 °C (Potter 1977).

Mean homogenization temperature measured from the primary to pseudo-primary aqueous biphase (L-V) fluid inclusions in CCC is 179 °C (FIA = 50). Mean homogenization temperature measured from the primary to pseudo-primary aqueous biphase (L-V) fluid inclusions in CIF is 183 °C (FIA = 11). The range for the homogenization temperatures are approximately ±14 °C and ±9 °C respectively. Given the regional geothermal gradient is from ~ 40 °C/km to up to 55 °C/km during orogenic events (Morrow et al. 1993; Davies and Smith 2006), and a mean surface temperature of 25 °C, this will give an estimated burial depth of ~ 4 to 4.5 km for CCC and CIF for their

time of precipitation in burial setting, or ~ 2.5 to 3 km during orogenic events. The pressure-temperature-fluid composition corrected range for the homogenization temperature is approximately ± 5 °C (Potter 1977).

6.2.3 Coarsely to very coarsely crystalline blocky calcite in vugs (CCC) in a structural geology framework

Eight samples of CCC were analyzed for fluid inclusion microthermometry. The mean homogenization temperature measured from the primary to pseudo-primary aqueous biphase (L-V) fluid inclusions in CCC is 179 °C (FIA = 50). The range is from 165 to 190 °C among the mean values of the 8 analyzed samples.

The primary to pseudo-primary aqueous biphase (L-V) fluid inclusions in a CCC sample from a-67-D/94-O-13, 5221.3 m have a mean homogenization temperature of 187 °C (FIA = 3), in which the present burial depth of the sample (a-67-D/94-O-13, 5221.3 m) is ~1200 m deeper than the majority of the CCC samples. Furthermore, the primary to pseudo-primary aqueous biphase (L-V) fluid inclusions in another CCC sample from c-10-E/94-N-7, 1823.0 m have a mean homogenization temperature of 165 °C (FIA = 8), in which the present burial depth of the sample is ~2000 m shallower than the majority of the CCC samples. Moreover, these two CCC samples are over 50 km apart, and over 3200 m difference in present day burial depth which was the final product of the three orogenies and most likely the last Laramide Orogeny. If these two calcite samples

precipitated during the Laramide Orogeny, the homogenization temperatures measured in the primary to pseudo-primary aqueous biphase (L-V) fluid inclusions would vary greatly and have a difference of over 100 °C, due to different burial depth hence geothermal gradient.

The similarity in homogenization temperatures for the primary to pseudo-primary aqueous biphase (L-V) fluid inclusions indicate that those 2 calcite samples were likely to have precipitated at approximately the same burial depth with the majority of the CCC. These date back to the Late Devonian to Middle Mississippian before the F1 fold as indicated in Fig. 2.7 and Fig. 4.16.

6.2.4 Carbonic (vapor only?) fluid inclusions and stable carbon isotopes

CO_2-dominated carbonic (vapor only?) fluid inclusions occurred as pseudo-secondary to secondary inclusions in CCC and CIF. The presence of CO_2-(CH_4-volatiles) fluid inclusions suggest decomposition and organic maturation. The $\delta^{13}C$ values of CCC and CIF varied from -11.23 to -1.71 ‰ V-PDB and -10.63 to -1.74 ‰ V-PDB, respectively. The $\delta^{13}C$ values are depleted and varied. These suggest significant but varied input of lighter carbon isotope possibly sourced by organic matters, or the parent diagenetic fluid(s) that precipitated the CCC and CIF (Brand and Veizer 1981; Anderson and Arthur 1983).

Base on the vitrinite reflectance study by Morrow et al. (1993), the Middle Devonian

strata including the Stone and Dunedin formations subsided and reached a maximum burial depth of ~ 4.5 to 5 km during the Triassic to Jurassic, uplifted by ~ 0.5 km during the Early Cretaceous, and reburied to ~ 4.5 to 5 km again during the Middle Cretaceous to Tertiary. Organic maturation and gas generation for the Devonian and older strata would have peaked during the Permian and Triassic for the Devonian strata (Morrow et al. 1993).

However, more cutting-edge fluid inclusion analysis is needed in order to determine if the CO_2-dominated carbonic (vapor only?) fluid inclusions contain hydrocarbons. Then further analysis would be needed to match the hydrocarbons to their source rock(s). Also the lighter carbons that cause the depleted carbon isotope values could have been sourced by hydrocarbons, decayed organic matters in the Liard basin, or the parental diagenetic fluid(s) that precipitated CCC and CIF. Nevertheless, these two elements together indicate carbon input into the CCC and CIF (Chi pers. comm.), which might be related to the peak organic maturation and gas generation for the Devonian and older strata.

6.3 Timing of precipitation for the coarsely to very coarsely crystalline nonplanar-e saddle dolomite and blocky calcite in vugs (CSD & CCC)

Based on the new evidence collected in this study, two interpretations on the timing of CSD and CCC precipitation are proposed:

6.3.1 During and immediately after the Antler Orogeny

CSD is interpreted to have precipitated during the Mississippian (Early Carboniferous) at the final stage of the Antler Orogeny:

1) CSD predates most of the structural deformation features as observed in cores and petrographic studies.

2) The uncorrected mean homogenization temperature measured from the primary to pseudo-primary aqueous biphase (L-V) fluid inclusions in CSD is 198 °C (FIA = 61). This would put CSD at a burial depth of ~ 3.5 km during the late stage of the Antler Orogeny which geothermal gradient was at ~55 °C/km (Fig. 6.10). The pressure-temperature-fluid composition corrected range for the homogenization temperature is approximately ± 5 °C (Potter 1977).

3) The spatial variation of the fluid inclusion homogenization temperatures and stable oxygen isotope values in Fig. 6.5 and Fig. 6.7 indicated that CSD was precipitated when the Stone and Dunedin strata was least deformed. Based on the seismic profile in Fig. 2.7, a time constraint can be placed before the Carboniferous/Permian.

4) CSD has $\delta^{18}O$ V-SMOW values from ~ 0 to +12 ‰ V-SMOW. The majority of the $\delta^{18}O$ V-SMOW values for CSD fall within the upper range of the $\delta^{18}O$ V-SMOW values of evaporated Middle Devonian seawater (Knauth and Beeunas 1986). On the other hand, radiogenic $^{87}Sr/^{86}Sr$ isotopic ratios of CSD are only 0.001 to 0.008 more

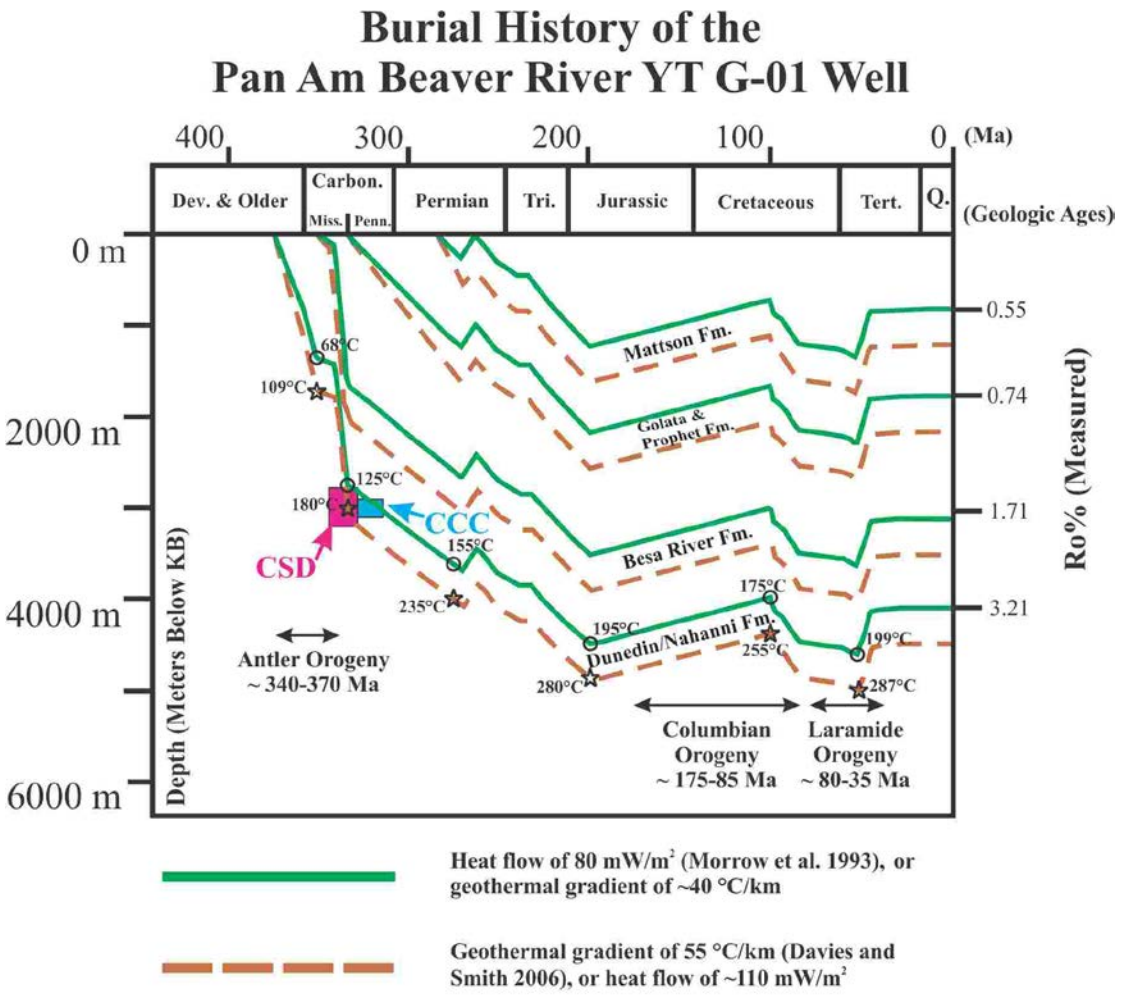

Figure 6.10: Burial history and interpretation: burial history and organic maturation plot of the Pan Am Beaver River YT G-01 by Morrow et al. (1993; see Fig. 2.4 for the location of Pan Am Beaver River YT G-01). Interpretation: coarsely to very coarsely crystalline nonplanar-e saddle dolomite in vugs (CSD) is interpreted to have precipitated during the Mississippian (Early Carboniferous). Coarsely to very coarsely crystalline blocky calcite in vugs (CCC) is interpreted to have precipitated during the Pennsylvanian (Middle to Late Carboniferous).

This plot used the decompaction program of Osadetz and Mottershead (1992) based on vitrinite reflectances Ro% with EASY%Ro algorithm (Sweeney and Burnham 1990). Two calibrations were used: 1) the geothermal heat flow as 80 mW/m^2 (geothermal gradient of ~40 °C/km; Morrow et al. 1993); 2) the geothermal gradient as 55 °C/km (heat flow of ~110 mW/m^2; Davies and Smith 2006). (original in color)

enriched in $^{87}Sr/^{86}Sr$ ratios when compared to the Middle Devonian seawater dolomite (Fig. 6.2). Eight samples of CSD fall into the experimental range of Phanerozoic basinal shales while 3 samples are in between the experimental range of Phanerozoic basinal shales and lower limit of Proterozoic Muskwa slate/quartzite. These are interpreted to be hydrothermal fluid circulation during the late stage of the Antler Orogeny, which the fluid was likely to be heated, evaporated Devonian seawater. Strontium input from deep basin was still limited.

CCC is interpreted to have precipitated during the Pennsylvanian (Middle to Late Carboniferous immediately after the Antler Orogeny:

1) CCC predates most of the structural deformation features as observed in cores and petrographic studies.

2) The uncorrected mean homogenization temperature measured from the primary to pseudo-primary aqueous biphase (L-V) fluid inclusions in CCC is 179 °C (FIA = 50). This would put CCC at a burial depth of ~ 3.5 km after the Antler Orogeny which the geothermal gradient was between ~40 °C/km and ~55 °C/km (Fig. 6.10). The pressure-temperature-fluid composition corrected range for homogenization temperature is approximately ± 5 °C (Potter 1977).

3) The spatial variation of the fluid inclusion homogenization temperatures and stable oxygen isotope values in Fig. 6.8 indicated that CCC was precipitated when the

Stone and Dunedin strata was least deformed. Based on the seismic profile in Fig. 2.7, a time constraint can be placed before Carboniferous/Permian.

4) CCC and CIF have the highest radiogenic strontium isotopic ratios among the diagenetic phases, which exceed the experimental range of Phanerozoic basinal shales and approach the range of Proterozoic slate and Cambrian sandstone. This is interpreted to have resulted from fluid flow induced by the Antler Orogency, which the fluid(s) that is enriched in Sr from the older Cambrian and Proterozoic rocks was introduced into the fluid conduit.

6.3.2. Alternative interpretation: during the Permian

CSD could have precipitated during the Early to Middle Permian based on the fluid inclusion microthermometric data (Fig. 6.11). All other structural elements and the interpreted diagenetic fluid composition still hold. CCC could have precipitated during the Middle to Late Permian based on the fluid inclusion microthermometric data (Fig. 6.11). All other structural components, interpreted diagenetic fluid composition, and fluid inclusion petrographic data still hold.

6.4 Conclusions

- Core study has identified twenty carbonate sedimentary facies in the Stone and Dunedin formations. The lower to middle Stone Formation comprises of a subtle vertical

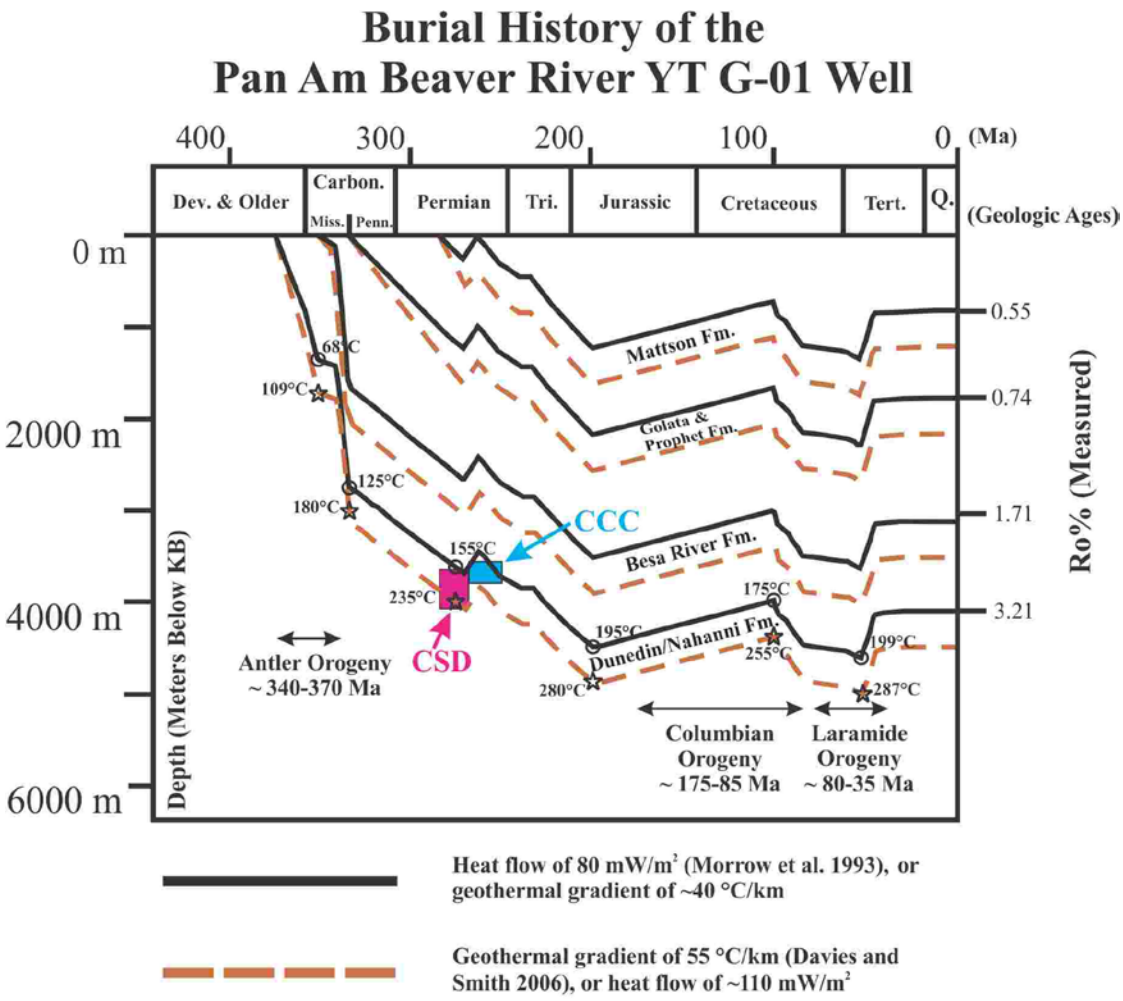

Figure 6.11: Burial history and alternative interpretation: burial history and organic maturation plot of the Pan Am Beaver River YT G-01 by Morrow et al. (1993; see Fig. 2.4 for the location of Pan Am Beaver River YT G-01). Alternative interpretation: coarsely to very coarsely crystalline nonplanar-e saddle dolomite in vugs (CSD) is interpreted to have precipitated during the Early to Middle Permian. Coarsely to very coarsely crystalline blocky calcite in vugs (CCC) is interpreted to have precipitated during the Middle to Late Permian.

This plot used the decompaction program of Osadetz and Mottershead (1992) based on vitrinite reflectances Ro% with EASY%Ro algorithm (Sweeney and Burnham 1990). Two calibrations were used: 1) the geothermal heat flow as 80 mW/m^2 (geothermal gradient of ~40 °C/km; Morrow et al. 1993); 2) the geothermal gradient as 55 °C/km (heat flow of ~110 mW/m^2; Davies and Smith 2006). (original in color)

facies transition from intertidal mudstones to lagoonal wackestones and amphiporid floatstone. The upper Stone Formation in c-10-E/94-N-7 comprises of dominantly clast-rich silty dolomudstone to silty dolomudstone (LF7), which is interpreted to have deposited in peritidal settings and represent the middle Chinchaga depositional break caused by the middle Eifelian regression. The Stone Formation as a whole is interpreted to be shallowing upward sequence. The Dunedin Formation comprises of a vertical facies transition from mudstones of restricted shallow marine origin, to reefal floatstones and boundstones, and to clast-bearing crystalline rock of slope facies. These are interpreted to be a deepening upward sequence.

- Finely crystalline dolomite(s) (FCD): FCD in limestone to calcitic dolomite and FCD in dolostone appear almost identical in petrographic studies. Stable oxygen and carbon isotopes values as well as radiogenic strontium $^{87}Sr/^{86}Sr$ ratios for FCD in both lithological units are very similar. It is concluded that FCDs were possibly altered during the diagenetic processes when the calcitic phase(s) precipitated in deep burial settings. No fluid inclusion microthermometric data could be acquired.

- Medium crystalline dolomite (MCD): MCD-2 appears to be the altered form of MCD-1. Stable oxygen and carbon isotopes values as well as radiogenic strontium $^{87}Sr/^{86}Sr$ ratios for MCD-1 and MCD-2 are very similar. However, the lack of limestone cores, sparse well spacing, and uncertainties in conducting rare earth elements as well as major and trace element analyzes, no further interpretation can be made. No fluid inclusion microthermometric data could be acquired.

- Coarsely to very coarsely crystalline nonplanar-e saddle dolomite in vugs (CSD) and dolomite in fractures (DIF): CSD is interpreted to have precipitated during the Mississippian (Early Carboniferous) at the final stage of the Antler Orogeny, based on the cross cutting relationships, fluid inclusion microthermometric data and spatial distribution of geochemical analytical data. An alternative interpretation on the timing of precipitation can be made based on the fluid inclusion microthermometric data. DIF were precipitated along fractures contemporaneously or immediately after CSD.

- Coarsely to very coarsely crystalline calcite in vugs (CCC) and calcite in fractures (CIF): CCC is interpreted to have precipitated during the Pennsylvanian (Middle to Late Carboniferous immediately after the Antler Orogeny, based on the cross cutting relationships, fluid inclusion microthermometric data, spatial distribution of geochemical analytical data, and fluid inclusion analysis of carbonic (vapor only?) inclusions. An alternative interpretation on the timing of precipitation can be made based on the fluid inclusion microthermometric data. CIF were precipitated along fractures contemporaneously or immediately after CCC.

6.5 Closing remarks

The achievements of this thesis can be summarized as follows:

- Identified and mapped 20 sedimentary facies in the Stone and Dunedin formations.

- Conducted combined diagenesis and fracture analysis studies; used structural deformation as a time constraint in studying diagenetic phases.
- Discovered new evidences from the diagenetic studies and reinterpreted the timing of CSD and CCC precipitations with the newly acquired evidences.

This thesis has also laid foundations in the following new research areas:

- Establishing a sedimentologic framework for the Stone and Dunedin formations.
- Combining fracture analysis and fluid inclusion analysis to solve geologic problems.
- Applying concepts of geochemical stratigraphy and fluid inclusion stratigraphy to solve geologic problems.

List of References

Allan, J.R., and W.D. Wiggins, 1993. Dolomite reservoirs: Geochemical techniques for evaluating origin and distribution. American Association of Petroleum Geologists, Continuing Education Course Notes, Series no. 36, 129 p.

Anderson, T.F., and M.A. Arthur., 1983. Stable isotopes of oxygen and carbon and their application to sedimentologic and paleoenvironmental problems. In: Stable isotopes in sedimentary geology. M.A. Arthur, T.F. Anderson, I.R. Kaplan, J. Veizer, and L.S. Land (eds.). Society of Economic Paleontologist and Mineralogists Short Course 10, p.1-1 to 1-151.

Aulstead, K., 1987. Origin and diagenesis of the manetoe facies, southern Yukon and Northwest Territories, Canada. University of Calgary unpublished M.Sc. thesis, 143 p.

Belyea, H.R., 1970. Significance of an unconformity within the Chinchaga Formation, northern Alberta and northeastern British Columbia. In: Report of Activities, Part B, Geological survey of Canada, Paper 70-1B, p. 76-79.

Belyea, H.R., and Norris, A.W., 1962. Middle Devonian and older Paleozoic formations of southern District of Mackenzie and adjacent areas. Geological Survey of Canada, Paper 62-15.

Blakey, R.C., 2009. Paleogeography Library. Department of Geology, Northern Arizona University. Website: http://cpgeosystems.com/index.html. Retrieved 20 Oct 2009.

Bourque, P.A. Amyot, G., Desrochers, A., Gignac, H., Gosselin, C., Lachambre, G. and Laliberté, J.Y. 1986. Silurian and Lower Devonian reef and carbonate complexes of the Gaspé Basin, Québec - a summary. Bulletin of Canadian Petroleum Geology, v. 34, p. 452-489.

Brand, U. and J. Veizer, 1981. Chemical diagenesis of a multicomponent carbonate system – 2: Stable isotopes. Journal of Sedimentary Petrology, v. 51, p. 987-997.

Braun, W.K., A.W. Norris, and T.T. Uyeno. 1988. Late Givetian to Early Frasnian biostratigraphy of Western Canada: The Slave Point - Waterways boundary and related events. In: Devonian of the World, Proceedings of the Second international Symposium on the Devonian System. N.J. McMillan, A.F. Embry, and D.J. Glass (eds.). Canadian Society of Petroleum Geologists, Calgary, v. III, p. 93-111.

Burne, R.V., J. Bauld and P. De Decker, 1980. Saline lake charophytes and their geological significance. Journal of Sedimentary Petrology, v. 50, p. 281-293.

Cavell, P. A., and H.G. Machel, 1997. Concentrations and isotopic compositions of strontium leached from Upper Devonian shales of the Alberta Basin - implications for regional paleofluid flow. CSPG-SEPM Joint Convention, Program with Abstracts, p. 57.

Cecile, M.P., D.W. Morrow, and G.K. Williams, 1997. Early Paleozoic (Cambrian to Early Devonian) tectonic framework, Canadian Cordillera. Bulletin of Canadian Petroleum Geology, v. 45, p. 54-74.

Chi, G., and P. Ni, 2007. Equations for calculation of $NaCl/(NaCl+CaCl_2)$ ratios and salinities from hydrohalite-melting and ice-melting temperatures in the H_2O-$NaCl$-$CaCl_2$ system. Acta Petrologica Sinica, v. 23, p. 33-37.

Choquette, P.W., and N.P. James, 1987. Diagenesis #12. Diagenesis in limestones – 3. The deep burial environment. Geoscience Canada, v. 14, p. 3-35.

Clayton, R.N., I., Friedman, D.L., Garf, T.K., Mayeda, W.F. Meents, and N.F. Shimp, 1966. The origin of saline formation waters, I. Isotopic composition. Journal of Geophysical Research, v. 71, p. 3869-3882.

Coniglio, M.I. and G.R. Dix, 1992. Carbonate slopes. In: Facies models: Response to sea level change. R.G. Walker and N.P. James (eds.), Geological Association of Canada, p. 349-373.

Crickmay, C.H., 1960. The older Devonian faunas of the Northwest Territories. Published by the author. Calgary, Canada. 12 p.

Davies, G., and L. B. Smith, 2006. Structurally controlled hydrothermal dolomite reservoir facies: An overview. American Association of Petroleum Geologist Bulletin, v. 90, p. 1641-1690.

Demicco, R.V., and L.A. Hardie, 1994. Sedimentary structures and early diagenetic features of shallow marine carbonate deposits. Society of Economic Paleontologists and Mineralogists Atlas Series 1, 255 p.

Dickson, J.A.D., 1966. Carbonate identification and genesis as revealed by staining: Journal of Sedimentary Petrology, v. 36, p. 491-505.

Douglas, R.J.W. and D.K. Norris, 1960. Virginia Falls and Sibbeston Lake map areas, Northwest Territories. Geological Survey of Canada, Paper 59-6.

Dunnington, H.V., 1967. Aspects of diagenesis and shape change in stylolitic limestone reservoirs: World Petroleum Congress, 7th, Mexico, Proc. v. 2, p. 339-352.

Embry, A. F., and J.E. Klovan, 1971. A Late Devonian reef tract on northeastern Banks Island, NWT. Bulletin of Canadian Petroleum Geology, v. 19, p. 730-781.

Faure, G., 1986. Principles of isotope geology. 2nd ed. John Wiley & Sons Inc. New York, 589 p.

Faure, G., and J. L. Powell, 1972. Strontium isotope geology. Springer-Verlag, Berlin. 188 p.

Folk, R.L., 1987. Detection of Organic-Matter in Thin-Sections of Carbonate Rocks using a White Card. Sedimentary Geology, v. 54, p. 193-200.

Frank, J.R., A.B. Carpenter, and T.W. Oglesby, 1982. Cathodoluminescence and composition of calcite cement in the Taum Sauk Limestone (Upper Cambrian), Southeast Missouri. Journal of Sedimentary Petrology, v. 52, p. 631-638.

Friedman, I., and J.R. O'Neil, 1977. Compilation of stable isotope fractionation: Factors of geochemical interest. In: Data of Geochemistry 6th edition. M. Fleischer (ed.). Geology Survey Professional Paper, Vol. KK. United States Geological Survey.

Goldstein, R. H., (2003). Petrographic analysis of fluid inclusions. In: Fluid Inclusions: Analysis and Interpretation. I. Samson, A. Anderson and D. Marshall (eds.). Mineralogical Association of Canada Short Course, v. 32, p. 9-53.

Griffin, D.L., 1967. Devonian of northeastern British Columbia. In: International Symposium on the Devonian System. D.H. Oswald (ed.). Alberta Society of Petroleum Geologists, p. 803-826.

Gosselin, E. G., L. Smith, and D.J.C. Mundy, 1989. The Golden and Evi reef complexes, Middle Devonian, Slave Point Formation, northwestern Alberta. In Reefs – Canada and adjacent areas. H.H.J. Geldsetzer, N.P. James, and G.E. Tebbutt (eds). Canadian Society of Petroleum Geologist Memoir 13, p. 440-447.

Hage, C.O., 1945. Geological reconnaissance along the lower Liard River, British Columbia, Yukon and Northwest Territories. Geological Survey of Canada, Paper 45-22.

Hladil, J., 2007. The earliest growth stages of *Amphipora*. – In: Fossil, Corals and Sponges. Hubmann, B., and Piller, W.E. (eds.). Proceedings of the 9th International Symposium on Fossil Cnidaria and Porifera. – Österr. Akad. Wiss., Schriftenr. Erdwiss. Komm. 17, p. 51-65.

House, M.R., and F.M. Gradstein, 2004. The Devonian Period. In: Geologic Time Scale. J. Gradstein, A. Ogg, and A. Smith (eds.). Cambridge University Press, Cambridge. p. 202-221.

Irwin, H., C. Curtis, and N. Coleman, 1977. Isotopic evidence for source of diagenetic carbonates formed during burial of organic-rich sediments. Nature, v. 269, p. 209-213.

James. N.P., and P.W. Choquette, 1990. Limestones – the sea-floor diagenetic environemnts. In: Diagenesis: Geoscience Canada Reprint Series 4. I.E. McIlreath and D.W. Morrow (eds.). Geologic Association of Canada. p. 13-34.

James, N.P., and P. Bourque, 1992. Reefs and mounds. In: Facies Models: Response to Sea Level Change. R.G. Walker and N.P. James (eds.). Geologic Association of Canada. p. 323-347.

Jones, B., and A. Desrochers, 1992. Shallow platform carbonates. In: Facies models: Response to sea level change. Walker, R.G., and James, N.P. (eds.). Geologic Association of Canada, p. 277-301.

Knauth, L. P., and M. A. Beeunas, 1986. Isotope geochemistry of fluid inclusions in Permian halite with implications for the history of ocean water and the origin of saline formation waters. Geochimica et Cosmochimica Acta, v. 50, p. 419-433.

Kobluk, D.R ., 1975. Stromatoporoid paleoecology of the south-east margin of the Miette carbonate complex, Jasper Park, Alberta. Bulletin of Canadian Petroleum Geology. v. 23, p. 224-277.

Land, L.S., 1980. The isotopic and trace element geochemistry of dolomite: The state of the art. In: Concepts and models of dolomitization. D.H. Zenger, J.B. Dunham, and R.L. Etherington (eds). SEPM Special Publication 28, p. 87-110.

Land, L.S., 1983. The application of stable isotopes to the studies of the origin of dolomite and to problems of diagenesis in clastic sediments, in M.A. Arthur, T.F. Anderson, I.R. Kaplan, J.Veizer, and L.S. Land (eds.). Stable isotopes in sedimentary geology, SEPM Short Course 10, p. 4.1-4.22.

Land, L.S., Salem, M.R. I. and Morrow, D.W. 1975. Paleohydrology of ancient dolomites:geochemical evidence. American Association of Petroleum Geologists Bulletin, v. 59, p. 1602-1625.

Law, J., 1955. Geology of northwestern Alberta and adjacent areas. American Associstion of Petroleum Geologists, Bulletin, v. 39, p. 1927-1975.

Lister, G.S., M.A. Etheridge, and P.A. Symonds, 1991. Detachment models for the formation of passive continental margins. Tectonics, v. 10, p. 1038-1064.

Lonnee, J. S., 1999. Sedimentology, dolomitisation and diagenetic fluid evolution of the Middle Devonian Sulphur Point Formation, Northwestern Alberta. University of Windsor. Unpublished M.Sc. thesis. 133 pages.

Lonnee, J. S., 2005. Diagenetic evolution of the slave point formation, Clarke Lake, B.C. Canada. University of Alberta. Unpublished PhD. thesis. 434 pages.

Lonnee, J.S., and H.G. Machel, 2006. Pervasive dolomitization with subsequent hydrothermal alteration in the Clarke Lake gas field, Middle Devonian Slave Point Formation, British Columbia. Canada. American Association of Petroleum Geologists Bulletin, v. 90, p. 1739-1761.

MacLean, B.C., and D.W. Morrow, 2004. Bovie structure: Its evolution and regional context. Bulletin of Canadian Petroleum Geology, v, 52, p. 302-324.

Machel, H.G., 1987. Some aspects of diagenetic sulphate-hydrocarbon redox reactions, In: Diagenesis of Sedimentary Sequences. J.D. Marshall (eds.). Geological Society Special Publication 36, p. 15-28.

Machel, H.G., 1999. Effects of groundwater flow on mineral diagenesis, with emphasis on carbonate reservoirs: Hydrogeology Journal, v. 7, p. 94-107.

Machel, H.G., and Hunter, I.G., 1994. Facies models for Middle to Late Devonian shallow marine carbonates, with comparison to modern reefs: a guide for facies analysis. Facies, v. 30, 155-176.

Machel, H. G., and P. A. Cavell, 1999. Low-flux, tectonically induced squeegee fluid flow (‘‘hot flash’’) into the Rocky Mountain foreland basin. Bulletin of Canadian Petroleum Geology, v. 47, p. 510-533.

Meijer Drees, N. C., 1994. Devonian Elk Point Group of the Western Canada sedimentary basin. In: Geological atlas of the Western Canada sedimentary basin. G. D. Mossop and I. Shetsen (compilers). Canadian Society of Petroleum Geologists and Alberta Research Council, p. 129-147.

Morrow, D.W., 1978. The Dunedin Formation: A transgressive shelf carbonate sequence. Geological Survey of Canada, Paper 76-12, 35 p.

Morrow, D.W., and H.H.J. Geldsetzer, 1988. Devonian of the eastern Canadian Cordillera. In: Denovian of the World, Proceedings of the Second International Symposium on the Devonian System. N.J. McMillan, A.F. Embry and D.J. Glass (eds.). Canadian Society of Petroleum Geologists, Memoir 14, v. 1, p. 85-121.

Morrow, D.W., and K.L. Aulstead, 1995. The Manetoe dolomite – a Cretaceous-Tertiary or a Paleozoic event? Fluid inclusion and isotopic evidence. Bulletin of Canadian Petroleum Geology, v. 43, p. 267-280.

Morrow, D.W., and R. Shinduke, 2003. Liard Basin, Northeast British Columbia: An exploration frontier. Canadian Society Exploration Geophysicts Convention, Calgary, Alberta, Canada. Abstract#283S0131.

Morrow, D.W., G.L. Cumming, and R.B. Koepnick, 1986, Manetoe facies — A gas-bearing, megacrystalline, Devonian dolomite, Yukon and Northwest Territories, Canada. AAPG Bulletin, v. 70, p. 702-720.

Morrow, D.W., G.L. Cumming, and K.L. Aulstead, 1990. The gas-bearing Devonian Manetoe facies, Yukon and Northwest Territories. Geological Survey Canada Bulletin, v. 400, 54 pp.

Mountjoy, E., H. Qing, and R. McNutt, 1992. Sr isotopic composition of Devonian dolomites, Western Canada Sedimentary Basin: Significance as sources of dolomitizing fluids. Applied Geochemistry, v. 7, p. 57-75.

Morrow, D.W., J. Potter, B. Richards, and F. Goodarzi, 1993. Paleozoic burial and organic maturation in the Liard Basin region, northern Canada: Bulletin of Canadian Petroleum Geology, v. 41, p. 17-31.

Morrow, D.W., M. Zhao, and L.D. Stasiuk, 2002. The gas-bearing Devonian Presqu'ile Dolomite of the Cordova Embayment region of British Columbia, Canada: Dolomitization and the stratigraphic template: American Association of Petroleum Geologists Bulletin, v. 86, p. 1609-1638.

Morse, J.W. and Mackenzie, F.T., 1990. Geochemistry of sedimentary carbonates. Developments in sedimentology 48. Elsevier, Amsterdam, The Netherlands.

Nadjiwon, L.M., 2001. Facies analysis, diagenesis and correlation of the middle Devonian Dunedin and Keg River Formations, Northeastern British Columbia. Unpublished M.S. thesis, Univ. of Waterloo, Waterloo, Ontario. 167 pp.

National Energy Board, 2000. Northeast British Columbia natural gas resource assessment 1992-1997. Technical Report, 10 p.

National Energy Board, 2001. Petroleum resource assessment of the Liard Plateau, Yukon Territory, Canada. 2001. National Energy Board for Energy Resources Branch, Government of Yukon, 63 p.

Osadetz, K.G., and K.E. Mottershead, 1992. BURIAL, a program that calculates and plots the burial history curves and thermal maturity history of a stratigraphic section. Geological Survey of Canada, Paper 91-19.

Peck, R.E., and G.A. Morales., 1966. The Devonian and Lower Mississippian charophytes of North America. Micropaleontology, v.12, p. 303-324.

Pelzer, E.E., 1966. Mineralogy, geochemistry and stratigraphy of the Besa River Shale, British Columbia. Bulletin of Canadian Petroleum Geology, v. 14, p. 273-321.

Petrel Robertson Consulting, 2003, Exploration assessment of deep Devonian gas plays, northeastern British Columbia: Report prepared for British Columbia Ministry of Energy and Mines, 24 p.

Pratt, B.R., N.P. James, and C.A. Cowan., 1992. Peritidal Carbonates. In: Facies models: Response to sea level change. Walker, R.G., and James, N.P. (eds.). Geologic Association of Canada, p. 303-322.

Potter, R.W. 1977. Pressure corrections for fluid inclusion homogenization temperatures volumetric properties of the sytem NaCl-H2O. Journal of Research of the U.S. Geological Survey 5, 603-607.

Qing, H., 1991. Diageneous of Middle Devonian Presqu'ile dolomite, Pine Point NWT and adjacent subsurface. Unpublished Ph.D. thesis. McGill University, Montreal, 287 p.

Qing, H., 1998. Petrography and geochemistry of early-stage, fine- and medium crystalline dolomites in the Middle Devonian Presqu'ile Barrier at Pine Point, Canada. Sedimentology, v. 45, p. 433-446.

Qing, H., and E.W. Mountjoy, 1994. Formation of coarsely crystalline, hydrothermal dolomite reservoirs in the Presqu'ile Barrier, Western Canada Sedimentary Basin. American Association of Petroleum Geologists Bulletin, v. 78, p. 55-77.

Reimer, J.D., and M.R. Teare, 1992. Deep burial diagenesis and porosity modification in carbonate rocks by thermal organic sulphate reduction and hydrothermal dolomitization: TSR-HTD. In: Subsurface dissolution porosity in carbonates: Recognition, causes and implications. Canadian Society of Petroleum Geologists Short Course Notes, 26 p.

Reineck, H.E., and F. Wunderlich., 1968. Classification and origin of flaser and lenticular bedding. Sedimentology, v. 11, p. 99-104.

Roedder, E., 1984. Fluid inclusions: Mineralogical Society of America Reviews in Mineralogy, v. 12, 644 p.

Rosenbaum, J., and S.M.F. Sheppard, 1986. An isotopic study of siderites, dolomites and ankerites at high-temperatures. Geochimica et Cosmochimica Acta, v. 50, p. 1147-1150.

Richards, B.C., 1989. Uppermost Devonian and Lower Carboniferous stratigraphy, sedimentation, and diagenesis, southwestern District of Mackenzie and southeastern Yukon Territory. Geological Survey of Canada, Bulletin 390, 135 p.

Salad Hersi, O., K. Khan and W. Walsh, 2006. Subsurface stratigraphic mapping of the Middle Devonian carbonates: Beaver River gas field, Liard Basin, Northeastern British Columbia. CSPG CSEG CWLS Joint Convention. Poster presentation #158.

Schaefer, M., 2002. Paleoproterozoic Mississippi Valley–type Pb-Zn deposits of the Ghaap Group, Transvaal Supergroup in Griqualand West, South Africa. Unpublished PhDdissertation, Rand Afrikaans University, Johannesburg. South Africa. 367 p.

Shackleton, N.J., and J.P. Kennett., 1975. Paleotemperature history of the Cenozoic and the initiation of Antarctic glaciation: oxygen and carbon isotope analyses in DSDP sites 277, 279 and 281. In: Initial reports of the Deep Sea Drilling Project, vol. 29, Lyttleton, N.Z. to Wellington, N.Z.; March-April 1973. Texas A & M University, Texas, USA., p. 743-755.

Snowdon, D.M., 1977. Beaver River gas field; a fractured carbonate reservoir. In: The Geology of Selected Carbonate Oil, Gas, and Lead Zinc Reservoirs in Western Canada. I.A. McIlreath and R.D. Harrison (eds.). Fifth Canadian Society of Petroleum Geologists core conference, v. 5, p. 1-18.

Stearn, C.W., 1982. The shapes of Paleozoic and modern reef builders: A critical review: Paleobiology, v. 8, p. 228-241.

Swart, P.K., S.J. Burns., and J.J. Leder, 1991. Fractionation of the stable isotopes of oxygen and carbon in carbon dioxide during the reaction of calcite with phosphoric acid as a function of temperature and technique. Chemical Geology, v. 86, p. 89-96.

Sweeney, J.J., and A.K. Burnham, 1990. Evaluation of a simple model of vitrinite reflectance based on chemical kinetics: AAPG Bulletin, v. 74, p. 1559-1570.

Taylor, G.D., 1967a, Stone Formation. In: Lexicon of Canadian Stratigraphy, Vol. 4, Western Canada, Including Eastern British Columbia, Alberta, Saskatchewan, and Southern Manitoba. Glass, D.J. (ed.), Canadian Society of Petroleum Geologists. 1990 p.

Taylor, G.D., 1967b. Dunedin Formation. In: Lexicon of Canadian Stratigraphy, Vol. 4, Western Canada, Including Eastern British Columbia, Alberta, Saskatchewan, and Southern Manitoba. Glass, D.J. (ed.), Canadian Society of Petroleum Geologists. 1990 p.

Taylor, H.P. Jr., 1979. Oxygen and hydrogen isotope relationships. In: Hydrothermal Mineral Deposits, H. L. Barnes (Ed.). Geochemistry of Hydrothermal Ore Deposits, 236-277.

Taylor, G.C., and W.S. Mackenzie, 1970. Devonian stratigraphy of northeastern British Columbia. Geological Survey of Canada, Bulletin 186.

Taylor, G.C., and D.F. Stott, 1973. Tuchodi Lakes map-area, British Columbia; Geological Survey of Canada, Memoir 373, 37 p.

Taylor, G.C. and W.S. MacKenzie, 1976. Dunedin Formaion. In: Lexicon of Canadian Stratigraphy, Vol. 4, Western Canada, Including Eastern British Columbia, Alberta, Saskatchewan, and Southern Manitoba. Glass, D.J., (Ed.), Canadian Society of Petroleum Geologist, 1990 p.

Tucker, M.E., 1981. Sedimentary petrology – an introduction: Blackwell Scientific Publications, Oxford, 252 p.

Tucker, M.E., and V.P. Wright, 1990. Carbonate sedimentology: Blackwell Scientific Publications, Oxford, 482 p.

Veizer, J., 1983. Chemical diagenesis of carbonates: theory and application of trace element techniques, in M.A. Arthur, T.F. Anderson, I.R. Kaplan, J. Veizer, and L.S. Land, eds., Stable isotopes in sedimentary geology: Society of Economic Paleontologists and Mineralogists Short Course 10, p. 3-1 to 3-100.

Veizer, J., D. Ala, K. Azmy, P. Bruckschen, D. Buhl, F. Bruhn, G. Carden, A. Diener, S. Ebneth, Y. Godderis, T. Jasper, C. Korte, F. Pawellek, O.G. Podlaha, and H. Strauss, 1999. $^{87}Sr/^{86}Sr$, $\delta^{13}C$ and $\delta^{18}O$ evolution of Phanerozoic seawater, Chemical Geology, v. 161, p. 59-88.

Vopni, L.K., and J.F. Lerbekmo, 1972. The Horn Plateau Formation: A Middle Devonian coral reef, Northwest Territories, Canada. Bulletin of Canadian Petroleum Geology, v. 20, p. 498-548.

Walsh, W., O. Salad Hersi, and M. Hayes, 2005. Liard Basin – Middle Devonian Exploration. In: Summary of Activities 2005, British Columbia Ministry of Energy and Mines, 38-41.

Wendte, J., I.S. Al-Aasm, G. Chi, and D.G. Sargent, 2007. Isotopic and fluid inclusion analysis of diagenetic mineral phases of the Upper Devonian Jean Marie Member (Redknife Formation) in the July Lake area of northeastern British Columbia. Geological Survey of Canada, Open File 5661, 7 p.

Zhang, Y.G., and J.D. Frantz, 1992. Hydrothermal reactions involving equilibria between minerals and mixed-volatiles. II) Investigations of fluid properties in the CO_2-CH_4-H_2O system using synthetic fluid inclusions. Chemical Geology, v. 100, p. 51-70.

APPENDIX A: List of Cores Studied

UWID	Core #	Interval	Formation (IHS formation tops)	Recovery
200/C-045-K	4	3858.6 ~ 3867.7 m	Dunedin	9.1 m
094-N-16/00	5	3937.8 ~ 3945.7 m	Stone	7.9 m
	6	4007.8 ~4022.4 m	Stone	13.4 m
	7	4022.4 ~4040.1 m	Stone	17.7 m
	8	4040.1 ~4048.5 m	Stone	8.4 m
	9	4048.8 ~4051.3 m	Stone	2.4 m
	10	4051.3 ~4055.6 m	Stone	3.4 m
	11	4078.6 ~ 4087.7 m	Stone	9.1 m
	12	4087.7 ~ 4091.3 m	Stone	3.5 m
	13	4091.3 ~ 4093.2 m	Stone	1.9 m
	14	4111.8 ~ 4114.0 m	Stone	2.2 m
	15	4145.3 ~ 4150.8 m	Stone	5.5 m
	16	4206.2 ~ 4217.8 m	Arnica	11.6 m
	17	4252.0 ~ 4266.6 m	Arnica	14.6 m
	18	4315.1 ~ 4324.8 m	Arnica	9.7 m
	19	4383.3 ~ 4386.7 m	Arnica	3.4 m
	20	4450.1 ~ 4455.6 m	Arnica	5.5 m
	21	4482.1 ~ 4482.7 m	Arnica	0.6 m
	22	4482.7 ~ 4486.7 m	Arnica	4.0 m
200/c-010-E	36	1627.3 ~1628.7 m	Dunedin	1.2 m
094-N-07/00	37	1628.7 ~1633.4 m	Dunedin	4.7 m
	38	1712.7 ~1721.8 m	Dunedin	9.1 m
	39	1793.1 ~1802.2 m	Dunedin	9.1 m
	40	1802.2 ~1812.0 m	Dunedin	9.8 m
	41	1812.0 ~1823.6 m	Dunedin	11.6 m
	42	1823.6 ~1833.1 m	Dunedin	9.4 m
	43	1833.1 ~1848.0 m	Stone/ Dunedin	14.9 m
	44	1848.0 ~1859.0 m	Stone	11.0 m
	45	1859.0 ~1873.0 m	Stone	14.0 m
	46	1873.0 ~1883.7 m	Stone	10.7 m
	47	1883.7 ~1890.1 m	Stone	6.4 m

UWID	Core #	Interval	Formation (IHS formation tops)	Recovery
200/b-019-K	1	3777.8 ~ 3781.2 m	Muskwa	2.7 m
094-N-16/00	2	3781.2 ~ 3785.4 m	Muskwa	4.2 m
	3	3827.5 ~ 3834.2 m	Dunedin	2.4 m
	5	3896.1 ~ 3900.9 m	Dunedin	1.5 m
	6	3934.8 ~ 3941.8 m	Dunedin	6.7 m
	7	3941.8 ~ 3951.5 m	Dunedin	9.7 m
	8	4027.7 ~ 4035.4 m	Dunedin	7.6 m
	9	4035.4 ~ 4053.0 m	Dunedin	17.3 m
	10	4113.1 ~ 4120.7 m	Stone	7.6 m
	11	4120.7 ~ 4127.7 m	Stone	7.0 m
	12	4188.7 ~ 4206.6 m	Stone	17.9 m
	13	4233.5 ~ 4237.7 m	Stone	3.9 m
	14	4237.7 ~ 4240.5 m	Stone	2.1 m
200/a-067-D	1	5128.3 ~ 5142.0 m	Nahanni	13.4 m
094-O-13/00	2	5211.2 ~ 5229.5 m	Nahanni	17.3 m
200/c-054-K	1	3527.0 ~ 3536.1 m	Dunedin	8.8 m
094-N-16/00	2	3536.1 ~ 3554.4 m	Dunedin	18.1 m
	3	3617.8 ~ 3630.3 m	Dunedin	11.8 m
	4	3697.0 ~ 3715.3 m	Dunedin	17.6 m
	5	3837.2 ~ 3855.5 m	Stone	18.2 m
	7	4036.9 ~ 4055.1 m	Stone	18.2 m
200/d-073-K	1	3782.4 ~ 3785.4 m	Nahanni	~3.0 m
094-N-16/00	2	3818.0 ~ 3825.4 m	Nahanni	6.7 m
	3	4127.0 ~ 4133.4 m	Stone	4.0 m
200/c-027-K	1	3744.3 ~ 3753.1 m	Dunedin	9.1 m
094-N-16/00	2	3808.2 ~ 3826.5 m	Dunedin	17.6 m
	3	3886.6 ~ 3895.5 m	Dunedin	8.3 m
	4	3957.3 ~ 3972.6 m	Dunedin	14.6 m
	5	4033.5 ~ 4051.8 m	Stone	18.2 m
	6	4114.6 ~ 4123.4 m	Stone	8.8 m
	7	4184.4 ~ 4202.8 m	Stone	18.4 m
200/c-016-A	1	3650.0 ~3668.0 m	Dunedin	16.8 m
094-N-15/00	2	3764.0 ~3782.2 m	Dunedin	18.2
	3	3782.2 ~3800.0 m	Dunedin	17.8 m
	4	3800.0~ 3818.0 m	Dunedin	18 m

UWID	Core #	Interval	Formation (IHS formation tops)	Recovery
200/c-016-A	5	3847.5 ~3650.6 m	Dunedin	3.1 m
094-N-15/00	6	3968.0 ~3972.6 m	Stone	2.6 m
	7	3972.6 ~3975.2 m	Stone	2.1 m
	8	4040.0 ~4049.5 m	Stone	9.5 m
	9	4120.0 ~4121.0 m	Stone	0.6 m
	10	4252.0 ~4268.2 m	Arnica	16.2 m
200/b-021-G 094-O-06/00	1	2647.1 ~2662.6 m	Nahanni	15.2 m
200/d-064-K	22	3489.8 ~ 3500.8 m	Dunedin	11.2 m
094-N-16/00	23	3500.8 ~ 3510.5 m	Dunedin	9.7 m
	24	3510.5 ~ 3523.0 m	Dunedin	12.5 m
	25	3523.0 ~ 3535.5 m	Dunedin	12.5 m
	26	3535.5 ~ 3547.7 m	Dunedin	2.1 m
	27	3547.7 ~ 3551.1 m	Dunedin	3.3 m
	28	3551.1 ~ 3560.5 m	Dunedin	8.2 m
	29	3560.5 ~ 3566.0 m	Dunedin	3.9 m
	30	3566.0 ~ 3569.6 m	Dunedin	2.9 m
	31	3569.6 ~ 3581.8 m	Dunedin	9.1 m

APPENDIX B: List of Thin Sections

Thin Section	Well ID	Depth (m)
1.8	c-45-K/94-N-16	4148.1
1.15	c-45-K/94-N-16	4045.5
1.16	c-45-K/94-N-16	4040.3
1.17	c-45-K/94-N-16	4038.3
1.21	c-45-K/94-N-16	3940.3
1.22	c-45-K/94-N-16	3867.6
1.23	c-45-K/94-N-16	3863.0
1.25	c-45-K/94-N-16	3792.4
1.28	c-45-K/94-N-16	3718.0
1.29	c-45-K/94-N-16	3717.3
1.30	c-45-K/94-N-16	3716.7
1.31	c-45-K/94-N-16	3712.5
1.32	c-45-K/94-N-16	3649.7
1.33	c-45-K/94-N-16	3648.8
1.34	c-45-K/94-N-16	3653.3
1.35	c-45-K/94-N-16	3652.1
D1-1	c-45-K/94-N-16	4486.1
D1-3	c-45-K/94-N-16	4324.1
D1-4	c-45-K/94-N-16	4214.5
D1-5	c-45-K/94-N-16	4032.0
D1-5B	c-45-K/94-N-16	4026.3
D1-6	c-45-K/94-N-16	4018.8
2.2	c-10-E/94-N-07	1835.0
2.5	c-10-E/94-N-07	1814.4
2.6	c-10-E/94-N-07	1810.9
2.8	c-10-E/94-N-07	1802.4
2.10	c-10-E/94-N-07	1713.0
2.12	c-10-E/94-N-07	1630.4
D2-2	c-10-E/94-N-07	1839.0
D2-3	c-10-E/94-N-07	1823.0
D2-4	c-10-E/94-N-07	1813.3

Thin Section	Well ID	Depth (m)
4.2	b-19-K/94-N-16	4191.9
4.3	b-19-K/94-N-16	4116.6
4.4	b-19-K/94-N-16	4119.9
4.5	b-19-K/94-N-16	4116.6
4.7	b-19-K/94-N-16	4113.6
4.8	b-19-K/94-N-16	4047.4
4.10	b-19-K/94-N-16	4040.4
4.11	b-19-K/94-N-16	4037.4
4.12	b-19-K/94-N-16	4034.0
4.13	b-19-K/94-N-16	4029.8
4.14	b-19-K/94-N-16	3949.9
4.16	b-19-K/94-N-16	3941.1
4.17	b-19-K/94-N-16	3938.0
4.18	b-19-K/94-N-16	3896.3
D4-2	b-19-K/94-N-16	4192.6
D4-7a	b-19-K/94-N-16	4046.3
D4-7b	b-19-K/94-N-16	4046.3
D4-8	b-19-K/94-N-16	3947.1
5.1	a-67-D/94-O-13	5225.1
5.2	a-67-D/94-O-13	5221.3
5.3	a-67-D/94-O-13	5212.5
5.4	a-67-D/94-O-13	5141.7
5.5	a-67-D/94-O-13	5133.7
5.6	a-67-D/94-O-13	5139.2
6.1	c-54-K/94-N-16	4048.4
6.2	c-54-K/94-N-16	4039.5
6.4	c-54-K/94-N-16	3850.4
6.6	c-54-K/94-N-16	3846.1
6.7	c-54-K/94-N-16	3841.1
6.8	c-54-K/94-N-16	3711.7
6.9	c-54-K/94-N-16	3708.5
6.11	c-54-K/94-N-16	3704.5
6.12	c-54-K/94-N-16	3699.1

Thin Section	Well ID	Depth (m)
6.13	c-54-K/94-N-16	3630.2
6.14	c-54-K/94-N-16	3552.1
6.15	c-54-K/94-N-16	3541.2
6.16	c-54-K/94-N-16	3536.0
6.17	c-54-K/94-N-16	3528.1
D6-1	c-54-K/94-N-16	3551.8
D6-2	c-54-K/94-N-16	3537.8
D6-4	c-54-K/94-N-16	3531.9
D6-5	c-54-K/94-N-16	3697.8
D6-7	c-54-K/94-N-16	3620.1
D6-8	c-54-K/94-N-16	3851.6
D7-1	d-73-K 94-N-16	3783.6
D7-3	d-73-K 94-N-16	3818.4
8.1	c-27-K/94-N-16	4048.4
8.2	c-27-K/94-N-16	4033.7
8.4	c-27-K/94-N-16	3963.9
8.5	c-27-K/94-N-16	3893.5
8.6	c-27-K/94-N-16	3821.7
8.7	c-27-K/94-N-16	3810.6
8.8	c-27-K/94-N-16	3747.8
D8-4	c-27-K/94-N-16	3958.4
D8-6	c-27-K/94-N-16	3894.7
D8-7	c-27-K/94-N-16	4045.5
D8-9	c-27-K/94-N-16	3816.0
D8-10	c-27-K/94-N-16	3815.3
D8-11	c-27-K/94-N-16	3744.4
17.1	d-16-A/94-N-15	3801.2
17.2	d-16-A/94-N-15	3779.4
17.3	d-16-A/94-N-15	3766.8
17.4	d-16-A/94-N-15	3660.7
17.6	d-16-A/94-N-15	3654.3
D17-1	d-16-A/94-N-15	3817.0

Thin Section	Well ID	Depth (m)
D17-2	d-16-A/94-N-15	3810.9
D17-3	d-16-A/94-N-15	3816.8
D17-4	d-16-A/94-N-15	3805.5
D17-5	d-16-A/94-N-15	3795.7
D17-6	d-16-A/94-N-15	3783.5
D17-6B	d-16-A/94-N-15	3783.5
D17-7	d-16-A/94-N-15	3781.8
D17-8	d-16-A/94-N-15	3764.3
D17-A	d-16-A/94-N-15	3775.5
D17-I	d-16-A/94-N-15	3768.1
D17-J	d-16-A/94-N-15	3769.1
D17-D	d-16-A/94-N-15	3765.8
D18-1	b-21-G/94-O-6	2657.8
26.2	d-64-K/94-N-16	3533.9
26.3	d-64-K/94-N-16	3503.7
26.4	d-64-K/94-N-16	3491.8
D26-1	d-64-K/94-N-16	3574.2
D26-2	d-64-K/94-N-16	3570.7
D26-3	d-64-K/94-N-16	3536.6
D26-4	d-64-K/94-N-16	3519.4
D26-5	d-64-K/94-N-16	3514.8
D26-6	d-64-K/94-N-16	3506.5
D26-7	d-64-K/94-N-16	3491.1

APPENDIX C: Isotopic Analytical Results

Sample Number	Diagenetic Phase	$\delta^{18}O$ (‰, V-PDB)	$\delta^{13}C$ (‰, V-PDB)	$^{87}Sr/^{86}Sr$ Isotopic Ratio
17.4 Cal MC	Limestone	-12.03	-2.10	-
2.2 Cal MC	Limestone	-10.32	-1.81	-
5.5 Cal Micrite	Limestone	-10.05	-0.89	-
D2-3 Cal MC	Limestone	-10.90	-2.23	-
D2-4 Cal MC	Limestone	-11.89	-2.74	-
17.4 Dolo FM	FCD in limestone to calcitic dolomite	-12.17	-0.57	0.70949
2.8 Dolo FM	FCD in limestone to calcitic dolomite	-8.42	-1.79	0.71365
5.5 Dolo FM	FCD in limestone to calcitic dolomite	-9.86	-0.97	0.70897
4.5 Dolo FM	FCD in dolostone	-9.59	-1.79	-
D4-2 Dolo Matrix	FCD in dolostone	-9.53	-1.40	0.71014
D8-10 Dolo FCM	FCD in dolostone	-10.46	-1.54	-
D1-3 Dolo Matrix	FCD in dolostone	-8.28	-1.16	0.71218
5.2 Dolo FM	FCD in dolostone	-14.87	-3.75	-
D1-4 Dolo FM	FCD in dolostone	-8.63	-1.07	0.71017
D18-1 Dolo FM	FCD in dolostone	-12.99	-2.06	0.71114
D4-7A Dolo FM	FCD in dolostone	-9.69	-2.84	0.71001
D4-8 Dolo FM	FCD in dolostone	-10.53	-0.69	-
1.30 Dolo G. Matrix	MCD-1	-11.51	-1.19	-
D17-3 Dolo Matrix	MCD-1	-10.69	-2.40	0.70973
D17-8 Dolo MSM	MCD-1	-10.77	-1.79	0.70927
D4-8 Dolo MSM	MCD-1	-10.98	-1.50	0.71210
D6-7 Dolo MSM	MCD-1	-11.36	-1.29	-
D8-4 Dolo G. Matrix	MCD-1	-10.03	-2.24	0.70922
D6-8 Dolo MSM	MCD-2	-10.40	-2.05	0.70919
1.34 CSM	MCD-2	-10.83	-1.26	0.70947
1.8 Dolo CSD	MCD-2	-9.44	-1.66	0.71161
6.6 CSD	MCD-2	-11.65	-2.15	-
8.1 Dolo MSM	MCD-2	-10.47	-1.74	-
D7-1 Dolo MSM	MCD-2	-12.33	-2.49	0.70997
D8-10 Dolo MSM	MCD-2	-10.48	-1.53	0.71082

Sample Number	Diagenetic Phase	$\delta^{18}O$ (‰, V-PDB)	$\delta^{13}C$ (‰, V-PDB)	$^{87}Sr/^{86}Sr$ Isotopic Ratio
D1-3 Dolo Type 1	MSD	-13.25	-3.40	-
D6-8 Dolo Type 1	MSD	-11.39	-2.09	-
5.2 Dolo	CSD	-12.18	-2.56	-
D1-1 Dolo SD	CSD	-12.25	-3.40	-
D1-3 Dolo T2	CSD	-16.55	-6.79	0.71378
D1-4 Dolo FFSD	CSD	-16.63	-9.02	0.71516
D17-8 Dolo T2	CSD	-11.43	-2.25	0.71053
D4-2 Dolo Type 2	CSD	-13.40	-6.21	0.71582
D4-8 Dolo	CSD	-11.35	-1.64	0.71138
D6-7 Dolo	CSD	-11.77	-1.55	0.70914
D6-8 Dolo Type 2	CSD	-11.87	-2.28	0.71005
D7-1 Dolo	CSD	-11.79	-1.51	0.70953
D8-10 Dolo T2	CSD	-11.05	-1.74	0.71104
D8-4 Dolo Type 2	CSD	-10.01	-1.89	0.70961
D17-3 Dolo FF	CSD	-9.09	1.05	0.71013
D1-5B Cal	CCC	-14.51	-11.23	-
D17-8 Cal	CCC	-15.50	-7.98	0.71225
D2-3 Cal	CCC	-12.65	-3.14	0.71009
D4-2 Cal	CCC	-12.10	-7.50	0.71151
D7-1 Cal	CCC	-15.05	-8.00	0.71250
D8-10 Cal	CCC	-9.80	-1.71	0.71354
D8-4 Cal	CCC	-12.92	-5.75	0.71092
D17-6B	CCC	-13.72	-9.81	-
D17-K	CCC	-12.07	-5.08	0.71226
D17-Q	CCC	-14.33	-9.34	-
1.17 HF	DIF	-11.30	-2.28	-
1.25 SVF	DIF	-10.64	-2.56	-
1.30 VF	DIF	-13.80	-3.80	-
17.2 HF	DIF	-10.85	-1.54	-
17.3 HF	DIF	-11.51	-2.59	-
5.1 VF	DIF	-11.23	-2.29	-
8.6 VFI	DIF	-11.15	-1.59	-
D1-1 VF	DIF	-11.09	-3.24	-
D17-1 VF	DIF	-11.85	-3.50	-
D17-2 VF	DIF	-11.02	-2.21	0.71228
D17-5 VF	DIF	-14.28	-3.72	-
D17-8 vein	DIF	-11.72	-2.73	-

Sample Number	Diagenetic Phase	$\delta^{18}O$ (‰, V-PDB)	$\delta^{13}C$ (‰, V-PDB)	$^{87}Sr/^{86}Sr$ Isotopic Ratio
D4-7B VF	DIF	-10.16	-2.71	-
D6-2 VF	DIF	-12.24	-1.71	-
D8-4 HVein	DIF	-10.64	-1.97	0.70995
D8-7 HF	DIF	-11.21	-1.81	-
D8-9 VF	DIF	-11.40	-1.69	-
D17-O	DIF	-14.09	-7.17	-
17.1 VF	CIF	-13.11	-6.43	-
D17-A	CIF	-11.61	-1.74	0.71751
D17-D	CIF	-13.26	-7.35	-
D17-D rpt	CIF	-13.25	-7.35	-
D17-E	CIF	-12.22	-2.54	-
D17-F	CIF	-13.24	-6.16	-
D17-G	CIF	-12.41	-7.03	0.71862
D17-H	CIF	-13.00	-10.54	-
D17-H rpt	CIF	-13.05	-10.63	-
D17-I	CIF	-13.01	-6.61	-
D17-J	CIF	-13.20	-5.19	0.71384
D17-M	CIF	-12.42	-6.52	-
D17-3 Cal	CIF	-13.49	-7.52	0.71436

APPENDIX D: Fluid Inclusion Microthermometric Data

Fluid inclusion microthermometric data for medium crystalline, nonplanar-c, saddle dolomite in vugs (MSD)

Well ID (Depth)	Diagenetic Phase	Occurrence of the FIAs	Size (μm)	Vapor (%)	Tm-first (mean °C; n)	Tm-HH (mean °C; n)	Tm-H_2O (range °C; n)	Tm-H_2O (mean °C)	Th (range °C; number of inclusion)	Th (mean °C)	XNaCl (mean; n; Chi and Ni 2007)	Salinity (mean wt. %; n; Chi and Ni 2007)
c-45-K/ 94-N-16 4324.1 m D1-3	MSD	Random	3	5	-	-	-	-	204 – 209 (2)	207	-	-
		Random	3	5	-	-	-	-	186 (1)	186	-	-
		Random	3	5	-	-	-	-	209 (1)	209	-	-
		Random	3	5	-	-	-	-	207 (1)	207	-	-
		Cluster	3 – 5	6	-56 (1)	-24 (1)	-13.5 (1)	-13.5	186 – 194 (4)	189	0.7 (1)	17.2 (1)
		Random	5	7	-	-	-	-	183 (1)	183	-	-
c-54-K/ 94-N-16 3851.6 m D6-8	MSD	Random	7	5	-	-	-	-	193 (1)	193	-	-
		Random	7	5	-	-	-	-	189 (1)	189	-	-
		Random	4	5	-	-	-	-	192 (1)	192	-	-
		Random	6	6	-	-	-	-	186 (1)	186	-	-
		Cluster	3 – 4	5	-	-	-	-	174 – 184 (5)	177	-	-

Fluid inclusion microthermometric data for coarsely to very coarsely crystalline, nonplanar-e, saddle dolomite in vugs (CSD)

Well ID/ Depth/ Sample Number	Diagenetic Phases	Occurrence of the FIAs	Size (μm)	Vapor (%)	Tm-first (mean °C; n)	Tm-HH (mean °C; n)	Tm-H_2O (range °C; n)	Tm-H_2O (mean °C)	Th (range °C; number of inclusion)	Th (mean °C)	XNaCl (mean; n; Chi and Ni 2007)	Salinity (mean wt. %; n; Chi and Ni 2007)
c-45-K/ 94-N-16 4324.1 m D1-3	CSD	Random	3	6	-	-	-	-	214 – 221 (3)	217	-	-
		Random	5	6	-55 (1)	-25 (1)	-14.0 (1)	-14.0	214 (1)	214	0.6 (1)	17.5 (1)
		Random	3	6	-	-	-	-	197(1)	197	-	-
		Random	5	7	-	-	-16.0 (1)	-16.0	192 (1)	192	-	19.5 (1)
		Random	3	6	-	-	-	-	197 (1)	197	-	-
		Random	6	7	-	-	-	-	197 (1)	197	-	-
		Random	5	5	-	-	-	-	193 (1)	193	-	-
		Random	15	5	-	-25 (1)	-	-	186 (1)	186	0.6 (1)	-
b-19-K/ 94-N-16 4192.9 m D4-2	CSD	Random	6	8	-56 (1)	-24 (1)	-18.0 (1)	-18.0	173 (1)	173	0.7 (1)	20.5 (1)
		Random	6	8	-55 (2)	-24 (1)	-15.7 (1)	-15.7	203 – 214 (2)	209	0.7 (1)	18.9 (1)
		Random	2 – 6	7	-57 (1)	-25 (1)	-18.7 (1)	-18.7	184 – 186 (2)	185	0.6 (1)	20.8 (1)
		Random	4	8	-	-	-	-	178 (1)	178	-	-
		Cluster	2 – 4	10	-	-	-	-	197 (3)	197	-	-
		Random	4	10	-	-	-	-	201 (1)	201	-	-
		Random	4 – 6	7	-	-	-	-	169 – 171 (2)	170	-	-
		Random	4	10	-57 (1)	-	-17.2 (1)	-17.2	193 – 195 (3)	194	-	20.4 (1)
		Random	3 – 6	8 – 10	-55 (1)	-25 (2)	-14.8 – -14.7 (2)	-14.8	221 (2)	221	0.6 (2)	18.1 (2)
		Random	8	6	-54 (1)	-25 (1)	-15.2 (1)	-15.2	212 (1)	212	0.6 (1)	18.4 (1)
b-19-K/ 94-N-16 3947.1 m D4-8	CSD	Random	2 – 5	6	-	-	-	-	189 – 204 (2)	197	-	-
		Random	4	6	-	-	-	-	193 – 194 (3)	194	-	-
		Random	7	6	-	-24 (1)	-	-	178 – 181 (2)	180	0.7 (1)	-
		Random	3 – 9	6	-	-24 (1)	-14.9 (1)	-14.9	171 – 178 (3)	174	0.7 (1)	18.3 (1)
a-67-D/ 94-O-13 5221.3 m 5.2	CSD	Cluster	2 – 6	5	-56 (2)	-25 (2)	-16.9 – -17.1 (2)	-17.0	189 – 206 (7)	195	0.6 (2)	19.7 (2)

Well ID/ Depth/ Sample Number	Diagenetic Phases	Occurrence of the FIAs	Size (µm)	Vapor (%)	Tm-first (mean °C; n)	Tm-HH (mean °C; n)	Tm-H2O (range °C; n)	Tm-H2O (mean °C)	Th (range °C; number of inclusion)	Th (mean °C)	XNaCl (mean; n; Chi and Ni 2007)	Salinity (mean wt. %; n; Chi and Ni 2007)
c-54-K/ 94-N-16 3620.1 m D6-7	CSD	Cluster	3 – 7	5	-55 (2)	-25 (3)	-17.7 (1)	-17.7	182 – 187 (4)	185	0.6 (3)	20.2 (1)
		Random	2 – 7	5	-	-24 (1)	-15.2 (1)	-15.2	171 – 190 (5)	182	0.7 (1)	18.5 (1)
		Random	2 – 6	5	-55 (1)	-24 (1)	-15.9 (1)	-15.9	176 – 178 (2)	177	0.7 (1)	19.0 (1)
		Random	2 – 5	5	-56 (1)	-24 (1)	-15.5 (1)	-15.5	173 – 177 (2)	175	0.7 (1)	18.7 (1)
c-54-K/ 94-N-16 3851.6 m D6-8	CSD	Random	5 – 9	6	-55 (1)	-26 (1)	-15.5 (1)	-15.5	181 – 184 (3)	182	0.5 (1)	18.6 (1)
		Random	11	6	-	-	-	-	174 (1)	174	-	-
		Random	8	6	-	-	-	-	182 (1)	182	-	-
		Random	8	6	-	-	-	-	184 (1)	184	-	-
		Random	4	5	-	-	-	-	168 (1)	168	-	-
		Random	4	5	-	-	-	-	193 (1)	193	-	-
		Random	4	5	-54 (1)	-24 (1)	-	-	208 (1)	208	0.7 (1)	-
		Random	3 – 5	6	-55 (1)	-	-	-	200 (2)	200	-	-
		Random	4 – 5	6	-	-	-	-	187 – 193 (2)	190	-	-
		Random	3 – 5	6	-	-25 (1)	-17.3 (1)	-17.3	168 – 172 (3)	170	0.6 (1)	19.9 (1)
		Random	4 – 7	6	-54 (1)	-25 (1)	-15.9 (1)	-15.9	179 – 194 (3)	186	0.6 (1)	18.9 (1)
		Random	5	6	-	-	-	-	201 (1)	201	-	-
		Random	3	5	-	-	-	-	178 (1)	178	-	-
d-73-K/ 94-N-16 3783.6 m D7-1	CSD	Cluster	4 – 5	6 – 7	-	-26 (5)	-12.8 – -12.2 (3)	-12.4	204 – 220 (7)	213	0.5 (5)	16.2 (3)
		Random	5 – 6	6 – 7	-56 (1)	-27 (1)	-18.7 – -18.9 (2)	-18.8	176 – 192 (3)	185	0.5 (1)	20.7 (2)
		Random	8 – 12	5	-55 (1)	-26 (1)	-19.2 (1)	-19.2	166 – 181 (2)	174	0.5 (1)	21.0 (1)
		Random	3	7	-	-26 (1)	<-15 (1)	-	181 – 186 (3)	184	0.5 (1)	-
		Isolated	5	7	-56 (1)	-25 (1)	-13.8 (1)	-13.8	231 (1)	231	0.6 (1)	17.4 (1)
		Isolated	3	5	-	-26 (1)	-13.2 (1)	-13.2	176 (1)	176	0.5 (1)	16.8 (1)
c-27-K/ 94-N-16 3958.4 m D8-4	CSD	Random	4 – 6	5 – 7	-	-26 (1)	<-13 (1)	-	198 – 208 (4)	202	0.5 (1)	-
		Isolated	6	5	-53 (1)	-	-19.8 (1)	-19.8	173 (1)	173	-	22.2 (1)
		Random	4 – 8	5	-56 (1)	-25 (2)	-19.8 (1)	-19.8	214 – 218 (3)	216	0.6 (2)	21.5 (1)

Well ID/ Depth/ Sample Number	Diagenetic Phase	Occurrence of the FIAs	Size (µm)	Vapor (%)	Tm-first (mean °C; n)	Tm-HH (mean °C; n)	Tm-H_2O (range °C; n)	Tm-H_2O (mean °C)	Th (range °C; number of inclusion)	Th (mean °C)	XNaCl (mean; n; Chi and Ni 2007)	Salinity (mean wt. %; n; Chi and Ni 2007)
c-27-K/ 94-N-16 3815.3 m D8-10	CSD	Random	3	5	-	-	-	-	187 (1)	187	-	-
		Random	3	5	-	-	-	-	224 (1)	224	-	-
		Random	3	5	-	-	-	-	198 (1)	198	-	-
		Random	5 – 7	5	-	-23 (1)	<-7 (1)	-	222 – 224 (2)	223	0.8 (1)	-
		Random	5	7	-54 (1)	-24 (1)	<-11 (1)	-	221 (1)	221	0.7 (1)	-
d-16-A/ 94-N-15 3816.8 m D17-3	CSD	Random	3 – 5	5	-56 (1)	-25 (1)	-16.0 (1)	-16.0	202 – 207 (3)	205	0.6 (1)	19.0 (1)
		Random	3	5	-	-	-	-	206 – 208 (2)	207	-	-
		Random	3	5	-	-	-16.1 (1)	-16.1	197 – 198 (3)	198	-	19.5 (1)
		Random	2 – 7	5	-55 (4)	-24 (1)	-	-	185 – 212 (7)	200	0.7 (1)	-
		Random	3 – 5	5	-	-	-	-	186 – 194 (3)	189	-	-
		Cluster	5 – 7	5 – 6	-56 (1)	- 26 (2)	-	-	194 – 204 (3)	197	0.5 (2)	-
d-16-A/ 94-N-15 3764.3 m D17-8	CSD	Random	3 – 6	5 – 7	-55 (1)	-25 (2)	-16.8 – -17.0 (2)	-16.9	191 – 228 (7)	209	0.6 (2)	19.6 (2)

Fluid inclusion microthermometric data for medium to coarsely crystalline, nonplanar-c dolomite in fractures (DIF)

Well ID/ Depth/ Sample Number	Diagenetic Phase	Occurrence of the FIAs	Size (µm)	Vapor (%)	Tm-first (mean °C; n)	Tm-HH (mean °C; n)	Tm-H_2O (range °C; n)	Tm-H_2O (mean °C)	Th (range °C; number of inclusion)	Th (mean °C)	XNaCl (mean; n; Chi and Ni 2007)	Salinity (mean wt. %; n; Chi and Ni 2007)
c-45-K/	DIF	Random	3	6	-	-	-	-	173 (1)	173	-	-
94-N-16		Random	3	6	-	-	-	-	213 (1)	213	-	-
3716.7 m		Random	3	6	-	-	-	-	211 (1)	211	-	-
1.30		Random	3	6	-	-	-	-	216 (1)	216	-	-
		Random	3	6	-	-	-	-	177 (1)	177	-	-
		Random	3 – 5	6	-	-	-	-	179 – 181 (2)	180	-	-
		Random	3	6	-	-	-	-	213 (1)	213	-	-
		Random	3	6	-	-	-	-	188 (1)	188	-	-
		Random	3	6	-	-	-	-	193 (1)	193	-	-
		Random	3 – 4	6	-	-	-	-	199 – 218 (3)	208	-	-
		Random	3	6	-	-	-	-	192 (1)	192	-	-
		Cluster	3 – 5	6	-	-	-	-	194 – 199 (5)	197	-	-
		Random	6	6	<-48 (1)	-24 (1)	-14.5 (1)	-14.5	226 (1)	226	0.7 (1)	18.0 (1)
		Random	3 – 5	6	-	-	-	-	209 – 210 (2)	210	-	-
		Random	3	6	-	-	-	-	222 – 226 (2)	224	-	-
b-19-K/	DIF	Random	6	6	-	-	-	-	189 (1)	189	-	-
94-N-16		Random	5 – 7	6	-	-	-	-	199 – 200 (2)	200	-	-
3947.1 m		Random	8	6	-55 (1)	-24 (1)	-	-	200 (1)	200	0.7 (1)	-
D4-8		Random	6 – 8	7	-55 (1)	-	-	-	194 – 196 (2)	195	-	-
		Random	6 – 8	6	-	-	-	-	172 – 176 (3)	174	-	-
a-67-D/	DIF	Random	4	6	-	-	-	-	184 (2)	184	-	-
94-O-13		Random	4	6	-	-	-	-	187 (1)	187	-	-
5225.1 m												
5.1												

Well ID/ Depth/ Sample Number	Diagenetic Phase	Occurrence of the FIAs	Size (µm)	Vapor (%)	Tm-first (mean °C; n)	Tm-HH (mean °C; n)	Tm-H_2O (range °C; n)	Tm-H_2O (mean °C)	Th (range °C; number of inclusion)	Th (mean °C)	XNaCl (mean; n; Chi and Ni 2007)	Salinity (mean wt. %; n; Chi and Ni 2007)
c-54-K/ 94-N-16 3851.6 m D6-8	DIF	Random	4	7	-	-	-	-	187	187 (1)	-	-
		Random	6	7	-55 (1)	-25 (1)	-	-	201	201 (1)	0.6	-
		Random	4	6	-	-	-	-	161	161 (1)	-	-
		Random	4	6	-	-	-	-	178	178 (1)	-	-
		Random	7	6	-55 (1)	-	-	-	192	192 (1)	-	-
		Random	4	6	-	-	-	-	190	190 (1)	-	-
		Random	6	6	-	-	-	-	217	217 (1)	-	-
		Random	6	6	-54 (1)	-24 (1)	-16.0 (1)	-16.0	186	186 (1)	0.7	19.1
c-27-K/ 94-N-16 3821.7 m 8.6	DIF	Random	8	6	-55 (1)	-	-	-	176 (1)	176	-	-
		Cluster	2 – 11	6	-	-	-	-	176 (1)	176	-	-
		Cluster	3 – 4	6	-	-	-	-	206 (1)	206	-	-
		Random	3	6	-	-	-	-	186 (1)	186	-	-
d-16-A/ 94-N-15 3810.9 m D17-2	DIF	Random	2 – 3	6	-	-	-	-	184 – 185 (3)	184	-	-
		Random	3	6	-	-	-	-	194 (1)	194	-	-
		Random	5	7	-55 (1)	-	-	-	213 (1)	213	-	-
		Random	5	6	-	-	-	-	203 (1)	203	-	-
		Cluster	2 – 8	6	-54 (1)	-	-	-	187 – 203 (6)	195	-	-

Fluid inclusion microthermometric data for coarsely to very coarsely crystalline, blocky calcite in vugs (CCC)

Well ID/ Depth/ Sample Number	Diagenetic Phase	Occurrence of the FIA	Size (µm)	Vapor (%)	Tm-first (mean °C; n)	Tm-HH (mean °C; n)	Tm-H_2O (range °C; n)	Tm-H_2O (mean °C)	Th (range °C; number of inclusion)	Th (mean °C)	XNaCl (mean; n; Chi and Ni 2007)	Salinity (mean wt. %; n; Chi and Ni 2007)
c-16-A/	CCC	Cluster	6 – 8	6	-	-24 (1)	-14.2 (1)	-14.2	170 – >261 (2)	170*	0.7 (1)	17.7 (1)
94-N-16		Random	6	6	-54 (1)	-25 (1)	-	-	144 (1)	144	0.6 (1)	-
3569.9 m		Isolated	7	7	-54 (1)	-24 (1)	-	-	149 (1)	149	0.7 (1)	-
D1-5B		Random	4	5	-	-25 (1)	-	-	179 (1)	179	0.6 (1)	-
		Random	4	6	-54 (1)	-25 (1)	-	-	183 – 206 (2)	195	0.6 (1)	-
c-10-E/	CCC	Random	8 – 10	6	-52 (2)	-23 (1)	-11.4 – -10.9 (3)	-11.2	131 – 149 (3)	141	0.8 (1)	15.2 (3)
94-N-7		Random	4 – 20	5	-53 (1)	-23 (1)	-13.2 – -12.7 (2)	-13.0	185 (1)	185	0.8 (1)	16.8 (2)
1823.0 m		Cluster	10 – 11	5	-	-24 (1)	-13.6 – -13.0 (3)	-13.3	163 – 173 (3)	168	0.7 (1)	17.0 (3)
D2-3		Random	6 – 9	5	<-46 (1)	-22 (2)	-14.0 – -13.2 (3)	-13.7	158 – 166 (3)	162	0.9 (2)	17.4 (3)
		Cluster	5 – 11	4 – 5	-51 (1)	-23 (2)	-12.9 – -12.6 (2)	-12.8	164 – 169 (3)	167	0.8 (2)	16.6 (2)
		Random	7	6	-	-	-	-	168 (1)	168	-	-
		Random	7	5	-	-	-	-	158 – 165 (2)	162	-	-
		Random	4 – 9	5	-52 (1)	-23 (1)	-12.8 (2)	-12.8	164 – 172 (2)	168	0.8 (1)	16.6 (2)
b-19-K/	CCC	Random	11 – 16	5	-54 (2)	-24(1)	-16.1 – -15.9 (2)	-16.0	137 – 138 (2)	138	0.7 (1)	19.1 (2)
94-N-16		Random	20 – 24	5	-	-	-14.7 – -12.7 (2)	-13.5	193 – 196 (2)	195	-	17.3 (2)
4192.9 m		Isolated	15	6	-	-	-		202 (1)	202	-	-
D4-2		Isolated	14	6	-54 (1)	-25 (1)	-17.4 (1)	-17.4	209 (1)	209	0.6 (1)	20.0 (1)
		Random	16 – 28	4 – 5	-54 (1)	-24 (3)	-18.4 – -14.1 (3)	-16.2	176 – 216 (4)	189	0.7 (3)	19.1 (3)
		Isolated	13	5	-54 (1)	-23 (1)	-16.0 (1)	-16.0	154 (1)	154	0.8 (1)	19.2 (1)
		Random	10 – 31	5 – 6	-53 (2)	-23 (2)	-15.0 – -13.7 (2)	-14.4	147 – 164 (2)	156	0.8 (2)	17.9 (2)
		Isolated	11	6	-53 (1)	-23 (1)	-17.0 (1)	-17.0	170 (1)	170	0.8 (1)	19.9 (1)
		Random	8 – 11	5	-	-24 (2)	-17.8 – -17.2 (2)	-17.5	151 – 162 (2)	157	0.7 (2)	20.2 (2)
		Random	12	5	-	-	-	-	181 (1)	181	-	-
		Random	20	5	-53 (1)	-24 (1)	-16.3 (1)	-16.3	183 (1)	183	0.7 (1)	19.3 (1)
		Isolated	16	~100	-	-	-	-	-53.1V (1)	-53.1V	-	-
		Trail	36	~100	-	-	-	-	-54.2V (1)	-54.2V	-	-
		Trail	14	~100	-	-	-	-	-56.0V (1)	-56.0V	-	-
		Trail	11	~100	-	-	-	-	-52.5V (1)	-52.5V	-	-
a-67-D/	CCC	Random	6	5	-	-	-	-	188 (1)	188	-	-
94-O-13		Random	2 – 3	5	-54 (1)	-23 (2)	-	-	177 – 196 (5)	185	0.8 (2)	-
5221.3 m		Random	2 – 5	5 – 6	-54 (1)	-24 (2)	-15.0 – -14.2 (2)	-14.6	180 – 193 (7)	188	0.8 (2)	18.1 (2)
5.2		Random	9	~100	-	-	-	-	-52.1V (1)	-52.1V	-	-

Well ID/ Depth/ Sample Number	Diagenetic Phase	Occurrence of the FIAs	Size (μm)	Vapor (%)	Tm-first (mean °C; n)	Tm-HH (mean °C; n)	Tm-H2O (range °C; n)	Tm-H2O (mean °C)	Th (range °C; number of inclusion)	Th (mean °C)	XNaCl (mean; n; Chi and Ni 2007)	Salinity (mean wt. %; n; Chi and Ni 2007)
d-73-K/	CCC	Random	23	4	-	-	-	-	174 (1)	174	-	-
94-N-16		Random	8 – 22	5 – 7	-	-	-	-	207 (2)	207	-	-
3783.6 m		Random	20	4	-51 (1)	-21 (1)	-11.1 (1)	-11.1	180 (1)	180	1.0 (1)	15.1 (1)
D7-1		Random	19	5	-50 (1)	-21 (1)	-10.7 (1)	-10.7	178 (1)	178	1.0 (1)	14.7 (1)
		Random	15 – 21		-49 (1)	-22 (2)	-12.4 – -9.3 (2)	-10.9	178 – 224 (3)	208	0.9 (2)	14.8 (2)
		Random	23 – 37	4 – 5	-49 (1)	-21 (1)	-12.0 (1)	-12.0	158 – 172 (4)	164	1.0 (1)	16.0 (1)
		Random	31	~100	-	-	-	-	-51.4 V (1)	-51.4V	-	-
		Trail	21	~100	-	-	-	-	-53.2 V (1)	-53.2V	-	-
		Random	17 – 21	~100	-	-	-	-	-54.0V – -53.6V (2)	-53.8V	-	-
		Trail	10 – 17	~100	-	-	-	-	-54.4V – -51.8V (3)	-52.7V	-	-
c-27-K/	CCC	Cluster	6 – 34	6 – 9	-54 (3)	-25 (7)	-19.6 – -16.0 (8)	-18.5	183 – 203 (8)	187	0.6 (7)	20.2 (8)
94-N-16		Random	48	8	-	-	-19.3 (1)	-19.3	199 (1)	199	-	21.9 (1)
3958.4 m		Random	13 – 16	5 – 9	-	-	-	-	183 – 187 (3)	185	-	-
D8-4		Random	2 – 6	5	-	-	-	-	184 – 205 (6)	192	-	-
		Random	8 – 14	7 – 8	-53 (1)	-24 (3)	-18.0 (1)	-18.0	182 – 189 (3)	186	0.7 (3)	20.5 (1)
c-27-K/	CCC	Random	7 – 9	6	-53 (1)	-23 (1)	-12.9 (1)	-12.9	186 – 198 (2)	192	0.8 (1)	16.7 (1)
94-N-16		Random	9 – 14	6	-52 (1)	-24 (2)	-13.5 – -12.6 (2)	-13.1	194 – 195 (2)	195	0.7 (2)	16.8 (2)
3815.3 m		Isolated	6	6	-	-23 (1)	-16.9 (1)	-16.9	164 (1)	164	0.8 (1)	19.9 (1)
D8-10		Random	3 – 5	6 – 7	-54 (1)	-24 (2)	-16.6 – -16.4 (3)	-16.5	173 – 179 (3)	177	0.8 (2)	19.5 (2)
		Trail	14 – 16	~100	-	-	-	-	-54.7V (1)	-54.7V	-	-
d-16-A/	CCC	Random	6 – 10	5 – 6	-53 (1)	-23 (2)	-15.1 – -14.8 (2)	-15.0	188 – 191 (2)	190	0.8 (2)	18.4 (2)
94-N-15		Random	18	5	-50 (1)	-24 (1)	-14.0 (1)	-14.0	196 (1)	196	0.7 (1)	17.6 (1)
3764.3		Cluster	8 – 24	6 – 10	-	-25 (2)	-18.5 – -16.0 (5)	-17.5	188 – 199 (5)	193	0.6 (2)	19.8 (2)
D17-8		Random	8 – 11	5	-	-22 (1)	-15.5 – -13.2 (2)	-14.4	186 – 191 (2)	189	0.9 (1)	18.0 (2)
		Random	17 – 33	6	<-46 (1)	-23 (1)	-14.8 – -14.5 (3)	-14.7	165 – 166 (3)	166	0.8 (1)	18.2 (3)
		Random	10 – 12	6	-52 (1)	-23 (1)	-16.3 – -15.3 (3)	-15.8	174 – 193 (3)	182	0.8 (1)	19.1 (3)
		Random	18	6	<-46 (1)	-23 (1)	-13.3 (1)	-13.3	194 (1)	194	0.8 (1)	17.1 (1)
		Random	8 – 14	6	-	-23 (2)	-18.5 – -18.2 (2)	-18.4	184 – 186 (2)	185	0.8 (2)	20.1 (2)

* The wide range in T_h within a FI assemblage is interpreted to reflect potential heterogeneous trapping or post-trapping modification; the minimum T_h is suggested to represent trapping temperature.

Fluid inclusion microthermometric data for medium to coarsely crystalline calcite in fractures (CIF).

Well ID/ Depth/ Sample Number	Diagenetic Phase	Occurrence of the FIAs	Size (μm)	Vapor (%)	Tm-first (mean °C; n)	Tm-HH (mean °C; n)	Tm-H_2O (range °C; n)	Tm-H_2O (mean °C)	Th (range °C; number of inclusion)	Th (mean °C)	XNaCl (mean; n; Chi and Ni 2007)	Salinity (mean wt. %; n; Chi and Ni 2007)
d-16-A/	CIF	Random	18	5	-53 (1)	-24 (1)	-17.3 (1)	-17.3	187 (1)	187	0.7 (1)	20.0 (1)
94-N-15		Random	7	5	-54 (1)	-25 (1)	-20.8 (1)	-20.8	179 (1)	179	0.6 (1)	22.1 (1)
3816.8 m		Random	10	5	-53 (1)	-24 (1)	-19.3 (1)	-19.3	193 – 195 (2)	194	0.7 (1)	21.3 (1)
D17-3		Random	9	6	-53 (1)	-24 (1)	-16.3 (1)	-16.3	176 (1)	176	0.7 (1)	19.3 (1)
		Random	8	6	-53 (1)	-24 (2)	-15.1 (1)	-15.1	191 – 193 (2)	192	0.7 (2)	18.4 (1)
		Random	12	6	-52 (1)	-23 (1)	-	-	189 (1)	189	0.8 (1)	-
		Random	11	6	-	-23 (1)	-	-	192 (1)	192	0.8 (1)	-
d-16-A/	CIF	Cluster	5 – 15	6	-	-23 (3)	-12.0 – -11.7 (2)	-11.9	172 – 175 (7)	174	0.8 (3)	15.8 (1)
94-N-15		Cluster	6 – 12	6	-49 (3)	-24 (3)	-16.3 – -15.7 (3)	-16.0	174 – 189 (6)	180	0.7 (3)	19.1 (1)
3768.1 m		Random	11 – 13	~100	-	-	-	-	-52.4V – -51.5V (2)	-52.0V	-	-
D17-I		Isolated	20	~100	-	-	-	-	-51.0V (1)	-51.0V	-	-
		Random	15	~100	-	-	-	-	-52.6V (1)	-52.6V	-	-
		Trail	10	~100	-	-	-	-	-54.2V (1)	-54.2V	-	-
		Isolated	10	~100	-	-	-	-	-56.5V (1)	-56.5V	-	-
		Isolated	11	~100	-	-	-	-	-49.5V (1)	-49.5V	-	-
d-16-A/	CIF	Random	10 – 13	6	<-45 (1)	-23 (1)	-16.3 (1)	-16.3	172 (2)	172	0.8 (1)	19.4 (1)
94-N-15		Isolated	15	6	-52 (1)	-24 (1)	-16.1 (1)	-16.1	175 (1)	175	0.7 (1)	19.2 (1)
3769.1 m		Trail	14	~100	-	-	-	-	-55.3V (1)	-55.3V	-	-
D17-J		Trail	7 – 11	~100	-	-	-	-	-57.6 – -55.9V (2)	-56.8V	-	-
		Isolated	8	~100	-	-	-	-	-57.3V (1)	-57.3V	-	-
		Random	12	~100	-	-	-	-	-57.4V (1)	-57.4V	-	-
		Random	6	~100	-	-	-	-	-58.6V (1)	-58.6V	-	-
		Cluster	6 – 10	~100	-	-	-	-	-59.5V – -57.4V (2)	-58.5V	-	-
		Isolated	6	~100	-	-	-	-	-55.9V (1)	-55.9V	-	-
		Cluster	10 – 16	~100	-	-	-	-	-52.2V – -51.5V (2)	-51.9V	-	-
		Isolated	23	~100	-	-	-	-	-58.7V (1)	-58.7V	-	-

D-4: Fluid inclusion microthermometric data for coarsely to very coarsely crystalline, blocky calcite in vugs (CCC)

Well ID/ Depth/ Sample Number	Diagenetic Phase	Occurrence of the FIA	Size (µm)	Vapor (%)	Tm-first (mean °C; n)	Tm-HH (mean °C; n)	Tm-H_2O (range °C; n)	Tm-H_2O (mean °C)	Th (range °C; number of inclusion)	Th (mean °C)	XNaCl (mean; n; Chi and Ni 2007)	Salinity (mean wt. %; n; Chi and Ni 2007)
c-16-A/	CCC	Cluster	6 – 8	6	-	-24 (1)	-14.2 (1)	-14.2	170 – >261 (2)	170*	0.7 (1)	17.7 (1)
94-N-16		Random	6	6	-54 (1)	-25 (1)	-	-	144 (1)	144	0.6 (1)	-
3569.9 m		Isolated	7	7	-54 (1)	-24 (1)	-	-	149 (1)	149	0.7 (1)	-
D1-5B		Random	4	5	-	-25 (1)	-	-	179 (1)	179	0.6 (1)	-
		Random	4	6	-54 (1)	-25 (1)	-	-	183 – 206 (2)	195	0.6 (1)	-
c-10-E/	CCC	Random	8 – 10	6	-52 (2)	-23 (1)	-11.4 – -10.9 (3)	-11.2	131 – 149 (3)	141	0.8 (1)	15.2 (3)
94-N-7		Random	4 – 20	5	-53 (1)	-23 (1)	-13.2 – -12.7 (2)	-13.0	185 (1)	185	0.8 (1)	16.8 (2)
1823.0 m		Cluster	10 – 11	5	-	-24 (1)	-13.6 – -13.0 (3)	-13.3	163 – 173 (3)	168	0.7 (1)	17.0 (3)
D2-3		Random	6 – 9	5	<-46 (1)	-22 (2)	-14.0 – -13.2 (3)	-13.7	158 – 166 (3)	162	0.9 (2)	17.4 (3)
		Cluster	5 – 11	4 – 5	-51 (1)	-23 (2)	-12.9 – -12.6 (2)	-12.8	164 – 169 (3)	167	0.8 (2)	16.6 (2)
		Random	7	6	-	-	-	-	168 (1)	168	-	-
		Random	7	5	-	-	-	-	158 – 165 (2)	162	-	-
		Random	4 – 9	5	-52 (1)	-23 (1)	-12.8 (2)	-12.8	164 – 172 (2)	168	0.8 (1)	16.6 (2)
b-19-K/	CCC	Random	11 – 16	5	-54 (2)	-24(1)	-16.1 – -15.9 (2)	-16.0	137 – 138 (2)	138	0.7 (1)	19.1 (2)
94-N-16		Random	20 – 24	5	-	-	-14.7 – -12.7 (2)	-13.5	193 – 196 (2)	195	-	17.3 (2)
4192.9 m		Isolated	15	6	-	-	-		202 (1)	202	-	-
D4-2		Isolated	14	6	-54 (1)	-25 (1)	-17.4 (1)	-17.4	209 (1)	209	0.6 (1)	20.0 (1)
		Random	16 – 28	4 – 5	-54 (1)	-24 (3)	-18.4 – -14.1 (3)	-16.2	176 – 216 (4)	189	0.7 (3)	19.1 (3)
		Isolated	13	5	-54 (1)	-23 (1)	-16.0 (1)	-16.0	154 (1)	154	0.8 (1)	19.2 (1)
		Random	10 – 31	5 – 6	-53 (2)	-23 (2)	-15.0 – -13.7 (2)	-14.4	147 – 164 (2)	156	0.8 (2)	17.9 (2)
		Isolated	11	6	-53 (1)	-23 (1)	-17.0 (1)	-17.0	170 (1)	170	0.8 (1)	19.9 (1)
		Random	8 – 11	5	-	-24 (2)	-17.8 – -17.2 (2)	-17.5	151 – 162 (2)	157	0.7 (2)	20.2 (2)
		Random	12	5	-	-	-	-	181 (1)	181	-	-
		Random	20	5	-53 (1)	-24 (1)	-16.3 (1)	-16.3	183 (1)	183	0.7 (1)	19.3 (1)
		Isolated	16	~100	-	-	-	-	-53.1V (1)	-53.1V	-	-
		Trail	36	~100	-	-	-	-	-54.2V (1)	-54.2V	-	-
		Trail	14	~100	-	-	-	-	-56.0V (1)	-56.0V	-	-
		Trail	11	~100	-	-	-	-	-52.5V (1)	-52.5V	-	-

Well ID/ Depth/ Sample Number	Diagenetic Phase	Occurrence of the FIAs	Size (μm)	Vapor (%)	Tm-first (mean °C; n)	Tm-HH (mean °C; n)	Tm-H2O (range °C; n)	Tm-H2O (mean °C)	Th (range °C; number of inclusion)	Th (mean °C)	XNaCl (mean; n; Chi and Ni 2007)	Salinity (mean wt. %; n; Chi and Ni 2007)
a-67-D/		Random	6	5	-	-	-	-	188 (1)	188	-	-
94-O-13		Random	2 – 3	5	-54 (1)	-23 (2)	-	-	177 – 196 (5)	185	0.8 (2)	-
5221.3 m		Random	2 – 5	5 – 6	-54 (1)	-24 (2)	-15.0 – -14.2 (2)	-14.6	180 – 193 (7)	188	0.8 (2)	18.1 (2)
5.2		Random	9	~100	-	-	-	-	-52.1V (1)	-52.1V	-	-
d-73-K/		Random	23	4	-	-	-	-	174 (1)	174	-	-
94-N-16		Random	8 – 22	5 – 7	-	-	-	-	207 (2)	207	-	-
3783.6 m		Random	20	4	-51 (1)	-21 (1)	-11.1 (1)	-11.1	180 (1)	180	1.0 (1)	15.1 (1)
D7-1		Random	19	5	-50 (1)	-21 (1)	-10.7 (1)	-10.7	178 (1)	178	1.0 (1)	14.7 (1)
		Random	15 – 21		-49 (1)	-22 (2)	-12.4 – -9.3 (2)	-10.9	178 – 224 (3)	208	0.9 (2)	14.8 (2)
		Random	23 – 37	4 – 5	-49 (1)	-21 (1)	-12.0 (1)	-12.0	158 – 172 (4)	164	1.0 (1)	16.0 (1)
		Random	31	~100	-	-	-	-	-51.4 V (1)	-51.4V	-	-
		Trail	21	~100	-	-	-	-	-53.2 V (1)	-53.2V	-	-
		Random	17 – 21	~100	-	-	-	-	-54.0V – -53.6V (2)	-53.8V	-	-
		Trail	10 – 17	~100	-	-	-	-	-54.4V – -51.8V (3)	-52.7V	-	-
c-27-K/		Cluster	6 – 34	6 – 9	-54 (3)	-25 (7)	-19.6 – -16.0 (8)	-18.5	183 – 203 (8)	187	0.6 (7)	20.2 (8)
94-N-16		Random	48	8	-	-	-19.3 (1)	-19.3	199 (1)	199	-	21.9 (1)
3958.4 m		Random	13 – 16	5 – 9	-	-	-	-	183 – 187 (3)	185	-	-
D8-4		Random	2 – 6	5	-	-	-	-	184 – 205 (6)	192	-	-
		Random	8 – 14	7 – 8	-53 (1)	-24 (3)	-18.0 (1)	-18.0	182 – 189 (3)	186	0.7 (3)	20.5 (1)
c-27-K/		Random	7 – 9	6	-53 (1)	-23 (1)	-12.9 (1)	-12.9	186 – 198 (2)	192	0.8 (1)	16.7 (1)
94-N-16		Random	9 – 14	6	-52 (1)	-24 (2)	-13.5 – -12.6 (2)	-13.1	194 – 195 (2)	195	0.7 (2)	16.8 (2)
3815.3 m		Isolated	6	6	-	-23 (1)	-16.9 (1)	-16.9	164 (1)	164	0.8 (1)	19.9 (1)
D8-10		Random	3 – 5	6 – 7	-54 (1)	-24 (2)	-16.6 – -16.4 (3)	-16.5	173 – 179 (3)	177	0.8 (2)	19.5 (2)
		Trail	14 – 16	~100	-	-	-	-	-54.7V (1)	-54.7V	-	-
d-16-A/		Random	6 – 10	5 – 6	-53 (1)	-23 (2)	-15.1 – -14.8 (2)	-15.0	188 – 191 (2)	190	0.8 (2)	18.4 (2)
94-N-15		Random	18	5	-50 (1)	-24 (1)	-14.0 (1)	-14.0	196 (1)	196	0.7 (1)	17.6 (1)
3764.3		Cluster	8 – 24	6 – 10	-	-25 (2)	-18.5 – -16.0 (5)	-17.5	188 – 199 (5)	193	0.6 (2)	19.8 (2)
D17-8		Random	8 – 11	5	-	-22 (1)	-15.5 – -13.2 (2)	-14.4	186 – 191 (2)	189	0.9 (1)	18.0 (2)
		Random	17 – 33	6	<-46 (1)	-23 (1)	-14.8 – -14.5 (3)	-14.7	165 – 166 (3)	16	0.8 (1)	18.2 (3)
		Random	10 – 12	6	-52 (1)	-23 (1)	-16.3 – -15.3 (3)	-15.8	174 – 193 (3)	182	0.8 (1)	19.1 (3)
		Random	18	6	<-46 (1)	-23 (1)	-13.3 (1)	-13.3	194 (1)	194	0.8 (1)	17.1 (1)
		Random	8 – 14	6	-	-23 (2)	-18.5 – -18.2 (2)	-18.4	184 – 186 (2)	185	0.8 (2)	20.1 (2)

D-5: Fluid inclusion microthermometric data for medium to coarsely crystalline calcite in fractures (CIF)

Well ID/ Depth/ Sample Number	Diagenetic Phase	Occurrence of the FIAs	Size (μm)	Vapor (%)	Tm-first (mean °C; n)	Tm-HH (mean °C; n)	Tm-H_2O (range °C; n)	Tm-H_2O (mean °C)	Th (range °C; number of inclusion)	Th (mean °C)	XNaCl (mean; n; Chi and Ni 2007)	Salinity (mean wt. %; n; Chi and Ni 2007)
d-16-A/	CIF	Random	18	5	-53 (1)	-24 (1)	-17.3 (1)	-17.3	187 (1)	187	0.7 (1)	20.0 (1)
94-N-15		Random	7	5	-54 (1)	-25 (1)	-20.8 (1)	-20.8	179 (1)	179	0.6 (1)	22.1 (1)
3816.8 m		Random	10	5	-53 (1)	-24 (1)	-19.3 (1)	-19.3	193 – 195 (2)	194	0.7 (1)	21.3 (1)
D17-3		Random	9	6	-53 (1)	-24 (1)	-16.3 (1)	-16.3	176 (1)	176	0.7 (1)	19.3 (1)
		Random	8	6	-53 (1)	-24 (2)	-15.1 (1)	-15.1	191 – 193 (2)	192	0.7 (2)	18.4 (1)
		Random	12	6	-52 (1)	-23 (1)	-	-	189 (1)	189	0.8 (1)	-
		Random	11	6	-	-23 (1)	-	-	192 (1)	192	0.8 (1)	-
d-16-A/	CIF	Cluster	5 – 15	6	-	-23 (3)	-12.0 – -11.7 (2)	-11.9	172 – 175 (7)	174	0.8 (3)	15.8 (1)
94-N-15		Cluster	6 – 12	6	-49 (3)	-24 (3)	-16.3 – -15.7 (3)	-16.0	174 – 189 (6)	180	0.7 (3)	19.1 (1)
3768.1 m		Random	11 – 13	~100	-	-	-	-	-52.4V – -51.5V (2)	-52.0V	-	-
D17-I		Isolated	20	~100	-	-	-	-	-51.0V (1)	-51.0V	-	-
		Random	15	~100	-	-	-	-	-52.6V (1)	-52.6V	-	-
		Trail	10	~100	-	-	-	-	-54.2V (1)	-54.2V	-	-
		Isolated	10	~100	-	-	-	-	-56.5V (1)	-56.5V	-	-
		Isolated	11	~100	-	-	-	-	-49.5V (1)	-49.5V	-	-
d-16-A/	CIF	Random	10 – 13	6	<-45 (1)	-23 (1)	-16.3 (1)	-16.3	172 (2)	172	0.8 (1)	19.4 (1)
94-N-15		Isolated	15	6	-52 (1)	-24 (1)	-16.1 (1)	-16.1	175 (1)	175	0.7 (1)	19.2 (1)
3769.1 m		Trail	14	~100	-	-	-	-	-55.3V (1)	-55.3V	-	-
D17-J		Trail	7 – 11	~100	-	-	-	-	-57.6 – -55.9V (2)	-56.8V	-	-
		Isolated	8	~100	-	-	-	-	-57.3V (1)	-57.3V	-	-
		Random	12	~100	-	-	-	-	-57.4V (1)	-57.4V	-	-
		Random	6	~100	-	-	-	-	-58.6V (1)	-58.6V	-	-
		Cluster	6 – 10	~100	-	-	-	-	-59.5V – -57.4V (2)	-58.5V	-	-
		Isolated	6	~100	-	-	-	-	-55.9V (1)	-55.9V	-	-
		Cluster	10 – 16	~100	-	-	-	-	-52.2V – -51.5V (2)	-51.9V	-	-
		Isolated	23	~100	-	-	-	-	-58.7V (1)	-58.7V	-	-